UNIVERSITA' DEGLI STUDI DI PAVIA

FACOLTA' DI INGEGNERIA
DIPARTIMENTO DI INGEGNERIA INDUSTRIALE E DELL'INFORMAZIONE

DOTTORATO DI RICERCA IN
BIOINGEGNERIA, BIOINFORMATICA E TECNOLOGIE PER LA SALUTE
XIV CICLO - 2021

DESIGN AND CHARACTERIZATION OF *CRISPRi*-BASED SYNTHETIC CIRCUITS TO INHIBIT ANTIBIOTIC RESISTANCES IN BACTERIA

PhD Thesis by

ANGELICA FRUSTERI CHIACCHIERA

Advisor:
Prof. Paolo Magni
Prof. Lorenzo Pasotti

PhD Program Chair:
Prof. Silvana Quaglini

A te Edoardo,
per tutto l'amore che custodisci
e che ogni giorno rinnovi.

Abstract (English)

Bacterial evolution is driven by rapid adaptation to changing environments where adverse conditions must be faced. The horizontal exchange of genetic information, along with the inherent bacterial genome plasticity, are key players in the evolution of microbial populations with increased tolerance towards physical or chemical agents, including the arsenal of antimicrobials (antibiotics, antivirals, antifungals etc.) used in different settings (from clinical to agriculture sector) to treat infectious diseases. The abuse and misuse of these medicines drive the evolution and selection of microbes able to survive exposure to an antimicrobial agent that was originally effective to kill the cell or arrest its growth. This phenomenon is defined as Antimicrobial Resistance (AMR) and, to date, it represents one of the major global health threat especially because of the spread of antibiotic resistance which, day by day, erodes the efficacy of available antibiotics and compromises our ability to cure life-threatening infections. This scenario, worsened by a gap in the discovery of innovative compounds with meaningful clinical benefits over existing drugs, poses an urgent need for new strategies to counteract AMR. With this regard, Synthetic Biology may significantly contribute to the development of non-traditional therapies able to supplant or accompanying antibiotics use. For instance, to treat a localized AMR-associated infection, sophisticated living systems can be rationally programmed to sense a distinctive environmental signal and respond through the *in situ* delivery of an antimicrobial agent able to selectively kill resistant bacteria. This genetic program can be encoded in a synthetic circuit by leveraging a collection of biological regulatory parts and the strong programmable nature of CRISPR technology. The latter allows to design sequence-specific antimicrobials as a guide RNA can be *ad hoc* designed to drive the cleavage of Cas9 nuclease towards target genes encoding for resistance determinants. The Cas9-mediated degradation of target DNA results in bacterial death or re-sensitization to antibiotic therapy. Although this approach has already been explored with promising results, at least two

major hurdles still have to be faced: the risk of generating new variants of resistance genes in escaper cells that have survived CRISPR targeting, and the need to develop a robust delivery strategy to mobilize *in vivo* the synthetic circuit in target bacteria. Both challenges were addressed with the research work presented in this thesis. First, to avoid the threatening consequences of Cas9 cleavage, a synthetic circuitry based on CRISPRi technology was developed as it relies on the ability of dCas9 protein to inhibit the expression of target genes without damaging the relative nucleotide sequence. The circuitry is expected to exert re-sensitization of target pathogens, acting as a trojan horse in the repression of resistance genes. Second, a delivery platform based on bacterial conjugation was exploited to mobilize the CRISPRi circuitry in target resistant bacteria. A mathematical model was implemented with the purpose to simulate the effect of a CRISPRi-based therapy on AMR pathogens and to compare different biological scenarios including the targeting and the delivery mechanisms, and eventually gaining insight into the best therapeutic strategies for *in vivo* use.

In Chapter 1, the biological background of AMR is described with a particular focus on the following topics: causes driving the evolution of antibiotic resistance on global scale; brief overview from antibiotic discovery to the current status of the antibacterial development pipeline; role of Synthetic Biology and CRISPR technology in the development of non-traditional therapies; summary on the State of the Art concerning the scientific works in which CRISPR-based antimicrobials have already been characterized. Finally, the purpose of this thesis is described and the activities conduced to reach the final goal are illustrated.

In Chapter 2, the CRISPRi platform designed and characterized in this work is presented. The circuit architecture is detailed and characterized in two main configurations, constitutive and inducible, including an *rfp* reporter gene as target expression cassette to evaluate platform performance. Along with the approaches exploited to optimize the efficiency of this circuitry, the flexibility and tunability of this platform is demonstrated in specific case studies dealing with the design of synthetic circuits for information processing tasks.

In Chapter 3, a proof of concept of the CRISPRi-based silencing of resistance genes is provided. The new synthetic circuitry, based on the pre-characterized platform, is described and characterized in terms of repression efficiency and multi-targeting capability, which are addressed in two case studies: transcriptional inhibition of model- and clinically-relevant resistance genes. The results derived from the analysis of escaper cells, whose behaviour was investigated with quantitative assays and sequencing analysis, are discussed with a particular focus on the hot-spot sequences susceptible

to nucleotide mutations. Finally, by considering two recipient populations of bacteria harbouring distinct resistance genes, the conjugative transfer of the CRISPRi circuitry is investigated and its performances discussed in terms of *conjugation* and *killing efficiency*.

In Chapter 4, the mathematical modelling of a CRISPR-based therapy is described by simulating and then comparing a set of therapeutic solutions based on two different delivery strategies (bacterial conjugation and phage infection) and targeting mechanisms (CRISPR/Cas9 and CRISPRi technology). Once the model architecture is defined, along with the differential equations systems used to model each biological process, the results generated by model simulations are discussed and compared with previously published and herein measured experimental data to evaluate the predictive power of the developed model.

In Chapter 5, the summary of this work is reported along with the overall conclusions and the future perspectives.

Abstract (Italian)

L'evoluzione delle specie batteriche è un processo guidato da un rapido adattamento alle mutevoli, e spesso avverse, condizioni ambientali. Lo scambio di materiale genetico attraverso meccanismi di trasferimento genico orizzontale, unito alla plasticità intrinseca del genoma batterico, gioca un ruolo fondamentale nell'evoluzione di microorganismi con potenziate capacità di adattamento nei confronti di svariati agenti chimici o fisici, tra i quali si distingue l'arsenale di agenti antimicrobici (antibiotici, antivirali, antifungini etc.) utilizzati in vari settori (dal contesto clinico a quello agricolo) per trattare le malattie infettive. L'abuso e l'uso improprio degli antimicrobici guida l'evoluzione e selezione di microorganismi in grado di sopravvivere al trattamento con farmaci precedentemente risultati efficaci per debellare l'infezione da essi provocata. Questo fenomeno si definisce Resistenza Antimicrobica (AMR) e, ad oggi, costituisce una seria minaccia per la salute pubblica mondiale specialmente a causa della rapida diffusione della resistenza antibiotica che, giorno dopo giorno, erode l'efficacia degli antibiotici attualmente disponibili e minaccia la capacità di trattare efficacemente infezioni potenzialmente letali. Lo scenario descritto è aggravato dall'insoddisfacente sviluppo e/o scoperta di nuovi composti con capacità terapeutiche superiori a quelli correntemente in uso e porta di conseguenza alla luce la necessità urgente di sviluppare terapie innovative capaci di sostituire o affiancare l'uso degli antibiotici. In questo contesto, la Biologia Sintetica può dare un contributo significativo. Riscrivendo il programma genetico di una cellula, i biologi sintetici possono infatti progettare sofisticati organismi in grado di percepire uno stimolo caratteristico di un distretto corporeo in cui ha luogo l'infezione e, in risposta al segnale, rilasciare una molecola battericida che agisca selettivamente sulla popolazione di patogeni da debellare. Questo programma genetico può essere codificato all'interno di un circuito sintetico sfruttando una collezione di parti biologiche e l'elevata versatilità della tecnologia CRISPR, che consente di progettare agenti antimicrobici selettivi in

grado di colpire una sequenza distintiva nel genoma del batterio bersaglio. Disegnando opportunamente la sequenza di una guida a RNA è infatti possibile pilotare il taglio della nucleasi Cas9 sui geni che conferiscono resistenza agli antibiotici: la degradazione del DNA bersaglio si risolve poi nella morte cellulare o nel ripristino della sensibilità antibiotica. Sebbene questo approccio sia già stato esplorato con promettenti risultati, almeno due questioni fondamentali rimangono ancora aperte: il rischio di incoraggiare l'evoluzione di nuove varianti dei geni di resistenza nelle cellule che sfuggono alla morte tramite una riparazione del DNA danneggiato, e la necessità di sviluppare una piattaforma in grado di garantire anche *in vivo* un trasferimento efficace della circuiteria CRISPR nei batteri resistenti. Entrambe queste sfide sono state affrontate nel progetto di ricerca presentato in questa tesi. In primo luogo, per aggirare i rischi connessi al taglio del DNA nelle cellule target, è stata progettata una circuiteria sintetica basata sulla tecnologia CRISPRi, la quale sfrutta la capacità della proteina dCas9 di silenziare l'espressione di un gene target senza tuttavia comprometterne la sequenza nucleotidica. In secondo luogo, una piattaforma di trasferimento genico basata sulla coniugazione batterica è stata sviluppata per veicolare il circuito CRISPRi nei batteri resistenti. Infine, è stato implementato un nuovo modello matematico per simulare l'effetto di una terapia che impiega il sistema CRISPRi, mettendo a confronto diversi scenari riguardanti il meccanismo di inibizione e il trasferimento della circuiteria, al fine di predire *in silico* la strategia terapeutica più efficace da utilizzare *in vivo*. Il lavoro di ricerca svolto in questa tesi si snoda attraverso i capitoli presentati di seguito.

Nel Capitolo 1 il problema della resistenza antimicrobica viene presentato attraverso una panoramica generale che pone una particolare attenzione sui seguenti temi: cause che spingono l'evoluzione della resistenza antibiotica a livello globale; breve excursus storico dalla scoperta degli antibiotici allo stato attuale della pipeline clinica relativa alle nuove molecole in via di sviluppo; contributo che la Biologia Sintetica e la tecnologia CRISPR possono fornire nel processo di sviluppo di terapie innovative; riassunto sui principali lavori scientifici in cui, ad oggi, la tecnologia CRISPR è stata impiegata per la progettazione di agenti antimicrobici. Infine, lo scopo della tesi sarà descritto scandendo le attività svolte per raggiungere l'obiettivo finale.

Nel Capitolo 2 viene presentata la piattaforma circuitale CRISPRi che è stata progettata e caratterizzata in questo lavoro. L'architettura di tale piattaforma è descritta e caratterizzata in due principali configurazioni, constitutiva e inducibile, entrambe progettate per inibire una cassetta di espressione per il gene reporter *rfp*, scelto come target modello per valutare le performance del sistema CRISPRi. Gli approcci utilizzati per ottimizzare l'efficienza di repressione di questa circuiteria sono descritti e adottati in

specifici casi di studio riguardanti la progettazione di circuiti sintetici.

Nel capitolo 3 il focus del lavoro di ricerca è dirottato sull'inibizione dei geni di resistenza antibiotica mediante la tecnologia CRISPRi. In primo luogo viene descritta la nuova circuiteria sintetica, basata sulla piattaforma genetica caratterizzata nel precedente capitolo, per la quale è stata svolta una caratterizzazione in termini di efficienza di repressione e capacità di *multi-targeting* in due casi di studio: inibizione di resistenze antibiotiche modello e ad alto impatto clinico. Il comportamento di cellule escaper, sopravvissute al *targeting* mediante CRISPRi e al trattamento antibiotico è inoltre discusso partendo dai risultati ottenuti mediante saggi quantitativi in liquido e dal sequenziamento dei siti più esposti all'insorgenza di mutazioni. Infine, lo studio della coniugazione batterica come strumento di trasferimento della circuiteria CRISPRi in cellule resistenti è affrontato in due popolazioni microbiche riceventi che si distinguono per il gene di resistenza. Le performance del processo coniugativo sono valutate in termini di *efficienza di coniugazione* e *killing*.

Nel Capitolo 4 viene descritta la modellizzazione matematica di una terapia che impiega la tecnologia CRISPRi come strumento per l'eradicazione di infezioni da batteri multi-resistenti. L'obiettivo è stato affrontato attraverso la simulazione e il confronto di diverse soluzioni terapeutiche basate sull'impiego di due differenti sistemi di trasferimento del DNA ingegnerizzato (coniugazione batterica o infezione fagica) e due strategie di *targeting* (CRISPR/Cas9 o CRISPRi). In primo luogo, viene definita l'architettura del modello e i sistemi di equazioni differenziali impiegati per descrivere ciascun processo biologico; in seguito, i risultati delle simulazioni sono discussi e anche confrontati con dati sperimentali ricavati dalla letteratura e da questa attività di tesi per valutare le performance predittive del modello.

Nel Capitolo 5 sono trattate le conclusioni finali ricavate dal lavoro di ricerca qui presentato e potenziali sviluppi futuri sono inoltre suggeriti.

List of Abbreviations

AMR Antimicrobial resistance

ARG Antimicrobial resistance gene

DSB Double-strand break

HAI Healthcare-associated infection

HGT Horizontal gene transfer

HR Homologous recombination

MDR Multidrug-resistant

MGE Mobile genetic element

NHEJ Non-homologous end-joining

WHO World Health Organization

Contents

List of Figures

List of Tables

Chapter 1

Introduction

1.1 Antimicrobial Resistance

Throughout history, infectious diseases like plague, cholera, malaria and tuberculosis have represented a major threat to human health. Pathogenic microorganisms such as viruses, bacteria, fungi and parasites have always been responsible for the emergence and spread of severe infections with pandemic potential. Since the 20th century, morbidity and mortality from infectious diseases have declined remarkably due to public health improvements in sanitation, childhood vaccination programs and discovery of antimicrobials. Antimicrobials (antibiotics, antivirals, antifungals and antiparasitics) are natural or synthetic agents able to kill or inhibit the growth of pathogenic microorganisms in humans, animals and plants. Since their introduction in clinical practice, they have contributed to the near eradication of several infectious diseases worldwide [1, 2, 3].

However, in recent decades, the public health sector has witnessed the alarming emergence and global dissemination of multidrug-resistant pathogens, i.e. microorganisms that have acquired or developed the ability to survive the action of an antimicrobial drug used to prevent and treat the infections they are responsible for. As a consequence, current available medicines result insufficient to arrest the spread of severe and even lethal illness. This phenomenon, known as antimicrobial resistance (AMR), has been included in the top 10 global health threat list edited by the World Health Organization (WHO) in 2019 [4]. In this context, of great concern is the increasing number of multi- and pan-resistant bacteria (also known as "superbugs"), which give rise to persistent infections that are harder to treat with available antibiotics, including those classified as last-resort drugs [5]. The global spread of antibiotic resistance is driven by a combination of factors such as close contact

with infected people or animals and exposure to contaminated surfaces, food or water. Often, the most deadly AMR-associated infections take place in healthcare facilities and spread through patients. Without appropriate control actions, resistant microorganisms can spill over into communities which, in turn, are connected on global scale [6]. The epidemiological impact of AMR reflects on the global increase of morbidity and mortality from resistant infections: only in the United States, 2.8 millions of individuals acquire an antibiotic-resistant infection, leading to the death of 35000 people/year [6]; in Europe, 33000 deaths annually are estimated as a direct consequence of an infection due to resistant pathogens [7]. Finally, the O'Neil report predicts that AMR could cause 10 million deaths by 2050, exceeding the current number of deaths from cancer [8]. Along with clinical impact, the economic cost of AMR is significant. Resistant infections involve prolonged hospitalizations, intensive care with more expensive medicines than first-line drugs and global investments into antimicrobials R&D. In the World Bank report (2017) it is predicted that the impact of AMR on healthcare costs will increase globally with an annual price ranging from 300 billion dollar to more than 1 trillion dollar by 2050 [9].

The stark increase in the incidence of multidrug resistant pathogens can be attributed to a variety of causes at different levels. First of all, as a natural evolutionary process encouraged by bacterial genome plasticity, AMR may occur through spontaneous genetic mutations that provide a microbe with defense mechanisms to survive antibiotic exposure [10]. Antibiotic resistance genes (ARGs) can also be acquired via horizontal gene transfer (HGT) of mobile genetic elements such as a plasmids, transposons or integrons carrying the resistance determinants [11]. Furthermore, the misuse and abuse of antibiotics in clinic, agriculture and veterinary medicine have established a selective evolutionary pressure which, encouraged by bacterial genome plasticity, has accelerated the spread of multi-drug resistant microorganisms [12]. In fact, according to several studies, antibiotic resistance can arise when bacteria are exposed to sub-inhibitory concentrations of antibiotics. This treatment might kill susceptible bacteria, but also enriches for resistant clones that survive, proliferate and may also share resistance genes with other members of bacterial community, even beyond species boundaries [11, 13]. This way, the selective pressure of antibiotics acts as an agent in the proliferation and dissemination of resistant bacteria, allowing for co-selection mechanisms such as co-resistance and cross-resistance. Co-resistance refers to the presence of different genes responsible for resistant phenotypes in the same genetic element such as plasmid, transposon or integron. Cross-resistance occurs when the resistance to multiple antimicrobial agents, even belonging to different classes, is conferred by a single molecular mechanism. An example of cross-resistance

is the multi-drug resistance (MDR) pump in *Listeria monocytogenes* able to efflux antibiotics and metals [13, 14]. In this regard, the major defense strategies evolved to withstand antibiotic activity includes: up-regulation of efflux pumps to expel the drug from the cell, restricted access to the antibiotic by reducing cell wall or outer membrane permeability, antibiotic inactivation through enzymatic degradation and target modification [11, 15].

Despite their role in resistance evolution, antibiotics have revolutionized modern medicine making not only the treatment of infectious diseases possible, but also complex surgeries such us tumor excision, organ transplants and open-heart surgery. The history of antibiotics starts with the accidental discovery of penicillin by Alexander Flaming in 1928, which led scientists to investigate the role of microbes as producers of antimicrobial compounds. Waksman, awarded with the Nobel Prize in Medicine or Physiology in 1952 for the discovery of streptomycin, the first successful agent isolated against tuberculosis, defined an antibiotic as "a compound made by a microbe to destroy other microbes" [16]. Indeed, antibiotics are small molecules able to inhibit essentials pathways for bacterial viability such as cell wall synthesis, protein translation and DNA replication [17]. Based on their spectrum of activity, they can be classified as narrow-spectrum or broad-spectrum antibiotics: the former act on a specific type of bacteria, whereas the latter target a wide range of bacteria.

Waksman's pioneering work on soil-actinomycetes, an order of actinobacteria identified as fruitful producers of antimicrobial compounds, opened the golden age of antibiotic discovery from 1940s to 1970s. During this period, multiple classes of antibiotics derived from natural products were discovered, encouraging an extensive use in clinic and led to an impressive advance in human health. However, the race to find and develop new antibiotics, including synthetic compounds, have stalled from 1980s onward. In fact, all the following research efforts to uncover innovative compounds, defined as agents that do not show known cross-resistances to existing antibiotics, ended with poor results [4, 16, 18]. This is a crucial point in the development of new classes of antimicrobial compounds because the resistance to one antibiotic is often correlated with resistance to multiple antibiotics belonging to the same class. According to the WHO report on the antibacterial clinical development pipeline, the majority of products that have reached the clinic in the latest years, along with agents that are currently under development worldwide, are derivatives of existing classes of natural or synthetic antibiotics, rather than new molecules. The same report points out that the current antibiotic discovery pipeline, mainly based on the improvements of existing drugs, is insufficient to support the development of new agents that fulfil innovative criteria (new chemical structure, new binding site or mode of action).

Only few molecules included in the clinical pipeline target the WHO priority pathogens, that are grouped under 3 priority tiers and represent the 12 classes of most threatening resistant bacteria identified to date. The pipeline also highlights that the molecules in development have only limited benefits over existing drugs and only three show activity towards *NDM-1* gene, one of the most threatening ARGs which confers resistance to carbapenems, a class of broad spectrum antibiotics used as the last line of defence against MDR bacteria [4, 7].
The described scenario threatens a return to the pre-antibiotic era, where common infections and minor injuries could be lethal again for millions of people. Therefore, the global crisis imposed by AMR requires urgent and multisectoral actions ranging from the improvement of infection prevention and appropriate antibiotic use, careful containment strategies to avoid environmental spread of resistant germs, additional research to identify new antibiotics and investigation of non-traditional approaches able to supplant or accompanying antibiotics use [6]. Among the new therapeutic strategies in drug discovery and development, of great interest are: monoclonal antibodies against virulence factors like toxins and effector proteins of specialized secretion systems; inhibitors of adhesins (proteins that allow bacterial adhesion to cell surface) and defense structures like biofilms; microbiome-modifying therapies based on the transplantation of human natural microbiota or rationally selected cocktails of beneficial microorganisms; genetically engineered bacteria, bacteriophages and nanoparticles as vehicles for the *in situ* delivery of therapeutic agents that selectively kill resistant pathogens without threatening the communities of commensal microbes [19]. An example of this innovative approach is provided by the engineering of bacterial therapeutics based on CRISPR technology; as a highly programmable genetic tool, CRISPR technology can support the design of synthetic circuits that could be delivered by engineered microorganisms in microbial communities in order to allow for the precision killing of target bacteria [20].
The development of non-traditional therapies is a promising future perspective but, before their introduction in clinical practice, many challenges like regulatory issues and meaningful clinical benefits over existing drugs must be addressed [19].

1.2 Synthetic Biology and CRISPR technology

The dramatic rise of MDR pathogens, along with the worring gap in the discovery of new molecules more effective than the currently available drugs, pose an urgent need for new strategies to tackle antibiotic resistance. In this

scenario, Synthetic Biology may play a crucial role in the development of innovative technologies targeting the most critical resistant bacteria. Synthetic Biology is a branch of bioengineering with a strong interdisciplinary nature in which knowledge and expertise from several research fields converge, including engineering, biology, chemistry, computer science and social science. Applying engineering rules to the biological world, Synthetic Biology aims to design sophisticated living systems in a reliable, efficient and predictable manner. Indeed, as an electronic circuit, a specific genetic program can be assembled into synthetic gene networks to implement specific functionalities in known organisms or create novel biological systems that do not exist yet in nature [21]. Paradigms of rational design, such as modularity and standardization of components, drive the construction of complex genetic circuits with predictable behaviour: basic biological parts deposited in libraries of well-characterized standard DNA components (promoters, ribosome binding sites-RBSs, transcription factors, etc.) can be interconnected to construct genetic programs that encode specific user-defined tasks; the resulting genetic circuit can be incorporated into a desired host organism through, for example, a plasmid vector, exploiting the endogenous molecular machinery for replication, transcription and translation [22]. The entire process can be supported by mathematical models which can assist synthetic biologists in the choice of optimal components to meet the design specifications. The most representative research fields of Synthetic Biology applications include: biomaterials, such as high-value polymers produced by engineered microorganisms [23]; biofuels, through the use of genetically modified bacteria able to convert waste materials into renewable fuels [24]; diagnosis, supported by the use of living biosensors equipped with a "sense-logic report module" able to detect disease-related molecules [25]; therapeutics, represented by the development of cell-based therapies to target cancer cells or microbiome manipulation to treat infections, metabolic or inflammatory bowel diseases (IBDs) [19, 26, 27]. These examples highlight the great potential of Synthetic Biology to address real global problems, including antibiotic resistant pathogens.

The spectrum of strategies explored by Synthetic Biology in the fight against MDR pathogens includes the discovery of new antibiotics as well as the development of non-traditional therapies to replace antibiotics or accompanying their use. In the first case, the drug discovery process passes through the identification of novel drug targets, the development of screening platform for the isolation of new bioactive candidates or the directed engineering of known gene clusters to produce novel drug leads [28]. In the second case, alternatives to antibiotics are represented by vaccines, antibodies and microbiome-modifying therapies. As the human microbiome is intimately connected with

the host health state [29], the ability to manipulate and engineer our resident bacteria provides an attractive platform to treat metabolic, human inherited and communicable diseases [19, 26, 29]. Indeed, scientific evidence shows that antibiotics administration can result in gut dysbiosis (imbalance in normal microbial composition) which can increase the susceptibility to infectious diseases such as *Clostridium difficile* infection (CDI). Transplantation of human intestinal microbiota [30] as well as the re-colonization of gut flora with cocktails of rationally selected bacteria contribute to restore a healthy community of microbes, which can compete with pathogenic bacteria and limit their proliferation. Furthermore, using Synthetic Biology, commensal and probiotic bacteria can be *ad hoc* engineered to detect infections by sensing pathogen-specific quorum sensing molecules; destroy defense structure like biofilms; deliver antimicrobial compounds and peptides (i.e. bacteriocines) to selectively kill target bacteria without affecting the growth of commensal microbes [31, 32]. Synthetic genetic circuits, which encode for sequence-specific antimicrobials, can also be transferred from engineered microbes to health-threatening pathogens in order to delete or inhibit the expression of resistance or virulence genes. To achieve this goal, which is an example of *in situ* microbiota engineering, CRISPR technology could be a key resource.

CRISPR-Cas (Clustered Regularly Interspaced Short Palindromic Repeats-associated protein) system is an ancestral form of adaptive immunity evolved by prokaryotes (bacteria and archaea) against the invasions of exogenous nucleic acids such as that of plasmids, phages or other mobile genetic elements (MGEs). All known CRISPR systems consist of CRISPR loci and CRISPR-associated (Cas) genes. CRISPR loci comprise a CRISPR array which preserves the immunological memory of bacteria as each array is made of short-palindromic repeats (repeats, 24-40 base pairs) interspaced by unique variable sequences (spacers, 20-58 base pairs) originated from the foreign DNA (protospacers) [33, 34, 35]. The defense mechanism mediated by CRISPR immunity acts with a conserved sequence of events: upon entry of exogenous MGEs, a short fragment of the invading DNA, flanked by a conserved sequence known as PAM (protospacer-adjacent motifs), is integrated as a new spacer in the CRISPR array (adaption); if a second infection occurs, the CRISPR array is transcribed (pre-crRNAs) and processed into mature crRNAs (expression) which guide Cas proteins to the recognition and subsequent degradation of the target DNA at a site complementary to the crRNA (interference) [36]. To prevent the risk of auto-immunity, potentially caused by self-targeting events at CRISPR loci, prokaryotes evolved a mechanism of self - non self discrimination based on the presence of the PAM sequence proximal to target site. In fact, the recognition of PAM on invading DNA guarantees first protospacer selection and then target degradation; its absence in CRISPR array

prevents self-targeting events [37]. To date, two main classes of CRISPR-Cas systems have been identified and further classified into 6 subtypes: class I and class II of CRISPR-Cas systems act, respectively, with effector modules made by multiple or single multi-domain Cas proteins [38]. Nowadays, type II CRISPR-Cas9 system (Class II) from *Streptococcus pyogenes* is the most widely used tool for genome engineering purposes and several other applications. Its success is mainly due to an essential and easy to design composition, which includes the Cas9 endonuclease from *S. pyogenes* and a guide RNA (gRNA) that specifies the target site. The ability of Cas9 to introduce DSBs (double-strand breaks) at sites sharing complementarity with the gRNA, led CRISPR-Cas9 immunity to rapidly evolve into a successful technology for precise genome editing in animals, bacteria and plants. In fact, the presence of a DSB in a DNA molecule induces the SOS response which mediates the activation of endogenous repair pathways, thus leading to the introduction of alterations in the nucleotide sequence of the damaged DNA [39]. By leveraging this mechanism, site-specific DSBs mediated by Cas9:gRNA complex may restore the original function of a gene (*Knock in* through homologous recombination pathway, HR) or definitively inactivate its expression (*Knock out* through non-homologous end-joining pathway, NHEJ). This way, CRISPR-Cas9 has provided a versatile and highly programmable molecular tool to meet several research challenges: generation of animal and cellular models bearing genetic alterations resembling those present in human diseases; precision medicine through the *in vivo* correction of genetic and epigenetic defects; genetic engineering of plant genomes to create crops more robust and resistant to environmental and biological stresses; manipulation of metabolic pathways in host cells to optimize the production of drugs, biofuels and other useful synthetic materials [34, 40, 41]. To accomplish all of these research works, the design process of CRISPR technology has been optimized through the replacement of the original crRNA with a chimeric gRNA, called sgRNA, made of three functional domains: the base pairing region of 20 nucleotides (nt), the dCas9 handle and a transcriptional terminator from *S. pyogenes* [42]. In recent years, different versions of Cas9 protein have been engineered in order to extend the application fields of CRISPR technology beyond the genome-editing. In particular, thanks to the introduction of point mutations in the nuclease domains HNH and RuvC, a catalytically deactivated version of Cas9 (dCas9) has been purposed as an RNA-guided transcriptional regulator of gene expression. It has been proven that the gene silencing induced by the expression of dCas9:sgRNA complex results from the inhibition of the transcriptional process: depending on the recognized site, the repressor complex can block transcription initiation (by preventing the binding of RNA polymerase to promoters) or transcription elongation (by blocking transcript

elongation within protein-coding regions) [43, 44]. This strategy, known as CRISPR *interference* (CRISPRi), represents an efficient and orthogonal platform for transcriptional regulation in prokaryotes and eukaryotes: on the one hand it can be exploited to repress the transcription of a target gene in a reversible way and without altering the sequence (unlike *Knock in* or *Knock out* techniques); on the other hand, transcriptional fusions of the dCas9 protein to effector modules, can reprogram the function in order to regulate biological processes such as transcriptional activation, epigenetic modifications, etc.[45].

Thanks to its programmable nature, CRISPR technology can also support the development of sequence specific-antimicrobials as the sgRNA sequence can be *ad hoc* designed to target genes encoding for resistance determinants. CRISPR-Cas9 system has already been used to this aim. Indeed, Cas9 cleavage of chromosomal DNA is usually lethal in bacteria as the NHEJ repair pathway is rare or no intact template is available for HR. Otherwise, the cleavage of resistance genes encoded by plasmids, does not lead to bacterial death but restores antibiotic susceptibility in the resistant strain. The main drawback of this strategy is that some cells can survive Cas9 cleavage of target DNA, leading to the generation of escape mutants. A recent study [46] shows that DNA damage can be tolerated when Cas9 cleavage is inefficient: the repair pathways induced by SOS response may support HR with intact homologous template if all the copies of bacterial chromosome are not cut simultaneously, thus restoring the original DNA sequence; moreover, in the absence of an available sister chromosome, HR can still occurs between REP (repetitive extragenic palindromic) elements or micro-homologies along the damaged DNA, resulting in large chromosomal deletions; NHEJ pathway, absent in the majority of studied bacteria but present in pathogens like *M. tuberculosis* [47], can also assist DSBs repair through small INDEL mutations (even in frame) at the target site; finally, SOS response induces a transient increase in mutation rate, which provides the cell with the possibility to mutate the target sequence, making it unrecognizable to CRISPR system [46]. The worst consequence of this scenario is the risk of generating new variants of resistance genes, immune to CRISPR targeting and still encoding for functional proteins. To overcome these issues, CRISPRi technology could represent a smart solution. In fact, the dCas9:sgRNA repressor complex can inhibit the expression of resistance genes without causing DNA damage, thus bypassing the threatening consequences of SOS response (see Figure 1.1). Nonetheless, the major challenge of CRISPR-based therapeutics is the development of a suitable delivery vehicle for CRISPR circuitry at the site of infection. To date, the delivery of CRISPR antimicrobials has been entrusted to conjugative plasmids [48],bacteriophages [49] engineered

phagemids [50, 51], synthetic nanoparticles [52] and mobile genomic islands [53] (see Figure 1.2). This biological background highlights that a CRISPR-based therapeutic treatment of antibiotic resistance can be developed by leveraging different delivery strategies and DNA targeting technologies. All the possible therapies that could be implemented in an *in vivo* experimental set-up can also be studied through the support of mathematical models able to simulate the desired scenario. Indeed, in latest years, several models have been proposed to describe different biological processes: bacterial growth in batch culture or dynamic system dependent on available nutritional resources [54], [55]; DNA transfer into microbial communities through bacterial conjugation [56] and phage infection [57]; CRISPR-Cas9 based genome editing and gene regulation [58] and so on. Taking advantage from these studies, a complete mathematical model that describes a CRISPR-based therapy of MDR bacteria could be implemented in order to investigate *in silico* its main strengths and weaknesses.

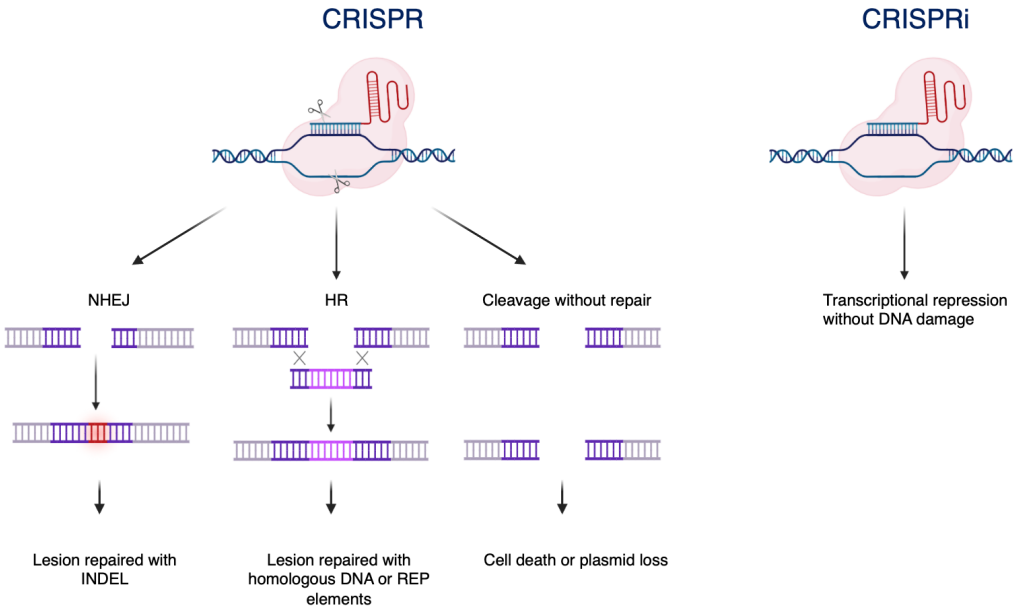

Figure 1.1: **Comparison between the outcomes of CRISPR and CRISPRi technologies on target DNA.** CRISPR and CRISPRi technologies can be used to target resistance genes. CRISPR-Cas9 mediated cleavage of target DNA generates a DSB that could result in: cell death or plasmid loss (depending on the location of the target gene); restoration of the original sequence, insertions or deletions within the target DNA supported by HR pathway; INDEL mutations as a consequence of NHEJ-mediated repair of the damage. Otherwise, CRISPRi technology acts as a trasnscriptional repressor of the resistance gene without introducing lesions in the target DNA.

1.3 State of the Art: focus on CRISPR-based antimicrobials

In the fight against AMR, targeted delivery of CRISPR-based antimicrobials has recently been explored as a therapeutic alternative to antibiotic treatment [59, 60, 61]. Towards this goal, two main approaches have been proposed and are illustrated in Figure 1.2: by harnessing endogenous Cas nuclease activity, self-targeting CRISPR arrays can be delivered in order to lethally turn cell own CRISPR immunity against themselves; otherwise, a totally exogenous Cas-gRNA expression system can be transferred into resistant cells. Moreover, target specificity of CRISPR systems, which is dependent on the careful design of guide RNAs, allows for the discrimination of specific pathogenic bacteria in a mixed population in the human gut microbiome, thus preventing deleterious effect on the rest of commensal community. Essential genes, as well as resistance or virulence determinants, can be chosen as CRISPR targets. However, depending on the location of the target sequence, the therapeutic outcome can be different: Cas9 cleavage of chromosomal loci usually results in bacterial cell death; conversely, restoration of sensitivity to antibiotics may be achieved by targeting plasmids harbouring resistance genes as the plasmid loss does not kill the cell but disarms it from the ability to resist antibiotics. These two different outcomes reflect the activity of CRISPR systems based on RNA-guided endonucleases, while the CRISPRi-mediated repression of genes encoded from chromosomal or plasmid DNA always re-establishes the susceptibility of resistant strains to existing antibiotics, thus preserving drug efficacy and preventing the risk of SOS response.

The first evidence of cell death induced by CRISPR-mediated self-cleavage derives from the pioneering work of Qimron et al. who engineered the type I-E CRISPR-Cas system from *E. coli* to target a λ prophage integrated in the bacterial chromosome, leading to the death of 98% of target cells [62]. Identifying unique PAM-flanked sequences in the genome of *E. coli*, *S. enterica* and *S. thermophilus*, Gomaa et al. showed that Type I and Type II CRISPR systems can be efficiently employed to selectively kill specific bacteria even within a mixed population composed of closely related bacterial strains [63]. Later, other research groups harnessed the endogenous CRISPR systems to pilot Cas nucleases activity towards essential genomic loci. Selle et al. reprogrammed the endogenous type I-B CRISPR-Cas system of *C. difficile* to redirect the cleavage of Cas3 nuclease towards chromosomal DNA. A self-targeting CRISPR array was delivered in the target population through a recombinant bacteriophage converted from temperate to obligately lytic

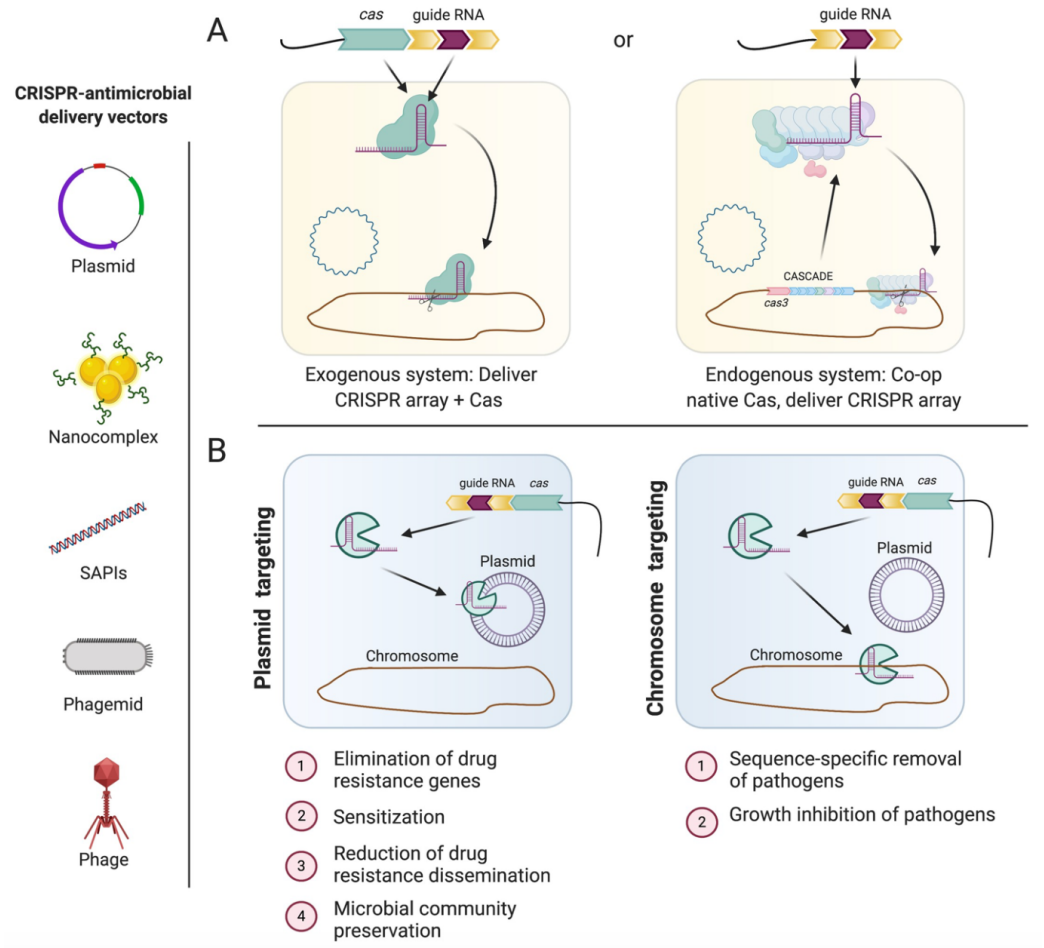

Figure 1.2: **CRISPR-based stategies to tackle AMR.** **A.** Comparison between approaches available to deliver CRISPR-encoding circuits in target cells: a complete exogenous system can be transferred in order to provide the cell with a functional Cas:gRNA complex; alternatively, endogenous Cas nuclease activity can be coupled with exogenous CRISPR arrays programmed to target resistance genes. **B.** Guides RNA can be *ad hoc* designed to drives the activity of Cas proteins towards chromosomal loci, leading to cell death, or plasmid sequences, leading to plasmid curing and re-sensitization of resistant cell to antibiotic treatment. On the left, a set of different delivery vehicles repurposed for the transfer of CRISPR-antimicrobials in target bacteria [59].

in order to improve the killing efficiency [49]. Bacteriophages are natural bacterial predators which invade the host by the injection of their nucleic acid. Thanks to their great species-level specificity, phages can be engineered to kill specific pathogens within complex bacterial populations. To this aim, genetic circuits carrying CRISPR technology can be inserted into phage genomes [49] or encapsulated into phage capsids by encoding the genetic circuits in phagemids vectors (plasmids designed to be packaged into phage capsids). This approach was successfully explored by Citorik et al. and Bikard et al.[51, 50], who engineered the Type II CRISPR-Cas9 of *S.*

pyogenes to target virulence and antibiotic resistance genes carried either on the chromosome or on the plasmids of *E. coli* [51] or *S. aureus* [50]. Both studies entrusted the delivery of complete exogenous CRISPR-Cas9 systems to recombinant phagemids based on ϕNM1 [50] or M13 [51] phages. These two research groups studied the efficacy of this approach in *in vitro* cultures and *in vivo* models by comparing the efficiency of CRISPR antimicrobials to existing antibiotics. To improve the ability to discriminate between sensitized and still resistant bacteria, Yosef et al. proposed a strategy to confer a selective advantage to re-sensitized bacteria. They designed a CRISPR array carrying a set of spacers targeting NDM1 and ctx-M-15 genes (which confer resistance to β-lactam antibiotics), naturally present in target plasmids but even transferred in the genome of lytic T7 phage. Only cells which had received CRISPR system, delivered by temperate phages, destroyed plasmids harbouring resistance genes and survived the subsequent T7 infection, thus promoting the enrichment of antibiotic-sensitized bacteria [64]. Despite their promising application, phage-based delivery vectors present some limitations such as a narrow host range, the evolution of resistance in target bacteria (e.g. through mutations in surface receptors) and challenges in regulatory issues and manufacturing process [65].

Another strategy proposed for the delivery of CRISPR antimicrobials harnesses bacterial conjugation, a natural mechanism evolved by bacteria to horizontally transfer MGEs, plasmids in particular, into microbial communities. In general, during a conjugation, a donor cell mobilizes a conjugative plasmid to a recipient cell, which acquires new genetic materials. Self-transmissible conjugation occurs when the transfer and replication functions necessary to support this mechanism, as well as the oriT sequence (origin of transfer) from which the transfer initiates, are encoded in *cis* on the conjugative plasmid; instead, a non-self-transmissible conjugation occurs when the conjugative machinery is expressed in *trans* from helper plasmids or chromosomal DNA, while the oriT sequence is carried by the mobilizable plasmid. Recently, Hamilton et al. explored both mechanisms to develop *cis* and *trans* conjugative systems based on IncP RK2 plasmid. Using *E. coli* as donor strain, a CRISPR circuitry based on tevSpCas9 and single or multiplexed sgRNAs was delivered in *S. enterica* to successfully target essential and non-essential genes [48]. In the same year, with the focus on MDR Gram positive bacteria, Rodrigues et al. deployed a pheromone-responsive plasmid (PRP) as delivery vehicle of CRISPR-machinery in *E. faecalis*. Since the same plasmid encoded a bacteriocin, its uptake by resistant-recipient bacteria led to degradation of plasmid-borne resistance genes (*ermB*, erythromycin resistance, and *tetM*, tetracycline resistance) but also conferred immunity against the toxic protein, which kills recipients that failed to acquire the en-

gineered PRP plasmid [66]. The delivery of conjugative plasmids can also be achieved with donor strains that provide in *trans* all the molecular functions necessary for conjugation, which are encoded from genes integrated into the chromosome. This approach was explored by Dong et al. who used *E. coli* strain S17-1 to mobilize a conjugative plasmid carrying a CRISPR-Cas9 system designed to target a plasmid-borne mcr-1 gene (colistin resistance) and restore polymyxin susceptibility in resistant *E. coli* strain [67]. As demonstrated in these research works, the major advantages of CRISPR-encoding conjugative plasmids are their broad-host range, cellular receptor independence and large coding capacities; on the other hand, the major limitation is the low efficiency of conjugative transfer. All the above mentioned studies reveal the great potential of CRISPR technology to develop sequence specific antimicrobials, but also warn about the emergence of escaper cells that survive CRISPR targeting, as anticipated in Section 1.2. Sequencing analysis has unveiled that these mutants can evolve different mechanisms to escape death. In fact, CRISPR machinery can be inactivated through: transposon insertion, whole gene deletion as well as single loss of function mutation in Cas9 gene [50, 51, 68, 69]; spacer mutations or deletions within the CRISPR array and transposable elements insertion in tracrRNA or sgRNA cassettes [48, 51, 63, 68]; delivery of an already defective CRISPR systems from donor conjugative strain or phagemid [50, 70]; mutations or deletions in the target sequence that impede the recognition and binding of Cas9:gRNA complex [46, 48, 70, 71, 72]. Indeed, it is known that resistance genes, especially those harboured by plasmids, can be flanked by recombinase or transposase which may support recombination events in the target sequence: the consequence could be the selection of new plasmid variants or the integration of resistance cassette into the chromosome. In a recent study, Reuter et al. demonstrated that Cas9-induced DSBs in the chromosome of *E. coli* and *C. rodentium* resulted in generation of escaper cells with inactivating mutations in Cas9 gene (38.7% and 42.8%) or target sequence (61.3% and 57.2%) [70]. Since the application of CRISPR-Cas9 systems involves the risk of generating new variants of resistance genes, a strategy based on CRISPRi technology could provide the optimal solution to circumvent this undesirable consequence. To date, only few research groups have investigated this approach. The first report on exploiting a CRISPRi system to target antibiotic resistances is provided by Wang et al. who designed a gRNA:dCas9 repressor complex able to reduce mecA gene expression (methicillin resistance) by 77% in *S. aureus* [73]. Li et al. engineered an inducible CRISPRi to target class I integron (intI) in *E. coli*, a type of MGE which is involved in the dissemination of resistance genes especially among Gram-negative bacteria. By targeting the Pc promoter, which was present within intI and drove the expression of

dfrB2 or *sul1* cassettes (encoding trimethoprim and sulfamethoxazole resistances), CRISPRi significantly alleviated the resistance to both antibiotics as the relative IC_{50} (half-maximal inhibitory concentrations) were reduced by 8 to 32 fold, respectively. It was also demonstrated that transcriptional inhibition of intI gene contributed to reduce the HGT rate of ARGs like *aadA1* and *aadB*: indeed, intI integrase is responsible for the integration of resistance gene cassettes within conjugative plasmids that can be mobilized into recipient cells, thus encouraging the spread of resistance determinants [74]. Later, a constitutive CRISPRi system was engineered by Reuter et. al in order to target a plasmid-born bla_{OXA-48} gene, which confers resistance to a broad range of β-lactam antibiotics, carbapenem included. By harnessing the conjugative machinery expressed in *trans* by the F plasmid, a non-self-transmissible conjugation was employed to deliver the repressor complex into resistant-recipient cells [70]. Together these works confirm that even CRISPRi technology could provide an attractive platform for the design of effective therapeutics against MDR pathogens. However, there are still some aspects which require further investigation to properly characterize the antimicrobial power of a CRISPRi-based circuitry. For instance, considering that resistance genes can be placed on bacterial virulence plasmids with different copy-number, the repression capability of dCas9:gRNA complex must be demonstrated even towards highly expressed target genes. Moreover, the multiplex capability of CRISPRi system can be explored by reprogramming dCas9 protein to target multiple loci within the same or different genes. This strategy could enhance repression efficiency but also expand the range of target genes. Another important aspect to consider is the rescue of escaper cells: although dCas9 targeting is not expected to induce target mutations, a deep characterization of survivor cells still needs to be carried out in order to investigate the evolution of inactivating mutations within CRISPRi circuitry and prove that target sequence is preserved from any DNA modifications. Finally, to date, the delivery of CRISPRi circuitry was addressed only in one study [70] in which an oriT$_{\mathrm{F}}$-carrying vector was mobilized to resistant cells by the conjugation machinery expressed in *trans* from F' plasmid. Although this system can be efficiently employed to mobilize synthetic circuits from *E. coli* to closely related *Enterobacteriaceae*, a conjugative platform based on a broad-host range plasmid could instead be explored to expand the range of targeted cells.

1.4 Project Aim

Antibiotic resistance is a global concern which threatens human health and poses huge and multisectoral efforts to arrest the spread of MDR bacteria. The abuse of antibiotics in clinical and agricultural sectors has been eroding the efficacy of even broad-spectrum antibiotics, highlighting the urgent need for novel therapeutics able to evade bacterial defence strategies. Thanks to its programmable nature, CRISPR technology provides a highly performing platform to address a wide range of scientific challenges as it can be repurposed for the design of sequence-specific antimicrobials. The flexibility of gRNA design pilots the specificity of CRISPR-based synthetic circuits, while their transfer into target bacteria can be achieved through different vehicles inspired by existing natural strategies. Based on this concepts, the aim of the PhD project is twofold: design and characterization of a CRISPRi circuitry *ad hoc* programmed to inhibit the expression of resistance genes in bacteria; development of a conjugation-based platform suitable for the delivery of CRISPRi circuitry in resistant cells. The general overview of the ideal therapeutic treatment proposed in this project is described below: the therapy of a patient affected by an intestinal infection can start with the oral administration of a probiotic bacterium engineered with the CRISPRi circuitry; by leveraging the ability of probiotics to colonize the gastrointestinal tract, the engineered microorganism can reach the site of infection and deliver the synthetic circuit encoding the CRISPRi platform to antibiotic-resistant bacteria; cells that have received the dCas9:gRNA complex are disarmed from their ability to resist antibiotic exposure as the inhibition of target genes restore drug susceptibility; subsequent antibiotic administration is necessary to kill re-sensitized bacteria (Figure 1.3). The main novel aspect of this approach is the application of CRISPRi, instead of the CRISPR technology, to target resistance genes. The above mentioned studies have unearthed the emergence of escaper cells that survive Cas9 cleavage through target DNA modification assisted by DNA damage repair pathways. Without damaging the DNA molecule, CRISPRi repressor complex can instead enter the cell undisturbed like a trojan horse, circumventing SOS response and inhibiting the expression of ARGs. This way, CRISPRi efficacy will not be measured by its ability to instantly kill the pathogen but to re-sensitize the cell to antibiotic treatment. Moreover, without killing the cell, the silent strategy allows for the spread of CRISPRi among pathogens via self-transmissible conjugation. The feasibility evaluation of CRISPRi technology to be used as a potent antimicrobial agent was addressed in the *E. coli* bacterium through the following experimental activities that define the specific aims of this thesis work:

- implement a CRISPRi-based platform in synthetic genetic circuits in order to characterize repression efficiency, suitable regulatory parts, contribution to cell load and reliable design rules towards the fine-tuning of CRISPRi-regulated transcriptional repression;

- reprogram the characterized CRISPRi circuitry towards the *bla* and *tetA* genes, two model ARGs that encode for ampicillin and tetracycline resistances, respectively, by using single gRNAs that individually target each resistance gene and eventually measuring their repression efficiency;

- investigate two different guide RNA architectures (*Double sgRNA Cassettes* and *CRISPRi Array*) in order to explore the multi-targeting capability of CRISPRi system and the effect on repression efficiency caused by the sharing of intracellular resources. A comparison between these two architectures was carried out in order to highlight design and cloning constrains as well as suitability in target gene repression;

- address the competition between guide RNAs sharing the same limited pool of dCas9 protein, an issue arising from the characterization of the aforementioned circuits; fine-tuning of dCas9 expression was thus carried out by an inducible promoter. This strategy aimed to find an optimal dCas9 expression level by regulating the intra-cellular amount of the common resource;

- once the CRISPRi-mediated silencing of model ARGs was confirmed, reprogram the synthetic circuitry to target *NDM1* and *mcr-1* genes, two examples of antibiotic resistances relevant in clinical settings as they are responsible for some of the most serious HAIs. A bioinformatic analysis of all known variants of *NDM* and *mcr* genes allowed for the identification of conserved regions used as CRISPRi targets. Once identified, guide RNA sequences were implemented as single or double spacers in the CRISPRi Array architecture, generating 4 different combinations of circuits to be tested in resistant bacteria;

- develop a platform for the delivery of CRISPRi circuitry to test the full workflow including HGT and killing of a target microbe. As a first attempt, the HGT mechanism known as non-self-transmissible conjugation was exploited to mobilize the engineered CRISPRi Arrays into resistant strains, in order to restore the susceptibility to target antibiotics;

- characterize the escaper cells, emerged from a background of re-sensitized bacteria, by carrying out liquid culture assays and sequencing analysis, in order to study the behavioural phenotype and the mutated genotype;
- finally, implement a mathematical model to simulate a CRISPR-based therapy; by comparing DNA-targeting technologies (CRISPR/Cas9 and CRISPRi) and delivery mechanisms (bacterial conjugation and phage infection), the model aimed at identifying the therapeutic strategy that, overall, could be most effective in eradicating antibiotic resistance, based on simulations and integration of experimental data.

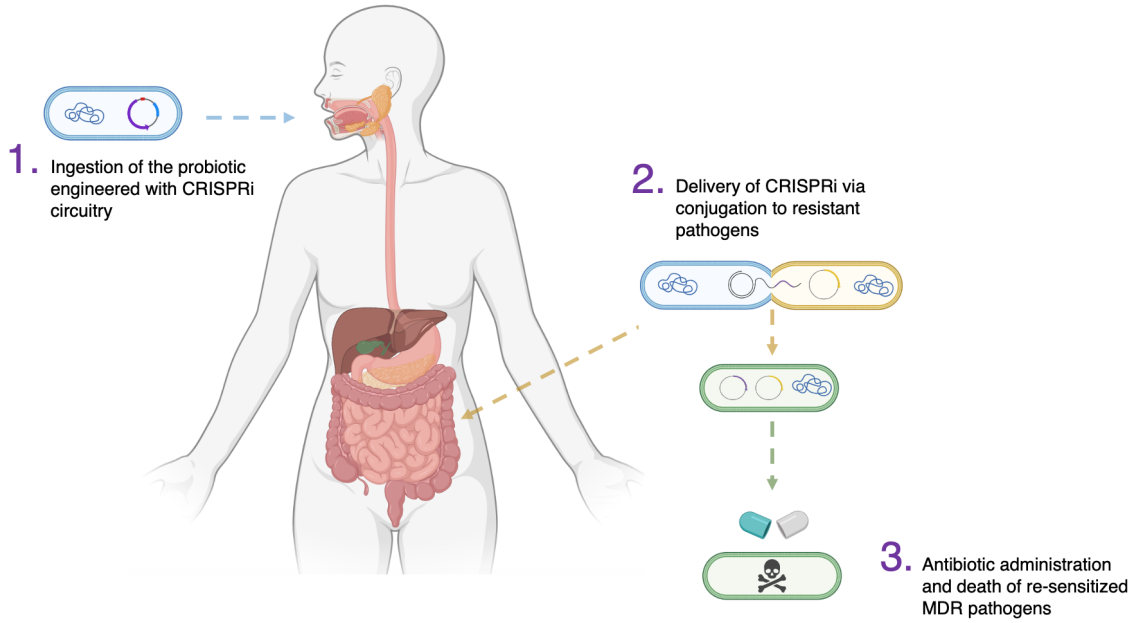

Figure 1.3: **General overview of the CRISPRi-based therapy.** **1.** Oral administration of a probiotic bacterium (blue) engineered with a CRISPRi circuitry programmed to target MDR pathogens. **2.** Once the site of infection (intestine) is reached, the probiotic can deliver the synthetic circuit to target bacteria (yellow) via conjugation. **3.** Trascriptional inhibition of resistance genes disarms the cell from its ability to survive antibiotic exposure (green), whose final administration is necessary to eradicate the bacterial infection.

Chapter 2

CRISPRi platform circuitry [1]

Compared with other genetic tool that carry out gene repression, a major advantage of CRISPRi technology is the easy "programmability" of sgRNAs to tune the repression of any gene of interest. In the global crisis imposed by AMR, CRISPRi can be thus repurposed to target resistance genes in a silenced and effective manner. In this chapter, the characterization of CRISPRi repression efficiency was first addressed by evaluating the performances of a CRISPRi-based synthetic platform programmed to target the *rfp* reporter gene. This circuitry was designed and quantitatively characterized in order to evaluate the repression capability and to investigate if an optimal balance between efficiency and metabolic load could be found. The modules composing the CRISPRi circuitry are described in order to provide essential information about: the model circuit architecture used in this study, the regulatory parts exploited to implement constitutive and inducible devices and the main features derived from the *in-vivo* characterization of the CRISPRi platform. In particular, the two main configurations in which the circuitry was tested are described by detailing the biological parts composing each module responsible for the constitutive or inducible expression of both sgRNA and dCas9 protein (Section 2.1.1). Starting from these two configurations, the performances of all the circuits characterized are discussed with a particular focus on their repression efficiency and burden properties (Section 2.2.1). After finding a proper dCas9 expression level to successfully balance repression efficiency and cell load, the developed genetic platform was applied to different case studies to demonstrate its flexibility. Such case studies included the fixing of synthetic circuits carrying out information processing tasks including a NOT gate with a too high repression strength (Section

[1] The content of this chapter is published in the article "CRISPR interference modules as low-burden logic inverters in synthetic circuits" [75].

2.2.2), a transcriptional cascade with high resource-consuming components, or a NOT gate to be re-designed to add more inputs, thus generating a NOR gate (Section 2.2.3). The tunability of the platform was addressed by modifying sgRNA sequences, thus providing not only a genetic tool to be customized for the desired application, but also approaches to guarantee its fine tuning.

2.1 *In-vivo characterization*

2.1.1 Circuit design

The model architecture of the circuits analysed in this chapter is described in Figure 2.1. All circuits relied on four gene cassettes for the expression of dCas9, sgRNA, RFP and GFP. These modules were interconnected in order to obtain and characterize two different configurations for the CRISPRi platform, both composed of two plasmids (Figure 2.2). The circuit architecture resembled the structure of logic NOT gate in which an input-controlled gene inverted the detectable circuit output, in this case RFP signal.

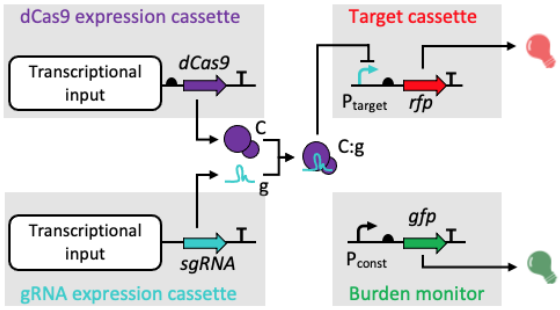

Figure 2.1: **Model architecture of the CRISPRi platform circuitry.** The CRISPRi platform is made of four gene cassettes for the expression of dCas9, sgRNA, RFP and GFP. Straight arrows represent protein-coding genes or sgRNA, curved arrows represent promoters, half ovals represent ribosome binding sites, and T shapes represent transcriptional terminators. Thin truncated arrows represent repression, while red and green bulbs indicate fluorescent outputs. The C, g and C:g symbols correspond to the dCas9 protein, sgRNA molecule and their complex, respectively. Generic transcriptional inputs are shown for the dCas9 and sgRNA cassettes, which may be provided by constitutive or inducible promoters. P_{const} is the J23100 promoter which drives the constitutive expression of GFP in the cell load monitor cassette, and P_{target} is the P_{LtetO1} or P_{LlacO1} promoter.

The first configuration included (Figure 2.2 A): a high copy vector bearing the target cassette under the control of the P_{LtetO1} or P_{LlacO1} promoter; a low copy plasmid with an HSL-inducible dCas9 module and a constitutive sgRNA cassette driven by one of three different promoters (J23116, J23100 or J23119, ordered from the weakest to the strongest one) which transcribed gPet or gPlac sgRNA. In the HSL-inducible cassette, the expression of dCas9 was placed under P_{Lux-3A} promoter, which is the wild-type

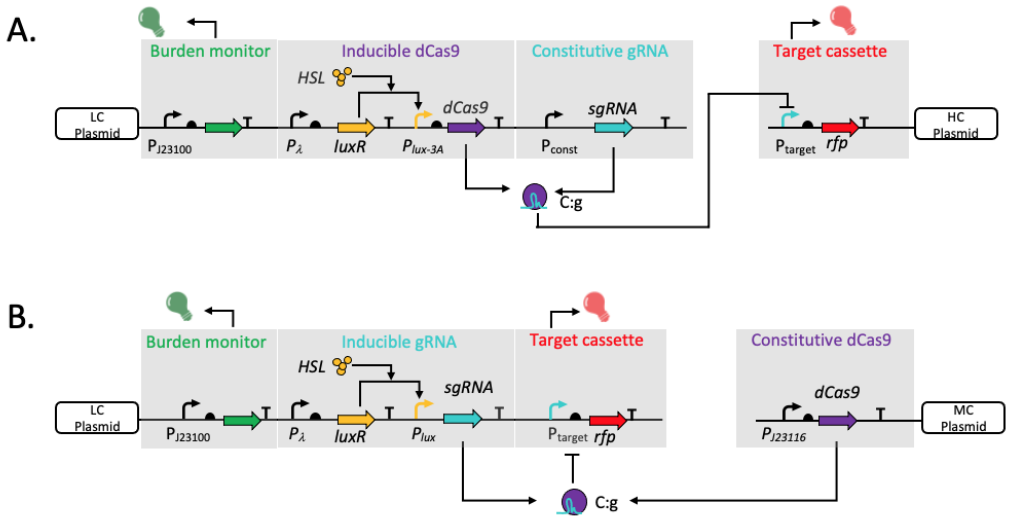

Figure 2.2: **CRISPRi platform: two different configurations.** The CRISPRi platform comprises four gene cassettes for the expression of dCas9, sgRNA, RFP and GFP. Two main configurations are obtained upon the interconnection of these modules. **A.** In the first configuration a low copy plasmid bears an inducible-dCas9 module driven by P_{Lux-3A} promoter and a constitutive sgRNA cassette transcribing gPtet or gPlac under the control of three different promoters of diverse strengths (indicated as P_{const}). The target cassette is placed on a high copy plasmid in which P_{LtetO1} or P_{LlacO1} (indicated as P_{target}) drives the expression of the *rfp* gene. **B.** In the second configuration, a constitutive dCas9 cassette is placed in a medium copy plasmid under P_{J23116} promoter, while a low copy plasmid bears the target cassette downstream P_{LtetO1} (indicated as P_{target}) and an HSL-inducible gRNA cassette transcribing gPtet downstream the wild-type P_{Lux} promoter. In each inducible module, luxR is constitutively expressed and the activation of P_{Lux} is regulated by the binding of LuxR:HSL active complex. A GFP expression module (burden monitor) driven by a constitutive promoter is also present in low copy plasmid to monitor cell load. The C, g and C:g symbols correspond to the dCas9 protein, sgRNA molecule and their complex, respectively. Colored bulbs indicate green or red fluorescence outputs. Curved thin arrows represent promoters, half ovals represent RBSs, colored arrows represent coding sequences or sgRNA as indicated, truncated arrows represent transcriptional repression and also transcriptional terminators downstream of coding sequences or sgRNAs.

P_{lux} promoter (BBa_R0062) without the last three adenine nucleotides that are downstream of the transcription start site of the original sequence. The second configuration (Figure 2.2 B), with an opposite structure, included: a medium copy plasmid bearing the dCas9 module under the control of a constitutive promoter (J23116 from the Anderson collection [76]) coupled with the strong RBS BBa_B0034; a low copy vector including both the target cassette downstream P_{LtetO1} and an HSL-inducible sgRNA cassette driven by the wild-type P_{Lux} promoter which transcribed gPtet. In both configurations, the HSL-inducible block, placed in low-copy plasmid, was composed of: luxR downstream the constitutive P_R promoter with RBS BBa_B0030; P_{Lux} promoter upstream RBS BBa_B0034 if followed by a gene cassette (Figure 2.2 A) or without RBS if followed by an sgRNA cassette (Figure 2.2 B). The target cassette, either assembled on high or low copy plasmid, was always constitutively expressed by the P_{LtetO1} or P_{LlacO1} promoter with RBS

BBa_B0034. The HSL-inducible device driving the expression of dCas9 or sgRNAs was properly selected not to interfere with the regulation of RFP. Finally, a GFP expression cassette was also included in each circuit, assembled in the low-copy vector, as a proxy of cell load. The complete list of all the biological parts used to assemble the circuits obtained in this study is reported Appendix A.2 and Table A.3, while all the final synthetic constructs are listed in Table A.4.

2.1.2 Circuit characterization

Fluorescence and absorbance of recombinant strains were measured over time in a microplate reader as previously described in [77]. Briefly, bacteria from a glycerol stock were streaked on a selective LB agar plate. After an overnight incubation at 37°C, 0.5 ml of selective M9 supplemented medium was inoculated with a single colony in 2−ml tubes. After a 21-h incubation at 37°C, 220rpm in an orbital shaker, cultures were 100-fold diluted in $200\mu l$ in a 96-well microplate. Two microliters of HSL were added when required to reach the desired final inducers concentration. Cultures were not placed in the external wells of the plate to avoid intensive evaporation. The microplate was incubated with lid in the Infinite F200Pro reader (Tecan) programmed with the $i-control^{TM}$ software to perform a kinetic cycle as follows: 15s linear shaking (3 mm amplitude), 5s wait, absorbance (600 nm) measurement, fluorescence measurements (gain 50 or 80), 5-min sampling time. Red and green fluorescence signals by RFP and GFP were measured with the 535/620 and 485/540 nm filter pairs, respectively. Control wells were also included, as described in the following Data Processing section 2.1.3, to measure the background signals of absorbance and fluorescence, and to provide internal control references for relative activity calculations. At least three biological replicates, starting from different colonies, were assayed for each strain.

2.1.3 Data processing

Data analysis and graphs were carried out via GraphPad Prism 8.0.1, Microsoft Excel and Matlab R2017b (MathWorks, Natick, MA). Raw absorbance and red fluorescence time series acquired from microplate experiments were background-subtracted as reported in [77] to obtain OD_{600} and RFP time series, proportional to the per-well cell density and fluorescent protein number. Sterile medium and a non-fluorescent TOP10 culture were used to measure absorbance and red fluorescence background, respectively. Since a significant cell density-dependent and growth rate-dependent autofluorescence was previously reported for GFP measurements with the adopted

experimental setup [77], green fluorescence was background-subtracted via a different procedure:

$$GFP_{auto}(t) = e^{q+m \cdot OD_{600}(t)} \tag{2.1}$$

in which OD600 is the cell density of the culture, and m and q describe the linear relation between $\ln(OD_{600})$ and GFP autofluorescence level. The m and q coefficients are growth rate (μ)-dependent parameters. This curve was used to estimate the green fluorescence background of a target culture, given its OD_{600} at each time point. The GFP_{auto}value was subtracted from the raw fluorescence of the target culture to obtain a signal proportional to the GFP level in the whole culture. Growth rate was estimated with the following procedure: OD_{600} values relatives to the exponential phase were selected within the $0.05 < OD_{600} < 0.18$ window; through the linear regression fitting of $\ln(OD_{600})$ values selected, the growth rate (μ) was obtained as the slope of the curve.

The fluorescence outputs of recombinant strains from microplate experiments were selected over time in the exponential growth phase ($0.05 < OD600 < 0.18$). These values were computed in terms of steady-state RFP and GFP synthesis rates per cell ($S_{cell\ RFP}$, and $S_{cell\ GFP}$ in arbitrary units per cell per time unit), expressing the output of synthetic circuits and the cellular capacity indicating the load of the circuit ([78]). The outputs were computed as:

$$S(t) = \frac{dF(t)}{dt} \cdot \frac{1}{OD_{600}} \tag{2.2}$$

$$S_{cell} = \frac{S_{ave}}{S_{ave,ref}} \tag{2.3}$$

where F(t) is the background-subtracted fluorescence time series of RFP or GFP and S_{ave} is the average of S(t) over the exponential phase. To normalize the obtained values, $S_{cell\ RFP}$ or $S_{cell\ GFP}$ were divided by the average S_{cell} of a reference strain ($S_{ave,ref}$) constitutively expressing RFP or GFP under the BBa_J23101 promoter. Reference strains for RFP and GFP have the BBa_J107029 and BBa_K173001 expression cassettes, respectively.

2.2 CRISPRi to engineer low burden and tunable synthetic circuits

2.2.1 Constitutive and inducible dCas9 or sgRNA expression systems

CRISPR interference technology is a key resource for the design of synthetic circuits encoding for complex and even finely regulated genetic programs. To this aim, rationally designed CRISPRi modules can be implemented in genetic circuits suitable for the expression in a desired host. However, the design process of a gene expression platform must take into account the influence of context-dependent sources that could affect the predictability of the desired host organism behaviour. In this regard, one of the major unpredictability sources is cell burden, the unnatural metabolic load caused by the expression of heterologous genes in host cells. This is mainly caused by the limitation of translational resources [78, 79] which may decrease upon expression of multiple, or even single, transcriptional regulators-encoding genes [77]. Compared with the traditionally adopted transcriptional regulator proteins, which could represent a source of cell load, CRISPRi modules have a substantial advantage: as sgRNAs are only transcribed and the only actors that undergo translation are dCas9 and the target genes, a depletion in translational resources is expected non to be observed in the CRISPRi case.

Based on these concepts, the CRISPRi circuitry must be designed to act not only as an efficient transcriptional repressor of targeted genes but also as a low burden device able to avoid the metabolic load that could affect the predictable function of the synthetic circuit. A CRISPRi platform able to meet these two main features was obtained upon the interconnection of the functional modules described below and represented in Figure 2.1:

- dCas9 expression cassette responsible for the synthesis of the protein under the control of a constitutive promoter, if present in medium copy plasmid, or inducible device, if cloned in low copy vector;
- sgRNA expression cassette in which the transcription of the chimeric guide RNA was driven either by an inducible or constitutive promoter in a low copy plasmid;
- constitutive target expression cassette encoding for the RFP reporter gene placed downstream the target promoter in low or high copy vector;
- constitutive GFP expression cassette in low copy plasmid (Burden monitor).

In the system described above, the expression of dCas9 and sgRNA cassettes led to the formation of a functional interference complex able to repress the transcription of the reporter gene by sterically hindering the recruitment of RNA polymerase to the target promoter. In particular, each sgRNA was *ad hoc* designed to inhibit the transcriptional activity of a target promoter cloned upstream of the *rfp* reporter gene encoding for a fluorescent protein. This way, RFP signal was used as an indicator of the CRISPRi repression efficiency, while growth rate and GFP were adopted to quantify cell load, since the GFP level was expected to decrease as a function of the metabolic load derived from the expression of heterologous gene within the host cell. Two configurations of the above mentioned CRISPRi platform were characterized in order to investigate the repression efficiency and the low burden property. The circuit scheme of these two configurations is reported in Figure 2.2. The architecture of the first combination of circuits characterized in this study (described in Figure 2.2 A) includes an inducible dCas9 cassette in a low-copy plasmid and a constitutive sgRNA cassette. The inducible system adopted for the expression of dCas9 relied on the Lux circuitry. That consists of the P_{Lux} promoter and the LuxR protein, which acts as a transcriptional activator of the cognate promoter in presence of N-(3-oxohexanoyl)-L-homoserine lactone (HSL). The LuxR-HSL active complex binds the lux box of the P_{Lux} promoter, thereby activating the transcription of the downstream gene, which is then translatd into protein. As dCas9 cassette was placed under P_{Lux}, the presence of HSL was required to trigger the transcription of the protein. In this study, a previously optimized variant of the P_{Lux} promoter was employed. The new version of the promoter, referred to as P_{Lux-3A}, was obtained by removing the three adenine nucleotides after the transcription start site (TSS) of the original P_{Lux} sequence. This modification made the toxicity of the HSL-inducible dCas9 circuit negligible at high inducer level and allowed to investigate the effects of dCas9 over a wide range of values without significant cell load or toxicity. On the other hand, the constitutive transcription of two sgRNA called gPtet and gPlac was driven by weak (J23116), medium (J23100) or strong (J23119) promoter. The two gRNAs were designed to target the P_{LtetO1} or P_{LlacO1} promoter (BBa_R0062 and BBa_R0011 from the Registry of Standard Biological Parts) that drive the expression of the *rfp* reporter gene in a high-copy plasmid. A set of six circuits with the described architecture was finally obtained and called AE$_{\text{-3A}}$d_J116/J100/J119 gPtet or gPlac. Control strains were included for each target promoter and had a non-specific sgRNA transcribed by the J23100 medium-strength promoter, i.e., gPtet for P_{LlacO1} and gPlac for P_{LtetO1} (see Appendix A.2 for the Cloning protocols and Table A.4 for the complete list of constructs). Thanks to the orthogonality of the two sgRNA binding sites, the RFP output was expected

to be unaffected in the absence of a complementary sgRNA. This first configuration enabled the study of dCas9 level-dependent repression of target genes, in presence of sgRNAs at three different expression levels. The results reported in Figure 2.3 showed that the configuration tested, which was indicated as "sgRNA in low-copy and target in high-copy", had a high level of tunability. In specific, although none of the tested circuits reached the same RFP level of their respective controls at zero induction, RFP expression was high for HSL concentrations up to 0.1 nM and reached a repressed state for HSL values of 1 nM. Qualitatively, the same trends were observed for both gPtet and gPlac. The control strains with non-specific guides were not affected by HSL and exhibited a high RFP expression, as expected. Growth rate and GFP showed a slight decrease only for high dCas9 expression levels, while no sgRNA expression-dependent burden was observed. Moreover, GFP showed an expression peak at 1 nM of HSL, corresponding to a situation in which RFP expression is low and dCas9 expression is not toxic. In other words, this observation demonstrated that, under a certain dCas9 induction, an active CRISPRi complex could alleviate the metabolic load caused by the expression of an heterologus gene. Indeed, systematically lower GFP level was observed for the controls compared with their respective circuits in the same conditions with specific guides, most probably due to the higher load caused by RFP expression.

Taken together, the results showed that none of the six tested circuits exhibited cell load as a function of sgRNA expression strength and the repression capability was extremely high for all the circuits, starting from the 1 nM inducer concentration. These results were significant not only because they demonstrated that dCas9, a potential source of cell load, could be placed under an inducible system to obtain an optimal expression level with minimal burden, but also because they revealed that the expression of the dCas9:gRNA complex even from a low-copy plasmid could be sufficient to successfully inhibit the transcription of a gene harboured by a high copy plasmid. This is a relevant aspect to be considered in the design of synthetic circuit reprogrammed to target genes placed on high copy vectors.

The second combination of circuits herein presented and described in Figure 2.2 B included a constitutive dCas9 cassette coupled with and inducible sgRNA module. The design of these model systems resembled the structure of actual logic inverters in which the gene expressed in an input-dependent fashion is the sgRNA. In these circuits, the expression of dCas9 was entrusted to a constitutive minimal burden gene cassette, constructed and validated in a previous work [80], in which the J23116 promoter was chosen to drive the dCas9 gene in a medium-copy vector. The wild-type P_{Lux} promoter was instead used in the HSL-inducible sgRNA cassette to drive

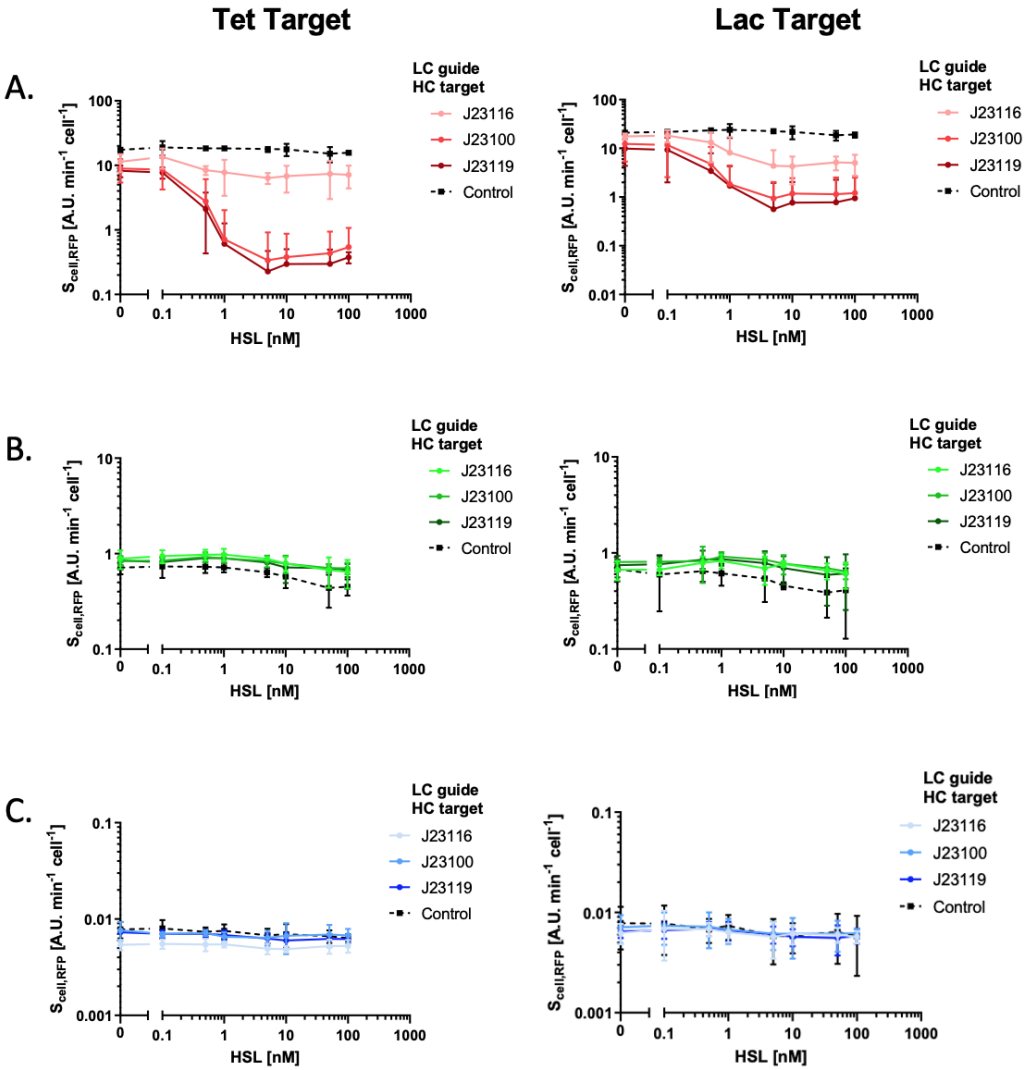

Figure 2.3: **Characterization of a CRISPRi circuitry with inducible dCas9 and constitutive sgRNA** The configuration of the CRISPRi circuitry includes an HSL-inducible dCas9 and a constitutive sgRNA cassette under the control of three constitutive promoters of diverse strengths (weak, medium and strong for J23116, J23100 and J23119, respectively). Two different targeting systems (Tet and Lac) are reported: gPtet and gPlac, which repress the P_{LtetO1} and P_{LlacO1} promoters, respectively, that drive RFP in a high copy plasmid. Each graph includes four curves: three of them correspond to circuits with the sgRNA under the control of one constitutive promoter and the fourth curve corresponds to a non-specific targeting control in which the medium-strength J23100 promoter constitutively transcribes a non-targeting sgRNA: gPlac and gPtet for the P_{LtetO1} and P_{LlacO1} promoters in the Tet and Lac systems, respectively. Characterization in terms of **A.** RFP, **B.** GFP and **C.** growth rate output of the six circuits and the respective controls consistent with the configuration described. In all the graphs, x-axis indicates HSL concentration [nM], while in y-axis data are shown as the average RFP or GFP synthesis rate per cell or average growth rate value. Data points represent the average value and error bars represent the standard errors of the mean of at least 3 independent experiments.

the transcription of the guide gPtet targeting the P_{LtetO1} promoter that expressed RFP; both sgRNA and target cassettes were cloned in the same

low-copy plasmid downstream the burden monitor and the resulted circuit was named AEgPtet_PtetRFP. A similar circuit, called X1T and including TetR instead of the sgRNA, was used for comparison in order to demonstrate that CRISPRi platform can also provide a low-burden alternative to the traditionally adopted transcriptional regulators. Indeed, in [77], it was demonstrated that the expression of TetR in X1T preserved the designed logic function of the synthetic circuit but also resulted in a high translational demand which generated a relevant cell load detected through the burden monitor. The obtained input-output data for this example of sgRNA-based logic inverter and the relative control circuit are shown in Figure 2.4.

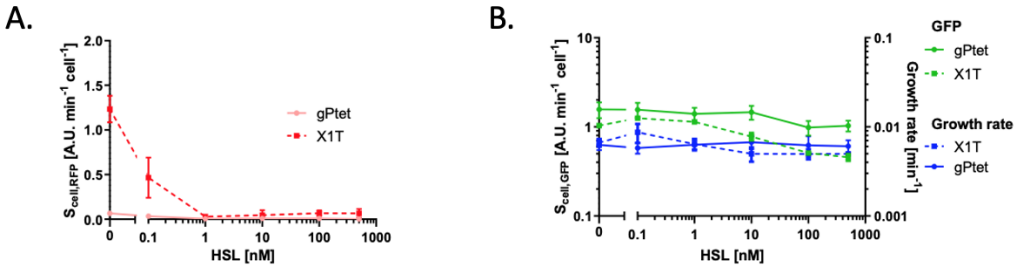

Figure 2.4: **Comparison between TetR-based and CRISPRi-based NOT gate.** The configuration of the CRISPRi-based NOT gate includes a constitutive dCas9 cassette and an HSL-inducible sgRNA module targeting the P_{LtetO1} promoter upstream *rfp* gene. The input-controlled guide is gPtet, with a perfect-matched sequence. X1T circuit has the same topology of the CRISPRi-based NOT gate with TetR repressor instead of gPtet. Characterization in terms of **A.** RFP, **B.** GFP and growth rate output. In all the graphs, x-axis indicates HSL concentration [nM], while in y-axis data are shown as the average RFP or GFP synthesis rate per cell or average growth rate value. Data points represent the average value and error bars represent the standard errors of the mean of at least 3 independent experiments.

As demonstrated by the RFP output, the expression of the reporter protein in the CRISPRi-based NOT gate (simply identified as "gPtet") was close to the maximum level of repression already at null inducer concentration, while the respective control circuit bearing the TetR repressor showed a gradual decrease in RFP value in response to HSL increase. Therefore, these data confirmed the repression capability of the CRISPRi circuitry but also revealed that the repression efficiency was too high for low copy targets due to the leakiness in the synthesis of the sgRNA. These findings were consistent with the results derived by the characterization of a previously obtained collection of circuits with same topology and target cassette cloned either on medium or high-copy plasmid [80]. Again, in these circuits, the repression efficiency was too high for medium-copy targets, while a wide repression range was observed with high copy plasmid bearing the target cassette, demonstrating that the output range was highly dependent on the target copy number. On the other hand, GFP and growth rate data (Figure 2.4) confirmed the suc-

cessful replacement of the resource consuming transcriptional regulator TetR with the CRISPRi circuitry. In fact, if the sgRNA transcription caused no relevant burden, the expression of the TetR-based NOT gate resulted in a decrease of GFP level, confirming the effect on depletion in cellular resources caused by TetR expression.

The two configurations of circuits characterized, obtained upon the interconnection of constitutive and inducible dCas9 or sgRNA expression cassettes, resulted to be efficient in the repression of *rfp* gene without causing a relevant load to the cells. However, the repression efficiency of the second configuration described, based on constitutive dCas9 and inducible sgRNA cassette, was too high for low copy targets, demonstrating that the CRISPRi platform needed to be tuned in order to widen its repression range.

2.2.2 Approaches to improve CRISPRi tunability

The CRISPRi platform described in Section 2.2.1 revealed a great potential to be used as an effective transcriptional repressor with low metabolic load. However, in case of low-copy targets, the repression capability of the device must be optimized in order to widen the induction range and achieve a fine-tuning of the high repression strength. To address the tunability of the CRISPRi module, an approach based on modifications of the perfectly matching gRNA sequence was exploited. Indeed, it was previously reported that alterations in the annealing region of the sgRNA have the potential to affect the binding affinity between the repressor complex and target sequence and, consequently, decrease the repression strength [42, 43, 81, 82, 83]. To evaluate if this strategy could effectively improve the output range of CRISPRi modules, the AEgPtet_PtetRFP (CRISPRi-based NOT-gate described in 2.2.1) circuit was used as a model system to investigate the effect on repression efficiency caused by different modifications in gPtet annealing sequence. Moreover, by comparing the RFP transfer function of the new collection of modified circuits with the one of X1T, we evaluated if the tuning of the CRISPRi module could also resemble the input-output RFP behaviour shown by TetR. To this aim, a library of sgRNA with non-canonical sequence was created: through a mutagenic PCR of the template plasmid AEgPtet_PtetRFP, the original gPtet guide was engineered by combining primers RV Plux (-3A), RV Plux AAA and FWgPtet with the desired mutated sequence. This way, RNA guides with truncated sequence were obtained along with sgRNA harbouring two mismatches in the base-paring region (see Appendix A.2.2 for the Mutagenesis protocol adopted and Table A.2 for the list of primer used in this study). In specific, five variants of gPtet were constructed by deleting nucleotides at its 5' end. The resulting guides, with the truncation of 4, 7,

10, 11, 15 nucleotides were tested but, as reported in Figure 2.5, the resulting NOT gates did not show the desired tuning of the repression efficiency, due to a too low output range or too high basic activity. Interestingly, the expression of the 11-nt deleted gPtet was not tolerated by cells, which stopped growth upon HSL addition at concentrations higher than 0.1 nM. The toxicity of specific guides has already been reported, although this variant did not include any of the reported toxicity-related features [84].

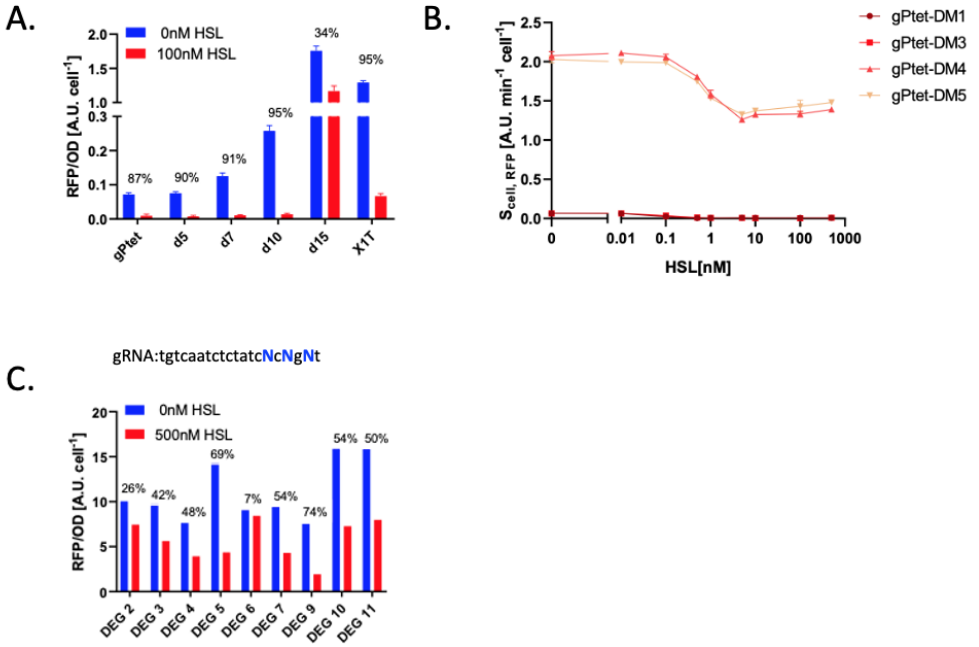

Figure 2.5: **Library of gPtet variants with truncated or mismatched sequences.** gPtet variants obtained through a mutagenic PCR of the original perfectly matching guide. **A.** sgRNAs with truncations and their effect on the HSL-inducible sgRNA circuit with constitutive dCas9 in MC and target in LC. All of them are transcribed with the three adenines present in the wild-type P_{Lux} promoter. The number of deleted nucleotides at the 5' end of the guide is reported and the bars show the RFP output in the no induction and full induction conditions. **B** Characterization in terms of RFP output of four gPtet variants with rationally designed mismatches. In the graph, x-axis indicates HSL concentration [nM], while in y-axis data are shown as the average RFP synthesis rate per cell. **C.** Screening of nine degenerate gPtet guide variants without inducer or with 500 nM of HSL. The output is expressed as RFP/OD600. Data points and bars represent the average value, and error bars represent the standard errors of the mean of at least 3 independent experiments. The numbers above the bars indicate the percent repression.

Since deletions failed to provide an sgRNA candidate with the desired affinity, the mismatch-based strategy was explored to design four new sgRNA candidates ($gPtet_{DM1,\ DM3,\ DM4,\ DM5}$). To achieve a gradual decrease in repression efficiency, two mismatched nucleotides were introduced from the 5' to the 3' end of the sgRNA that is the region most sensitive to sequence modification because of its proximity to PAM. The rational design of internal mismatches was also supported by the use of a free-energy based model able

to predict the decrease in binding strength for each mutagenized sgRNA[2]. Unfortunately, sgRNA with rationally designed mismatches did not exhibit the desired transfer function of XIT because, as described in Figure 2.5, the binding affinity was irreversibly altered by the mismatches ($gPtet_{DM4,\ DM5}$) or because the repression efficiency was still too high ($gPtet_{DM1,\ DM3}$). Being unable to generate a proper diversity in repression affinity, to reach the desired repression range with a rational approach we created and screened a library of randomly mutagenized sgRNAs. Again, AEgPtet_PtetRFP was used as template plasmid in a mutagenic PCR perfomed with RV Plux AAA and FWgPtet_degenerate; the latter was a mix of primers containing different substitutions of three bases along its sequence (Figure 2.5 C). Based on these degenerate primers, a screening test was performed in order to obtain 20-nt gPtet variants with mismatches in three specific positions of the annealing sequence (see Figure 2.5 C and Appendix A.2.2 for the Mutagenesis protocol). The screening included the per-cell measurement of RFP of several strains bearing the NOT gate with mismatched gPtet variants, among which the one with the high output range and low basic activity trade-off, named $gPtet_{DEG9}$, was selected and sequenced. Its sequence was tgtcaatctctatc**g**c**gg****a**t, in which the degenerate nucleotides are written in bold type. When tested at different HSL concentrations, the circuit with $gPtet_{DEG9}$ showed a transfer function that resembled the target one of X1T, as reported in Figure 2.6 A. Moreover, by comparing growth rate and GFP outputs of $gPtet_{DEG9}$ and X1T, the sgRNA-based NOT gate confirmed low cell load for any input value, Figure 2.6 B.

All data reported for truncated and mismatched gPtet variants were relative to guides downstream of the wild-type P_{Lux} promoter, thus including the three adenines in the transcribed region of the sgRNA. To demonstrate that the removal of these three nucleotides did not result in relevant changes in the $gPtet_{DEG9}$ transfer function, an identical circuit with the P_{Lux-3A} promoter was constructed according to the protocol described in Appendix A.2.2; as shown in Figure 2.7, a 3-mismatching nucleotide extension did not significantly alter guide affinity and also confirmed that the P_{Lux} transcriptional activity is not affected by this modification.

The results described in this section demonstrated that the repression range of the CRISPRi device can be widen by altering the 20-nt targeting sequence of the sgRNA. Although the approach based on truncated or rationally mutagenized gPtet variants failed in this case study, the same strategies

[2]The choice of point mutations in specific sites of the sgRNA annealing region was supported by the use of a python script based on [58], kindly provided by Prof. H.M. Salis (Penn State University). The tool was used to predict the relative decrease in binding strength of altered sgRNAs compared with a perfectly matching 20-nt guide.

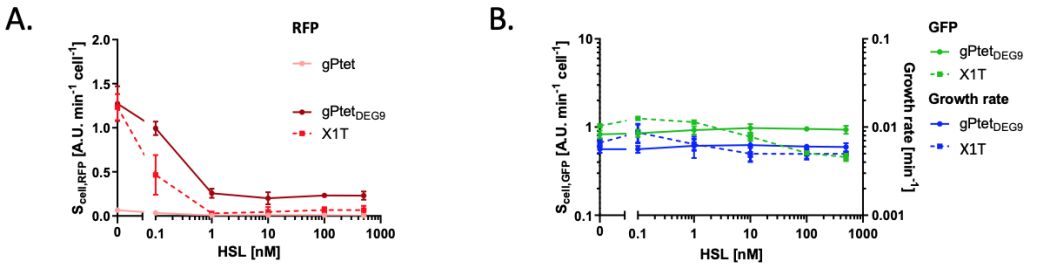

Figure 2.6: **Comparison between TetR-based and CRISPRi-based NOT gate with original or mismatched sgRNA.** The configuration of the CRISPRi-based NOT gate includes a constitutive dCas9 cassette and an HSL-inducible sgRNA module targeting the P_{LtetO1} promoter upstream *rfp* gene. The input-controlled guide can be gPtet, with a perfect-matched sequence, or $\text{gPtet}_{\text{DEG9}}$, with two mismatches in the annealing region. X1T circuit has the same topology of the CRISPRi-based NOT gate with TetR repressor instead of gPtet. **A.** Characterization in terms of RFP output of the three NOT gates with gPtet, $\text{gPtet}_{\text{DEG9}}$ and TetR. **B.** Characterization in terms of GFP and growth rate output of $\text{gPtet}_{\text{DEG9}}$ and X1T. In all the graphs, x-axis indicates HSL concentration [nM], while in y-axis data are shown as the average RFP or GFP synthesis rate per cell or average growth rate value. Data points represent the average value and error bars represent the standard errors of the mean of at least 3 independent experiments.

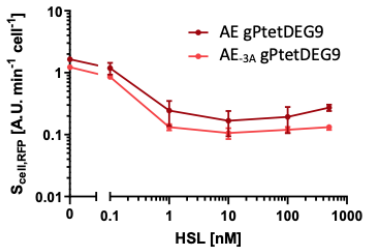

Figure 2.7: **Comparison between the $\text{gPtet}_{\text{DEG9}}$ variant when expressed by the wild-type P_{Lux} and the modified P_{Lux-3A} promoters.** The configuration of the CRISPRi-based NOT gate includes a constitutive dCas9 cassette and an HSL-inducible sgRNA module targeting the P_{LtetO1} promoter upstream *rfp* gene. The input-controlled guide is $\text{gPtet}_{\text{DEG9}}$ under the wilde-type P_{Lux} or the modified P_{Lux-3A} promoter ($\text{AEgPtet}_{\text{DEG9}}$_PtetRFP and $\text{AE}_{\text{-3A}}\text{gPtet}_{\text{DEG9}}$_PtetRFP circuits, respectively). Characterization in terms of RFP output of the two circuits. In the graph, x-axis indicates HSL concentration [nM], while in y-axis data are shown as the average RFP synthesis rate per cell. Data points represent the average value and error bars represent the standard errors of the mean of at least 3 independent experiments.

gave promising results in the tuning of sgRNA affinity for a previously obtained collection of guide RNA targeting the P_{LuxH} promoter in a medium copy plasmid [75]. Here, to adjust the high repression strength of gPtet, only the screening of a library of sgRNA harbouring random mismatches provided the best performing guide $\text{gPtet}_{\text{DEG9}}$, able to resemble the desired input-output behaviour of the X1T circuit expressing TetR.

These findings demonstrate that reliable design rules for sgRNAs with the desired repression efficiency must take into account different factors such as nucleotide composition and target copy number. Moreover, while truncated guides are easy to design and require a limited range of constructs to test their

efficiency, the correct prediction of the mismatches identity or site specificity, as well as the the higher number of plasmids to be screened to find a candidate with desired properties, are still major hurdles to overcome for the mismatch-based approach.

2.2.3 Application of tunable CRISPRi to fix a non-functional transcriptional cascade

The architecture of the gene expression platform herein developed (Figure 2.1), the possibility to tune the CRISPRi repression efficiency and the low burden properties of the CRISPRi modules (Section 2.2.1) are useful features that can be together employed to build synthetic circuits able to carry out sophisticated functions. To prove the usefulness of the developed platform, the $gPtet_{DEG9}$-based NOT gate was used to fix the behaviour of a non-functional synthetic circuit from a collection of previously published transcriptional cascades [77]. As anticipated in Section 2.2.1, the cell load caused by the expression of heterologous proteins can affect, and even break, the function of a synthetic circuit [77, 85]. In the above mentioned transcriptional cascade, the main responsible of cell load was TetR protein when expressed at high levels. The considered cascade, assembled in low-copy vector, was named X1TL and included an HSL-inducible device upstream of a TetR- and LacI-based NOT gates with RFP as circuit output. The circuit scheme of the cascade is represented in Figure 2.8. Instead of showing a monotonically increasing HSL-dependent output, expected from the transfer function logic of the individual inverter blocks, the circuit exhibited an increasing and then decreasing RFP output (Figure 2.8 B). In the same work [77], TetR expression was confirmed as the main responsible for the unpredicatble behaviour observed by obtaining a variant of the circuit with a weaker RBS; the modified circuit showed a functional output, increasing with HSL. As an alternative to RBS variations, which do not guarantee the desired input-output transfer function, an sgRNA-based NOT gate could be used to replace the TetR expression cassette in the broken cascade. This approach was expected to fix the device without causing any input-dependent expression of resource-consuming components, while maintaining the desired input-output behaviour. Considering that $gPtet_{DEG9}$ successfully resembled the RFP output exhibited by TetR in X1T circuit, which represented a single-stage NOT gate of the complete cascade, the final circuit was constructed by including an HSL-inducible $gPtet_{DEG9}$ cassette instead of TetR expression module. The scheme of the sgRNA-based cascade is reported in Figure 2.8 A. As shown in Figure 2.8 B, the new low-burden cascade (indicated as "CRISPRi") had an

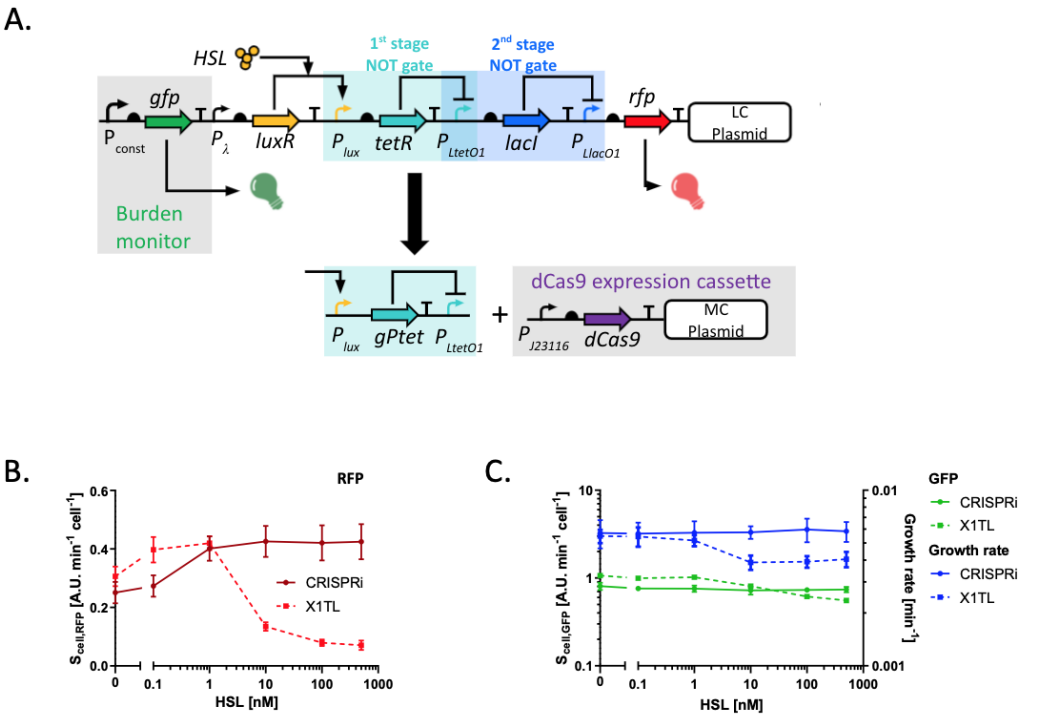

Figure 2.8: **Fixing of a non-functional transcriptional cascade.** **A.** Architecture of the non-functional cascade, including the LuxR, TetR and LacI regulators; it has HSL as input and RFP as output, and the main source of failure was the high resource usage of the TetR module, highlighted in light blue and indicated as the 1st stage NOT gate. This module has been replaced with gPtet$_{DEG9}$-based expression cassette, including the parts illustrated below the black arrow, and the obtained circuit was named Final Cascade (in the graph: CRISPRi). **B.** Characterization, in terms of RFP output, of the full transcriptional cascades: X1TL represents the original circuit for which an unexpected non-monotonically increasing HSL-dependent output was reported, and CRISPRi represents the fixed cascade with the gPtetDEG9 as repressor of the P$_{LtetO1}$ promoter. **C.** GFP and growth rate values for the same strains illustrated in graph B. In all the graphs, x-axis indicates HSL concentration [nM], while in y-axis data are shown as the average RFP or GFP synthesis rate per cell or average growth rate value. Data points represent the average value and error bars represent the standard errors of the mean of at least 3 independent experiments

about 2-fold output range and showed the expected monotonically increasing HSL-dependent output. As expected, GFP was essentially independent from HSL, demonstrating that sgRNA expression caused no relevant burden (Figure 2.8 C). On the other hand, the original circuit showed a GFP decrease for high HSL values, which corresponded to high TetR expression levels. Despite the sgRNA-based cascade exhibited no HSL-dependent GFP or growth rate decrease, its GFP value obtained in the no-HSL condition was slightly lower than in the original cascade, suggesting that an additional load was present, most probably caused by multiple plasmids in the same strain, as previously observed in [86] and not by dCas9 expression itself. Such effect was not observed in growth rate measurements.

The results presented in this section demonstrate that by combining a

minimal burden constitutive dCas9 cassette, an inducible sgRNA expression module and the mismatch-based approach is possible to build a CRISPRi circuitry that can efficiently fix the broken quantitative behaviour of a complex synthetic circuit by preserving the predicted logic function and the low metabolic load property.

2.3 Main considerations on CRISPRi circuitry functional features

Engineered microorganisms able to carry out a designed function can be created by encoding a specific genetic program into a synthetic circuit suitable for the expression in the host cell. However, as the expression of heterologous genes may cause a metabolic load able to alter the function of the circuit itself, a gene expression platform can be considered efficient if it satisfies the functional specifications and also shows minimal burden properties. For this reason, as CRISPRi technology was chosen as an essential component of the herein presented gene expression platform, we first addressed the characterization of the CRISPRi mediated transcriptional repression of the *rfp* target gene as well as the effect on cell load. Two configurations of the CRISPRi circuitry were analysed. In the first one, the constitutive expression of the sgRNA cassette under three promoters with increasing strength was coupled with an inducible dCas9 expression module. In this configuration, the CRISPRi components and the target gene were expressed from low and high copy plasmid, respectively. Despite the different copy number of the two plasmids, the dCas9:sgRNA complex efficiently inhibited the expression of the high copy target without showing relevant cell burden. The second combination of circuits characterized had an inverted configuration as it included a constitutive dCas9 cassette in a medium-copy plasmid and an inducible sgRNA module in a low-copy plasmid. In this case, the CRISPRi device showed a highly sensitive on/off response with low copy plasmids holding the target gene, leading to a too high repression efficiency. To improve the tunability of the system, the possibility to regulate the sgRNAs repression strength was explored by modifying their original perfect matching sequence with deletions or mismatched nucleotides. While the intervention based on deletion failed to regulate the sgRNA affinity, the mismatch-based approach provided the sgRNA $gPtet_{DEG9}$ with the wider output range than the original guide. Moreover, compared with a control circuit expressing TetR repressor instead of an sgRNA cassette, the $gPtet_{DEG9}$-based NOT gate significantly alleviated the metabolic load caused by the high resource consuming tran-

scriptional regulator. Finally, the broken quantitative behaviour of a three-gene transcriptional cascade was fixed by replacing TetR with gPtet$_{\mathrm{DEG9}}$, that efficiently restored the logic function predicted for the synthetic circuit. Taken together, these results demonstrated that a tunable and low burden CRISPRi platform can be engineered in synthetic circuits with predictable functions and no relevant cell load. However, it is worth mentioning that the tunability of the system still requires a deep understanding of sequence-dependent effects. Indeed, although computational tools have been proposed to support the prediction of mismatch effects, a random screening approach was here necessary to find the sgRNA with the desired repression efficiency.

In conclusion, the results discussed in this chapter prove that the CRISPRi platform developed could be efficiently employed to address the research project herein presented. First of all, the CRISPRi circuitry includes functional modules to drive the constitutive or inducible expression of both dCas9 and sgRNA; second, the circuitry turned out to be a tunable and low burden device; third, the genetic platform was able to exert a strong repression efficiency that was sufficient for the full inhibition of target genes in high-copy plasmids; finally, thanks to these two main features, CRISPRi modules can also be adopted to construct even complex genetic circuits by preserving the designed function. Taken together, the attractive features mentioned for the developed CRISPRi platform are suitable for the engineering of antibiotic resistance repression devices and for the tuning of other biological processes for different applications.

Chapter 3

CRISPRi-mediated silencing of antibiotic resistance genes

The CRISPRi platform developed and characterized in this study showed great potential for the design of synthetic circuits with high repression capability of target genes. Based on these findings, the CRISPRi repressor complex was redirected towards resistance genes by reprogramming the genetic platform described in Section 2.1. In particular, taking advantage of the easy programmability of sgRNA, the CRISPRi circuitry was *ad hoc* designed to inhibit the expression of model and clinically relevant resistance genes. To this aim, a new set of synthetic circuits was characterized with two main genetic architectures: sgRNA Cassette and CRISPRi Array, both implemented with single or double gRNAs. This way, four different combinations of circuits were obtained: single or double sgRNA Cassettes and CRISPRi Array with one or two spacers. First, the synthetic circuitry exploited in this work is detailed along with the description of liquid and plate culture assays used to quantitatively characterize its performances (Section 3.1). The first feasibility evaluation of CRISPRi technology to act as a sequence-specific antimicrobial was addressed in a case study in which two model ARGs, *bla* and *tetA*, represented the CRISPRi targets. With this purpose, the previously characterized sgRNA Cassette architecture was reprogrammed to individually target the two resistances with customized gRNAs (Section 3.2.1). Subsequently, in order to explore the multi-targeting capability of the CRISPRi system, the architecture of double sgRNA Cassettes and CRISPRi Array were characterized in the transcriptional inhibition of the same model ARGs. The first one was constructed by combining two single sgRNA Cassettes, the second one was implemented in a synthetic architecture inspired by native CRISPR systems (Section 3.2.2). By leveraging an inducible device, the tuning of dCas9 expression level was then addressed to counteract the competition between

gRNAs, emerged from the characterization of the above mentioned genetic architectures (Section 3.2.3). Once the CRISPRi-mediated silencing of model ARGs was demonstrated, a new CRISPRi circuitry was implemented with a set of CRISPRi Arrays rationally designed to inhibit the expression of *NDM-1* and *mcr-1* genes, two examples of antibiotic resistances relevant in clinical settings (Section 3.3). The nature of escaper cells that survived the antibiotic treatment even in presence of an active CRISPRi circuitry was studied through liquid assays and sequencing analysis in order to properly investigate their phenotype and genotype (Section 3.4). Finally, the delivery of CRISPRi-encoding circuits in resistant bacteria was addressed by exploiting an HGT mechanism known as bacterial conjugation. In particular, a non-self-transmissible platform was developed to deliver a mobilizable CRISPRi Array targeting *bla* or *mcr-1* gene. The performances of this platform were characterized both in terms of *conjugation* and *killing efficiency*, two parameters that measured the frequency of the conjugative transfer and the CRISPRi repression capability of resistance genes, respectively (Section 3.5).

3.1 *In-vivo characterization*

3.1.1 Circuit design

The model architecture of the circuits characterized in this chapter included three main modules for the expression of gRNAs, dCas9 and target gene encoding for a specific antibiotic resistance (See Figure 3.1). The gRNA module was placed in low-copy plasmid under the IPTG-inducible P_{LlacO1} promoter. This module was characterized with two different architectures: sgRNA Cassette, implemented as single or double Cassettes, and CRISPRi Array, expressing single or double spacers. Single sgRNA cassettes transcribed only a gRNA targeting *bla* or *tetA* gene: in the first case, the sgRNA could be gAmpRpromoter, targeting P_{bla} promoter placed upstream *bla* gene, or gAmpRgene targeting the coding sequence of the same gene; in the second case, the sgRNA was gtetA targeting the coding sequence of *tetA* gene. A double sgRNA Cassette was obtained by cloning in tandem gAmpRpromter- and gtetA-based single Cassette within the same low copy plasmid. The gRNA encoded in each sgRNA Cassette was provided with its own tracrRNA and transcriptional terminator (BBa_J107201). The second architecture, named CRISPRi Array, resembled the topology of native CRISPR systems. An array composed of one or two spacers (30-nt) flanked by two repeat sequences (36-nt) was placed downstream the P_{LlacO1} promoter. At the end of each array, the transcriptional terminator BBa_1006

was cloned. CRISPRi Arrays with single and double spacers were employed to target *bla*, *tetA*, *NDM-1* and *mcr-1* genes. In case of CRISPRi Array with single spacer, the gRNA transcribed could be: gNDM1 or gNDM2 targeting two different positions within the coding sequence of *NDM-1* gene. In case of CRISPRi Array with double spacers, the gRNAs pairs could be: gAmpRpromoter and gtetA; gNDM1 and gNDM2; gNDM1 and gmcr-1 targeting the coding sequence of *NDM-1* and *mcr-1* genes, as indicated. The transcriptional activity of the P_{LlacO1} promoter, either placed upstream of sgRNA Cassettes and CRISPRi Array, was inhibited by the LacI repressor, which was constitutively expressed in the $lacI^q$ locus of the *E. coli* TOP10 F' strain, used as host for the characterization of these circuits. If present, the inducer molecule IPTG bound to the LacI protein and released the tetrameric repressor from the lac operator, allowing the transcription of genes placed under P_{LlacO1} promoter. The dCas9 expression cassette was either constitutive or inducible. The former was placed in a medium copy plasmid under the control of the constitutive promoter BBa_J23116 coupled with the strong RBS BBa_B0034. The latter was an HSL-inducible module placed under the control of P_{Lux-3A} in a low copy vector along with double sgRNA Cassettes or CRISPRi Array. The topology of this circuit was compliant to the one described in Section 2.1.1 and Figure 2.2 A. The target cassette, encoding for a specific antibiotic resistance gene, was placed in endogenous or recombinant plasmids, characterized by different copy numbers. In specific, the *bla* gene encoding for ampicillin resistance was under the control of the constitutive P_{bla} promoter in the high copy vector I13521 belonging to the class pSB1A2. The *tetA* gene, responsible for tetracycline resistance, was expressed by the tn10 transposon placed in the endogenous low copy F' plasmid. *NDM-1* and *mcr-1* genes, conferring resistance to meropenem and colistin, were expressed from two medium copy plasmids (pGDP1 NDM-1, Addgene n. #112883; pGDP2-mcr1, Addgene n. #118404) under the control of P_{bla} and P_{LlacO1} promoter, respectively [87].

The three expression modules described were characterized in two main configurations, as represented in Figure 3.1. The first configuration included three plasmids: a low copy vector bearing the IPTG-inducible gRNA module implemented as single/double sgRNA Cassettes or CRISPRi array; a medium copy plasmid carrying the dCas9 module; a low or high copy plasmid bearing the target cassette (*bla* or *tetA* gene). The second configuration included two plasmid: a low copy vector bearing the IPTG-inducible gRNA module implemented as double sgRNA Cassettes or CRISPRi array along with the HSL-inducible dCas9 module; a low, medium or high copy vector bearing the target cassette (*bla*, *tetA*, *NDM1* and *mcr-1* genes). In the first configuration, a functional CRISPRi complex was obtained upon addition of the

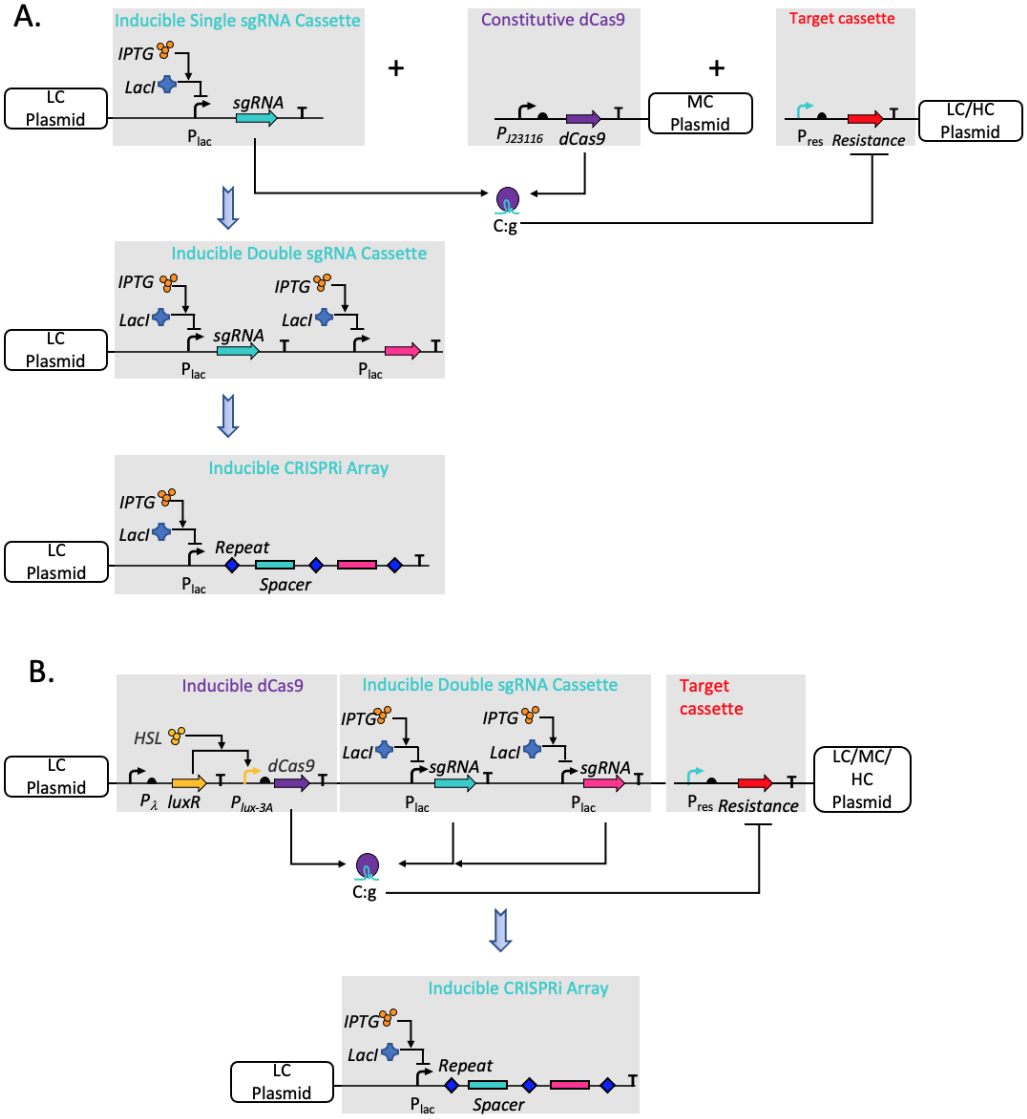

Figure 3.1: **CRISPRi circuitry to inhibit antibiotic resistances.** The CRISPRi platform comprises three gene cassettes for the expression of dCas9, gRNAs and antibiotic resistance genes. Two main configurations are obtained upon the interconnection of these modules. **A.** The first configuration includes three plasmids: a low copy vector holding the constitutive dCas9 cassette under P_{J23116} promoter; a low or high copy plasmid encoding for the target cassette downstream a constitutive promoter (indicated as P_{res}); a low copy copy plasmid bearing an IPTG-inducible gRNAs module implemented as single/double sgRNA Cassettes or CRISPRi Array. The expression of guide RNAs, either transcribed as sgRNA or spacer, is under the control of the LacI-regulated P_{LlacO1} promoter. If present, IPTG triggers the expression of the gRNA(s) downstream of P_{LlacO1}. **B.** The second configuration includes two plasmids: a low copy vector holding both an HSL-inducible dCas9 cassette and an IPTG-inducible gRNAs module implemented as double sgRNA Cassettes or CRISPRi Array; a low, medium or high copy vector bearing the target cassette downstream a constitutive promoter (indicated as P_{res}). Straight arrows represent protein-coding genes or sgRNA, while CRISPRi Array components are represented as rectangles if spacers or diamonds if repeat sequences. The C, g and C:g symbols correspond to the dCas9 protein, gRNA molecule and their complex, respectively.

inducer molecule IPTG; otherwise, in the second configuration, both IPTG and HSL were necessary to trigger the activity of the inducible promoters P_{LlacO1} and P_{Lux-3A} placed upstream of the gRNA module and dCas9, respectively. To perform conjugation assays, a new collection of circuits with the same topology reported in Figure 3.1 B was constructed by cloning the oriT sequence (Origin of transfer) from the pRK2 plasmid upstream of each CRISPRi Array (not shown in the figure). A non-self transmissible conjugation was carried out by leveraging the conjugative machinery expressed in *trans* by the pTA-Mob helper plasmid [88]. A schematic representation of the conjugative transfer is reported in Figure 3.2 (the protocols employed to construct the genetic circuits and the complete list of plasmids obtained in this study are reported in Appendix A).

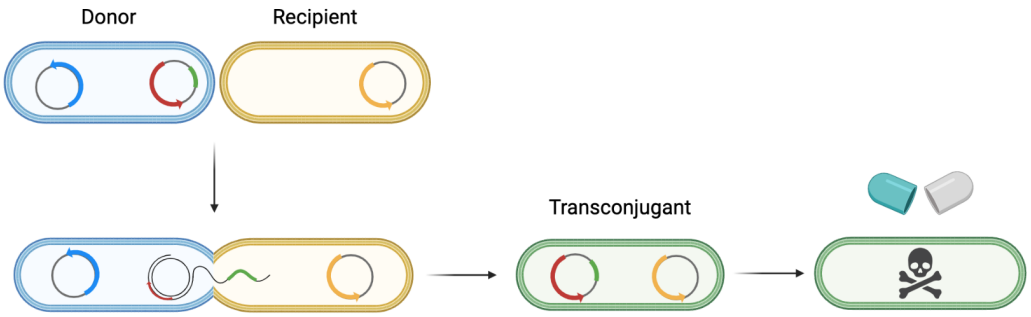

Figure 3.2: **Scheme of a non-self transmissible conjugation.** Trans-conjugative set-up employed to perform conjugation assays. A donor cell (blue) harbours two plasmid: a low copy vector bearing both CRISPRi circuitry (red arrow) and oriT_{RK2} sequence (green segment) and the helper plasmid pTA-Mob which provides in *trans* all the transfer and replication functions (blue arrow) necessary to support a non-self transmissible conjugation. The recipient strain (yellow) is represented by a cell carrying the resistance gene (yellow arrow) within an endogenous plasmid. During a conjugation event, the oriT_{RK2} sequence is recognized by the relaxase expressed in *trans* from pTA-Mob and a single DNA strand of the CRISPRi encoding plasmid is mobilized towards the recipient cell through a cytoplasmic bridge that connects the mating pair. At the end of conjugation, recipient cells become transconjugants, bearing both the plasmid encoding the resistance gene and the one carrying the CRISPRi machinery. The CRISPRi-mediated silencing of target gene restores antibiotic susceptibility in the resistant strain which is killed upon exposure to the drug.

3.1.2 Circuit characterization

Liquid and Plate Culture Assays

The bacterial growth of engineered strains with CRISPRi circuitry and relative controls was quantitative characterized through liquid culture assays, while plate culture assays were performed only for recombinant strains classified as *silenced strains*. The two protocols, which share the first steps, are described in Figure 3.3 and detailed below:

- bacteria from glycerol stock were streaked on a selective LB agar plate and incubated overnight at 37°C to isolate single colonies;

- the following day, 0.5 ml of selective LB were inoculated with a single colony in 2−ml tubes. The same colony was tested in two conditions, ON and OFF state. In case of ON state, IPTG and HSL inducers were added to the culture at a concentration of $200\mu M$ and 100 nM, respectively; in case of OFF state none of the inducers was added to the cultures. In both cases, the medium was supplemented only with the antibiotics necessary for plasmid maintenance but not with the final target antibiotic. Cultures were incubated overnight in an orbital shaker at 37°C, 220rpm. At this point, the two protocols diverged;

- in case of liquid assays, after a 20-h incubation, cultures grown in the ON and OFF state were 100-fold diluted in $200\mu l$ in a 96-well microplate. Two microliters of HSL and IPTG were added when required to maintain the same inducers concentration used for overnight cultures, while the target antibiotic was added in a range of concentrations. The microplate was incubated with lid in the Infinite F200Pro reader (Tecan) programmed with the $i - control^{TM}$ software to perform a kinetic cycle as follows: 5s linear shaking (3 mm amplitude), 5s wait, absorbance (600 nm) measurement, 5-min sampling time. Cultures were not placed in the external wells of the plate to avoid intensive evaporation. The experiment lasted 24h;

- in case of plate assays, only the overnight cultures grown in the ON state were serially diluted and $100\mu L$ plated on LB + inducers or LB + inducers + target antibiotic. HSL and IPTG were added to agar plates to maintain the same inducers concentration used for overnight cultures, while the target antibiotic was added in a single concentration. Plates were then incubated at 37°C overnight. Colonies were counted the following day in order to obtain the relative CFUs.

Growth curves from liquid culture assays were obtained by processing the absorbance acquired from microplate experiments. In specific, raw absorbance was measured over time and then background-subtracted as reported in [77] to obtain an OD_{600} measure proportional to the per-well cell density. Data analysis were carried out via Microsoft Excel. Using this method, the minimum inhibitory concentration (MIC) of each target antibiotics was determined along with the delay in growth recovery showed by escaper cells (See Figure 3.5). In case of plate culture assays, the number

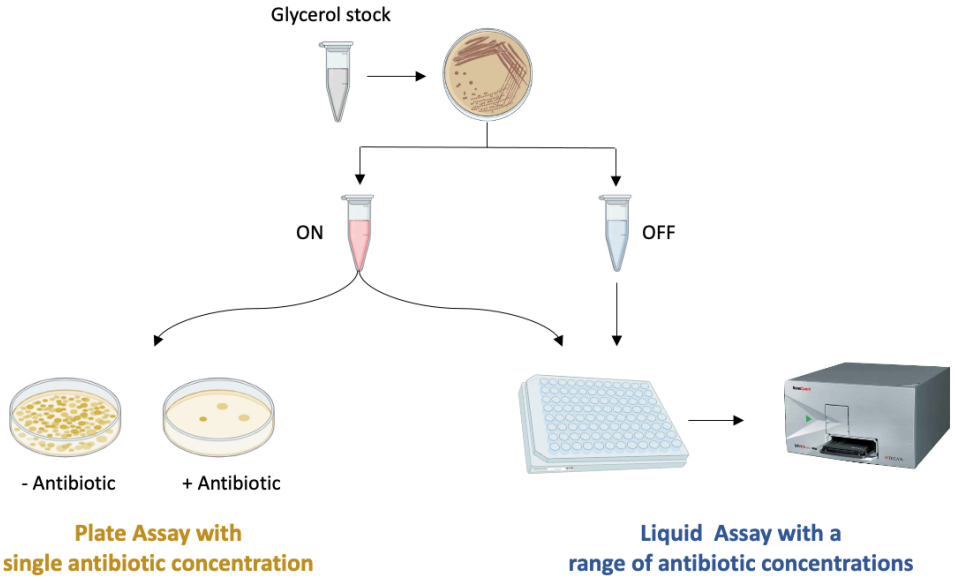

Figure 3.3: **Scheme of Liquid and Plate culture assays.** Bacteria engineered with CRISPRi circuitry and relative controls are streaked on selective LB plates and grown overnight. A single colony for each strain is cultivated in two conditions: ON state when the growth medium is supplemented with IPTG and HSL, OFF state if the inducers are are not added; in both conditions, the target antibiotic is absent. After an overnight incubation, bacteria cultivated in the ON and OFF state are diluted in a 96-well microplate and tested under a range of antibiotic concentrations. The multi-well is later incubated in a plate reader to measure the absorbance of the bacterial cultures over time (Liquid assay). Bacteria cultivated only in the ON state are serially diluted and plated on LB + inducers (- Antibiotic) or LB + inducers + target antibiotic (+ Antibiotic) added in a single concentration. Colonies were counted manually and the total amount of viable cells expressed as CFU/mL (Plate assay).

of viable bacteria present in each sample was estimated by plating serial dilution of the overnight liquid cultures on LB agar medium and then colony counting. The number of bacteria per milliliter (CFU/mL - colony forming units) was determined by multiplying the amount of colonies detected in the plate the respective dilution factor. This method was adopted to evaluate the efficiency of the CRISPRi circuitry in inhibiting the resistance gene by comparing the ratio of CFUs under two conditions in which the repressor complex was always activated (ON state) and the target antibiotic was either present or absent. The CRISPRi *repression efficiency* was thus estimated as:

$$Repression\ Efficiency = \left(1 - \frac{CFU_{+Ab}ON}{CFU_{-Ab}ON}\right) \cdot 100 \tag{3.1}$$

where $\mathrm{CFU_{+Ab}}$ refers to the total amount of cells bearing the CRISPRi circuitry detected on agar plate in presence of both target antibiotic and inducer molecules (ON state); $\mathrm{CFU_{-Ab}}$ refers to the total amount of cells bearing the CRISPRi circuitry detected on agar plate supplemented only with

inducer molecules (ON state without antibiotic target selection pressure).

Characterization of CRISPRi escape mutants

Liquid assays and sequencing analysis: escaper cells that have recovered from the antibiotic treatment at the end of the liquid culture assays were collected and further analysed in order to characterize the genotype and the behavioural phenotype. The experimental protocol employed is described in Figure 3.4 and detailed below:

- bacteria that have recovered from the highest antibiotic concentration during the first round experiment were streaked on selective LB agar plate and incubated overnight at 37°C;
- the following day, a single colony for each recovered culture was inoculated in selective LB and, after an overnight growth at 37°C and 220rpm, the culture was used to prepare a glycerol stock, stored at -80°C;
- starting from the long term stocks, each escape mutant was used to run another liquid culture assay with the same range of antibiotic concentrations used in the first round treatment. This method was adopted to study the temporal dynamics of the recovered culture and test whether it was represented by a sub-population of resistant or resilient cells;
- escaper cells from glycerol stocks were also cultivated overnight at 37°C, 220rpm in selective LB; the following day, cells were collected to extract plasmid DNA. The latter was used to perform restriction digest, plasmid copy number quantification and sequencing analysis with three different primers annealing the sequences of dCas9, CRISPRi Array and target resistance gene (see Table A.2). This method was adopted to characterize the genotype of escape mutants with a particular focus on CRISPRi machinery and target gene. In case of dCas9 protein, sequencing analysis covered only the initial sequence of the respective gene (about 700bp); to verify whether large DNA arrangements (e.g., deletions or insertions) occurred within dCas9 gene sequence, a restriction digest was performed by leveraging HindIII enzyme which generates two cuts within dCas9 gene.

Plasmid copy number quantification: plasmid DNA purified from recombinant strains was also used to carry out a plasmid copy number quantification in case of engineered strains harbouring two plasmids: a LC vector carrying the CRISPRi machinery and a MC vector bearing *NDM-1* or *mcr-1*

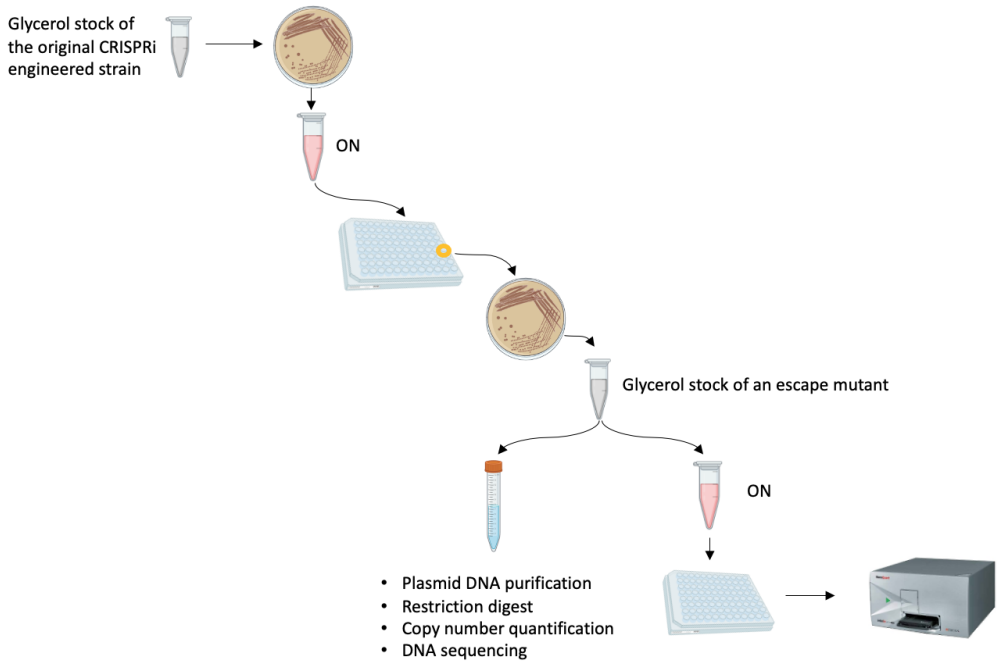

Figure 3.4: **Experimental protocol employed to characterize escaper cells.** Bacteria engineered with the CRISPRi circuitry, indicated as "original CRISPRi engineered strain", are tested according to the protocol described in Figure 3.3. Cells that survive antibiotic exposure are collected from the 96-well microplate (yellow circle), streaked on selective plates and used to prepare a glycerol stock. Plasmid DNA from each culture of escape mutant is purified and used to carry out restriction digest, plasmid copy number quantification and sequencing analysis. The same clones are used to run another liquid culture assay with the same range of antibiotic concentrations used in the first round treatment in order to investigate the temporal dynamic.

target gene. Plasmids were quantified through fluorescence measurements of their DNA fragments upon plasmid purification (Macherey-Nagel Plasmid Kit), restriction digests with the BglII enzyme (generating a single cut within each plasmid), and 1% agarose gel electrophoresis stained with ethidium bromide staining, assuming that the relative amount of all the plasmids does not change during extraction from bacterial cultures. Gel pictures were taken with an Imager CHEMI Premium (VWR) and the fluorescence intensity of bands was analysed via ImageJ [89]. The GeneRuler 1 Kb DNA ladder was used to assess the linearity of fluorescence intensity of bands as a function of their length, according to the DNA amount, available from the manufacturer, for each band.

Delay in growth recovery: in experiments with liquid culture, the speed of recovery after exposure to target antibiotic was measured as the delay in the time that escaper cells take to reach the OD_{600} value of 0.1 compared to the delay that the same culture showed in absence of target antibiotic. This

parameter, defined as "Delay in growth recovery", was estimated as:

$$Delay\ in\ growth\ recovery = T_{0.1[Ab]} - T_{0.1} \tag{3.2}$$

where $T_{0.1[Ab]}$ is the time that the strain engineered with the CRISPRi circuitry in the ON state takes to reach the OD_{600} value of 0.1 after exposure to a precise antibiotic concentration; $T_{0.1}$ is the time that the same strain takes to reach the OD_{600} value of 0.1 without antibiotic treatment (See Figure 3.5).

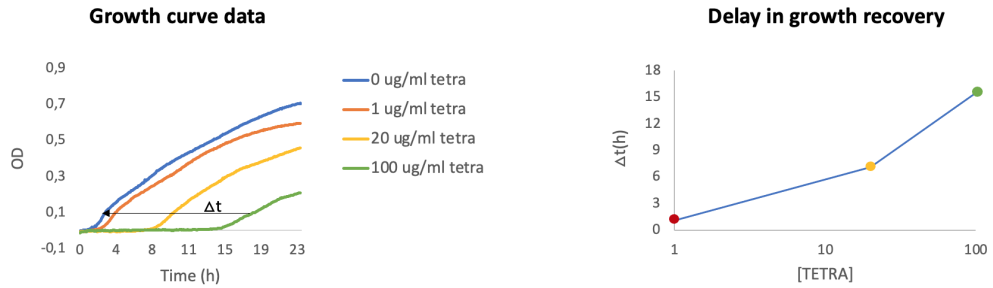

Figure 3.5: **Method used to measure the delay in growth recovery from growth curve data.** Example of growth delay computation. On the left: growth curve data derived from liquid culture assays. A bacterial strain, harbouring *tetA* gene along with a CRISPRi circuitry targeting the same resistance, is exposed to tetracycline treatment. In the graph, temporal series of bacterial density, measured as OD_{600}, are shown over time. On the right: for each antibiotic concentration, the delay in growth recovery is measured as the time taken to reach the OD value of 0.1 (orange, yellow and green curves on the left) in comparison to the growth of the same strain in absence of antibiotic (blue curve on the left). The delay is reported as Δt(h) and plotted as a function of tetracycline concentrations.

Supernatant Assay: at the end of the liquid culture assay, the supernatants from sensitive and CRISPRi engineered strains were collected by centrifuging the cultures grown in the 96-well microplate. Three microliters of both supernatants were dropped into the center of two different agar plates where a sensitive strain was previously plated. The plates were incubated at 37°C overnight and the zone of inhibition observed the following day as the area without bacterial growth. This method was employed to investigate the β-lactamase-mediated degradation of ampicillin and meopenem in liquid cultures.

Bacterial Conjugation Assay

The bacterial conjugation assay carried out in this study was optimized by using as a starting point the general conjugation protocol provided by the Barrick Lab [90]. A non-self-transmissible conjugation was performed in order to deliver the CRISPRi circuitry from a donor strain, carrying the helper

plasmid pTA-Mob, to a recipient strain harbouring the target antibiotic resistance gene. The conjugation assay, which is represented with a simplified scheme in Figure 3.6, was performed as follows:

- donor and recipient strains from a glycerol stock were streaked on selective LB agar plates and incubated overnight at 37°C;
- the following day, 5 ml of selective LB was inoculated with a single colony of each strain in 50 ml tubes. Cultures were then incubated overnight in an orbital shaker at 37°C, 220rpm;
- after the overnight incubation, donor and recipient strains were in stationary growth phase; to reach the exponential growth phase, both cultures were diluted and grown to an OD_{600} of about 0.25. Subsequently, 1 mL culture was taken from each tube, gently spun down and washed twice in PBS in order to remove residual antibiotics from donor and recipient cell cultures. After the washing steps, the optical density was measured and each culture was diluted or concentrated to reach the final OD_{600} of 0.5. Subsequently, mating pairs were combined at a donor to recipient ratio of 1:1 and $100\mu L$ of the mixture was plated onto non selective LB plate that was further incubated at 37°C. The mating proceeded for 20h;
- the following day, the conjugation mixture was scraped up from the agar plate and collected into a micro centrifuge tube with 1ml PBS. Conjugation was interrupted by vortexing and washing in PBS the mating mixture which was further diluted and $100\mu L$ spotted on agar plates containing appropriate antibiotics to select donor, recipient and transconjugant cells;
- after an overnight incubation at 37°C, colonies were counted in order to obtain the relative CFUs.

At the end of the conjugation assay, the number of CFUs was determined as previously described (see Section 3.1.2) and used to calculate two parameters: *conjugation efficiency* and *killing efficiency*. *Conjugation efficiency* was measured under a condition in which the CRISPRi circuitry was not expressed (OFF state) in order to evaluate only the efficacy of the genetic transfer without killing recipient cells. With this method, *Conjugation efficiency* provided an indication about the amount of cells transformed in transconjugants relative to total recipient cells and was estimated as follows:

$$Conjugation\ Efficiency = \frac{CFU_{trans}OFF}{CFU_{recip}} \cdot 100 \tag{3.3}$$

where CFU_{trans} refers to the total amount of transconjugant cells detected on agar plate in presence of target antibiotic and absence of inducer molecules (OFF state); CFU_{recip} refers to the total amount of recipient cells detected on a selective agar plate.

Killing efficiency was investigated under two conditions in which target antibiotic was always present and the CRISPRi circuitry was either expressed (ON state) or not (OFF state) in order to evaluate the repression capability of the CRISPRi-based conjugative platform. This parameter was the ratio between transconjugant cells with induced CRISPRi and transconjugant cells with repressed CRISPRi and was estimated as:

$$Killing\ Efficiency = \left(1 - \frac{CFU_{trans}ON}{CFU_{trans}OFF}\right) \cdot 100 \tag{3.4}$$

where $CFU_{trans}ON$ refers to the total amount of transconjugant cells detected on agar plate in presence of both target antibiotic and inducer molecules (ON state); $CFU_{trans}OFF$ refers to the total amount of transconjugant cells detected on agar plate in presence of target antibiotic and absence of inducer molecules. It is worth mentioning that the CRISPRi-mediated repression was not measured for all the recipient cells harbouring the resistance gene but only for those that have acquired the CRISPRi machinery through the conjugative transfer.

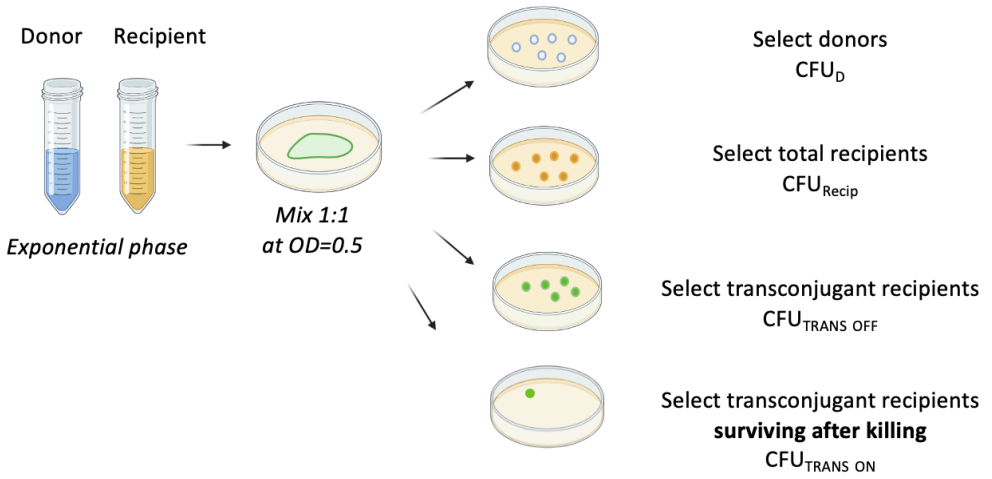

Figure 3.6: **Scheme of the bacterial conjugation assay.** Donor and Recipient strains are cultivated overnight in 50ml tubes and subsequently diluted to reach the exponential growth phase; 1ml culture from both tube is washed in PBS and concentrated to an OD_{600} of 0.5. The mating pair is combined at a donor to recipient ratio of 1:1 and the mixture spotted on non selective LB plate. After a 20-h incubation at 37°C, the conjugation mixture is collected, serially diluted and plated on selective LB plates to distinguish donor (blue), recipient (yellow) and transconjugant cells in the OFF and ON state (green).

3.2 Silencing of antibiotic resistances in model systems

The CRISPRi circuitry was first programmed to inhibit the expression of *bla* and *tetA*, two model ARGs that confer resistance to the antibiotics ampicillin and tetracycline, respectively. To this aim, customized gRNAs were implemented in two genetic architectures: sgRNA Cassette (used to test gRNAs individually and in combination) and CRISPRi Array (used to test gRNAs in combination). The CRISPRi platform was characterized by exploiting both configurations described in Figure 3.1 as the expression of gRNAs was coupled with a constitutive (Section 3.2.1 and 3.2.2) or inducible dCas9 module (Section 3.2.3).

3.2.1 Bla and tetA genes repression via single sgRNA Cassettes

A proof of concept of the CRISPRi-mediated silencing of resistance genes was achieved in a model system in which *bla* and *tetA* represented the final target genes. Bacteria harbouring these two ARGs are able to survive the antimicrobial action of ampicillin and tetracycline, respectively. Ampicillin is a bactericidal antibiotic derived from the penicillin group and belonging to the class of β lactam antibiotics; the latter inhibits the bacterial cell wall synthesis by irreversible binding the transpeptidase enzyme, which is necessary to build the peptidoglycan. This way, ampicillin definitively compromises cell wall integrity, which ultimately leads to cell lysis. In resistant bacteria, the *bla* gene encodes for a β lactamase enzyme which is secreted into the periplasm where it acts by hydrolyzing the β-lactam ring of ampicillin, thus inactivating the antibiotic [91]. Tetracyline, belonging to the tetracyclines family of compounds, is a bacteriostatic antibiotic that inhibits the bacterial protein synthesis; the molecule binds to the 30S ribosomal subunit and, by preventing the attachment of aminoacyl-tRNAs, blocks the translational process of mRNAs. Bacteria resistant to tetracyline express *tetA* gene which encodes for a membrane-bound efflux pump that active exports the drug outside the cell, thus preventing the increasing of intracellular amount [92]. The CRISPRi platform designed to inhibit the expression of *bla* and *tetA* genes was consistent with the one described in Figure 3.1 A. The target module was placed under a constitutive promoter in high copy vector (I3521) in case of *bla* gene or low copy plasmid (F' episome) in case of *tetA* gene.

To test the feasibility of CRISPRi-mediated inhibition of AMR, the modules responsible for the expression of dCas9 and sgRNA were cloned in a two-

plasmid system: the dCas9 cassette was placed downstream of a constitutive promoter (in medium-copy vector) while the gRNA module was driven by the IPTG-inducible P_{LlacO1} promoter (low-copy vector). The architecture of single sgRNA Cassette was first exploited to implement a gRNA module which transcribed a customized sgRNA to target *bla* or *tetA* gene. In particular, the trascriptional inhibiton of *bla* gene was studied with two sgRNAs targeting either the coding sequence (gAmpRgene) or the promoter region (gAmpRpromoter), while only a gRNA targeting the coding sequence of *tetA* gene was implemented within the sgRNA Cassette (gtetA). The CRISPRi-mediated repression of these model resistances was *in vivo* characterized through an experimental set-up that employed three main clones, described below and represented in Figure 3.7:

- *sensitive strain*, which was susceptible to antibiotic exposure as the plasmid carrying the resistance gene was absent;
- *resistant strain*, which was resistant to antibiotic treatment as the plasmid bearing the resistance gene was present along with a CRISPRi circuitry expressing a non-specific gRNA unable to inhibit the expression of target gene;
- *silenced strain*, which was expected to be susceptible to antibiotic exposure as the plasmid holding the resistance gene was present along with a functional CRISPRi circuitry.

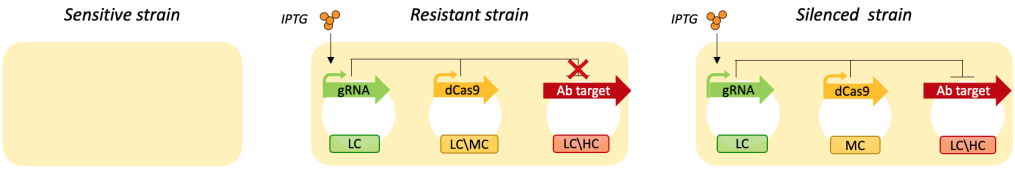

Figure 3.7: **Experimental set-up exploited to characterize CRISPRi efficiency with single sgRNA Cassettes.** The experimental set-up employed to perform *in vivo* experiments is composed of three clones: *sensitive strain*, susceptible to antibiotic exposure; *resistant strain*, able to survive antibiotic treatment as the resistance gene is present (indicated as Ab target) and not inhibited by CRISPRi circuitry; *silenced strain*, in which a functional CRISPRi complex restores antibiotic susceptibility by inhibiting the expression of the resistance gene. In *silenced strain*, the CRISPRi platform has an architecture consistent with the one described in Figure 3.1 A. Green arrows represent IPTG-inducible gRNA modules implemented as single sgRNA Cassette; yellow arrows indicate constitutive dCas9 expression module; red arrows represent the target cassette encoding for an antibiotic resistance gene placed on high (*bla* gene) or low copy vector (*tetA* gene).

In the described experimental set-up, the bacterial growth of *sensitive* and *resistant* strains was first characterized with microplate liquid assays in order to determine the Minimum inhibitory concentration (MIC) of target

antibiotics (ampicillin and tetracyline); this preliminary step was crucial to define a window of antibiotic concentrations suitable for the characterization of the *sensitive strain*. To this aim, the experimental protocol described in Section 3.1.2 was exploited. Briefly, all strains were cultivated overnight in a medium supplemented only with the inducer molecule IPTG; the following day, cultures were diluted in a 96-well microplate and treated with a range of ampicillin or tetracycline concentrations, by maintaining IPTG in the growth medium. This experimental condition, defined as ON state, was also carried out in absence of inducer (OFF state). For each target antibiotic, it was expected to find a very low MIC in *sensitive strain*; a MIC higher than the current antibiotic concentration adopted for plasmid maintainance in *resistant strain*; a MIC comprised between the other two values in case of *silenced strain*. The characterization of CRISPRi-mediated repression of *bla* gene was carried out by employing TOP10 F' as *sensitive strain*; TOP10 F' co-transformed with J116dCas9, I13521 (harbouring *bla* gene) and gtetA (non-specific gRNA) as *resistant strain*; TOP10 F' co-transformed with J116dCas9, I13521 and gAmpRpromoter/gAmpR gene (specific gRNAs) as *silenced strain* (see Table A.4 for the complete list of constructs obtained in this study). The MIC of each strain was determined by analysing the growth curves in the ON/OFF states and under a range of ampicillin concentrations. As shown in Figure 3.8, data were consistent with the expected outcomes.

Indeed, if *sensitive strain* was high susceptible to antibiotic exposure, *resistant strain* survived even the highest ampicillin concentration tested, without showing relevant growth defects. Either in the ON or OFF state, the MIC values determined for *sensitive* and *resistant* strains were [AMP=10$\mu g/ml$] and [AMP>5000$\mu g/ml$], respectively. The behaviour shown by *resistant strain* confirmed that, even in presence of a complete CRISPRi circuitry, the non-specific guide gtetA was unable to interfere with *bla* gene expression that provided the clone with the ability to degrade the antibiotic. On the other hand, by comparing ON and OFF experimental conditions, *silenced strains* clearly showed the effect on bacterial growth derived from *bla* gene repression. Both *silenced strains*, harbouring gAmpRpromoter or gAmpRgene single sgRNA Cassette, revealed the effect of a basal activity of P_{LlacO1} promoter in the OFF state. Indeed, a delay in bacterial growth could be observed at the highest ampicillin concentration as a little amount of CRISPRi repressor complex was already active in inhibiting *bla* gene expression. This delay could not be observed in the *resistant strain*. The ON state was fully achieved upon IPTG induction: in this condition, gAmpRpromoter showed a repression efficiency higher than the one exhibited by gAmpRgene as only the CRISPRi complex targeting the promoter sequence restored a complete susceptibility to ampicillin with a MIC value of [AMP=5000$\mu g/ml$]. Nev-

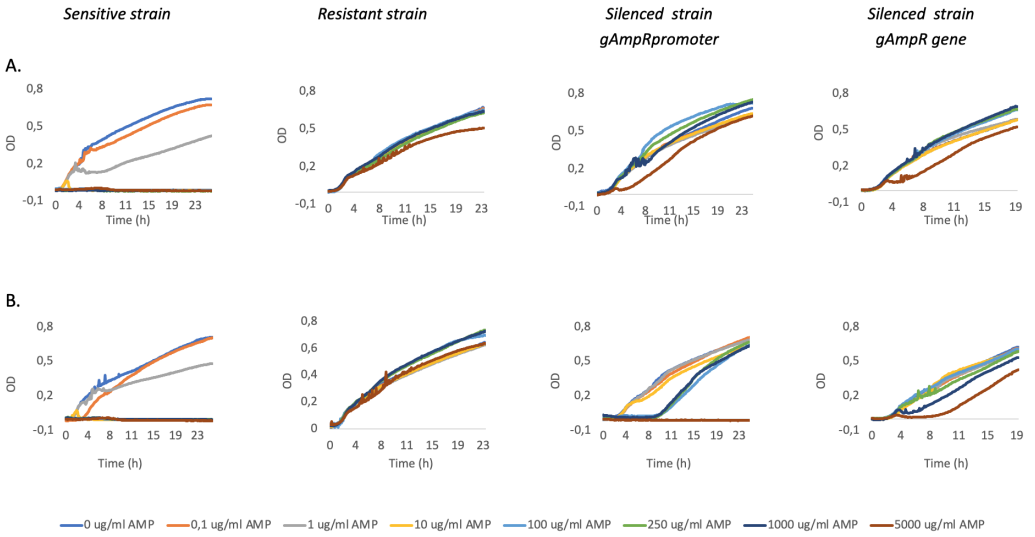

Figure 3.8: **CRISPRi-mediated repression of *bla* gene with single sgRNA Cassette.** Growth curve data derived from liquid culture assays. The CRISPRi circuitry includes an IPTG-inducible single sgRNA Cassette coupled with a constitutive dCas9 module. In each graph, temporal series of bacterial density, measured as OD_{600}, are shown over time. At t=0, *sensitive*, *resistant* and *silenced* strain (expressing gAmpR promoter or gAmpR gene) are treated with a range of ampicillin concentrations either in the OFF **A.** or ON **B.** state. Growth curves are representative of a single experiment from a set of three independent biological replicates that did not show significant variations in the observed trends.

ertheless, the CRISPRi repression efficiency could also be measured as a function of the delay in growth recovery that both *silenced strains* showed upon drug exposure (See Section 3.1.2). As reported in Figure 3.8 B, a sub-population of silenced clones recovered after 8-9h from time zero when bacteria were inoculated into microplate. Survivor cells could be represented by resistant clones, which have increased their capability to withstand antibiotic treatment, or resilient cells, that have recovered from the initial disturbance thanks to a community response. Resilience is a phenomenon that can be explained by detailing the bacterial response that occurs in case of treatment with β-lactam antibiotics, such as ampicillin [93]. In resistant cells, β-lactamase (*bla*) anchored in the bacterial periplasm degrades ampicillin that diffuses across the outer membrane, preserving the cell from the lethal effect of the drug. If *bla* gene expression is inhibited (CRISPRi ON) and a sufficient amount of ampicillin is administered, a sub-population of cells is killed, resulting in an initial decline of bacterial density. As long as the antibiotic acts against re-sensitized bacteria, β-lactamase is released in the growth medium because of cell lysis. If a sufficient amount of enzyme is released from killed cells, residual ampicillin is degraded in time for individual clones to recover and proliferate. To prove this hypothesis, a supernatant assay was

performed as described in Section 3.1.2. As expected, the supernatant from *silenced strains* did not contain enough ampicillin to inhibit the growth of a sensitive strain compared with the supernatant collected from the TOP10 F' control culture, which produced the expected inhibition zone on LB plate. As this particular phenomenon occurs, the delay in growth recovery exhibited by *silenced strains* provided an indication of CRISPRi efficiency and was thus measured as described in Section 3.1.2. Results are shown in Figure 3.9 and demonstrated a correlation between the increasing in antibiotic concentration and the delay in the time taken by *sensitive strains* to reach the OD value of 0.1 compared to the same non treated strains. The efficiency of CRISPRi circuitry to restore antibiotic susceptibility in *silenced strains* was also evaluated through plate culture assays performed as described in Section 3.1.2. By comparing the ratio of CFUs under two conditions in which ampicillin was either absent or added at a concentration of $100\mu g/ml$, the stronger repression efficiency of gAmpRpromoter over gAmpRgene was again demonstrated. In particular, as shown in Figure 3.9, gAmpRpromoter effectively re-sensitized almost the entire bacterial population to ampicillin treatment with the same ampicillin concentration used for selection of recombinant strains. Compared to liquid culture, this result could be interpreted as a snapshot at time zero of bacterial response: in liquid medium, the secreted β-lactamase was well distributed and supported the rescue of resilient cells during the overnight culture in microplate; this advantage was absent in solid medium during the selection of survivor cells, most probably due to the spatial separation of individual colonies on LB plate. The experimental set-up described in Figure 3.7 was also adopted to characterize the CRISPRi-mediated silencing of *tetA*. The protocol described in Section 3.1.2 was carried out by employing the following three clones: TOP10 as *sensitive strain*; TOP10 F' co-transformed with J116dCas9 and gAmpRgene (non-specific gRNA) as *resistant strain*; TOP10 F' co-transformed with J116dCas9 and gtetA (specific gRNA) as *silenced strain*. This time, the resistance gene was harboured by F' episome, present in the host cell. The MIC of each strain was determined by analysing the growth curves in the ON/OFF states and under a range of tetracycline concentrations. Data are reported in Figure 3.10. As expected, *sensitive strain* was highly susceptible to tetracycline and the MIC value determined was [TETRA=$10\mu g/ml$] either in the ON or OFF state. The response of *resistant strain* highlighted that tetracycline concentrations grater than $20\mu g/ml$ significantly affected bacterial growth; as previously observed, a MIC value could not be determined and IPTG induction did not alter the outcome. In *silenced strain*, targeting *tetA* coding sequence in both ON/OFF states determined a consistent reduction in bacterial growth, which resulted in a MIC value of [TETRA=$100\mu g/ml$] in presence of IPTG. This result

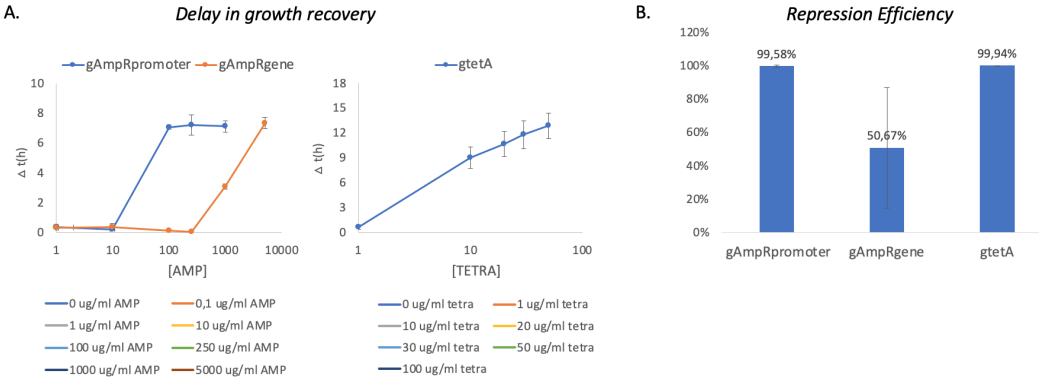

Figure 3.9: **CRISPRi-mediated repression of *bla* and *tetA* gene with single sgRNA Cassette: growth delays and plate assays.** **A.** Delays in growth recovery measured from liquid culture assays. The CRISPRi circuitry includes an IPTG-inducible single sgRNA Cassette coupled with a constitutive dCas9 module. CRISPRi repression efficiency of single sgRNA Cassette is measured as the delay in the time taken to reach the OD value of 0.1 in comparison to the growth of the same strain in absence of antibiotic. In each graph, the delay is reported as Δt(h) and plotted as a function of ampicillin concentrations (graph on the left) or tetracycline concentrations (graph on the right). Data points represent the average value measured for each antibiotic concentration. **B.** CRISPRi repression efficiency of single sgRNA Cassettes in plate culture assays. *Silenced strains* are selected on LB + IPTG or LB + IPTG + ampicillin /tetracycline to calculate the ratio of survivor cells to total non-treated bacteria and the relative CRISPRi repression efficiency. Error bars represent the standard errors of the mean of at least 3 independent experiments.

can be explained by considering two aspects: first, P_{LlacO1} promoter leakage resulted in a little amount of CRISPRi repressor complex already capable of inhibiting *tetA* gene expression even in the OFF state; second, the target gene was placed on F' episome, which is a low copy plasmid present in 1-2 copies per cell [94]. As observed with ampicillin, increasing tetracycline concentrations resulted in a delayed growth for *resistant* and *silenced* strains. Again, this phenomenon can be explained by detailing the bacterial response that occurs upon tetracycline treatment. The native tet resistance mechanism is based on two proteins, TetR and TetA: TetR is a transcriptional repressor that inhibits *tetA* expression in absence of tetracycline. If present, tetracycline diffuses across the cell membrane and binds TetR, thus triggering the expression of both *tetA* and *tetR*: the former actively exports antibiotic out of the cells, the latter maintains *tetA* expression under a potential toxic level and contributes to reducing the tetracycline intracellular amount by sequestering the molecule. In *silenced strain*, *tetA* expression was inhibited by the CRISPRi repressor complex, but TetR protein could still maintain its role in reducing the amount of antibiotic molecules available to kill the cell [95]. The delay in growth recovery exhibited by *silenced strain* was thus used as a mean to measure CRISPRi repression efficiency for tetracycline and could be due to antibiotic sequestration or mutations occurring in the CRISPRi system. Data are reported in Figure 3.9 A and clearly demonstrated that

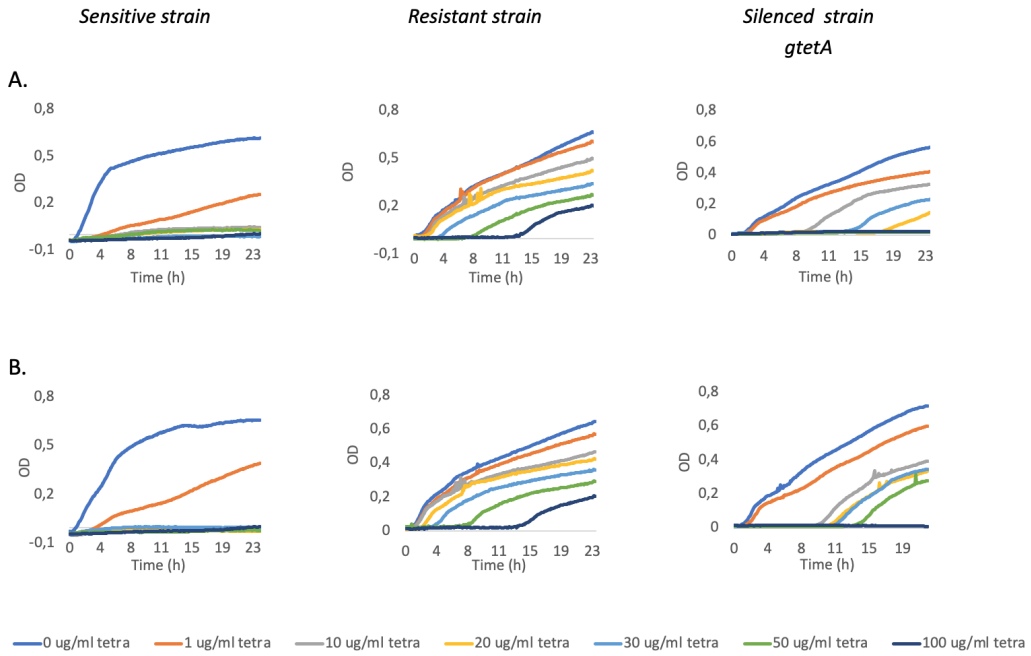

Figure 3.10: **CRISPRi-mediated repression of *tetA* gene with single sgRNA Cassette.** Growth curve data derived from liquid culture assays. The CRISPRi circuitry includes an IPTG-inducible single sgRNA Cassette coupled with a constitutive dCas9 module. In each graph, temporal series of bacterial density, measured as OD_{600}, are shown over time. At t=0, *sensitive*, *resistant* and *silenced* strain (expressing gtetA) are treated with a range of tetracycline concentrations either in the OFF **A.** or ON **B.** state. Growth curves are representative of a single experiment from a set of three independent biological replicates that did not show significant variations in the observed trends.

the time needed for population recovery increased as a function of antibiotic concentration. Results from plate culture assays are reported in Figure 3.9 B. By comparing the ratio of CFUs under two conditions in which tetracycline was either absent or added at a concentration of $15\mu g/ml$, the strong repression efficiency of the gtetA-based CRISPRi circuitry was confirmed. Indeed, almost the entire bacterial population was re-sensitized to tetracycline at the same concentration used for selection of TOP10 F' clones.
The results described in this section are extremely promising as they prove that the CRISPRi platform can be efficiently employed in the trascriptional repression of resistance genes. This case study highlighted that even target genes placed in high copy plasmid can be efficiently repressed, thus providing an encouraging result towards the treatment of highly expressed resistance genes. On the other hand, as already reported in the literature, the location of the target site may significantly affects repression efficiency, as demonstrated by the targeting of *bla* gene coding sequence. With regard to *tetA* gene, a higher repression level was detected, probably due to the low copy number of the target plasmid; the latter unearthed the leakage activity of

P_{LlacO1} promoter, thus preventing a clear differentiation between ON and OFF state. The designed systems were able to fully inhibit bacterial growth for 24h, i.e., a MIC could be established. Nonetheless, at intermediate antibiotic concentrations growth recovery was observed, probably due to the specific AMR mechanisms of the two model systems used or to mutations breaking the silencing capability of the CRISPRi system. The role of escape mutants will be in-depth characterized below when dealing with clinically relevant antibiotics.

3.2.2 Bla and tetA genes repression via double sgRNA Cassettes and CRISPRi Array

Once the efficiency of the CRISPRi circuitry based on single sgRNA Cassettes was demonstrated, two new synthetic circuits suitable for multi-targeting were developed. This step was addressed as the possibility to target multiple genes or different loci within the same gene is a crucial point in the design of CRISPRi-based systems with enhanced performances and it can also represent the only solution in case of MDR pathogens. To this aim, two different gRNAs were implemented as sgRNAs or CRISPR spacers within the same vector. The resulted circuits were indicated as "double sgRNA Cassettes" and "CRISPRi Array", respectively (see Figure 3.1). The main differences between these two architectures regarded dimension and processing mechanism. As detailed in Section 3.1.1, each sgRNA Cassette was provided with its own regulatory parts, thus the final length of a double sgRNA module was $\sim 1Kb$. The structure of CRISPRi Array resembled the one of native CRISPR systems, in which multiple guides (called "spacers") can be expressed under the control of a single promoter and terminator. This meant that, with the same guides transcribed, a CRISPRi Array with two spacers reached a final length of $\sim 0.4Kb$. Furthermore, if each sgRNA was expressed as a crRNA:tracrRNA complex (thanks to the synthetic tetra-loop connecting the two parts), CRISPRi Array encoded for a single tracrRNA shared among transcribed guides. Regarding processing mechanism, unlike sgRNA Cassette, the expression and processing of gRNAs from CRISPRi Array depends on Cas9, tracrRNA and RNAse III (see Section 1.2 for a detailed description of CRISPR Array maturation process).

With the purpose to target *bla* and *tetA* genes, gAmpRpromoter and gtetA were expressed using the above mentioned architectures and placed in low copy vectors; gAmpR_Promoter was preferred to gAmpR_gene due to its higher repression efficiency. The resulting circuits were named gAmpRpromoter_gtetA Cassettes and Array gAmpRpromoter_gtetA (see Table

A.4 for the complete list of constructs). The transcriptional regulatory elements were the same for both designs: an IPTG-inducible P_{LlacO1} upstream the gRNA expression module in LC plasmid; a dCas9 cassette in MC vector under the control of BBa_J23116 constitutive promoter; *bla* and *tetA* target genes in HC (I3521) and LC (F' episome) plasmids, respectively. The resulting expression system had an architecture consistent with the one described in Figure 3.1 A, in which the three main modules were placed in different vectors. The mentioned plasmids were first co-transformed in the TOP10 F' *E. coli* strain and than characterized with the protocol reported in Section 3.1.2. To separately evaluate the CRISPRi-mediated silencing of *bla* and *tetA* genes, ampicillin and tetracycline were administered individually; this way, it was possible to investigate the contribution of each guide in the repression of the respective target gene. The *E. coli* strains engineered with single sgRNA Cassettes were employed as controls in order to evaluate the effect on repression efficiency caused by the sharing of intracellular resources. Results obtained from liquid culture assays are shown in Figure 3.11 (only results from the ON state are shown). Growth curve data revealed a re-

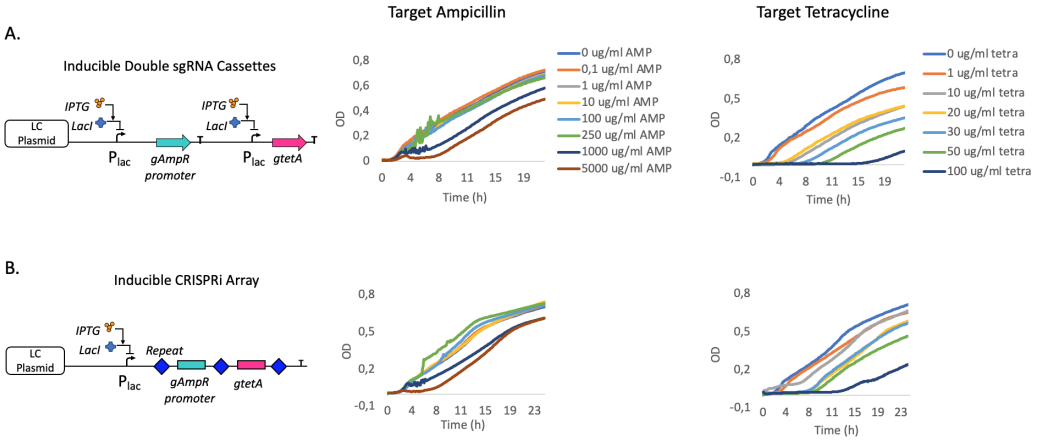

Figure 3.11: **CRISPRi-mediated repression of *bla* and *tetA* genes with double sgRNA Cassettes and CRISPRi Array.** On the left, schematic representation of double sgRNA Cassettes **A.** and CRISPRi Array **B.** inducible modules. ON the right, growth curve data derived from liquid culture assays. The CRISPRi circuitry includes the IPTG-inducible double sgRNA Cassettes or CRISPRi Array coupled with a constitutive dCas9 module. In each graph, temporal series of bacterial density, measured as OD_{600}, are shown over time. *Silenced strains* expressing both double sgRNA Cassettes **A.** or CRISPRi Array **B.** are treated with a range of ampicillin concentrations (first column) or tetracycline concentrations (second column). Growth curves are representative of a single experiment from a set of three independent biological replicates that did not show significant variations in the observed trends.

duction in repression efficiency with both architectures compared to single sgRNA Cassettes (see Figure 3.8 and Figure 3.10). Neither double sgRNA Cassettes nor CRISPRi Array restored a complete susceptibility to ampicillin or tetracycline, as a MIC value could not be determined for both antibiotics.

This observation could be explained by considering that the repression efficiency may be affected by gRNAs competition for the same pool of dCas9 protein. Indeed, dCas9 is a common resource and, even if the number of gRNAs was increased, the transcriptional level of the shared protein was not modified. Compared with circuits encoding for single sgRNA, a lower amount of gRNA:dCa9 complex can thus bind target sequences, resulting in a reduction of repression efficiency. In order to compare more accurately the performances of the two architectures, the speed of recovery of survivor cells upon exposure to both ampicillin and tetracycline was analysed. As shown in Figure 3.12 A, even delays in growth recovery measured from liquid assays did not show significant differences between the optimized designs and highlighted that a gRNA module implemented as single sgRNA Cassette was the best strategy to achieve the highest repression efficiency. Moreover,

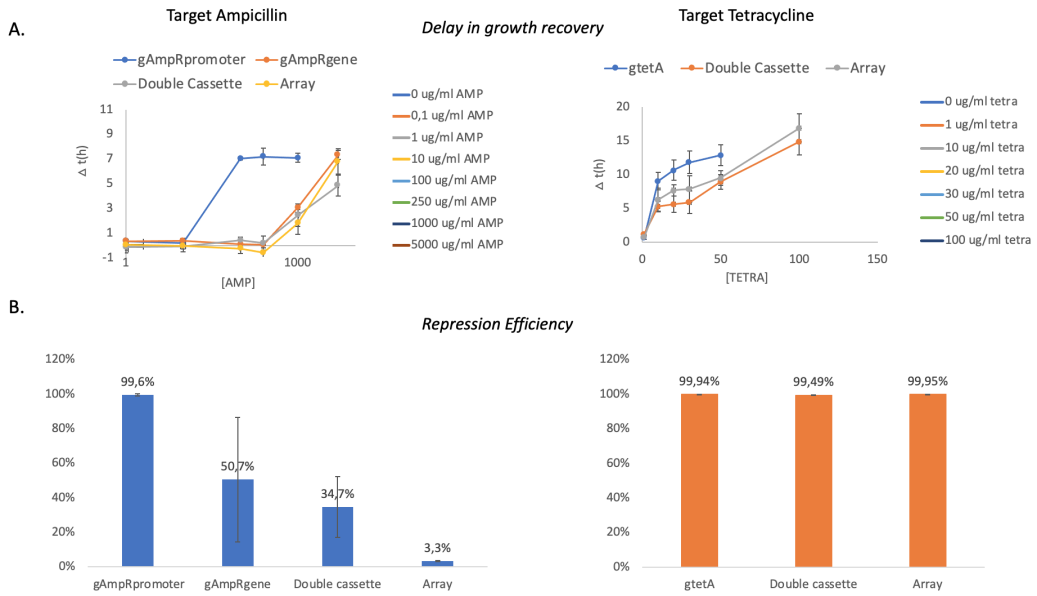

Figure 3.12: **CRISPRi-mediated repression of *bla* and *tetA* genes with double sgRNA Cassettes and CRISPRi Array: delay in growth recovery and plate assays.** **A.** Delays in growth recovery measured from liquid culture assays. The CRISPRi circuitry includes an IPTG-inducible single/double sgRNA Cassette or CRISPRi Array coupled with a constitutive dCas9 module. CRISPRi repression efficiency is measured as the delay in the time taken to reach the OD value of 0.1 in comparison to the growth of the same strain in absence of antibiotic. Data points represent the average value measured for each antibiotic concentration. In each graph, the delay is reported as Δt(h) and plotted as a function of ampicillin concentrations (first column) or tetracycline concentrations (second column). Data points represent the average value measured for each antibiotic concentration. **B.** CRISPRi repression efficiency of single/double sgRNA Cassette and CRISPRi Array in plate culture assays. *Silenced strains* are selected on LB + IPTG or LB + IPTG + ampicillin (first column) or tetracycline (second column) to calculate the ratio of survivor cells to total non-treated bacteria and the relative CRISPRi repression efficiency. Error bars represent the standard errors of the mean of at least 3 independent experiments.

the comparison between double sgRNA Cassettes and CRISPRi Array was

investigated by performing plate culture assays. Data are shown in Figure 3.12. To separately evaluate the CRISPRi-mediated silencing of *bla* and *tetA* genes, liquid culture grown overnight in presence of IPTG (ON state) were plated on LB solid medium supplemented only with IPTG or IPTG + target antibiotic; the latter was added at a fixed concentration of [AMP=100$\mu g/ml$] or [TETRA=15$\mu g/ml$]. As in liquid assays, this strategy was employed to investigate the contribution of each guide in the repression of the respective target gene. Making a comparison with the results obtained with single sgRNA cassettes, a consistent reduction in repression efficiency could be observed with both double Cassettes and Array in case of ampicillin resistance; none of the two architectures restored a complete susceptibility to the antibiotic, even though double Cassettes showed a higher repression efficiency than CRISPRi Array. In case of tetracycline resistance, no relevant differences could be observed between the two designs characterized as almost the entire bacterial population was effectively re-sensitized to tetracycline with double Cassettes and CRISPRi Array. It is worth mentioning that this result was due to the low copy number of F' plasmid carrying *tetA* gene. The results described in this section demonstrated that the CRISPRi circuitry can be expanded with additional gRNA modules in order to leveraging its multi-targeting capability. However, as a consequence of gRNAs competition for dCas9 protein, a general reduction in repression strength was observed for both target genes. This is a critical aspect to consider as it could limit the application of CRISPRi circuitry in case of multiple gene repression. To counteract competition and optimize the performances of the CRISPRi platform, a tuning of dCas9 expression was carried out and will be detailed in the following section.

3.2.3 Inducible dCas9 with double sgRNA Cassettes and CRISPRi Array

Considering the results described in Section 3.2.2 and assuming that a limitation in intracellular resources was the main responsible for the reduced repression efficiency exhibited by gAmpRpromoter_gtetA Cassettes and Array, the competition effect was addressed by tuning the intracellular amount of dCas9 protein. This strategy was implemented by replacing the original constitutive dCas9 module with an inducible expression cassette, with the final purpose to find an optimal expression level for target gene repression. The HSL-inducible dCas9 cassette described in Section 2.2 was thus employed, as the functional and minimal burden properties had already been demonstrated. The resulting CRISPRi platform was consistent with the one

described in Figure 3.1 B, in which an IPTG-inducible gRNA module and an HSL-inducible dCas9 cassette were placed on the same low copy vector. Both architectures for gRNA expression were maintained and the resulted circuits named AE$_{\text{-3A}}$d gAmpRpromoter_gtetA Cassettes and AE$_{\text{-3A}}$d Array gAmpRpromoter_gtetA. As the two main components of CRISPRi repressor complex were placed under inducible devices (P_{LlacO1} upstream gRNA module and P_{Lux-3A} upstream dCas9 cassette), both IPTG and HSL were required to trigger the expression of the CRISPRi circuitry. The described expression system was completed by a second plasmid holding the target cassette represented by *bla* or *tetA* placed in HC and LC vector, respectively (see Figure 3.1 B). For this set of experiments, the *E. coli* TOP10 F' strain was thus co-transformed with: AE$_{\text{-3A}}$d gAmpRpromoter _gtetA Cassettes/Array + I13521. The protocol described in Section 3.1.2 was carried out by modifying some steps. First, the CRISPRi repression efficiency was characterized only through liquid assays. Second, the bacterial growth of the engineered strains was studied only in the ON state: as for previously experiments, IPTG was present in the growth medium at a fixed concentration [IPTG=500μM], while HSL was added at 5 different concentrations maintained from the overnight culture to the experiment in the 96-well microplate. The strategy to couple an increasing concentration of HSL to a fixed amount of IPTG had the purpose to identify an HSL concentration able to bring the dCas9 expression level towards an optimal repression strength. dCas9 toxicity was monitored by characterizing the bacterial growth of the CRISPRi engineered strain under the same conditions (IPTG fixed + a range of HSL concentrations) but without administering target antibiotics, which were added individually to separately evaluate the CRISPRi-mediated silencing of *bla* and *tetA*. This way, once the antibiotic concentration was fixed, a set of 5 growth curves was obtained for each HSL value included in the tested window. Due to the large number of growth curve data derived from this experimental set-up, the results are shown in Figure 3.13 as delays in growth recovery upon exposure to ampicillin or tetracycline. Data revealed that, among the concentrations tested, [HSL=10nM] was the optimal solution to improve CRISPRi repression efficiency with both architectures. The control strain confirmed the absence of any dCas9 toxicity when treated with the same HSL concentration and in absence of target antibiotics (data not shown). Nonetheless, since the optimal HSL concentration was not the highest one tested, it is worth noting that the decreased repression efficiency for high induction levels was unexpected and might be due to overexpression issues beyond the scope of this work. The most promising results could be observed in case of tetracycline treatment as a complete susceptibility to the antibiotic was restored with a MIC value of [TETRA=100$\mu g/ml$], also ob-

served with single sgRNA Cassette. On the other hand, targeting *bla* with the new circuitry did not restore a complete susceptibility to ampicillin for the same concentration ranges tested previously, thus impeding to establish a MIC value also after the tuning of dCa9 expression. In this regard, it is worth mentioning that ampicillin resistance was expressed from a HC vector rather than a LC one like tetracycline resistance, thus a greater amount of repressor complex was needed to inhibit all the available intracellular targets. However, compered with the previously characterized platform with constitutive dCas9, a major improvement can be observed in terms of delay in growth recovery which resulted increased under ampicillin concentrations greater than $100\mu g/ml$. The improvement achieved with the tuning of dCas9 expression level is highlighted in Figure 3.14, in which a comparison between the two CRISPRi platforms is represented through growth curve data. In case of CRISPRi circuitry with inducible dCas9 cassettes, only growth curves relative to [HSL=10nM] concentration are shown for both genetic architectures targeting *bla* or *tetA* before and after dCas9 tuning.

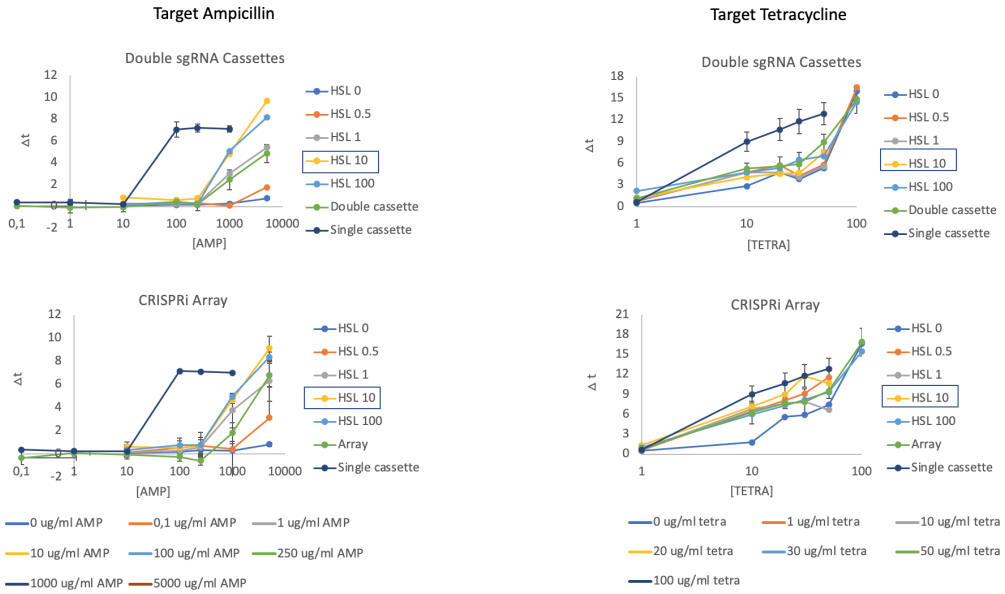

Figure 3.13: **CRISPRi-mediated repression of *bla* and *tetA* genes with double sgRNA Cassettes or CRISPRi Array and inducible dCas9: delay in growth recovery.** Delays in growth recovery measured from liquid culture assays. The CRISPRi circuitry includes the IPTG-inducible double sgRNA Cassettes or CRISPRi Array coupled with a HSL-inducible dCas9 module. CRISPRi repression efficiency is measured as the delay in the time taken to reach the OD value of 0.1, under a fixed HSL concentration, in comparison to the growth of the same strain in absence of antibiotic. In each graph, the delay is reported as Δt(h) and plotted as a function of ampicillin concentrations (first column) or tetracycline concentrations (second column). Data points represent the average value measured for each antibiotic concentration and error bars represent the standard errors of the mean of at least 3 independent experiments.

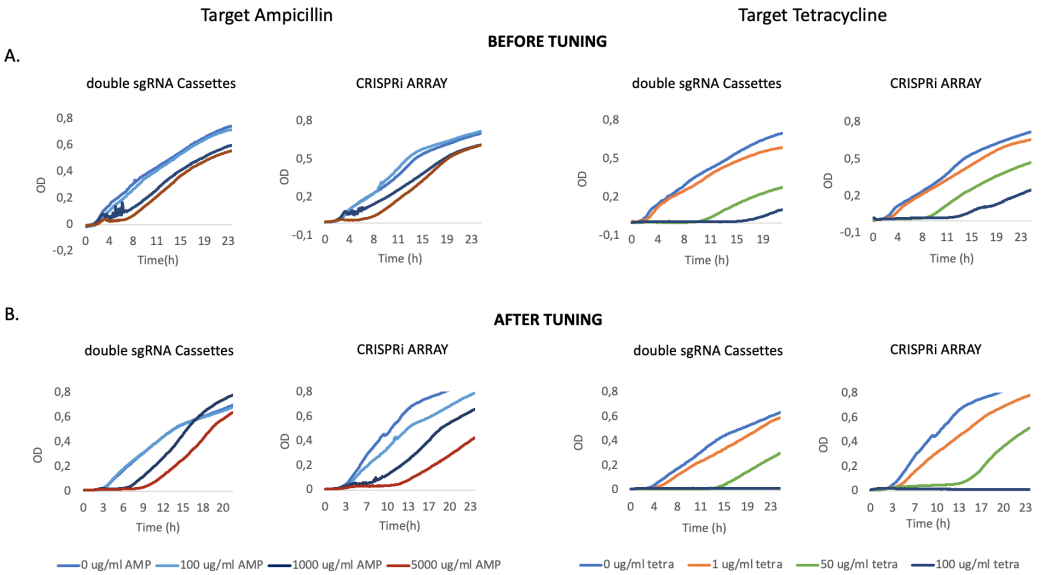

Figure 3.14: **Comparison between CRISPRi-mediated repression of *bla* and *tetA* genes with constitutive or inducible dCas9 module.** Growth curve data derived from liquid culture assays. **A.** The CRISPRi circuitry includes the IPTG-inducible double sgRNA Cassettes or CRISPRi Array coupled with a constitutive dCas9 module. **B.** The CRISPRi circuitry includes the IPTG-inducible double sgRNA Cassettes or CRISPRi Array coupled with a HSL-inducible dCas9 module. In each graph, temporal series of bacterial density, measured as OD_{600}, are shown over time. *Silenced strains* expressing both double sgRNA Cassettes or CRISPRi Array are treated with a range of ampicillin concentrations (on the left) or tetracycline concentrations (on the right). Growth curves are representative of a single experiment from a set of three independent biological replicates that did not show significant variations in the observed trends.

Two main considerations derived from the results described in this section. First, the repression efficiency of the CRISPRi circuitry was preserved even in the second configuration (Figure 3.1 B) in which the same plasmid carried both dCas9 expression cassette and gRNA module, either implemented as double sgRNA Cassettes or CRISPRi Array. This is an important aspect to consider as the final goal of the research project is to develop a CRISPRi platform encoded in a single conjugative vector suitable for the delivery in resistant bacteria. Second, by exploiting an inducible device, an optimal expression level for dCas9 protein was found, although the competition effect was not completely solved.

3.3 Silencing of antibiotic resistances relevant in clinical settings

Once a proof of concept of the CRISPRi-mediated silencing of resistance genes was achieved in the model system, the efficiency of the developed platform was investigated in a clinically relevant case study. To this aim, the genetic architecture based on CRISPRi Array was reprogrammed to target *NDM-1* and *mcr-1* genes which confer resistance to meropenem and colistin, respectively. These two antibiotics are extremely relevant in clinical settings as they represent an example of last resort drugs employed only in case of severe MDR infections.

3.3.1 NDM1 and mcr-1 genes repression via CRISPRi Array

The most life-threatening AMR-associated infections are caused by the dissemination, especially in clinical settings, of MDR pathogens able to withstand even the treatment with broad spectrum drugs. An example of last resort antibiotics used in these therapeutic treatments is provided by meropenem and colistin. Meropenem is an ultra-broad spectrum β-lactam antibiotic belonging to the family of carbapenem compounds. The molecule acts by inhibiting the bacterial cell wall synthesis and, to date, it is one of the main antimicrobial agents used to treat severe infections caused by both Gram-positive and Gram-negative bacteria. The resistance to this antibiotic is conferred by *NDM* gene (New Delhi metallo-β-lactamase) encoding for a β-lactamase enzyme able to hydrolyze a broad range of antibiotics including carbapenems, cephalosporins and penicillins. Moreover, *NDM* belongs to a family of MBLs (metallo-β-lactamase) enzymes that are largely distributed among carbapenem-resistant Enterobacteriaceae (CRE), able to survive in presence of clinically relevant concentrations of carbapenems [96]. CRE have also been classified as critical priority pathogens by WHO. Colistin is an antimicrobial peptide belonging to the family of polymyxins. The molecule acts by binding to lipids on the cell cytoplasmic membrane of Gram-negative bacteria thus disrupting cell wall integrity. To date, despite its adverse effects, colistin remains one of the last alternative for the treatment of MDR Gram-negative pathogens. The resistance to this antibiotic is conferred by *mcr*, encoding for a phosphoethanolamine transferase which acts by adding a phosphoethanolamine to lipid A, thus interfering with the binding of colistin to cell membrane [97]. A major concern with these resistance mechanisms is the possibility to isolate pathogens holding both resistance genes. Indeed, in clinical settings, CRE can be treated with colistin, which remains a key

resource in the therapeutic arsenal used against MDR pathogens. However, in latest years, an increasing number of CRE infections have been caused by pathogens that have also acquired resistance to colistin, thus reducing its efficacy as monotherapy treatment. As a result, a dual-therapy combing both meropenem and colistin is needed to treat this type of infections with high mortality risk [96, 98]. The CRISPRi platform developed to inhibit the expression of these two genes employed the genetic architecture of CRISPRi Array. The design process was supported by a bioinformatic analysis of all the known variants of *NDM* and *mcr* genes to select a conserved region suitable as CRISPRi target. Sequences of *NDM* and *mcr* variants were retrieved from the online database CARD (Comprehensive Antibiotic Resistance Database) and used to perform a multiple sequence alignment with Clustal Omega. With this approach, two conserved target regions were selected within the 28 variants of *NDM*, while a single conserved sequence was identified within the 9 variants belonging to the first class of *mcr* [99, 100, 101, 102]. Once identified, gRNAs sequences were implemented in four different combinations of CRISPRi Arrays to target resistant bacteria (See section 3.1.1 for a detailed description of the circuitry). In particular, to inhibit the expression of *NDM-1* gene, two different gRNAs (gNDM-1 and gNDM-2) targeting adjacent regions within the gene coding sequence were characterized as single or double spacers. The resulting Arrays were classified as: Array_NDM1, Array_NDM2 and Array_NDM1-NDM2. The latter combination, which included two guides targeting the same gene, was characterized for two main reasons: evaluate if an increase in repression efficiency could be achieved by targeting adjacent loci within the same CDS; verify if the multi-targeting based strategy could be employed to address the risk of mutations that may occur in the target region by increasing the number of repressible sequences. To implement a pair of gRNAs within the CRISPRi Array, a tail-to tail orientation was employed in order to avoid the potential steric hindrance caused by two proximal dCas9 proteins bound to the same DNA. To inhibit the expression of *mcr-1*, a single gRNA named gmcr1 was employed and cloned in tandem with gNDM1 within the same array, called Array_NDM1-mcr1; this strategy was employed to obtain a final construct suitable for the simultaneous repression of both genes. The resulting CRISPRi platform comprised two plasmids and was consistent with the one described in Figure 3.1 B: a MC vector which carried the target cassette represented by *NDM-1* or *mcr-1* gene; a LC plasmid bearing both a HSL-inducible dCas9 cassette and an IPTG-inducible CRISPRi Array module (to give an example, the complete name of the resulting LC vector was $AE_{\text{-}3A}$dArray_NDM1 but, henceforth, it will be simply identified as Array_NDM1). The experimental set-up described in Figure 3.15 was adopted to characterize the CRISPRi-mediated

silencing of *NDM-1* and *mcr-1*.

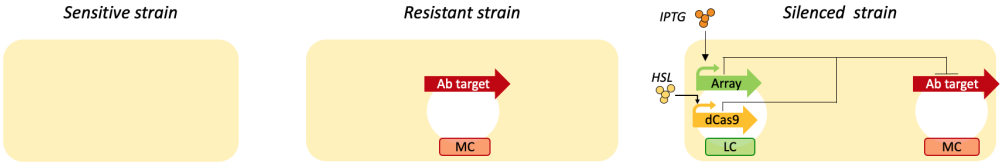

Figure 3.15: **Experimental set-up exploited to characterize the CRISPRi-mediated repression of *NDM-1* and *mcr-1* genes.** The experimental set-up employed to perform *in vivo* experiments is composed of three clones: *sensitive strain*, susceptible to antibiotic exposure; *resistant strain*, able to survive antibiotic treatment as the resistance gene (indicated as Ab target) is present in a MC vector; *silenced strain*, in which a functional CRISPRi complex restores antibiotic susceptibility by inhibiting the expression of the resistance gene. In *silenced strain*, the CRISPRi platform has an architecture consistent with the one described in Figure 3.1 B. The green arrow represents the IPTG-inducible gRNA module implemented as CRISPRi Array with single or double spacers; the yellow arrow indicates the HSL-inducible dCas9 cassette; red arrows represent the target cassette encoding for *NDM-1* or *mcr-1* resistance genes.

The bacterial growth of *sensitive* and *resistant* strains was first characterized in micro-plate liquid assays in order to determine the MIC of target antibiotics (meropenem and colistin); this preliminary step was crucial to define a window of antibiotic concentrations suitable for the characterization of *sensitive strains*. Once a MIC value for both antibiotics in the two control strains was identified, the protocol described in Section 3.1.2 was performed. In particular, the MIC of each strain was determined by analysing the growth curves in the ON/OFF states and under a range of meropenem or colistin concentrations. However, only the results relative to the ON condition are described in this section as they are more relevant for final considerations. The set of three clones employed to characterize the CRISPRi-mediated silencing of NDM1 gene included: TOP10 F' as *sensitive strain*; TOP10 F' co-transformed with pGDP1 NDM1-1 as *resistant strain*; TOP10 F' co-transformed with one of the four Arrays designed to target *NDM-1* + pGDP1 NDM1-1 as *silenced strain*. The results obtained from liquid culture assays are shown in Figure 3.16. The results were consistent with the expected outcomes as the *sensitive strain* was highly susceptible to antibiotic exposure, while the *resistant strain* withstood even the highest meropenem concentration tested, without showing relevant growth defects. The MIC value determined for *sensitive* strain was [MERO=1$\mu g/ml$]. On the other hand, *silenced strains* clearly showed the effect on bacterial growth derived from *NDM-1* gene repression. In particular, except for Array NDM2, the MIC value determined for the other combinations tested was [MERO=200$\mu g/ml$]. The lower repression efficiency exhibited by gNDM2 (for which no MIC could be established) was supposed to be dependent on the location of the target region that was more distant from the start codon

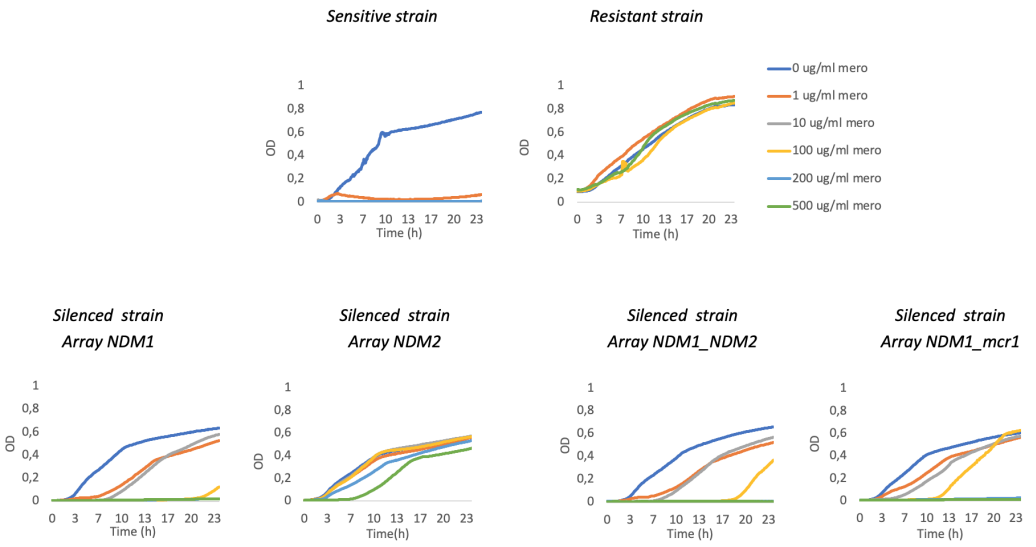

Figure 3.16: **CRISPRi-mediated repression of *NDM-1* gene with CRISPRi Arrays.** Growth curve data derived from liquid culture assays. The CRISPRi circuitry includes an IPTG-inducible CRISPRi Array coupled with a HSL-inducible dCas9 module. In each graph, temporal series of bacterial density, measured as OD_{600}, are shown over time. At t=0, *sensitive*, *resistant* and *silenced strain* (expressing 4 different combinations of Arrays targeting *NDM-1* gene) are treated with a range of meropenem concentrations in the ON state. Growth curves are representative of a single experiment from a set of three independent biological replicates that did not show significant variations in the observed trends.

than gNDM1 targeting sequence (see Appendix A.2.3 for more information about gRNAs design). This observation was coherent with data reported in the literature as a strong correlation between CRISPRi repression efficiency and distance from promoter region has already been demonstrated [43]. Results also revealed that targeting the resistance gene with a pair of gRNAs did not significantly increase the repression efficiency compared to a single spacer Array (Array_NDM1-NDM2 vs Array_NDM1), probably due to a combination of effects such as gRNA competition and low performances of gNDM2. Moreover, an interesting result derived from the comparison between Array_NDM1 and Array_NDM1-mcr1, which included a non-specific gRNA. Although in this configuration dCas9 is a shared resource, the competition between gNDM1 and gmcr1 did not result in a decrease of repression efficiency, as meropenem susceptibility was restored with both circuits and under the same MIC value. A common aspect shared with the CRISPRi-mediated repression of model ARGs is the delayed growth observed under sub-inhibitory concentrations of meropenem. This phenomenon was investigated more accurately by measuring the delay in growth recovery exhibited by all *sensitive strains* upon exposure to the drug. To this aim, growth curve data derived from liquid culture assays were processed as described in

Section 3.1.2. Results are shown in Figure 3.17. Even the analysis of de-

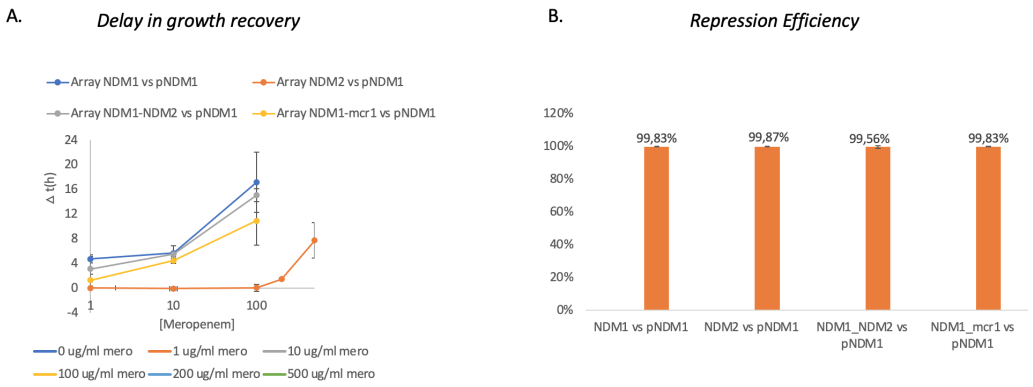

Figure 3.17: **CRISPRi-mediated repression of *NDM-1* gene with CRISPRi Arrays: growth delays and plate assays.** **A.** Delays in growth recovery measured from liquid culture assays. The CRISPRi circuitry includes an IPTG-inducible CRISPRi Array coupled with a HSL-inducible dCas9 module. CRISPRi repression efficiency of 4 different combinations of CRISPRi Arrays is measured as the delay in the time taken to reach the OD value of 0.1 in comparison to the growth of the same strains in absence of antibiotic. In each graph, the delay is reported as Δt(h) and plotted as a function of meropenem concentrations. Data points represent the average value measured for each antibiotic concentration. **B.** CRISPRi repression efficiency of 4 different combinations of CRISPRi Arrays in plate culture assays. *Silenced strains* are selected on LB + IPTG + HSL or LB + IPTG + HSL + meropenem to calculate the ratio of survivor cells to total non-treated bacteria and the relative CRISPRi repression efficiency. Error bars represent the standard errors of the mean of at least 3 independent experiments.

layed growth confirmed no relevant differences between repression efficiency of single or double spacer Arrays; on the other hand, for the same antibiotic concentrations, the Array encoding the non-specific guide gmcr1 showed a slight decrease in repression strength which could not be appreciated by the determination of MIC value from liquid assays. It is also worth mentioning that the population of survivor cells that recovered after the initial antibiotic administration could be represented by resistant or resilient cells, as observed with ampicillin treatment. Indeed, like *bla*, *NDM-1* encoded for a β-lactamase that can be released in the growth medium because of cell lysis. If a sufficient amount of enzyme is released from killed cells, residual meropenem can be degraded over time for individual clones to recover and proliferate. Consequently, a delay in growth recovery is observed with increasing meropenem concentrations. To prove this hypothesis, a supernatant assay was performed as described in Section 3.1.2. As expected, the supernatant from *silenced strain* expressing Array_NDM1 did not contain enough meropenem to inhibit the growth of a sensitive strain compared to the supernatant collected from TOP10 F' culture, which produced the expected inhibition zone on LB plate (data not shown). The efficiency of CRISPRi circuitry to restore antibiotic susceptibility was also evaluated through plate culture assays performed as described in Section 3.1.2. By comparing the

ratio of CFUs under two conditions in which meropenem was either absent or added at a concentration of [$64\mu g/ml$], as reported in [103], the high repression efficiency of all the combinations of CRISPRi Arrays was again demonstrated. As shown in Figure 3.17 B, targeting *NDM-1* with a CRISPRi Array encoding for single or double spacers effective re-sensitized almost the entire bacterial population to meropenem treatment with a MIC value of [MERO=$64\mu g/ml$]; in plate culture assays, differences in repression efficiency dependent on competition effect or target site location were thus overcome by the strong repression capability of the CRISPRi circuitry. This result could be interpreted as a snapshot at time zero of bacterial response. Indeed, compared to liquid culture where the secreted β-lactamase was well distributed in the growth medium and could support the rescue of resilient cells, in plate assays this advantage was absent during the selection of survivor cells. The experimental set-up described in Figure 3.15 was also adopted to characterize the CRISPRi-mediated silencing of *mcr-1* gene. The protocol described in Section 3.1.2 was carried out by employing the following three clones: TOP10 F' as *sensitive strain*; TOP10 F' co-transformed with pGDP2 mcr-1 as *resistant strain*; TOP10 F' co-transformed with Array_NDM1-mcr1 + pGDP2 mcr-1 as *silenced strain*. All the results obtained from liquid and plate culture assays are shown in Figure 3.18. As expected, growth curve data showed that the *sensitive strain* was highly susceptible to antibiotic exposure with a MIC value of [COLIS=$1\mu g/ml$]; on the other hand, *resistant strain* could not grow in presence of colistin concentrations grater than $8\mu g/ml$ thus the MIC value was fixed at [COLIS=$20\mu g/ml$]. This result clearly demonstrated the potent antimicrobial effect of this antibiotic even towards resistant strains. In *silenced strain*, the CRISPRi-mediated repression of *mcr-1* gene resulted in a MIC value of [COLIS=$4\mu g/ml$] and a consistent delay in growth recovery was also detected for lower antibiotic concentrations. Even in this case, the rescue of survivor cells was accurately investigated by measuring the delayed growth for each concentrations of colistin included in the tested window (Figure 3.18 B). A strong correlation between the increasing in antibiotic concentration and the delay in the time taken to reach the fixed OD value was observed even in this case study, confirming that the CRISPRi repression efficiency could also be measured as a function of the delay in growth recovery exhibited by *silenced strains* upon antibiotic exposure. Results derived from plate culture assays were also extremely promising. By comparing the ratio of CFUs under two conditions in which colistin was either absent or added at a concentration of $1\mu g/ml$, the high repression efficiency of the CRISPRi circuitry was again demonstrated. As shown in Figure 3.18 C, targeting *mcr-1* with a CRISPRi Array encoding for gmcr1 along with a non specific gRNA (gNDM1) effective re-sensitized almost the entire bacterial population to colistin treatment

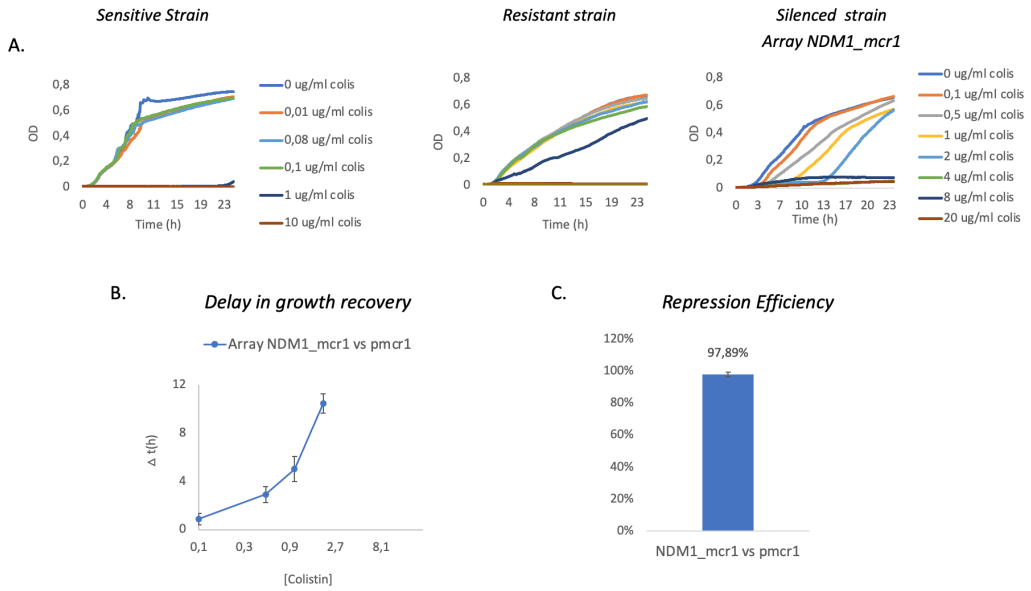

Figure 3.18: **CRISPRi-mediated repression of *mcr-1* gene with CRISPRi Array: growth curves, growth delays and plate assays.** **A.** Growth curve data derived from liquid culture assays. The CRISPRi circuitry includes an IPTG-inducible CRISPRi Array coupled with a HSL-inducible dCas9 module. In each graph, temporal series of bacterial density, measured as OD_{600}, are shown over time. At t=0, *sensitive*, *resistant* and *silenced* strain (expressing Array_NDM1-mcr1) are treated with a range of colistin concentrations in the ON state. Growth curves are representative of a single experiment from a set of three independent biological replicates that did not show significant variations in the observed trends. **B.** Delays in growth recovery measured from liquid culture assays. CRISPRi repression efficiency of CRISPRi Array_NDM1-mcr1 is measured as the delay in the time taken to reach the OD value of 0.1 in comparison to the growth of the same strain in absence of antibiotic. In each graph, the delay is reported as Δt(h) and plotted as a function of colistin concentrations. Data points represent the average value measured for each antibiotic concentration. **C.** CRISPRi repression efficiency in plate culture assays. *Silenced strains* are selected on LB + IPTG + HSL or LB + IPTG + HSL + colistin to calculate the ratio of survivor cells to total non-treated bacteria and the relative CRISPRi repression efficiency. Error bars represent the standard errors of the mean of at least 3 independent experiments.

with a concentration of [COLIS=$1\mu g/ml$]. As observed in the previous case studies, CRISPRi repression efficiency in plate assays resulted in an almost complete cell killing for antibiotic concentrations lower than the MIC value determined in liquid culture; this phenomenon must be investigated more accurately in order to highlight if a dependence on the type of growth medium could explain the different behaviour of survivor cells. Being the plate assays a means of providing snapshot data at the initial inoculum time, a possible explanation is the emergence of escape mutants that become enriched in the liquid culture but correspond to a few survivor colonies in plate assays.

In this Section, high-impact results have been presented. First, it was demonstrated that the CRISPRi platform herein developed can be efficiently employed to inhibit the expression of clinically relevant resistance genes. Compared with *resistant strains*, a reduction of MIC value for both target antibiotics, meropenem and colistin, was determined in liquid culture assays

for *silenced strains*. The analysis of growth delay, as well as the measurement of repression efficiency from plate assays, revealed that a CRISPRi Array encoding double spacers, both targeting *NDM-1* or *NDM-1* and *mcr-1*, did not suffer the competition effect derived from the expression of two gRNAs. This was an important result as it demonstrated that the multi-targeting capability of CRISPRi circuitry could be efficiently employed as its repression strength was not altered by the competition effect.

3.4 Analysis of escaper cells

The CRISPRi platform herein developed was programmed to target four different resistance genes: *bla*, *tetA*, *NDM-1* and *mcr-1*. For each case study, the results from liquid assays revealed that a sub-population of cells recovered from a background of re-sensitized bacteria upon the exposure to target antibiotics. The rescue of survivor cells, defined as "escapers", was accurately investigated with different methods. First, the delayed growth of *silenced strains* at the end of microplate assays was measured through the method describe in Section 3.1.2; results obtained from this analysis, along with those derived from supernatant assays, are discussed in Section 3.2. To better understand the nature of escaper cells and distinguish between resistant or resilient phenotype, cells that have recovered from the first round treatment were collected and re-exposed to the same range of target antibiotic concentrations according to the protocol described in Section 3.1.2. This analysis was particularly indicated to study the effect of CRISPRi repression on *bla* and *NDM-1* gene as, in both cases, the resistance mechanism is dependent on an enzyme that degraded β-lactam antibiotics (the effect on antibiotic degradation was proven with supernatant assays described in previous Section). This analysis was based on the assumption that the temporal dynamic of resilient cells after second round treatment must resemble the one observed upon the first administration of target antibiotic, as the rescue of resilient cells is only dependent on the β-lactamase-mediated degradation of residual drug. If, as a consequence of the antibiotic treatment, a population of mutants with increased tolerance is selected, a different response to drug exposure is expected to emerge from the analysis of time courses. Results included also the analysis of *mcr-1* escapers and are shown in Figure 3.19, in which some representative growth curve data are reported. Data revealed that, in some cases, the recovery of escaper cells was due to the selection of a sub-population of resilient cells (e.g., see Array_NDM1 in Figure 3.19), which was an observation consistent with the expected activity of β-lactamases secreted by killed cells [93]. In the remaining cases, the bacterial response

resulted in an increased MIC value as well as in a reduced delay in growth recovery, as expected from the selection of resistant mutants with increased tolerance.

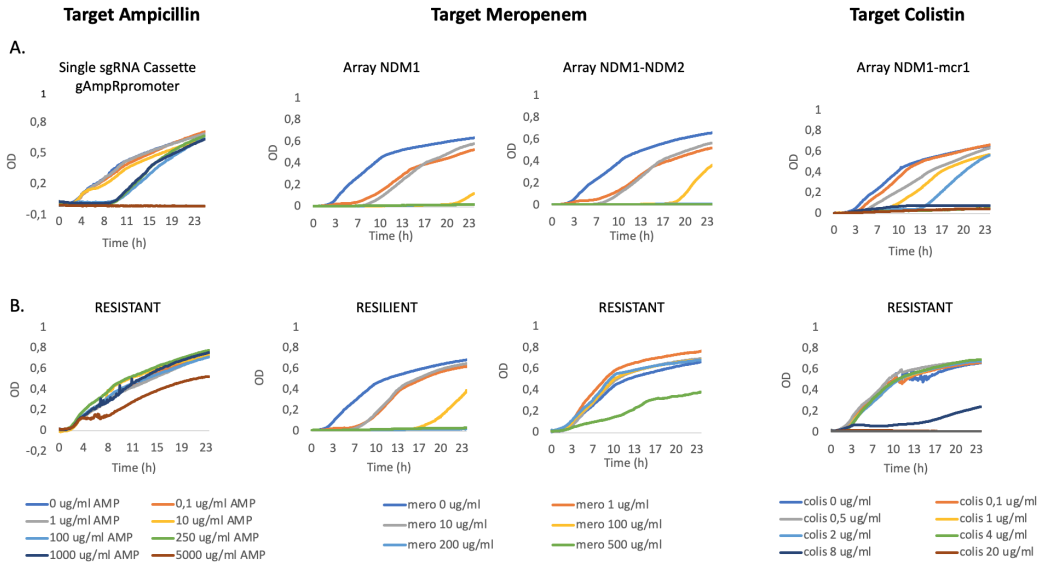

Figure 3.19: **Escaper analysis after first and second round treatment with target antibiotics.** Growth curve data derived from liquid culture assays. *Silenced strains* with CRISPRi circuitry in the ON state are treated with a range of target antibiotic concentrations. **A.** First round treatment of original clones never exposed to target antibiotic. **B.** Second round treatment of escaper cells that have recovered after antibiotic exposure in first round experiments. In each graph, temporal series of bacterial density, measured as OD_{600}, are shown over time. At t=0, *silenced strains* (expressing CRISPRi circuitry with the architectures of sgRNA Cassette or Array) are treated with a range of ampicillin (column on the left), meropenem (columns in the centre) or colistin (column on the right) concentrations.

To study more carefully the behaviour of cells that survived the treatment with meropenem and colistin, three escaper colonies from different experiments were isolated and characterized after exposure to a single antibiotic concentration. This procedure was employed to test whether the phenotype of a resistant or resilient cell was conserved among different experiments. *Resistant strains* as well as *original silenced strains* were included in the same test. At the end of the liquid assay, the measurement of delayed growth was expected to produce a similar result when comparing resilient escapers with *original silenced strains* and resistant escapers with *Resistant strains*. Results are shown in Figure 3.20.

In two out of three cases, escaper cells emerged from the CRISPRi-mediated silencing of *NDM-1* gene through Array-NDM1 and -NDM1-NDM2 were represented by a sub-population of resilient cells. Array_NDM1-mcr1 was the only exception as a population of resistant escapers was isolated in three out of three cases. The same phenotype was also exhibited by escaper

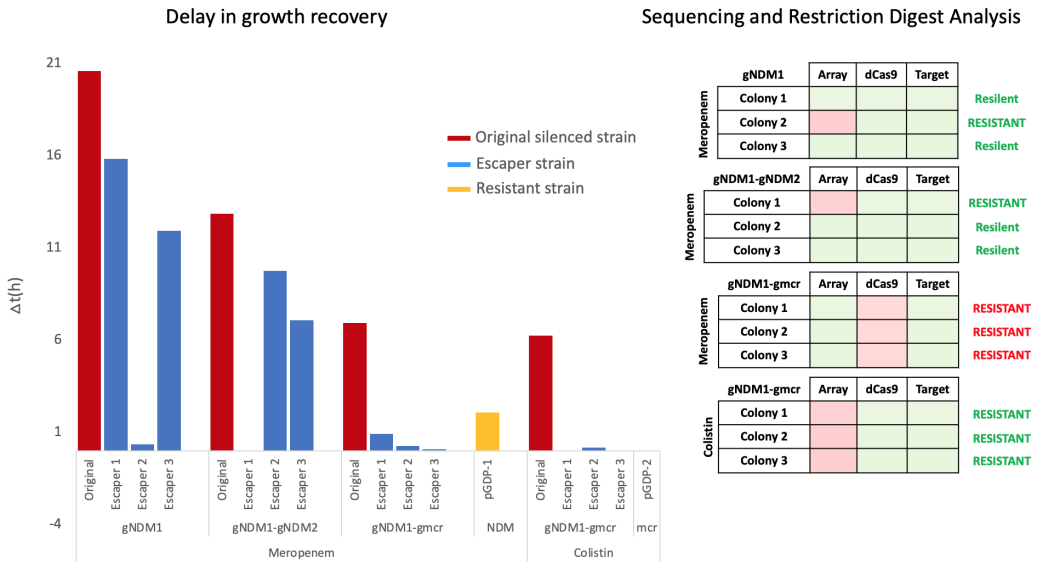

Figure 3.20: **Escaper analysis via liquid assays, DNA sequencing and restriction digest.** On the left, delays in growth recovery measured from liquid culture assays. Three different escaper colonies for each CRISPRi Array targeting *NDM-1* or *mcr-1* gene are isolated from first round experiments and characterized along with *resistant* and *original silenced strains* in a second round experiment with a single antibiotic concentration. CRISPRi repression efficiency is measured as the delay in the time taken to reach the OD value of 0.1 in comparison to the growth of the same strains in absence of antibiotic. In the graph, the delay is reported as Δt(h). On the right, plasmid DNA purified from escaper cells is analysed via sequencing analysis and restriction enzymes digestion. Results are reported in four different tables and each table refers to a single *escaper strain* expressing a specific CRISPRi Array. Results for single colonies are reported in rows, while the site covered by sequencing analysis or verified through restriction digest is reported in columns. Green boxes indicate unaltered sequences, while red boxes indicate mutated sequences bearing nucleotide mutations or DNA arrangements.

cells emerged from the CRISPRi-mediated silencing of *mcr-1* gene. To more accurately investigate the nature of escaper cells, the DNA regions assumed to be susceptible to nucleotide mutations were studied through sequencing analysis. In particular, the sequences of dCas9, Array and target gene were analysed to investigate whether the resistant phenotype of escaper cells could be dependent on mutations within CRISPRi circuitry or target sequence. Plasmids purified from escapers were also analysed via restriction enzymes digestion to identify large rearrangements within the CRISPRi-encoding circuit (not detectable via DNA sequencing) or an increase in the copy number of the plasmid bearing the resistance gene. To this aim, the protocol described in Section 3.1.2 was performed with the same set of escaper clones (three for each construct) characterized with liquid assays. Results are shown in Figure 3.20. In the majority of cases, the phenotype observed in liquid assays was correlated with the genotype resulted from sequencing analysis. Indeed, cells identified as resistant escapers showed a mutation within the CRISPRi Array sequence, in which the deletion of single or double spacers

was detected. In case of Array_NDM1-mcr1 targeting *NDM-1* gene, although sequencing analysis did not show nucleotide mutations within the considered sequences, restriction enzymes digestion revealed the presence of an insertion within the dCas9 expression module, thus justifying the observed resistant phenotype. Finally, compared to original engineered strains never exposed to target antibiotic, no significant variation in the copy number of plasmid carrying the resistance gene was detected.

The results described in this section are extremely interesting because, through the analysis of escaper cells, two different bacterial antibiotic responses were deep characterized: resistance and resilience. Moreover, except in one case, the majority of escaper cells showed a resilient or resistant phenotype that was consistent with results derived from sequencing analysis. Finally, the most relevant aspect highlighted in this study concerns the identification of loss of function mutations only within the CRISPRi Array sequence, while no alterations in the target gene were detected. This aspect is of great importance as it proves that a silencing strategy based on CRISPRi technology has the potential to preserve target DNA from the risk of generating new variants of resistance genes.

3.5 Full workflow: conjugation of CRISPRi devices and silencing of resistance genes

To date, the major challenge in the therapeutic deployment of CRISPR-based antimicrobials is the need to develop an efficient delivery strategy to mobilize synthetic circuits in target bacteria. Different transfer mechanisms, even inspired by existing natural strategies, have already been exploited to address this goal (Section 1.3). In this work, a synthetic platform based on bacterial conjugation was developed and characterized. First, the main features required by a conjugative system were studied in depth in order to design a mobilizable vector well suited for the delivery of the CRISPRi-encoding circuits previously characterized. A detailed description of the CRISPRi conjugative platform is provided in Section 3.5.1. Second, the conjugation between donor and resistant recipient strains was performed with an optimized experimental protocol that led the quantitative characterization of the conjugative transfer, using the *conjugation efficiency* index. Finally, the designed conjugative platform was successfully employed to mobilize the CRISPRi repressor complex in recipient bacteria harbouring *bla* (ampicillin resistance) or *mcr-1* (colistin resistance) gene and the transcriptional repression of both resistances was determined through the *killing efficiency* index

(Sections 3.5.2 and 3.5.3).

3.5.1 CRISPRi-based conjugative platform

Along with transformation and transduction, bacterial conjugation is a widespread HGT mechanism that provides plasticity to bacterial genome but is also involved in the dissemination of antibiotic resistances in microbial communities. Conjugative transfer is a phenomenon that occurs when a bacterial species, identified as donor strain, transfers DNA to a recipient bacterium in close contact. In case of Gram-negative bacteria, a bridge named conjugative pilus establishes a direct contact between the mating pair and allows transfer of genetic material, usually plasmid DNA, from donor to recipient cell. In Gram-positive bacteria, the conjugation occurs when a donor cell first responds to the presence of pheromones released by recipient cell and then starts to synthesize aggregation substances that allow the contact between the plasmid-bearing and plasmid-free cell. The set of genes responsible for the conjugative transfer are grouped in two main operons, *mpf* and *dtr*, that ensure mating pair formation and DNA processing and mobilization. When these genes are encoded by an autonomous conjugative plasmid, a self-transmissible conjugation occurs and all recipient cells that have received the plasmid became potential donors in subsequent rounds of conjugation. If the conjugative machinery is expressed in *trans* from helper plasmids or chromosomal DNA, a non-self-transmissible conjugation occurs and recipient cells that have received the mobilizable plasmid cannot become donors as they lack the transfer and replication functions needed to support a subsequent round of conjugation. With both mechanisms, autonomous conjugative and mobilizable plasmids contain a DNA sequence, named oriT (origin of transfer) which is recognized by the molecular machinery responsible for the DNA transfer. In this study, a non-self-transmissible conjugation was performed in order to deliver a mobilizable plasmid encoding for the CRISPRi circuitry to resistant recipient cells. To this aim, a *trans*-conjugative platform was developed by employing two vectors: the helper plasmid pTA-Mob [88], which provided all the HGT functions needed in a conjugation, and a mobilizable vector carrying both the CRISPRi circuitry and the oriT from RK2 plasmid recognized by the molecular machinery expressed in *trans* from pTA-Mob. Indeed, as a derivative of RK2, pTA-Mob is a broad-host-range plasmid that allows the use of several bacterial hosts as donors for conjugation of $oriT_{RK2}$-carrying vectors. A detailed scheme of a non-self-transmissible conjugation is provided in Figure 3.2. To construct this experimental set-up, pTA-Mob was kindly provided by Prof. Rahmi Lale (NTNU, Norway), while the oriT sequence was first amplified from RK2 plasmid and then cloned in $AE_{\text{-3A}}$d

Arrays vectors designed to target *bla* and *mcr-1* gene. As the complete nucleotide sequence of RK2 was not available on the main biological on line databases, a detailed bioinformatic analysis on previous works was carried out in order to identify the oriT sequence from the used primers and select only a functional region lacking undesirable promoter sequences. In the following two sections, results regarding the conjugative transfer of CRISPRi Arrays targeting *bla* and *mcr-1* gene are shown.

3.5.2 Conjugative transfer of CRISPRi Array to target bla gene

The conjugative transfer of CRISPRi circuitry was first addressed by employing a model system in which the donor strain harboured a mobilizable CRISPRi circuitry targeting *bla* and the recipient strain carried the target gene conferring ampicillin resistance. In detail, the conjugative system studied was composed of the following mating pair:

- *E. coli* DH10B co-transformed with oriT_AE$_{\text{-3A}}$dArray gAmpRpromoter _gtetA + pTA-Mob, which represented the donor strain;
- *E. coli* TOP10 F' transformed with I3521 plasmid carrying *bla* target gene as recipient strain.

As discussed in the previous section, this experimental set-up was exploited to perform a non-self-transmissible conjugation. In donor strain, pTA-Mob helper plasmid mobilized oriT_AE$_{\text{-3A}}$dArray gAmpRpromoter _gtetA vector (henceforth simply Array_Amp-tet) towards the recipient strain. At the end of the conjugation, a new population of cells defined as transconjugant was selected. In this case study, each transconjugant cell harboured both Array_Amp-tet and I3521 plasmids. As the repression efficiency of the CRISPRi Array targeting the promoter placed upstream of *bla* was previously demonstrated (see Section 3.2), the same synthetic circuit was employed to construct a CRISPRi-based mobilizable vector, carrying the oriT$_{\text{RK2}}$ sequence, constructed according to the protocol described in Appendix A.2. Since the final architecture of CRISPRi circuitry was consistent with the one described in Figure 3.1 B, the expression of the repressor complex was activated only upon the addition of two inducers molecules: IPTG, which triggered the activity of P_{LlacO1} promoter placed upstream CRISPRi Array module; HSL which activated the expression of dCas9 cassette under P_{Lux-3A} promoter. Taking advantage of this inducible system, the conjugative transfer of CRISPRi circuitry was studied in the OFF and ON state: the former was

needed to evaluate the efficiency of the conjugative transfer without compromising the growth of transconjugants; the latter was used to characterize the CRISPRi-mediated killing of resistant strain upon exposure to target antibiotic. Indeed, it was expected that the expression of *bla* gene was not inhibited by the gRNA:dCas9 complex in the OFF state, thus transconjugants could withstand the treatment with ampicillin. In the ON state, thus in presence of inducer molecules, an active repressor complex was assembled in resistant cells in which the CRISPRi-mediated silencing of *bla* restored antibiotic susceptibility. Before evaluating its killing efficiency, the conjugative transfer of CRISPRi circuitry was studied in the OFF state in order to verify that an efficient genetic transfer could be carried out in our experimental set-up. The performances of the conjugative platform were quantitatively characterized by determining the *conjugation efficiency* parameter, which provided an indication about the amount of cells transformed in transconjugants relative to total recipient cells. To this purpose, a conjugation experiment was performed with the mating pair described at the beginning of this paragraph and by selecting transconjugants on LB plates supplemented with chloramphenicol (Array_Amp-tet vector) and ampicillin (I13521 vector), according to the expected outcome (the complete list of inducers, antibiotics and the relative concentrations used in each assay are reported in Appendix A.1). Starting from a general protocol [90], the conjugation assay was optimized by modifying the following parameters:

- OD value at which donor and recipient cells were combined before conjugation;
- bacterial growth phase of both donor and recipient cells (stationary or exponential);
- dimension of the conjugation mixture spotted on non selective plate.

The first parameter was studied in order to evaluate if, by varying bacterial density, the efficiency of conjugative transfer could be improved. By employing the same mating pair, the conjugation was carried out in two different conditions: in the first one, the mating pair was combined at an OD value of 0.5; in the second one, liquid cultures of both donor and recipients were diluted to an OD value of 0.15 and combined in a conjugation mixture before the mating. As shown in Figure 3.21, results revealed that the efficiency of the genetic transfer depended on the "OD value parameter" as, by employing diluted cultures (OD=0.15), the conjugation efficiency was substantially decreased, probably due to a reduced cell to cell contact in the mating mixture. The second parameter investigated in this study was the

bacterial growth phase. It is known that the growth of a bacterial culture in "a close system" (batch culture) can be divided in the following phases: lag phase, during which the number of viable cells is not substantially increased; log phase, in which an exponential increase in the number of bacterial cells is observed; stationary phase, during which bacterial density reaches a plateau as the rate of cell division equals the rate of cell death; decline phase, in which a rapid decrease in the number of viable cells is registered due to the depletion in nutritional resources. As conjugation is a resource-consuming process that depends on the employment of different molecular machineries, it was expected that the conjugative transfer reached the best performance during log phase, when the cellular fitness is at the highest level. To test this hypothesis, the conjugation was carried out with the same mating pair but in two different conditions: in the first one, saturated cultures of donor and recipient cells in stationary phase were combined in the mating mixture; in the second one, the same liquid cultures were diluted and incubated again to reach the exponential growth phase and then combined in the conjugation mixture. In each condition, the OD value was varied (OD=0.2 - 0.5 - 1) in order to study the combined effect of both parameters on *conjugation efficiency*. Data revealed that the best result was achieved by combining donor and recipient cells in stationary phase at an OD value of 0.5. However, a complete analysis of the results suggested that, for different OD values, the *conjugation efficiency* obtained by employing cells in exponential phase resulted in a more stable range of values than the one observed in stationary phase. For this reason, the following conjugation assays were carried out with bacterial cultures in exponential growth phase. This experiment also demonstrated that the highest OD value among those tested (OD=1) did not increase *conjugation efficiency* but could even reduce it by two orders of magnitude. The last parameter considered in this study was the dimension of the conjugation mixture spotted onto the LB plate before the mating. Since bacterial growth is dependent on the presence of nutritional resources in the growth medium, we investigate whether a higher access to nutrients could improve the conjugative capability of the mating strains. To investigate this aspect, the distribution area of the conjugation mixture spotted on the solid medium was increased, thus enabling the access to nutrients to as many cells as possible. The conjugation was thus carried out with the same mating pair but varying the dimension of the spot containing the conjugation mixture. As it was a pilot test, the area of the spot containing the cultures was not measured and will be generically indicated as "regular" (spotted and then incubated) or "increased" (spotted, spread to enlarge the cultured area, and then incubated) if its size was comparable to or greater than the one obtained in previous conjugations. For this experiment, donor and recipi-

ent cells in exponential growth phase were combined at an OD value of 0.5. The comparison between the two conditions highlighted that an increased distribution area of the mating mixture did not substantially improve *conjugation efficiency*. Overall, the results described so far prove that CRISPRi

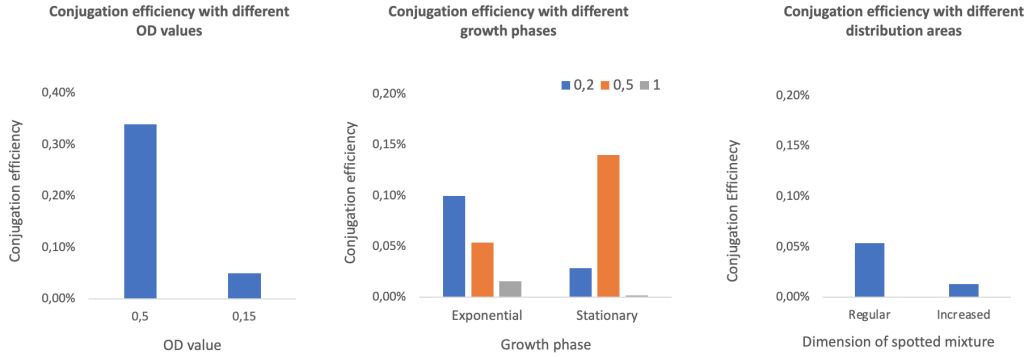

Figure 3.21: **Optimization of the conjugation protocol in a model case study.** A model conjugative system is composed of two actors: a donor strain, harbouring both pTA-Mob helper plasmid and a mobilizable CRISPRi circuit targeting *bla* gene; a recipient strain, carrying the target gene conferring ampicillin resistance. At the end of the conjugation, transconjugants are selected on LB + CM + AMP and recipients on LB + AMP. In each graph, conjugation efficiency is reported as the ratio of transconjugants to the total amount of recipient cells. On the left, conjugation efficiency measured by combining the mating pair at two different OD values before conjugation. In the centre, conjugation efficiency measured by combining the mating pair in two different growth phases. On the right, conjugation efficiency measured by combining the mating pair in a conjugation mixture having a distribution area comparable (regular) or greater (increased) than the one usually obtained.

circuitry can be delivered in resistant recipient cells through bacterial conjugation. By leveraging the *trans*-conjugative platform herein developed, a conjugation efficiency ranging from $3x10^{-3}$ to $1x10^{-5}$ was achieved by comparing all the tested conditions. Although the conjugation frequency is low in absolute terms, the values obtained were consistent with those reported in a scientific work where a conjugative platform based on pTA-Mob helper plasmid reached a conjugation efficiency ranging from $1x10^{-3}$ to $1x10^{-5}$ [48]. This observation demonstrated that the interventions carried out to optimize the conjugation assay were suitable to reach a result consistent with previously reported data. The optimized conjugation protocol is reported in Section 3.1.2. Once a proof of concept of the CRISPRi conjugative transfer was achieved and the conjugation protocol was properly optimized, the repression efficiency of the mobilizable circuit targeting *bla* was investigated by performing new conjugation assays. While *conjugation efficiency* was studied by maintaining the circuitry in the OFF state, the ON state was needed to assay the CRISPRi-mediated silencing of target gene. To this aim, *killing efficiency* was investigated under two conditions in which target antibiotic was always present at a concentration of [AMP= $1000\mu g/ml$] and the CRISPRi circuitry was either expressed (ON state) or not (OFF state).

Indeed, as ampicillin was needed to select transconjugant cells from the conjugation mixture, only the presence or absence of inducer molecules (OFF vs ON state) led the possibility to discriminate between susceptible bacteria and still resistant ones. This way, the repression capability of the CRISPRi-based conjugative platform was estimated as the ratio between transconjugant cells with induced CRISPRi and transconjugant cells with repressed CRISPRi (see Section 3.1.2). From an experimental point of view, a complete active state was reached by adding IPTG and HSL in the growth medium. Moreover, as the dynamic of gene expression depended on the inducer molecules used, the selection of transconjugants was carried out by exploiting two experimental conditions: in the first one, the induction of CRISPRi circuitry was achieved by adding the inducers in the solid growth medium used to select transconjugants at the end of the conjugation assay (induction and selection at the same time in solid medium); in the second condition, the mating mixture scraped-up from LB plate was first inoculated in liquid medium supplemented with IPTG + HSL in absence of ampicillin and, after 1h incubation at 37°C, the culture with CRISPRi machinery activated was plated on selective plates containing the same inducer molecules (induction in liquid medium before selection in solid medium). The first experimental condition was based on the assumption that the simultaneous administration of inducers and target antibiotic was sufficient to activate the repressor complex in time to restore antibiotic susceptibilty in transconjugant cells; otherwise, if the dynamics of gene expression required a longer time window for CRISPRi to reach an effective active state, than the best result would be achieved with the second experimental condition. As shown in Figure 3.22, almost the entire recipient population that have received the CRISPRi circuitry was effectively re-sensitized to ampicillin, with no relevant differences between the two experimental conditions analysed; this aspect was particularly advantageous as it demonstrated that a pre-incubation of mating mixture in liquid medium supplemented with inducers could be avoided in order to simplify an assay that resulted already functional with the first experimental set-up (induction and selection at the same time in solid medium). The results described in this section are extremely promising as they demonstrate that the complete workflow, including conjugative transfer and target gene repression, can be successfully reached in resistant bacteria. Indeed, although the efficiency of the genetic transfer was relatively low but consistent with previously reported data, almost the entire target population that received the CRISPRi circuitry was re-sensitized to ampicillin treatment. Moreover, the experimental protocol developed to investigate the dynamics of gene expression revealed that the selection of survivor transconjugants in the ON state could be performed by simultaneously administering inducers and tar-

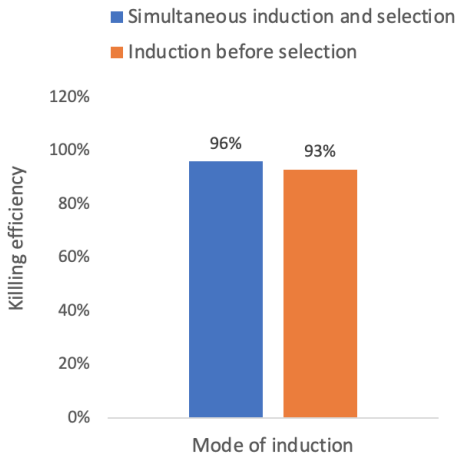

Figure 3.22: **Conjugative transfer of CRISPRi circuitry to inhibit the expression of *bla* gene.** The conjugative system is composed of two actors: a donor strain, harbouring both pTA-Mob helper plasmid and a mobilizable CRISPRi circuit targeting *bla* gene; a recipient strain, carrying the target gene conferring ampicillin resistance. At the end of the conjugation, transconjugants are selected under two conditions: the OFF state, by employing LB plates supplemented with CM + AMP; the ON state, by employing LB plates supplemented with CM + AMP + inducers. In the graph, killing efficiency is reported as the ratio of transconjugants detected in the ON state to transconjugants detected in the OFF state. At the end of the overnight incubation, transconjugants are selected from the mating mixture by exploiting two experimental conditions: in the first one (blue bar) inducer molecules and target antibiotic are added simultaneously on solid medium; in the second one (orange bar), inducers are added before selection during a pre-incubation in liquid medium.

get antibiotic in solid medium; this meant that the dynamics of CRISPRi expression was relatively fast and did not require a longer induction window to reach a functional active state. Based on these findings, the CRISPRi-conjugative platform was programmed to target a population of resistant bacteria harbouring *mcr-1* gene, which confers resistance to colistin, in order to provide a demonstration of full HGT-killing workflow in a clinically relevant case study.

3.5.3 Conjugative transfer of CRISPRi Array to target mcr-1 gene

The results derived from the characterization of a model conjugative system (Section 3.5.2) proved that the genetic platform herein developed, based on a *trans*-conjugative set-up, could be efficiently employed to deliver CRISPRi-based antimicrobials in resistant bacteria. Moreover, as the transcriptional inhibition of target gene was confirmed with encouraging results, the performances of the conjugative platform, both in terms of *conjugation* and *killing efficiency*, were investigated in a clinically relevant case study. This time, the population of resistant bacteria was represented by an *E. coli*

strain harbouring *mcr-1* gene which confers resistance to colistin, a broad-spectrum antibiotic used as last resort drug only in case of severe MDR infections. On the other hand, the donor strain was engineered with a mobilizable CRISPRi circuitry *ad hoc* designed to target *mcr-1* gene. In detail, the conjugative system studied was composed of the following mating pair:

- *E. coli* DH10B co-transformed with oriT_AE$_{\text{-3A}}$dArray NDM1_mcr1 + pTA-Mob, which represented the donor strain;
- *E. coli* DH5α with the recombinant plasmid pGDP2 mcr-1 carrying the target gene as recipient strain.

As discussed in the previous section, this experimental set-up was exploited to perform a non-self-transmissible conjugation. In donor strain, pTA-Mob helper plasmid mobilized oriT_AE$_{\text{-3A}}$dArray NDM1_mcr1 vector (henceforth simply Array_NDM1-mcr1) towards the recipient strain engineered with pGDP2 mcr-1 carrying colistin resistance. A the end of the conjugation, the population of transconjugants selected harboured both Array_NDM1-mcr1 and pGDP2 mcr-1 plasmids. As the repression efficiency of the CRISPRi Array targeting *mcr-1* gene was previously demonstrated (see Section 3.3), the same synthetic circuit was employed to construct a CRISPRi-based mobilizable vector. The latter, carrying the oriT$_{\text{RK2}}$ sequence, was constructed according to the protocol described in Appendix A.2. The final architecture of the CRISPRi circuitry was consistent with the one described in Figure 3.1 B, in which the expression of both dCas9 and gRNA modules was under the control of a HSL- and IPTG-inducible devices, respectively. This meant that the expression of the repressor complex was activated only upon addition of both inducer molecules. By leveraging this functional feature, the conjugative transfer and the subsequent CRISPRi-mediated repression of *mcr-1* gene were investigated in the OFF state to calculate *conjugation efficiency* and either in the OFF and ON state to calculate *killing efficiency*. Once the conjugation assay was optimized, the definitive protocol reported in Section 3.1.2 was performed in order to first confirm the conjugative transfer of the CRISPRi circuitry in recipient cells and second to verify if the activation on the repressor complex in transconjugants could effectively re-sensitize resistant strain to colistin treatment. The conjugation assay was thus carried out by combining donor and recipient cells in exponential growth phase at an OD value of 0.5 and by selecting transconjugants on LB plates supplemented with chloramphenicol + [colistin= $1\mu g/ml$] or chloramphenicol + [colistin= $1\mu g/ml$] + inducers to discriminate between OFF and ON state, respectively (the complete list of inducers, antibiotics and the relative concentrations used in each assay are reported in Appendix A.1). *Conjugation*

and *killing efficiencies* were calculated as described in Section 3.1.2. Even in this case study, the performances of CRISPRi circuitry were extremely promising. The ratio between transconjugants in the OFF state to total recipient cells resulted in a *conjugation efficiency* of 0.19%, a value that was consistent with the results showed in the previous section; the ratio between transconjugants in the ON to transconjugants in the OFF state resulted in a *Killing efficiency* of 99.58%, which again demonstrated that almost the entire target population that had received the CRISPRi circuitry was effectively resensitized to colistin treatment. Although these preliminary results must be confirmed in order to obtain a robust validation of the CRISPRi-based conjugative platform, they already highlight some aspects that require a deeper characterization. To give an example, even if the high repression capability of the CRISPRi circuitry was demonstrated in both case studies (ampicillin and colistin resistances), the leakage in the activity of the repressor complex in absence of inducer molecules must be taken into account. Indeed, during the selection of transconjugant cells, a complete discrimination between ON and OFF state could not be achieved due to the basal activity of the inducible platform. For this reason, an optimized strategy for the selection of transconjugants must be developed. For example, in case of resistant bacteria harbouring *mcr-1* gene, the selection of transconjugants in the OFF state could be carried out by employing LB plates supplemented with chloramphenicol and kanamycin, instead of colistin. Indeed, on the recombinant vector carrying *mcr-1* gene, a marker cassette encoding for kanamycin resistance is also present. This strategy could be useful not only to circumvent the leakage in the activity of CRISPRi circuitry, but also to properly calculate the *conjugation efficiency*, that can be under-estimated due to the basal activity of the repressor complex. The same strategy could not be applied in case of resistant bacteria harbouring *bla* gene as the backbone of I13521 plasmid does not contain other marker cassettes. The described issue is relevant for characterization purposes, in which the OFF state is important, while a final application of such circuits will have the CRISPRi circuitry in ON state.

3.6 Main considerations on CRISPRi-based silencing of resistance genes and bacterial conjugation as delivery strategy

The first scientific challenge addressed in the research project herein presented was the design and characterization of a CRISPRi circuitry to restore

antibiotic susceptibility in resistant bacteria. By harnessing the highly flexible nature of CRISPR technology, the genetic platform described in Section 2.1 was reprogrammed in order to target a set of genes classified as model or clinically relevant resistances. To this aim, an efficient CRISPRi platform was implemented in synthetic circuits by exploiting two main genetic architectures: sgRNA Cassette, expressing single or double sgRNAs, and CRISPRi Array, carrying one or two spacers. A proof of concept of the CRISPRi-mediated antimicrobial action was achieved in a model case study in which *bla* and *tetA*, conferring resistance to ampicillin and tetracycline, represented the final targets. The CRISPRi mediated silencing of model resistances revealed that even targets in high copy plasmids could be efficiently repressed, but also confirmed that the location of the target site could strongly affect repression strength. Moreover, a leakage in P_{LlacO1} promoter activity emerged from *tetA* gene repression, highlighting that a small amount of CRISPRi repressor complex was already present in the OFF state. The architectures designed to explore the multi-targeting capability of CRISPRi circuitry, double sgRNA Cassettes and CRISPRi Array, demonstrated that two ARGs can be repressed simultaneously, but also showed a reduction in repression efficiency compared to single Cassettes. As this result was supposed to be caused by a competition between gRNAs for the shared pool of dCas9 protein, an HSL-inducible device was placed upstream dCa9 gene in order to achieve a gradual increase in its intracellular amount (the same inducible module characterized in Section 2.1 was here re-used). This strategy contributed to find an optimal expression that maximized the repression efficiency, but it did not completely solve the competition effect. Once the CRISPRi-mediated silencing of model ARGs was demonstrated, the genetic architecture based on CRISPRi Array was reprogrammed to target *NDM-1* and *mcr-1* genes that confer resistance to meropenem and colistin, an example of multi-spectrum antibiotics used as last resort drugs in case of severe MDR infections. To this aim, a set of four different CRISPRi Arrays, encoding for single or double spacers, were *ad hoc* designed and characterized with the same quantitative assays. Even in this case study, the activation of CRISPRi circuitry efficiently restored antibiotic susceptibility in resistant strains. In particular, by comparing the repression efficiencies of CRISPRi Arrays carrying single or double spacers targeting *NDM-1* gene, no relevant differences were observed, demonstrating that even a properly designed single gRNA could be sufficient to guarantee an high transcriptional repression. Moreover, despite the presence of a non-specific gRNA, the CRISPRi Array designed to inhibit *mcr-1* gene contributed to effectively kill the population of resistant cells upon colistin treatment. To investigate the nature of escaper cells, able to recover from the background of re-sensitized bacteria after drug

administration, liquid assays, sequencing analysis and restriction enzymes digest were carried out. Two different bacterial antibiotic responses were identified and classified as resistant or resilient phenotype. Growth profiles of survivor cells, re-exposed to a second round treatment with the target antibiotic, were studied in order to distinguish between resistant and resilient populations. Data from liquid cultures were consistent with sequencing analysis results; indeed, the resistant phenotype exhibited by some escaper cells was due to the presence of nucleotide mutations within the CRISPRi Array or genetic rearrangements within dCas9 expression module, while the target sequence was always intact. This result is encouraging as it proves that CRISPRi technology could represent a valid and safe alternative to CRISPR-Cas9 system in the treatment of MDR bacteria. Once the characterization of all the synthetic circuits mentioned was completed, the second research challenge was addressed: development of a conjugative platform to support the delivery of CRISPRi circuitry in resistant bacteria. To this aim, a trans-conjugative system was implemented in donor strains to perform a non-self-transmissible conjugation with resistant recipient cells. In the trans set-up, the conjugative machinery was expressed by the helper plasmid pTA-Mob, while the CRISPRi circuitry was placed on a different plasmid carrying the $oriT_{RK2}$ sequence. Starting from a general protocol, the conjugation assay was optimized by varying three main parameters regarding cellular density, bacterial growth phase and distribution area of the mating mixture spotted on LB plate. This study was performed by employing a mating pair composed of a donor strain carrying a mobilizable CRISPRi Array targeting *bla* and a recipient strain harbouring the target gene. In this model conjugative system, the genetic transfer was quantitative characterized with the CRISPRi circuitry in the OFF state and through *conjugation efficiency*, which resulted in a range of values consistent with those reported in the literature. Once the delivery of the CRISPRi circuitry was demonstrated, the repression efficiency of the mobilizable platform was investigated in resistant bacteria harbouring *bla* or *mcr-1* genes. In both cases, almost the entire transconjugant population was efficiently re-sensitized to the treatment with ampicillin or colistin. From these preliminary results, some important considerations can be highlighted. First, if on the one hand bacterial conjugation provides an interesting strategy to mobilize synthetic circuits in target bacteria, on the other hand the low efficiency of the conjugative transfer could represent a substantial bottle-neck in the development of a meaningful delivery platform in clinical context. Second, the high repression capability of the CRISPRi circuitry was demonstrated by the almost complete re-sensitization of target bacteria to both antibiotics used as testbed. However, due to the basal activity of the CRISPRi circuitry in absence of inducer molecules, an

optimized strategy to discriminate between ON and OFF state should be further adopted to confirm the quantitative results of conjugation efficiency. Finally, although the conjugative transfer was performed with an efficiency comparable to the one reported in the literature, some interventions could be explored in order to increase the conjugation frequency. In this regard, three main approaches can be mentioned. The ratio between donor and recipient cells could be unbalanced with the purpose to increase the amount of donors in the mating mixture; with this approach, a greater number of recipients is expected to be involved in the conjugative transfer. An alternative strategy is based on the deployment of a self-transmissible vector: in this case, all the cells that have received the plasmid become potential donors in subsequent rounds of conjugation and it could contribute to amplify the dissemination of the CRISPRi circuitry. As last resource, the conjugation could be performed with a narrow-host range helper plasmid, in order to investigate whether the efficiency of the conjugative transfer could be enhanced by restricting the window of recipient strains.

Chapter 4

Mathematical modelling of CRISPR-based therapy to treat AMR infections

The biological background described in Section 1.1 provides an alarming picture about the health crisis imposed by AMR on global scale. To counteract the dissemination of MDR pathogens and preserve the efficacy of last-resort antibiotics, an extended spectrum of strategies has already been explored. However, the *in-vitro* studies needed to develop novel therapies can be guided and even improved through the mathematical modelling of the desired experimental set-up. This approach aims at generating realistic predictions about the final therapeutic outcome. Although a mathematical model may never be a complete representation of the complex biological word, it could at least provides useful information about the key variables affecting the output of the considered process. With regard to microbial communities, several models have already been implemented to describe bacterial growth, interactions between individuals competing for shared resources, horizontal gene transfer mechanisms like bacterial conjugation and bacteriaphage interactions, all of which are relevant to the new therapeutic strategies described in this thesis. In this chapter, to simulate the effect of a CRISPR-based therapy on the eradication of MDR bacteria, a mathematical model was developed by exploiting the mentioned studies. In particular, the model aimed at predicting the performances of a CRISPR-based therapy by comparing two different delivery strategies, bacterial conjugation and phage infection, and two DNA targeting mechanisms, CRISPR-Cas9 and CRISPRi technologies. First, a deep analysis of the literature was required to investigate the molecular mechanisms involved in each considered strategy and to retrieve a collection of models used to describe the underlying processes (Section 4.1.1). The model architecture was then defined through the following stages: the growth of bacterial cultures was modeled by considering the

interaction among different cells in a microbial community and the competition for shared nutritional resources (Section 4.1.2); the delivery of CRISPR encoding circuits was simulated with either bacterial conjugation and phage infection (Section 4.1.3); the Cas9-mediated cleavage or the transcriptonal inhibition of resistance genes was modeled along with the bacterial response to both targeting technologies (Section 4.1.4). Once the structure was defined, a set of specific parameters was retrieved from the literature or estimated from previously published data in order to properly simulate the desired scenario (Section 4.1.5). Then, all the above mentioned biological processes were included in the final model, implemented with Matlab (Section 4.2). Each therapeutic treatment was simulated by comparing delivery and targeting mechanisms; with this approach, a specific quantitative index was used to evaluate which scenario, among those proposed, minimized the concentration of resistant bacteria, thus resulting in the theoretically best therapeutic solution to tackle AMR (Section 4.3). Finally, to investigate whether the model was able to predict the results obtained from *in vitro* and *in vivo* experiments, a comparison between model predictions and previously published experimental data, or new experimental data described in this thesis, was carried out (Section 4.4).

4.1 Model definition

In this section, once a general overview on model implementation was provided, all the parts composing its architecture are individually described. Subsequently, the set of values used to parametrize the model is reported along with the methods used to estimate some of them from experimental data. Finally, the complete model is presented with the support of detailed schemes.

4.1.1 General overview on model implementation

The mathematical model developed in this study aims to simulate a non traditional therapy of AMR-associated infections in which an engineered probiotic bacterium is employed as a vehicle for the *in situ* delivery of CRISPR antimicrobial agents programmed to kill resistant pathogens. In particular, through model simulations, different scenarios were compared: delivery of CRISPR circuitry via two transfer mechanisms, bacterial conjugation or phage infection; targeting of resistance genes with CRISPR-Cas9 (henceforth CRISPRcut) or CRISPRi technology. Model implementation required a deep analysis of the literature in order to identify the models that, in a quanti-

tative way, best represented the proposed case study. Throughout years, several mathematical models have been proposed to describe bacterial physiology and the interaction among different members of a microbial community. From these studies, it emerged that the modelling of bacterial population behaviour must account for at least two aspects: spatial distribution of cells in the environment; different physiological states in which individual members of the same community can be due to the biological noise arising from intrinsic and extrinsic components (stochasticity in cellular processes). In our case study, the microbial population has an explicit spatial structure since it colonizes the intestine, where bacteria form communities called biofilms (aggregates of cells and extracellular polymeric matrix). Moreover, it has been observed that biofilms are heterogeneous community in which localized cell behaviours are determined by the spatial structure inherent to the population (versus well mixed-culture), which generates gradient of nutrients and gases [104]. To properly describe such a complex biological environment, where each cell is modeled as an individual entity with a specific spacial localization, individual-based models (IbMs) have been proposed [105]. However, as these models are significantly complex and computationally demanding, we started to simulate the desired scenario by implementing a deterministic model. As a result, the model always generates the same result under a given set of initial conditions and parameters. Moreover, the one proposed is a population-based model in which a microbial community composed of identical individuals is exposed to same events and described with a single equation: this way, the dynamic evolution of the entire population is described, rather than that of a single cell. The model was implemented with a set of ordinary differential equations (ODE) that describe the dynamic evolution of bacterial density for each considered population. Each state variable represents a physiological condition of a given species (probiotics, pathogens, phages), e.g., untreated pathogens, bacteria that received the CRISPR circuitry from the donor probiotics, or pathogens that have been successfully re-sensitized. To describe the dynamics of the entire system, the model was divided into three macro-areas:

- bacterial growth;
- transfer mechanisms for the delivery of CRISPR circuitry;
- CRISPR-mediated inhibition/degradation of target genes and response of pathogenic bacteria.

Once all these biological processes were individually modelled, the equations were assembled to simulate all the considered scenarios.

4.1.2 Bacterial growth

First, the basic equation describing the growth of a bacterial population in a batch culture was defined. Second, the modelling of bacterial growth in a dynamic system was addressed in order to obtain a more realist representation of the herein proposed case study: therapeutic treatment of a microbial community that colonizes the human intestine. With this purpose, each biological scenario was simulated in a laboratory device named chemostat [54].

In a batch culture, also defined as a "close system" in which nutrients are not added and waste not removed, the bacterial growth can be conventionally divided in four key stages: *lag phase*, an adaptation period during which the growth is slow due to the low amount of actively growing cells; *exponential phase*, in which bacterial growth follows an exponential increase due to nutrient abundance and free available space; *stationary phase*, during which bacterial density reaches a plateau as resources become limited and lead to a decrease in population growth; *decline phase*, in which the number of viable cells rapidly falls due to the depletion in nutritional resources and the accumulation of metabolic waste. The basic equation describing the bacterial growth curve is reported below [106]:

$$\frac{dx}{dt} = \lambda \cdot x \tag{4.1}$$

where x is bacterial density expressed as number of individual cells per unit of volume in a culture [#/ml], t is time [h] and λ represents the growth rate [h^{-1}]. This equation describes the dependence of bacterial growth on cell density and growth rate. Growth rate is a parameter that refers to the number of divisions per cell in a given time. This value can be considered constant only in case of unlimited nutrients and space. However, considering a batch culture with limited resources, the bacterial population consumes nutrients and grows by occupying the available space until the stationary phase is reached. At this point, growth rate is null as the rate of cell division equals the rate of cell death. This behaviour can be mathematically described with the *Monod* equation [107]:

$$\begin{cases} \dfrac{dx}{dt} = \lambda_{max} \cdot \left(\dfrac{N}{K_S + N} \right) \cdot x \\ \dfrac{dN}{dt} = -\dfrac{1}{\epsilon} \cdot \lambda_{max} \cdot \left(\dfrac{N}{K_S + N} \right) \cdot x \end{cases} \tag{4.2}$$

where

$$\lambda(N) = \lambda_{max} \cdot \left(\frac{N}{K_S + N} \right) \tag{4.3}$$

In the *Monod* equation, $\lambda_{\max}$ is the maximum growth rate that the bacterial culture can reach, N represents nutrients concentration $[\mu g/ml]$ and K_{S} is the half-saturation constant that represents the concentration of nutrients at which the rate is half the maximum. Both $\lambda_{\max}$ and K_{S} can be measured experimentally. The system also includes a second differential equation to model nutrients dynamics, in which ϵ is a yield constant reflecting the conversion of nutrients to organism, i.e. the amount of nutrients consumed per cell $[\mu g/\#]$. It could be determined as follows:

$$\epsilon = \frac{mass \quad of \quad the \quad organism \quad formed}{mass \quad of \quad the \quad substrate \quad used} \tag{4.4}$$

As already mentioned, the exponential growth is followed by a stationary phase caused by depletion in nutrients, accumulation of waste products and lack of physical space. As in this phase the number of viable cells equals the number of dying cells, the growth curve assumes a sigmoidal shape. Once the system of equations describing the bacterial growth in a batch culture with limited resources and space was defined, the mathematical modelling of an open and continuously changing system was addressed in order to simulate the desired scenario in a more realistic way. Indeed, as the human intestine represents the ecological habitat where the therapeutic treatment takes pace, the flux of nutrients in input as well as the removal of waste in output must be considered. To simulate this environment, the equation system describing the bacterial grow in a chemostat was employed [55]. The chemostat, also defined as a continuous-culture device, is an "open system" in which fresh nutrients are constantly supplied, while exhausted medium (containing both nutrients and cells) is removed at the same rate. Even in this case, although nutrients are supplied in a continuous flux, the stationary phase is reached as the positive contribution of bacterial growth is balanced by the negative contribution of washout. Two variables are thus added to the differential equations system: the concentration of nutrients supplied in input, N_{in}, and the rate of nutrient exchange defined as *washout rate* w $[h^{-1}]$. With this approach, the portion of bacteria removed in output is subtracted to the total amount of cells growing in the chemostat, while the concentration of nutrients is balanced by the flux of fresh medium provided in input and the flux of exhausted medium subtracted in output.

$$\begin{cases} \dfrac{dx}{dt} = \lambda_{max} \cdot \left(\dfrac{N}{K_S + N} \right) \cdot x - w \cdot x \\ \dfrac{dN}{dt} = -\dfrac{1}{\epsilon} \cdot \lambda_{max} \cdot \left(\dfrac{N}{K_S + N} \right) \cdot x + w \cdot N_{in} - w \cdot N \end{cases} \tag{4.5}$$

This equations system was refined by adding the contributions of DNA delivery and CRISPR-induced response in target bacteria, both modeled in the following sections. Overall, the scenario described in model simulations evolves through the following stages: a bacterial culture of resistant pathogens in stationary phase grows in the chemostat (representing the human intestine), under the aforementioned conditions (nutrients supplied in input and waste removed in output); at t=0, a population of probiotics engineered with CRISPR circuitry is added to the chemostat. The synthetic circuit is delivered to target bacteria (either through bacterial conjugation or phage infection) and antibiotic resistance genes can be degraded (CRISPR-cut) or transcriptionally inhibited (CRISPRi). Through model simulations, the evolution of the microbial communities colonizing the same habitat was followed over time in order to investigate the final outcome derived by the CRISPR-based therapy.

4.1.3 Delivery strategies: bacterial conjugation and phage infection

Although different transfer mechanisms have already been explored to deliver CRISPR-encoding circuits within a microbial population, in this work the investigation was focused on bacterial conjugation and phage infection. Bacterial conjugation, that has already been described in Sections 1.3 and 3.5.1, is a widespread HGT mechanism that allows the lateral gene transfer of genetic material, usually plasmid DNA, from a donor to a recipient cell, by harnessing a cytoplasmic bridge that establishes a cell to cell contact. Phage infection is an event that naturally occurs when a virus named bacteriophage, or simply phage, injects its nucleic acid into a bacterial cell. This can result in cell death, in case of virulent phages, or genomic integration, in case of temperate phages. The former produce a lytic cycle that kills the cell upon the release of a new progeny of phage particles assembled within the host; the latter initiate a lysogenic cycle by integrating their nucleic acid in the host genome, in which the phage remains in a dormant state (prophage) without killing its host. By leveraging their ability to infect a bacterial cell in a species- or even strain-specific manner, phages have already been engineered for several therapeutic purposes [108]. Considering the potential application of both transfer mechanisms, the therapeutic treatment herein proposed starts with the oral administration of probiotic bacteria engineered with a CRISPR circuitry either encoded on conjugative plasmid, delivered via bacterial conjugation, or engineered phages, released by the population of probiotics at the site of infection (human intestine). Both delivery strategies

were modeled by considering the time delays through which a cell naturally evolves during a biological process. To meet this requirement, a transit compartment model was implemented [109], i.e., a mathematical approximation which enables the representation of the time delays in a systems avoiding the use of time-delayed differential equation systems. Generally, mathematical models used in the literature to describe bacterial cultures assume that an event (e.g., bacterial replication, transcriptional events) occurs simultaneously for the entire population/state of the system without considering the heterogeneity, which naturally arises in biology. For example, considering a bacterial population for which an enzymatic pathway causing bacterial death in 1 hour was been activated, if all the bacteria die in exactly 1 hour, the mathematical function that describes this phenomenon will be the step function, which is not an appropriate representation of reality. In fact, the real behaviour is less homogeneous, in which many bacteria die in 1 hour and the remaining cells die slower or faster, dying after or before 1 hour, respectively. The middle compartments within the transit compartment model used in this case study describe this time-latency behaviour: the bacterial population is divided based on the single bacteria evolution states, of which the last state is the dead state and the backward transition is avoided. The transition between different states is regulated by kinetic constants. The differential equation system that describes the transition among the states was written as follows:

$$\begin{cases} \dfrac{dx_1}{dt} = -k \cdot x_1 \\ \dfrac{dx_2}{dt} = +k \cdot x_1 - k \cdot x_2 \\ \dfrac{dx_n}{dt} = +k \cdot x_{n-1} - k \cdot x_n \\ \dfrac{dx_n + 1}{dt} = +k \cdot x_n - k \cdot x_{n+1} \end{cases} \tag{4.6}$$

Where n is the number of transit compartments used to model the overall delay, x_i (i=1,. . . ,n+1) is the bacterial concentration in every evolution state and k is the transit rate between the compartments, computed as:

$$k = \frac{n+1}{\tau} \tag{4.7}$$

The Equations 4.1.3 can be graphically modeled as follows:

Every circle and arrow in Figure (4.1) represent a differential equation and the rate of transition among the states, respectively. The bold arrow represents the initial bacterial concentration of probiotics and the last thin

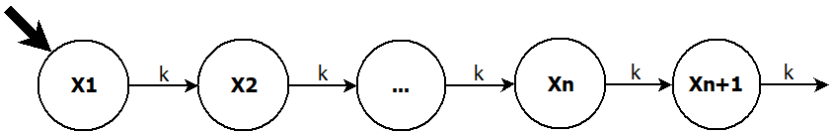

Figure 4.1: **Scheme of a transit compartment model.** The scheme represents the transition between different physiological states. Each state is identified by a circle connected to the others with a thin arrow that represents the rate of transition between states. Bold arrow represents the initial concentration of probiotic bacteria.

arrow represent the rate of bacterial death. Based on the number of compartments n, the mathematical model that describes the bacterial concentration changes between a first-order dynamic function (n=0) to the step function (n->∞). To properly model the considered biological processes, it was necessary to choose n high enough to model the latency effect of bacterial death and low enough not to overload the computation costs of the simulations. This time latency approximation was used to model the bacterial conjugation and to describe the release of phage particles from probiotic bacteria via a delayed but smooth dynamics.

The first scenario considered is the delivery via bacterial conjugation. In this case, probiotics and pathogens colonize together the chemostat and each microbial population grows with a rate dependent on its nutrient consumption: the competition for shared nutritional resources in a mixed population is the first example of microbial interaction. By co-existing in the same habitat, both populations reach an equilibrium in which the species with the highest growth rate overcome other bacteria by consuming the majority of nutrients and by occupying the largest portion of space. The contribution of probiotics in nutrient consumption was thus included in the differential equations system reported below:

$$\begin{cases} \dfrac{dT}{dt} = \lambda_{T,max} \cdot \left(\dfrac{N}{K_{T,S}+N}\right) \cdot T - w \cdot T \\ \dfrac{dP}{dt} = \lambda_{P,max} \cdot \left(\dfrac{N}{K_{P,S}+N}\right) \cdot P - w \cdot P \\ \dfrac{dN}{dt} = -\dfrac{\lambda_{T,max}}{\epsilon_T} \cdot \left(\dfrac{N}{K_{T,S}+N}\right) \cdot T - \dfrac{\lambda_{P,max}}{\epsilon_P} \cdot \left(\dfrac{N}{K_{P,S}+N}\right) \cdot P + w \cdot (N_{in} - N) \end{cases} \tag{4.8}$$

where T and P represent target pathogens and probiotic bacteria, respectively; the parameters $\lambda_{\max}$, ϵ and K_S are specific for the bacterial population considered, thus they generally differ between pathogens and probiotics. Bacterial conjugation can be described by mass-action kinetics between donor and recipient cells; during a conjugation, donors mobilize a copy of plasmid to

recipients which become transconjugants, whereas donor become temporarily exhausted cells. In fact, after a first round of conjugation, a lag time occurs before trasnsconjugant and donor cells can become or return active donors, respectively. In our system, donors are probiotics engineered with CRISPR circuitry, recipients are target resistant pathogens and transconjugants are represented by pathogens that, once received the conjugative plasmid, can mobilize the same to other target bacteria. In more detail, the conjugation simulated in our scenario involves the contribution of all the following bacterial populations:

- donor probiotics (PD), engineered probiotic bacteria that, upon oral administration, reach the site of infection (human intestine) where they can deliver the CRISPR circuitry to target pathogens via bacterial conjugation;

- exhausted donors (PL), probiotics that, after a first conjugation cycle, cannot initiate a second conjugative transfer before a lag time t_{L} has been occurred;

- target pathogens (T), target recipient bacteria that have not yet received the plasmid carrying the CRISPR circuitry;

- pathogens in latent state (TR), target bacteria which have received the plasmid carrying the CRISPR circuitry and that can become themselves donors after a lag time t_{R} required to express the conjugative machinery;

- donor pathogens (TD), target pathogens that act as donor cells in the delivery of the CRISPR circuitry to the population of resistant bacteria; in donor pathogens, CRISPR complex is already active in the degradation/inhibition of antibiotic resistances;

- exhausted pathogens (TL), target pathogens that have delivered the CRISPR circuitry and, after a lag time t_{L}, can perform a second round of conjugation; also in this case, CRISPR-mediated targeting of resistances is already active.

This scenario is described by the differential equations system reported below [56]:

$$\begin{cases} \frac{dT}{dt} = -\gamma \cdot T \cdot TD - \gamma \cdot T \cdot PD \\ \frac{dTR}{dt} = +\gamma \cdot T \cdot TD + \gamma \cdot T \cdot PD - lat_R \cdot TR \\ \frac{dTD}{dt} = -\gamma \cdot T \cdot TD + lat_R \cdot TR + lat_L \cdot TL \\ \frac{dTL}{dt} = +\gamma \cdot T \cdot TD - lat_L \cdot TL \\ \frac{dPD}{dt} = -\gamma \cdot T \cdot PD + lat_L \cdot PL \\ \frac{dPL}{dt} = +\gamma \cdot T \cdot PD - lat_L \cdot PL \end{cases} \tag{4.9}$$

where γ is the conjugation rate, while $lat_{\mathrm{L,R}}$ is the rate of exhausted cells becoming active donors, derived as $lat_{L,R} = {\tau_{\mathrm{R,L}}}^{-1}$ (in this example, contributions of bacterial growth, washout and nutrients consumption are not added to point out the equations system describing bacterial conjugation). A schematic representation of the states a cell can assume during the described conjugation steps is shown in Figure 4.2.

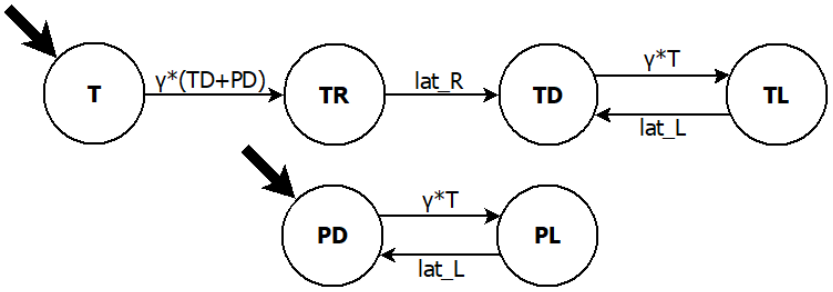

Figure 4.2: **Compartment model of bacterial conjugation.** Probiotics engineered with CRISPR circuitry (bold arrow and PD circle) are administered to a culture of target resistant pathogens (T) growing in a chemostat environment. Once the plasmid carrying CRISPR system is received via conjugation (TR), target bacteria can become themselves donors (TD) at rate lat_{R}. Once a first round of conjugation is completed, probiotics and target bacteria become exhausted donors (PL and TL); after a lag time, probiotics and pathogens return active donors at rate lat_{L}.

As anticipated, bacterial conjugation is described via a mass-action model in which the mating between recipient and donor cell allows the transition to a state in which both species are temporarily inactive; at the end of a lag time $\tau_{\mathrm{R,L}}$ during which conjugation does not occur, probiotics and pathogens can become active donors. The conjugation rate is described as a second order kinetics, as the event occurs between two species and its frequency depends on the relative concentration of both populations involved in the conugative transfer; in this case, the unit of measurement used is $[\mathrm{ml}/\# \cdot h]$. Conversely, the rates $lat_{R,\ L}$ describe a first order kinetics with the unit of

measurement h^{-1}, as the event occurs in a bacterium with an average lag time τ: this is an example of biological process that can be described with a transit compartment model. Rather than using a single state to model the lag time, several intermediate compartments can be added to describe the outcome of a biological process in a more realistic way. The resulting scheme, in which n intermediate compartments are added, is reported in Figure 4.3.

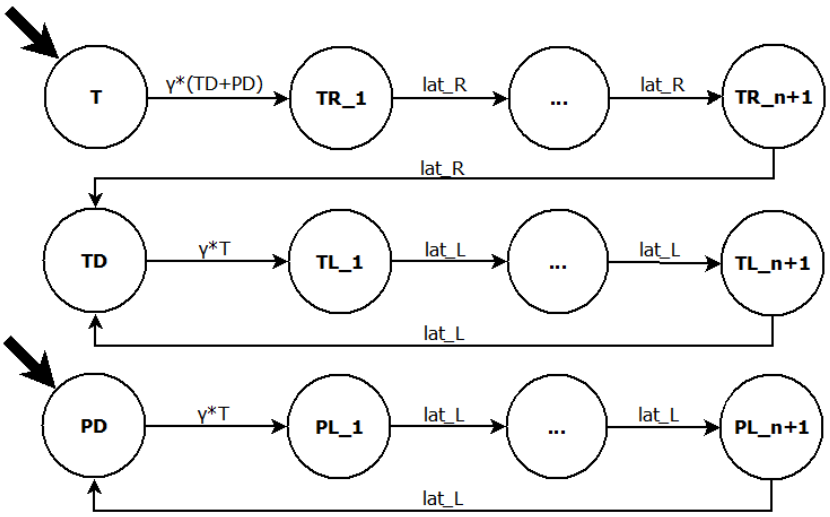

Figure 4.3: **Transit compartment model of bacterial conjugation.** Probiotics engineered with CRISPR circuitry (bold arrow and PD circle) are administered to a culture of target resistant pathogens (T) growing in a chemostat environment. Once the plasmid carrying the CRISPR system is received via conjugation (TR), target bacteria can become themselves donors (TD) at the end of a lag phase represented by several intermediate compartments through which the transition occurs at rate lat_{R}. Once a first round of conjugation is completed, probiotics and target bacteria become exhausted donors (PL and TL); after a lag time represented by several intermediate compartments (PL/TR_n+1), probiotics and pathogens return active donors at rate lat_{L}.

The differential equations system describing a bacterial conjugation modeled with a transit compartment model is reported below.

$$
\begin{cases}
\frac{dT}{dt} = -\gamma \cdot T \cdot TD - \gamma \cdot T \cdot PD \\
\frac{dTR1}{dt} = +\gamma \cdot T \cdot TD + \gamma \cdot T \cdot PD - lat_R \cdot TR_1 \\
\frac{dTR_i}{dt} = +lat_R \cdot TR_{i-1} - lat_R \cdot TR_i \\
\frac{dTR_{n+1}}{dt} = +lat_R \cdot TR_n - lat_R \cdot TR_{n+1} \\
\frac{dTD}{dt} = +lat_R \cdot TR_{n+1} - \gamma \cdot T \cdot TD + lat_L + TL_{n+1} \\
\frac{dTL_1}{dt} = +\gamma \cdot T \cdot TD - lat_L \cdot TL_1 \\
\frac{dTL_i}{dt} = +lat_L \cdot TL_{i-1} - lat_L \cdot TL_i \\
\frac{dTL_{\mathrm{n+1}}}{dt} = +lat_L \cdot TL_n - lat_L \cdot TL_{n+1} \\
\frac{dPD}{dt} = -\gamma \cdot T \cdot PD + lat_L \cdot PL_{n+1} \\
\frac{dPL_1}{dt} = +\gamma \cdot T \cdot PD - lat_{\mathrm{L}} \cdot PL_1 \\
\frac{dPL_i}{dt} = +lat_L \cdot PL_{i-1} - lat_L \cdot PL_i \\
\frac{dPL_{n+1}}{dt} = +lat_L \cdot PL_n - lat_L \cdot PL_{n+1}
\end{cases}
\tag{4.10}
$$

In this case, the rate $lat_{\mathrm{R,L}}$ is computed as follows:

$$
lat_{R,L} = \frac{n+1}{\tau_{R,L}} \tag{4.11}
$$

The second delivery strategy considered in this study is phage infection. Even in this case, the bacteria-phage interaction is modeled with a system of differential equations describing the following scenario: once they reach the site of infection, probiotics release a population of engineered phages via cell lysis; upon adsorption to target cell surface (attachment of a phage particle on cell membrane depends on the presence of specific receptors on the host surface), the nucleic acid within the phage particle, encoding for CRISPR machinery, is injected into the host cell in which antibiotic resistances can be cleaved (CRISPRcut) or inhibited (CRISPRi). The dynamic of bacteria-phage interaction, including the release from probiotics upon cell lysis and the adsorption on cell surface, is described with the equation system reported below [57]:

$$\begin{cases} \dfrac{dT}{dt} = -\delta \cdot T \cdot F \\ \dfrac{dTR}{dt} = +\delta \cdot T \cdot F - bs \cdot T(t-\tau) \cdot F(t-\tau) \\ \dfrac{dF}{dt} = -\delta \cdot T \cdot F + bs \cdot T(t-\tau) \cdot F(t-\tau) \end{cases} \tag{4.12}$$

where F identifies the population of free phages expressed as individuals per milliliter [#/ml]; TR represents infected pathogens in a temporarily latent state; δ is the adsorption rate (described with a second order kinetics and expressed as $[\mathrm{ml}/(\# \cdot h)]$); *bs* is the *burst size*, a parameter that identifies the number of phage particles released from a bacterium due to cell lysis; τ is the time required by the phage progeny to complete a lytic cycle. In the simulated scenario, the release of phage particles from probiotics is due to a bacterial lysis induced by a synthetic circuit carrying a sense-logic-actuation module (the latter is expressed from a recombinant plasmid harboured by donor probiotics; this genetic module, is responsible for the probiotic lysis upon sensing an endogenous stimulus at the site of infection), then phages are not assumed to be lytic for the target pathogen. The described dynamics was further refined as follows: delays were modeled by adding intermediate compartments to the equations; upon phage infection, a lag time was introduced as it naturally occurs before the expression of CRISPR machinery in target cells. A schematic representation of this scenario is reported in Figure 4.4.

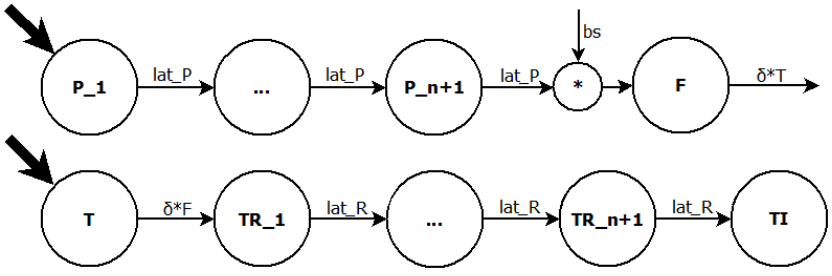

Figure 4.4: **Transit compartment model of phage infection.** Probiotics engineered with CRISPR circuitry (bold arrow and P circle) are administered to a culture of target resistant pathogens (T) growing in a chemostat environment. Probiotics evolve through several intermediate states at rate lat_{P} (*n+1* compartments) before releasing (bs) the progeny of phage particles (F). Once the plasmid carrying CRISPR circuitry is received via phage infection (TR), target bacteria evolve with a lag time (*n+1* compartments) towards the final state (TI) at rate lat_{R}; in this final state, antibiotic resistance genes can be degraded (CRISPRcut) or inhibited (CRISPRi).

The states a cell can assume during phage infection are described with the following differential equations system.

$$
\begin{cases}
\frac{dP_1}{dt} = -lat_P \cdot P_1 \\
\frac{dP_i}{dt} = +lat_P \cdot P_{i-1} - lat_P \cdot P_i \\
\frac{dP_{n+1}}{dt} = +lat_P \cdot P_n - lat_P \cdot P_{n+1} \\
\frac{dF}{dt} = +bs \cdot lat_P \cdot P_{n+1} - \delta \cdot F \cdot T \\
\frac{dT}{dt} = -\delta \cdot F \cdot T \\
\frac{dTR_1}{dt} = +\delta \cdot F \cdot T - lat_R \cdot TR_1 \\
\frac{dTR_i}{dt} = +lat_R \cdot TR_{i-1} - lat_R \cdot TR_i \\
\frac{dTR_{n+1}}{dt} = +lat_R \cdot TR_n - lat_R \cdot TR_{n+1} \\
\frac{dTI}{dt} = +lat_R \cdot TR_{n+1}
\end{cases}
\tag{4.13}
$$

The probiotic bacterium P evolves through several intermediate states (represented by *n+1* compartments) until the final lysis; at this point, phages F are released at the infection site where the adsorption to target cell surface allows the delivery of CRISPR machinery within the host cell; once infected, target pathogens TR evolves through several intermediate states (represented by *n+1* compartments) until the activation of CRISPR circuitry; in this final state, identified as TI, antibiotic resistances can be degraded or inhibited depending on the employed targeting technologies. The transition between intermediate states occurs at rate $lat_{\mathrm{P,\,R}}$ that were computed by employing the lag times τ_{P} and τ_{R}.

4.1.4 CRISPR-induced response in target bacteria

To properly investigate the therapeutic outcome of a CRISPR-based therapy, the bacterial response induced by the transfer and subsequent antimicrobial activity of the synthetic circuitry must be taken into account. To this regard, it is known that the uptake of exogenous DNA via HGT mechanisms (transformation, conjugation and transduction) can trigger the SOS response within the recipient cell. SOS is a bacterial stress response induced by the accumulation of single strand DNA (ssDNA) in response of exogenous DNA uptake or DNA damage (either due to physical and chemical agents). If an SOS response occurs, a set of gene involved in DNA replication and repair are activated, i.e. high and low-fidelity repair mechanisms like error-prone

translesion DNA polymerases. Moreover, the expression of low-fidelity polymerase is responsible for a transient increase in the mutation rate, which promotes the evolution of genetic diversity within a microbial population. This adaptive strategy provides microorganisms with the ability to withstand stressful environmental conditions but, in pathogenic bacteria, it could also represent a way to evolve new variants of resistance genes [110, 39]. Considering a CRISPR-based therapy, which acts as a sequence-specific antimicrobial, a mutation within the target DNA sequence could definitively impede the binding of CRISPR complex, thus inactivating its role in the degradation (CRISPRcut) or transcriptional inhibition (CRISPRi) of antibiotic resistances. In the literature, the transition from pathogens with original and mutated resistance genes is described with a first-order mutation rate [111]. In our model, was also included the possibility that spontaneous mutations can evolve within the genetic module encoding for the CRISPR circuitry, thus altering the sequence of gRNA or Cas9 gene. Due to these events, the antimicrobial activity of CRISPR system is compromised and resistant bacteria can preserve their ability to survive antibiotic treatment. This scenario was modeled with a set of compartments that describe the transition of the bacterial populations between different states. The nomenclature used in the scheme reported in Figure 4.5 is detailed below.

- T: pathogen without mutations in target gene;
- M: pathogen that has evolved mutations in target gene impeding CRISPR targeting;
- x: plasmid carrying a functional CRISPR circuitry;
- y: plasmid carrying a defective CRISPR circuitry where a loss of function mutation has evolved;
- Tx: pathogen harbouring a functional CRISPR system;
- Mx: pathogen with mutated target gene harbouring a functional CRISPR circuitry;
- Ty: pathogen harbouring a defective CRISPR system;
- My: pathogen with mutated target gene harbouring a defective CRISPR circuitry;
- mut_{M}: basal mutation rate of target bacterial genome $[h^{-1}]$ multiplied by the number NR of functional resistance copies (each copy of target gene can evolve a mutation and become immune to CRISPR targeting);

- mut_y: basal mutation rate of plasmid carrying CRISPR circuitry.

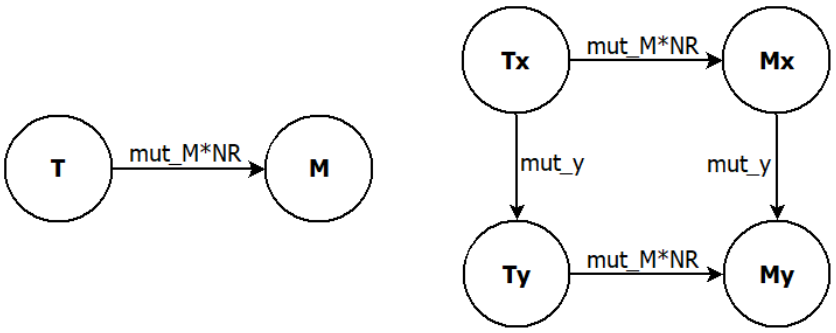

Figure 4.5: **Compartment model of basal mutations.** The evolution of spontaneous mutations within the genome of a target resistant pathogen or in the plasmid carrying the CRISPR circuitry is described with a compartment model where each compartment (represented as a circle) identifies a specific physiological state. The complete nomenclature is reported in the main text.

Among all the combinations listed above, only Tx can become susceptible to the antibiotic treatment as a functional CRISPR circuitry can target the sequence of the resistance gene not altered by spontaneous mutations. In all the remaining conditions, represented by bacteria that have not received the CRISPR system yet (T, M) or that have evolved one of the aforementioned mutations (Mx, Ty, My), resistance genes are still expressed and can provide immunity against antibiotic therapy. Starting from these considerations, a fundamental assumption is here introduced: even a single functional copy of the resistance gene, not susceptible to CRISPR targeting, is sufficient to provide antibiotic immunity to target cells. Usually, as the basal mutations rate is very low, this phenomenon is not expected to significantly affect the efficiency of the therapeutic treatment. However, as described below, some exceptions exist and can interfere with the final outcome of a CRISPR-based therapy. If we consider a target pathogen in the state identified as Tx, i.e. in a condition where a plasmid carrying a functional CRISPR circuitry has already been delivered and a sufficient lag time has occurred to express the synthetic circuit, the subsequent state to be implemented is the bacterial response induced by CRISPR targeting of resistance genes. Since mathematical models describing this phenomenon have not been found in the literature, experimental data derived from several research works were collected in order to retrieve or derive a set of parameters needed to parametrize the mathematical model (see Section 4.1.5). Starting from CRISPRi technology, only the transcripional inhibition of resistance genes was simulated. Indeed, as already mentioned, dCas9:gRNA complex can inhibit the expression of target genes without causing DNA damage, thus circumventing SOS response and preserving the original DNA sequence. As reported in a biophysical model

describing the Cas9-based binding of target genes [58], the dynamic through which CRISPR-Cas9 complex acts is much faster than the ones already described for other biological processes. Based on this consideration, the following assumption is introduced: dCas9-based binding or Cas9-based cleavage of target genes always follows a first-order kinetics whatever the number of antibiotic resistances. This hypothesis is considered plausible as the speed of CRISPR-based binding or cleavage is two orders of magnitude higher then other dynamics included in the system. This means that, if in a simulated scenario CRISPRi technology is employed as targeting mechanism and NR is the number of resistances within a single pathogen, the inhibition of a target gene will proceed in a single stage during which dCas9:gRNA complex binds all copies of the resistance gene. In this context, the transition between different states was modeled with the inhibition rate r_{inib} $[h^{-1}]$. Therefore, considering a scenario where a population of target pathogens is in the Tx state (i.e. NR resistance are intact and still functional) and spontaneous mutations can evolve, the resulting scheme is reported in Figure 4.6. In this scheme, Tx_{r0} (represented with a green circle) identifies a target pathogen in which all copies of the resistance gene were successfully inhibited, resulting in a complete restoring of antibiotic susceptibility.

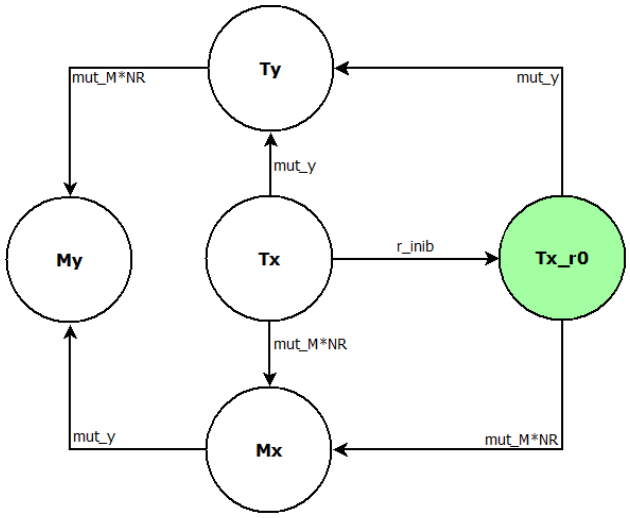

Figure 4.6: **Compartment model describing the CRISPRi-based targeting of resistance genes.** The evolution of spontaneous mutations within the genome of a target resistant pathogen or in the plasmid carrying the CRISPRi circuitry is described with a compartment model where each compartment (represented as a circle) identifies a specific physiological state. Green circle represents a pathogen in which all available resistances are inhibited. The complete nomenclature is reported in the main text.

The differential equations system describing the scheme in Figure 4.6, is reported below.

$$\begin{cases} \frac{dTx}{dt} = -(r_{inib} + mut_M \cdot NR + mut_y) \cdot Tx \\ \frac{dTx_{r0}}{dt} = +r_{inib} \cdot Tx - (mut_M \cdot NR + mut_y) \cdot Tx_{r0} \\ \frac{dTy}{dt} = +mut_y \cdot Tx + mut_y \cdot Tx_{r0} - mut_M \cdot NR \cdot Ty \\ \frac{dMx}{dt} = +mut_M \cdot NR \cdot Tx + mut_M \cdot NR \cdot Tx_{r0} - mut_y \cdot Mx \\ \frac{dMy}{dt} = +mut_M \cdot NR \cdot Ty + mut_y \cdot Mx \end{cases} \tag{4.14}$$

However, it is worth noting that even a pathogen in the $\mathrm{Tx_{r0}}$ state is not definitively re-sensitized to antibiotic treatment as both target gene or CRISPRi circuitry could evolve spontaneous mutations that can compromise targeting efficiency.

If we consider a CRISPRcut-based therapy of MDR pathogens, the simulated scenario changes significantly due to the induction of an SOS response within the target cell. Indeed, as Cas9 cleavage produces ssDNA, repair mechanisms such as homologous recombination are activated to fix the broken nucleotide sequence. Through this pathway, the original sequence could be efficiently restored if an intact homologous template is still available (not all copies of target gene are cut). Otherwise, the DSB could be repaired by leveraging micro-homologies spread through bacterial genome, resulting in a mutated version of the original gene (insertions or deletions within target sequence; for a more detailed explanation see also Section 1.2 and Figure 1.1). Considering this aspect, the homologous recombination rate r_{HR} was introduced in the system of differential equations by discriminating between the probability to achieve a correct or incorrect repair of damaged DNA: the former was defined as p_{cor}, the latter as p_{err} = 1-p_{cor}. Moreover, to properly simulate the bacterial response induced by Cas9 cleavage (represented with the rate r_{cut}), the location of target gene must be considered. Indeed, resistance genes can be placed at high or low copies on plasmid or chromosome, respectively. Depending on their position, the final outcome changes: in case of a plasmid-borne resistance, if the DSB is not repaired, the Cas9 cleavage results in plasmid curing (described with the degradation rate r_{deg}) without compromising cellular viability, but restoring antibiotic susceptibility (eradication of MDR pathogens is completed only upon antibiotic administration); in case of chromosome-borne resistance, if the damaged DNA is not repaired timely to enable the rescue of the cell, the enzymatic cascade responsible for cell death is triggered. Also this last condition is reached with the rate r_{deg}, which describes the dynamic through which a cleaved DNA evolves from a

state where it could be still repaired to a state in which the molecule is definitively compromised. This scenario is described with the scheme reported in Figure 4.7. Green circles represent target bacteria re-sensitized to antibiotic therapy. In this case, Tx_{r0} identifies a transient state in which all copies of resistance gene are cut, but HR can still occur to repair cleaved DNA. However, as the degradation rate is 7 orders of magnitude higher than the HR rate, Tx_{r0} is a labile state that quickly evolves towards bacterial death (in case of chromosome-borne resistance) or tx condition, in which all plasmids carrying antibiotic resistances are degraded, thus an HR-dependent repair of target DNA is no longer possible. Indeed, as shown in figure, this condition is still represented with a green circle as, even a mutation in CRISPRi circuitry, is unable to restore antibiotic susceptibility (Ty). The differential equations system describing this scenario is reported below and also includes the variable p_{cut}: if p_{cut}=1, then target bacteria evolve to Tx state due to the degradation of all copies of resistance gene; if p_{cut}=0, then Cas9 cleavage of chromosomal DNA induces cell death. The complete list of parameters, along with the methods used to estimate their values, are described in Section 4.1.5.

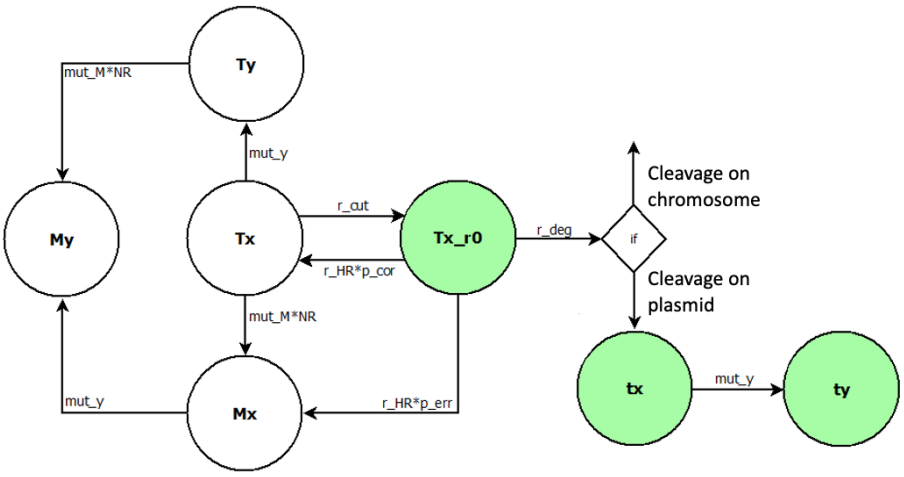

Figure 4.7: **Compartment model describing the CRISPRcut-based targeting of resistance genes.** The evolution of spontaneous mutations within the genome of a target resistant pathogen or in the plasmid carrying the CRISPRi circuitry is described with a compartment model where each compartment (represented as a circle) identifies a specific physiological state. Green circles represent pathogens in which antibiotic susceptibility is restored. The complete nomenclature is reported in the main text.

$$\begin{cases} \frac{dTx}{dt} = -(r_{cut} + mut_M \cdot NR + mut_y) \cdot Tx + r_{HR} \cdot p_{cor} \cdot Tx_{r0} \\ \frac{dTx_{r0}}{dt} = +r_{cut} \cdot Tx - r_{HR} \cdot Tx_{r0} - r_{deg} \cdot Tx_{r0} \\ \frac{dTy}{dt} = +mut_y \cdot Tx - mut_M \cdot NR \cdot Ty \\ \frac{dMx}{dt} = +mut_M \cdot NR \cdot Tx + r_{HR} \cdot p_{err} \cdot Tx_{r0} - mut_y \cdot Mx \\ \frac{dMy}{dt} = +mut_M \cdot NR \cdot Ty + mut_y \cdot Mx \\ \frac{dtx}{dt} = +r_{deg} \cdot p_{cut} \cdot Tx_{r0} - mut_y \cdot tx \\ \frac{dty}{dt} = +mut_y \cdot tx \end{cases} \tag{4.15}$$

4.1.5 Model Parameters

The majority of parameters used to implement the mathematical model herein presented was retrieved from the literature, by leveraging the large number of biological models and experimental data that are already available. The value of each parameter, along with the relative reference from which the same was retrieved or derived, is reported in Table 4.1.

Table 4.1: **Model parameters** List of parameters values used to implement the mathematical model. For each parameter reported in the first column, the unit of measurement, the relative value and the reference from which the same was retrieved are shown.

Parameter	Unit of measurement	Value	Reference
Chemostat			
N_{in}	$\mu g/ml$	100	[112]
w	h^{-1}	0.2 0.3 [0.2;0.45]	[112] [113] [114]
Bacterial growth rate			
λ_{max}	h^{-1}	0.86 0.7 0.7 [0.01;0.6] [0.2;0.8]	[111] [112] [113] [115] [116]
K_s	$\mu g/ml$	5	[112]
ϵ	$\mu g/\#$	$2 \cdot 10^{-6}$	[112]
Bacterial conjugation			

Continue on next page...

Table 4.1…*continued from previous page*

Parameter	Unit of measurement	Value	Reference
γ	$ml/\# \cdot h$	$3 \cdot 10^{-8}$ $6 \cdot 10^{-5}$ $6 \cdot 10^{-7}$	[56] [117] [118]
τ_{L}	h	0.5 [0.08; 0.5]	[56] [117]
τ_{R}	h	1.5 [0.57; 1.66]	[56] [117]
Phage infection			
δ	$ml/\# \cdot h$	10^{-7} $[10^{-9}; 10^{-7}]$ $3 \cdot 10^{-7}$ $[4 \cdot 10^{-10}; 2 \cdot 10^{-8}]$ 10^{-6} $6.24 \cdot 10^{-8}$ 10^{-9} $2 \cdot 10^{-7}$	[42] [112] [113] [114] [119] [120] [121] [122]
bs		1.55 100 80 [12 ; 60] [50 ; 150] 98 58 100	[111] [112] [113] [114] [119] [120] [121] [122]
τ_{P}	h	0.09 0.5 0.6 [0.3 ; 1.3] 0.5 0.5	[111] [112] [113] [114] [120] [121]
τ_{R}	h	the same of τ_{R} in conjugation	
CRISPR and DNA repair			
$\mathrm{r_{cut}}$ / $\mathrm{r_{inib}}$	h^{-1}	150	Derived from [83]
$\mathrm{r_{HR}}$	h^{-1}	10^{-6}	Derived from [123]
$\mathrm{p_{cor}}$		[0.5 ; 0.99]	Derived from [46]
$\mathrm{p_{err}}$		[0.01 ; 0.5]	Derived from [46]
$\mathrm{r_{deg}}$	h^{-1}	10	Derived from [124]
DNA mutation			
$\mathrm{mut_M}$/ $\mathrm{mut_y}$	h^{-1}	10^{-5} $8 \cdot 10^{-8}$ 10^{-6} $[4.1 \cdot 10^{-10}; 6.9 \cdot 10^{-10}]$	[111] [113] [122] [125]

As shown in Table 4.1, the only variables not available in the literature regarded the CRISPR-based targeting mechanism and the SOS response induced by DNA cleavage in target cells. These parameters were thus estimated from *in vitro* experiments performed

by other research groups.

In particular, to estimate the cleavage and inhibition rate of the CRISPR system, a model describing the *in vitro* experiment carried out by Sternberg et al. [83] was *ad hoc* implemented. The considered experiment aimed at investigating whether the binding of Cas9:gRNA complex to DNA products could prevent subsequent rounds of cleavage. In particular, the rate and yield of product formation upon Cas9 cleavage was measured with a plasmid assay in which an equimolar mixture of [Cas9:gRNA] was incubated with 25 nM of target DNA. Assuming that the amount of CRISPR complex exceeds the one of target DNA (in agreement with this case study), the relation between intact and cleaved DNA can be written as follows:

$$DNA_i + CAS \xrightarrow{r} DNA_t + CAS \tag{4.16}$$

where $\mathrm{DNA_i}$, $\mathrm{DNA_t}$ and CAS represent the relative nanomolar concentrations of intact DNA, cleaved DNA and Cas9:gRNA complex, respectively, while r indicates the cleavage rate (in this context, as the system evolves with a fast dynamics, DNA binding and cleavage are considered simultaneous events). Starting from this relation, the graph reported in Figure 4.8 is described via the following expression, derived from the kinetic model above:

$$DNA_t(t) = DNA_i(0) \cdot (1 - e^{r \cdot CAS \cdot t}) \tag{4.17}$$

Since the concentration of Cas9 protein affects the speed of reaction, the cleavage rate r is expressed as $[1/(s \cdot nM)]$. Considering a constant expression of the CRISPR complex within the cell and assuming that the proposed experiment is a good representation of *in vivo* behaviour, the cleavage rate included in the final model was derived as follows:

$$r_{cut} = r \cdot CAS \tag{4.18}$$

where $\mathrm{r_{cut}}$ is the constant rate used to obtain the best approximation of experimental data through a fitting process.

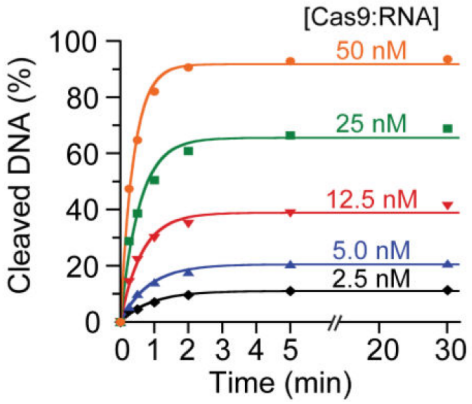

Figure 4.8: **DNA cleavage assay.** Cleavage yield of 25 nM plasmid DNA obtained by varying the molar ratios of Cas9:gRNA complex [83] .

The degradation rate of target DNA was derived by the research work of Kulka et al. [124]. In this study, the *mazEF*-dependent genetic program responsible for bacterial cell death was analysed. *mazEF* is a toxin-antitoxin module found in the chromosome of many

bacterial species and consists of two adjacent genes, *mazE* and *mazF*, transcribed by the same promoter P_2: *mazF* encodes for a stable toxin, while *mazE* encodes for an unstable antitoxin that *in vivo* is partially degraded by the ATP-dependent protease ClpPA. In case of normal physiological conditions, mazE inhibits the lethal effect of mazF. If a stressful condition occurs, e.g. a DNA damage induced by a double-strand break, the transcriptional activity of P_2 promoter decreases, thus resulting in a reduction of the intracellular level of both proteins. However, the amount of mazE is further reduced due to the ClpPA-mediated degradation. As a consequence, the toxic effect of mazF is no longer hampered by mazE and the genetic program responsible for cell death can initiate. This scenario could be a good representation of the SOS-induced bacterial response that arises in target cells upon Cas9 cleavage of resistance genes. In the same study, to investigate more accurately the role of mazEF as a stress-induced suicide module, the described physiological condition was mimicked by cloning *mazF* and *mazE* genes under two inducible promoters. With this approach, the time required to trigger cell death upon mazEF induction was estimated. Data presented in the aforementioned article were used to set a biological plausible variation range for the degradation rate parameter r_{deg}, which was computed as the reciprocal of the time constant for which 99% of cells have been killed by the induced-activated system.

To estimate the rate of homologous recombination, the work conducted by Huang et al. was exploited [123]. In particular, by considering the Cas9 cleavage of a chromosome-borne target gene, the value was computed as the ratio between killed and total bacteria (chromosome degradation usually results in cell death). As described in Section 1.2, HR pathway can repair a DSB by leveraging an homologous intact template or micro-homologies along the damaged DNA. In the study conducted by Huang et al., the consequences of HR-mediated repair were investigated in *E. coli*. In more detail, by programming CRISPR-Cas9 system to target the *lacZ* gene, the HR-dependent recombination frequency was estimated by providing an exogenous template *ad hoc* designed to be inserted in the same locus (successful HR-based repair results in the integration of the exogenous template within LacZ gene). To properly capture experimental data and estimate the HR rate, a differential equations system was implemented as reported below along with a scheme describing the consequences of Cas9 cleavage on double strand DNA (Figure 4.9).

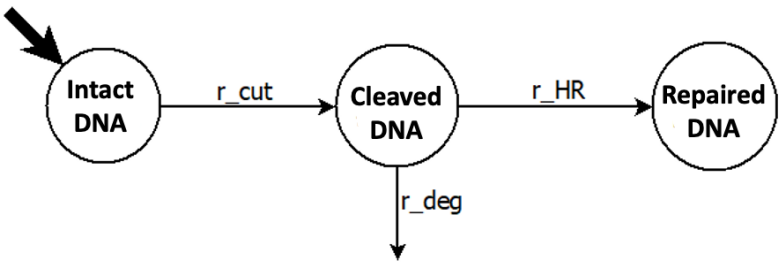

Figure 4.9: **Scheme of DNA cleavage and repair via HR.** The Cas9-mediated cleavage of a target gene generates a DSB at rate r_{cut}; cleaved DNA could be definitively degraded at rate r_{deg} or repaired via HR at rate r_{HR}.

$$\begin{cases} \dfrac{dDNA_i}{dt} = -r_{cut} \cdot DNA_i \\ \dfrac{dDNA_t}{dt} = +r_{cut} \cdot DNA_i - r_{HR} \cdot DNA_t - r_{deg} \cdot DNA_t \\ \dfrac{dDNA_r}{dt} = +r_{HR} \cdot DNA_t \end{cases} \tag{4.19}$$

The homologous recombination rate was computed from the steady-state solution of the equations system reported above by fixing the value of the parameters r_{cut} and r_{deg} (See Table 4.1). The resulting expression is:

$$r_{HR} = r_{deg} \cdot 10^{-7} \tag{4.20}$$

Considering Cas9 cleavage of a target gene, it is worth noting that HR pathway may repair a DSB by restoring the original DNA sequence or by introducing large nucleotide deletions if the recombination occurs with adjacent or even distant homologous sequences. To estimate the probability that a DSB can be repaired in a correct or incorrect way via HR, the research work conducted by Bikard et al. [46] was harnessed as a source of experimental data. This study demonstrated that DNA damage can be tolerated when Cas9 cleavage is inefficient: indeed, if not all copies of the target gene are cut simultaneously, HR pathway may support the repair of the damaged DNA with an intact homologous template (e.g. with sister chromosomes). This event results in a continuous cycle of cleavage and repair which leads to a constitutive SOS response within the cell. To more accurately investigate this aspect, in [46] CRISPR-Cas9 circuitry was programmed to target different positions spread throughout the *E. coli* chromosome. Among those performed, the following experiment was considered to determine the desired parameters. Two different positions within *lacZ* gene, lacZ1 and lacZ2, were chosen as CRISPR targets (Figure 4.10) in order to investigate the dependence of targeting efficiency from DNA sequence. As

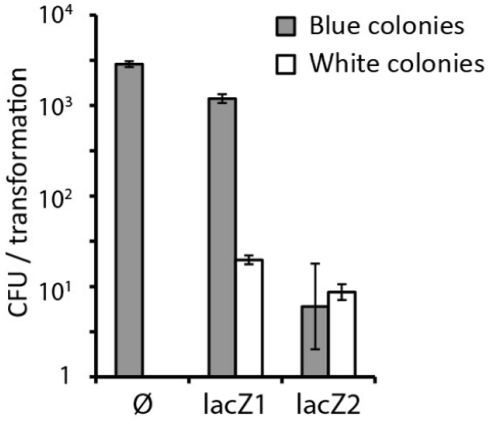

Figure 4.10: **Blue-white screening of E. coli cells engineered with a CRISPR-Cas9 circuitry targeting *lacZ* gene.** A CRISPR circuitry targeting the chromosome-borne *lacZ* gene is characterized in *E. coli* cells that constitutively express Cas9 protein. The targeting efficiency of LacZ1 and lacZ2 gRNAs, targeting two different positions within *lacZ*, is determined by counting the number of viable cells, further discriminated as blue colonies (still functional lacZ) or white colonies (inactivated lacZ). First bar refers to a guide less control [46].

the target sequences were integrated into the chromosome, CRISPR targeting efficiency was evaluated by counting the number of colony survived after Cas9 cleavage. Moreover, by leveraging a blue-white screening, the phenotype of survivors cells was determined in presence of X-gal. This screening relies on the activity of a β-galactosidase, encoded by *LacZ* gene, which can hydrolyzes X-gal resulting in the production of a blue pigment. This particular screening allowed to discriminate between cells where the HR-mediated repair of target gene efficiently restored the original sequence of *LacZ*, blue colonies, and cells where an alteration within target DNA (deletions) impeded the expression of a functional β-galactosidase (white colonies). As shown in Figure 4.10, targeting two adjacent loci within the same gene can result in different outcomes. Indeed, in case of LacZ1 site, the number of colonies that showed a blue phenotype (original sequence efficiently repaired) overcome the number of white colonies (deletion within target DNA) by 2-fold; otherwise, in case of lacZ2 site, the number of viable cells was significantly reduced and the probabilities to obtain a correct or incorrect HR-dependent repair were equal.

4.1.6 Final Model

All the individual biological processes described in previous sections were combined to capture the desired experimental set-up. All the therapeutic scenarios, composing the final model, were thus simulated by including the following sections:

- bacterial growth within the chemostat, a continuous-culture device in which nutrients are supplied in input and waste removed in output (washout);
- delivery of CRISPR circuitry to a population of resistant pathogens via bacterial conjugation or phage infection;
- bacterial response induced by the CRISPR targeting of resistance genes.

The following schemes, in which the contribution of each biological process is modelled, describe the 4 different scenarios analysed in this study.

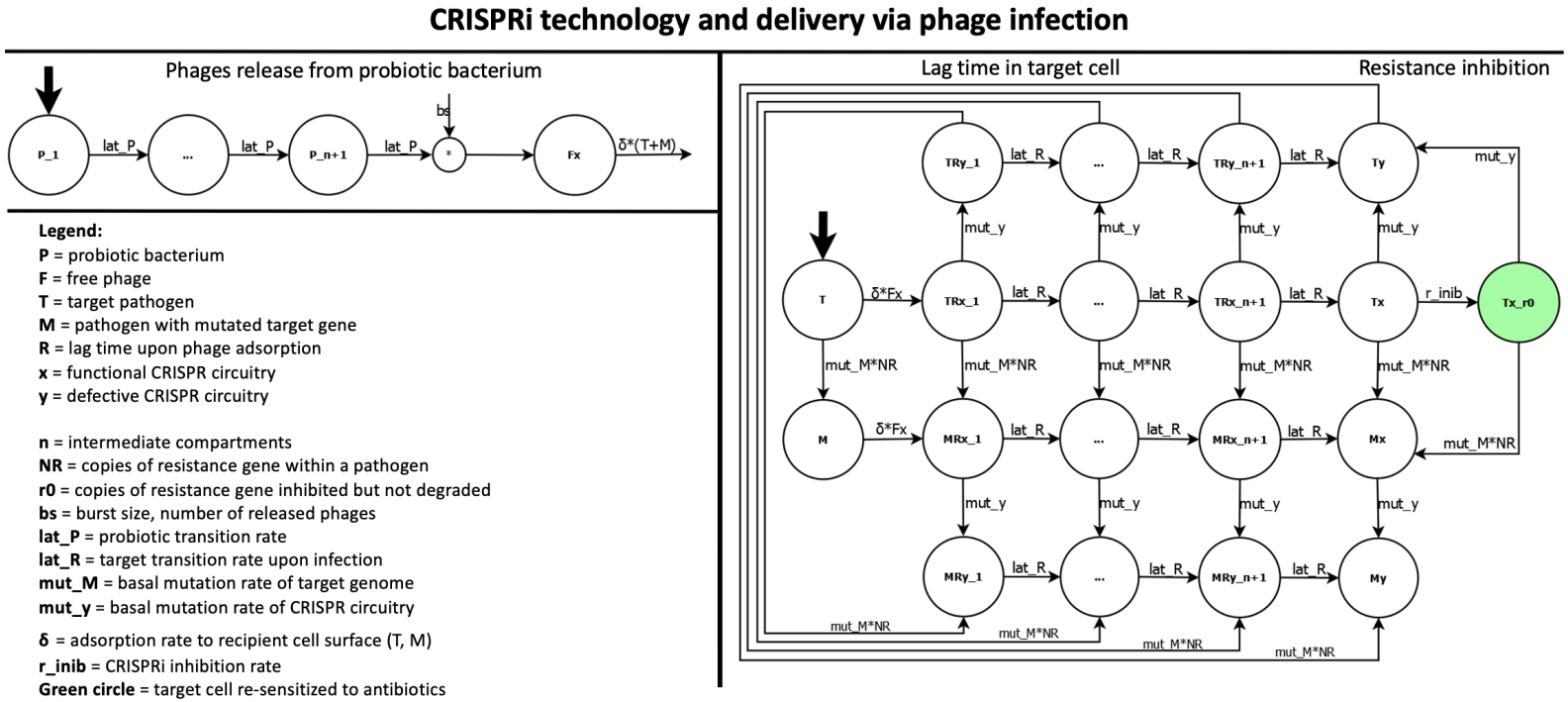

Figure 4.11: Final Model n.1: therapeutic treatment of AMR infections based on CRISPRi technology delivered via phage infection.

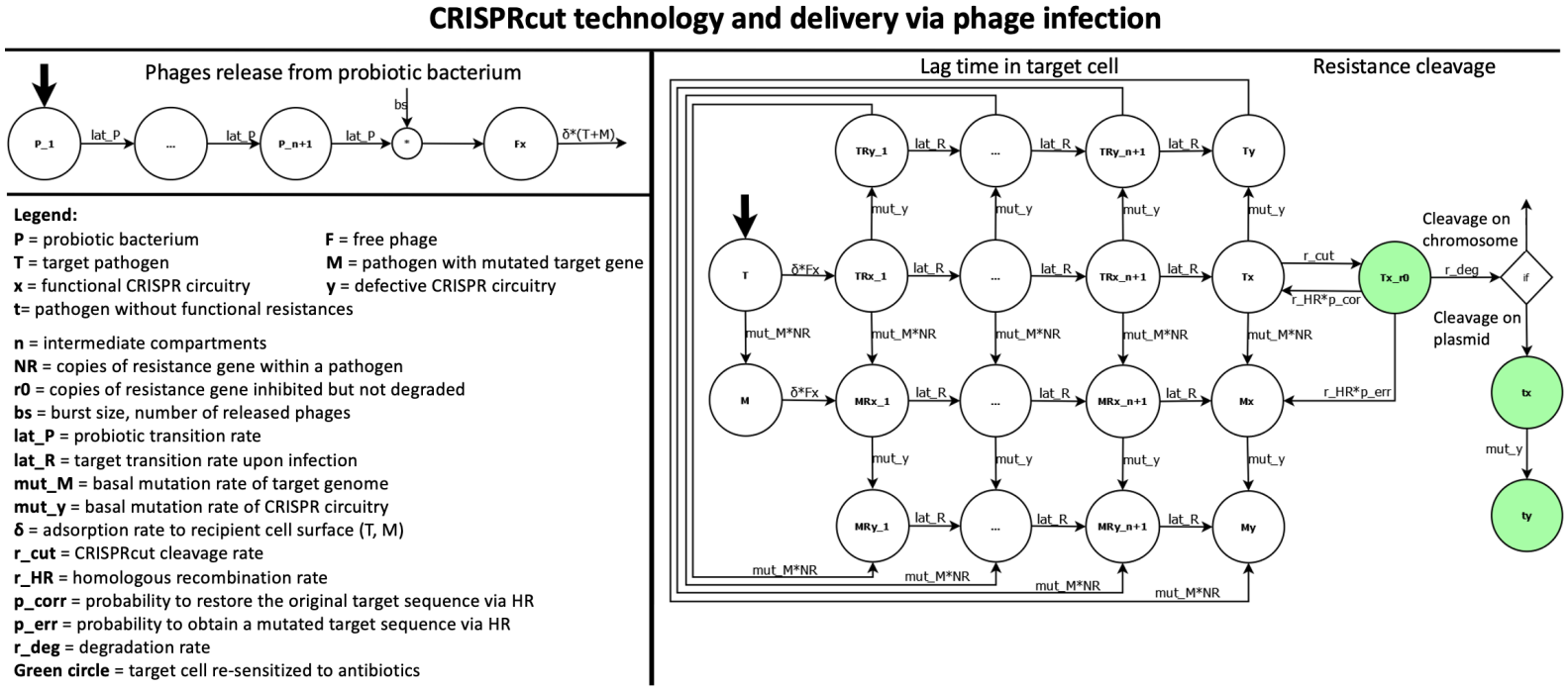

Figure 4.12: Final Model n.2: therapeutic treatment of AMR infections based on CRISPRcut technology delivered via phage infection.

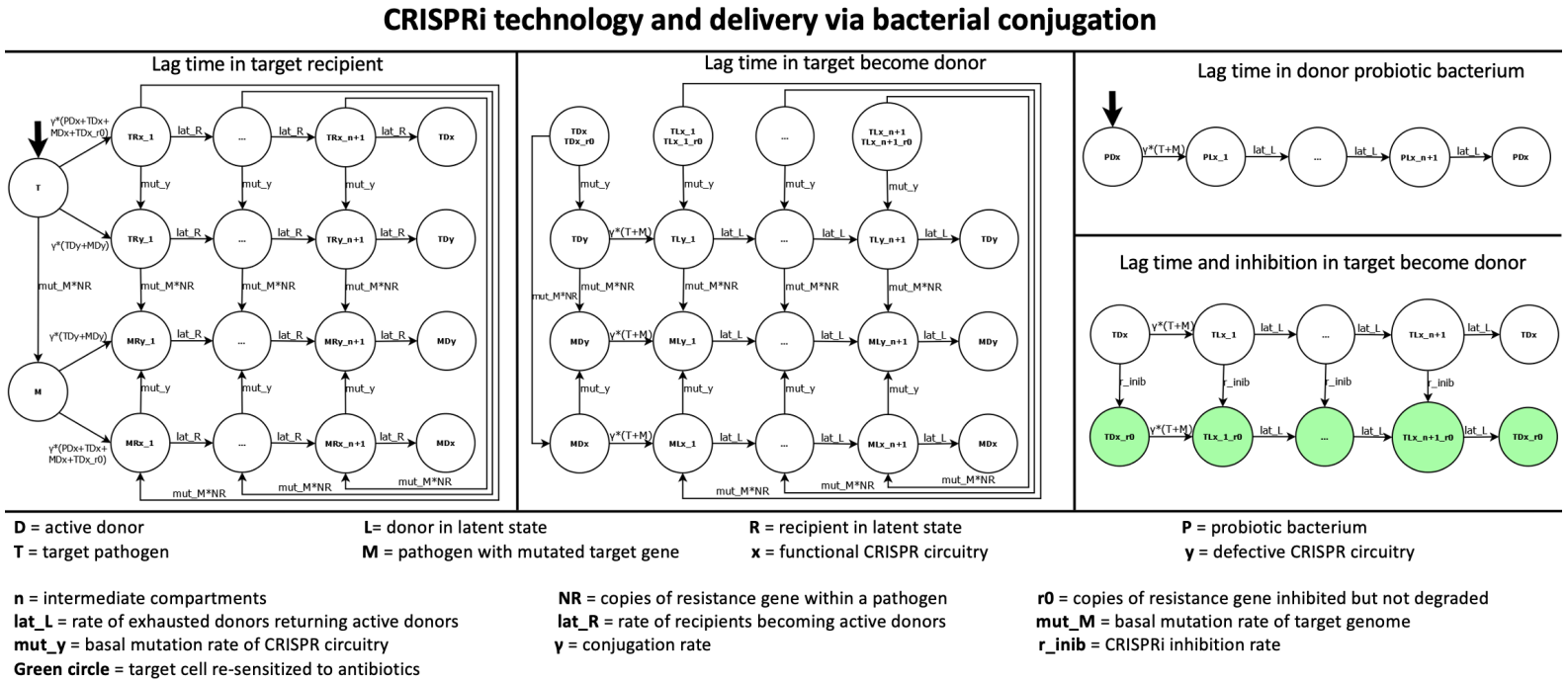

Figure 4.13: Final Model n.3: therapeutic treatment of AMR infections based on CRISPRi technology delivered via bacterial conjugation.

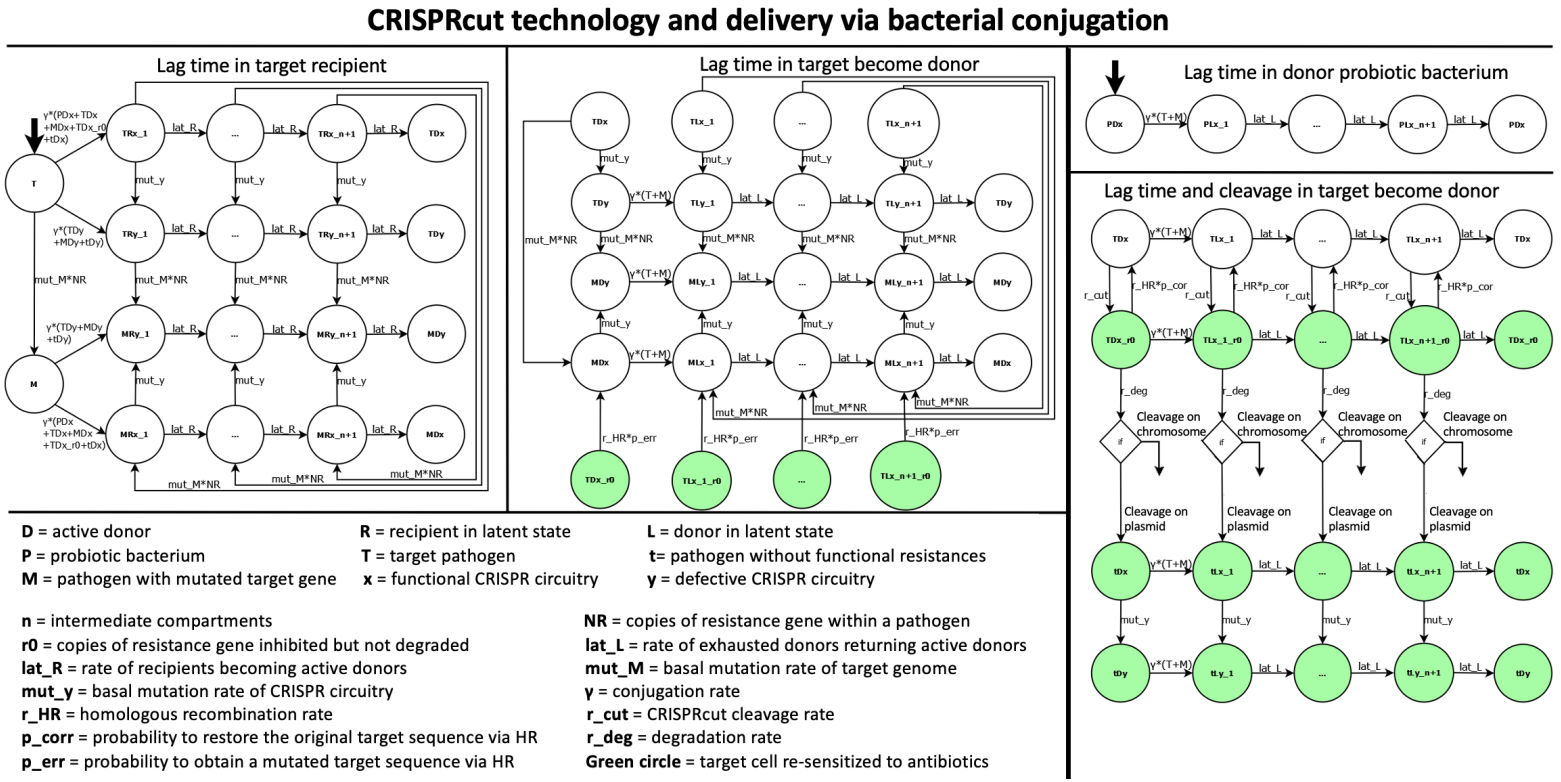

Figure 4.14: Final Model n.4: therapeutic treatment of AMR infections based on CRISPRcut technology delivered via bacterial conjugation.

4.2 Model implementation

The model was implemented through the software Matlab R2019b. To solve the system of differential equations, the *ode15s* routine was employed.

Model simulations were carried out using a time span of 20 hours in order to visualize in the resulting graphs the complete temporal dynamics of each considered scenario; the only exceptions were represented by the reactions describing the evolution of spontaneous mutations that required a longer simulation to reach the steady state, and a particular scenario in which the CRISPRcut technology was programmed to target a chromosome-borne resistance gene (discussed in the following section). Depending on the presence of commensal bacteria, initial conditions were set as described below.

- Scenario in absence of commensals
  - Pathogens: $1.9 \cdot 10^7$ bacteria/ml
  - Probiotics: $5 \cdot 10^6$ bacteria/ml
  - Nutrients: 2 $\mu g/ml$
  - N_{in}: 40 $\mu g/ml$
- Scenario in presence of commensals
  - Pathogens: $2 \cdot 10^7$ bacteria/ml
  - Probiotics: $5 \cdot 10^6$ bacteria/ml
  - Commensals: $8 \cdot 10^7$ bacteria/ml
  - Nutrients: 2 $\mu g/ml$
  - N_{in}: 200 $\mu g/ml$

Commensal bacteria are a population of non-pathogenic microbes that inhabit our organism and also represent an essential component of the gut microbiota. A differential equation system describing their growth dynamics and nutrient consumption was added to the model in order to simulate the interaction and the competition for nutritional resources among all the microbial communities included in each studied scenario. In model simulations, as commensals were not involved in bacterial conjugation or phage infection, only the contributions of bacterial growth, washout and nutrient competition were considered. At the end of the simulations, the number of resistant bacteria was computed as a quantitative index that allowed to identify the best therapeutic treatment of MDR pathogens among those compared.

4.3 Delivery of CRISPR/CRISPRi-based antimicrobials through phage infection or bacterial conjugation

In this section, the results generated by model simulations are discussed. A set of biological scenarios is first defined and then each comparison is individually described in order to highlight the theoretical strengths and weaknesses of the therapeutic treatments. Finally, to evaluate model performances, results predicted *in silico* are compared with experimental data provided by other research works and in this thesis.

4.3.1 Comparison between targeting strategies and delivery systems

With the purpose to investigate which targeting strategies (CRISPRcut vs CRISPRi) and delivery systems (bacterial conjugation vs phage infection) could provide the most effective therapeutic treatment of MDR pathogens, the comparison between the simulations were programmed by setting the same initial conditions and parameters. As described in the following sections, five different scenarios were simulated:

- comparison between targeting technologies (CRISPRi and CRISPRcut on plasmid or chromosomal DNA) and delivery through phage infection in absence of commensal bacteria. The aim was to investigate how the pathogen response, induced by two different targeting strategies, affected the final result;
- comparison between targeting technologies (CRISPRi and CRISPRcut on plasmid or chromosomal DNA) and delivery through phage infection in presence of commensal bacteria. This time, as another microbial community was present, the aim was to investigate how the interaction between commensal and pathogenic bacteria could affect the final result;
- comparison between delivery mechanisms (bacterial conjugation and phage infection) by employing CRISPRi technology in presence of commensal bacteria. The purpose was to identify the most effective delivery strategy between those proposed;
- comparison between delivery mechanisms (bacterial conjugation and phage infection) by employing a CRISPRcut circuitry programmed to target bacterial chromosome. This scenario was simulated in order to investigate how Cas9-mediated degradation of chromosomal DNA and subsequent death of pathogenic bacteria could affect the final result;
- comparison between self and non-self-transmissible conjugation in presence of commensal bacteria. The aim was to explore the result derived from the dissemination of CRISPR circuitry through a conjugative transfer performed with autonomous conjugative plasmids (even pathogenic bacteria could become donor in subsequent round of conjugations) or with mobilizable vectors (only probiotics acted as donor cells).

The graphs presented in the following sections show the results of all the transitions among different states modeled in the four schemes reported in Section 4.1.6, describing the dynamic evolution of target bacteria from the initial state of resistant pathogens (R) to the final state of susceptible bacteria (S). In particular, the population of re-sensitized pathogens was computed by considering all the green states reported in the schemes, while the population of resistant bacteria was represented by the residual cells in which the CRISPR circuitry was not delivered or did not efficiently interfere in the expression of resistance genes (mutations within target sequence or CRISPR module). To give an example, if we consider the scheme describing the scenario in which CRISPRcut technology is delivered through phage infection, R and S were computed as follows:

$$R = T + M + TRy + TRx + MRx + MRy + Ty + Tx + Mx + My \tag{4.21}$$

$$S = Tx\_r0 + tx + ty \tag{4.22}$$

Finally, bacterial density of probiotic and commensal bacteria is identified with P and C, respectively.

CRISPR-based targeting technologies and delivery with phage infection

The first comparison between CRISPRcut and CRISPRi technologies was performed in order to investigate whether the targeting mechanism could affect the final amount of resistant bacteria at the end of the simulation, by maintaining phage infection as the only delivery strategy. It is worth noting that the location of target gene has a crucial role to properly simulate the therapeutic outcome. Indeed, as already mentioned, resistance genes can be placed on plasmids or on the bacterial chromosome. In case of CRISPRi technology, the transcriptional inhibition of resistance genes, either integrated into plasmid or chromosome, always re-establishes the susceptibility of resistant strains to antibiotics. In case of CRISPRcut technology, depending on the location of the target sequence, the therapeutic outcome can be different: Cas9 cleavage of chromosomal loci induces the activation of an enzymatic cascade that ultimately results in bacterial cell death, thus antibiotic administration is not needed to complete the therapeutic treatment; otherwise, if the resistances are placed on plasmids, Cas9 cleavage results in plasmid curing which does not kill the cell but disarms it from the ability to withstand antibiotic treatment, which is subsequently administered in order to complete the eradication of the bacterial infection. For this reason, it was necessary to discriminate between two conditions where CRISPRcut is programmed to target resistance genes placed on plasmid or chromosome, and then both conditions were compared to CRISPRi outcome. Starting with the simulation of a scenario in which resistance genes are expressed from plasmid DNA, no relevant differences emerge from the comparison between CRISPRi (Figure 4.15) and CRISPRcut (Figure 4.16) technologies.

Considered scenario	**Resistant bacteria at 20h**
Phage infection - CRISPRi	41.7 bacteria/ml
Phage infection - CRISPRcut on plasmid	22.9 bacteria/ml

Indeed, both targeting strategies are extremely efficient as the target gene is quickly silenced or degraded. As shown in the figures above, after one hour from the administration of probiotics at time t=0h, the bacterial density of resistant pathogens (R) begins to decrease, while the one of susceptible bacteria (S) increases. After 4 hours, almost all pathogens are effectively re-sensitized to antibiotics. The only difference between the two targeting strategies emerges from the graph in semi-logarithmic scale: in case of CRISPRi, target bacteria that survive antibiotic treatment show a slight increase after about 10 hours. This observation could be explained by considering the CRISPRi-based molecular mechanism: dCas9:gRNA complex inhibits target gene without damaging the DNA molecule, thus the resistance determinant is always present; a mutation within the target sequence or the CRISPRi circuitry can compromise targeting efficiency, thus preserving pathogens from the re-sensitization to antibiotic treatment. The same outcome is not observed in case CRISPRcut technology. Indeed, although the sequence of target gene could be mutated as a consequence of HR-mediated repair, the process evolves with a very fast dynamics, thus pathogens cannot activate repair pathways timely to impede DNA degradation (all copies of resistance gene are cut simultaneously). In this scenario, resistant pathogens are represented by cells in which the target gene or the CRISPR circuitry was mutated before Cas9 cleavage. As a consequence, the amount of resistant bacteria at the end of the simulation is higher in case of CRISPRi technology even if, compared to the total number of bacteria, the population of pathogens is significantly reduced with both targeting strategies. Different results are obtained when the simulated scenario describes

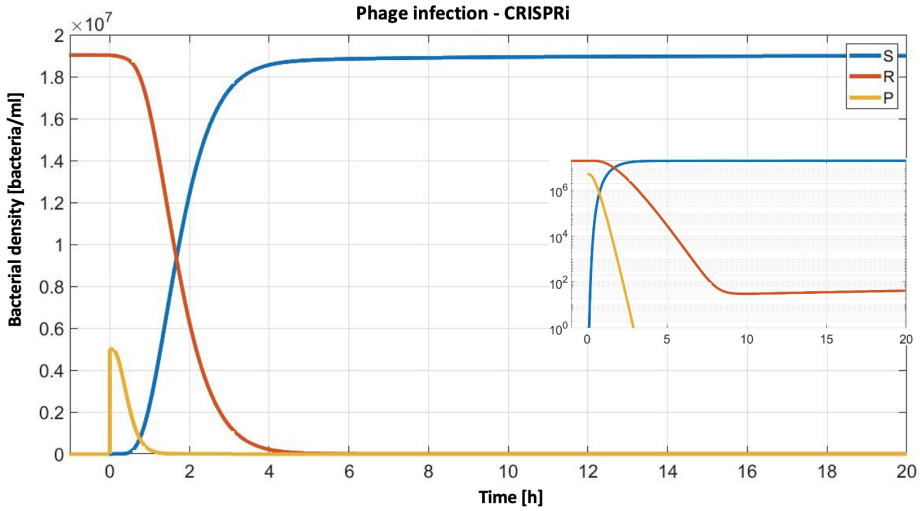

Figure 4.15: **Simulation of a CRISPRi-based therapy to target antibiotic resistances: delivery via phage infection.** Probiotic bacteria engineered with CRISPRi circuitry are added to a culture of resistant pathogens growing in a chemostat environment. CRISPRi circuitry is delivered via phage infection in absence of commensal microbes. In the graph, bacterial density is plotted over time (the inset refers to the same simulation but with semi-logarithmic scale on the y axis). S: susceptible cells; R: resistant pathogens; P: probiotics.

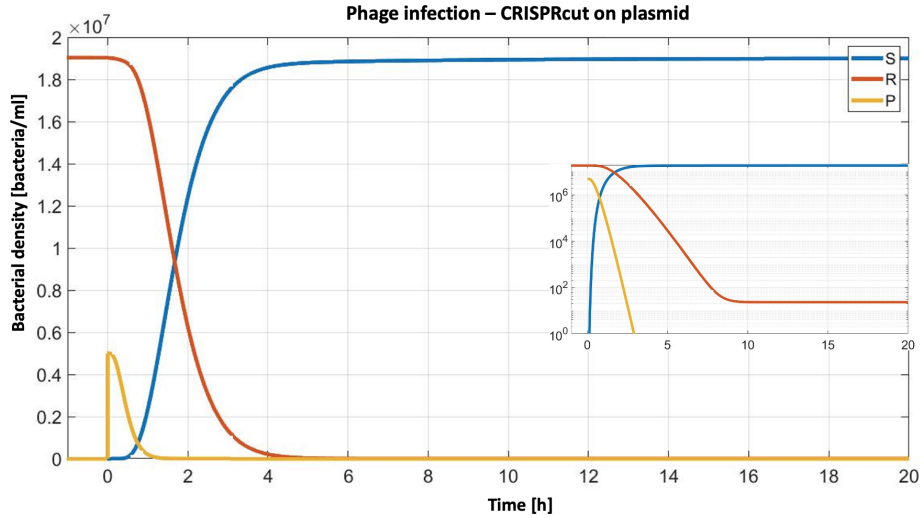

Figure 4.16: **Simulation of a CRISPRcut-based therapy to target plasmid-borne resistances: delivery via phage infection.** Probiotic bacteria engineered with CRISPRcut technology are added to a culture of resistant pathogens growing in a chemostat environment. CRISPRcut circuitry is delivered via phage infection in absence of commensal microbes. In the graph, bacterial density is plotted over time (the inset refers to the same simulation but with semi-logarithmic scale on the y axis). S: susceptible cells; R: resistant pathogens; P: probiotics.

the Cas9 cleavage of resistance genes integrated into the bacterial chromosome (Figure 4.17). This is the only condition in which 20 hours of simulation are not sufficient to reach a steady state; this observation also led to the introduction of a community of commensal

bacteria, as described in the following comparisons. In the considered scenario, once engineered phages are released from probiotics, the population of target pathogens is infected and the CRISPR circuitry can be expressed. In resistant cells, the Cas9:gRNA complex cleaves the chromosome-borne target gene, thus enabling the transition from resistant to susceptible state. Once this condition was achieved, the pathogen can evolve in two different ways as a consequence of the DNA damage: on the one hand, the DSB could be repaired via HR; on the other hand, cell fate can resolve in bacterial death if the DNA sequence is not efficiently repaired. However, as the degradation rate is seven orders of magnitude higher than the HR rate, bacterial death overcomes the survival of still resistant cells. As shown in Figure 4.17, a main difference with previous results, is that a transition from resistant to susceptible state cannot be clearly appreciated in resistant bacteria; indeed, the susceptibility state is so fast that, in few minutes, it evolves towards bacterial death. However, after 8 hours, bacterial density shows an exponential increase, encouraged by the absence of other microorganisms that can compete for nutritional resources (see the inset with semi-logarithmic scale on the y axis). In more detail, although the population of pathogens is successfully infected with phages that have delivered the CRISPRcut circuitry, some cells can evade Cas9 cleavage due to the evolution of mutations within the target gene or the synthetic circuitry. This way, at the end of the infection cycle, the majority of re-sensitized bacteria die while a little amount of resistant cells survive and proliferate. Starting from these considerations, the scenario within the chemostat changes: after 8 hours, a culture of resistant pathogens is provided with a continuous flux of nutrients without any form of competition with other bacterial communities. As a consequence, resistant cells can grow exponentially and, after 40 hours, reach a steady state. After 20 hours from the administration of probiotics, the total number of pathogens reaches the value of 21561 bacteria/ml thanks to the exponential growth supported by the absence of commensal bacteria. The same outcome is not observed when the effects of CRISPRcut and CRISPRi technologies are compared in the previous scenario, in which plasmid-borne resistances are considered. In this case, the population of infected pathogens is not killed and can grow in the chemostat environment by consuming the nutritional resources; the system then reaches an equilibrium in which the number of residual resistant cells does not further increase. Even in this context, the population of re-sensitized cells is eradicated upon antibiotic exposure, while residual resistant pathogens can grow exponentially due to the absence of a competition with other microbes. For this reason, a community of commensal bacteria was introduced into the model with a system of differential equations that describes the behaviour of a population non involved in phage infection or bacterial conjugation but only affected by the contributions of cell growth and washout. The introduction of a third bacterial community contributed therefore to represent in a more faithfully way the considered case study where different microbial populations, that colonize the same habitat, compete for shared nutrients and finally reach an equilibrium with each other.

CRISPR-based targeting technologies and delivery with phage infection in presence of commensal bacteria

The scenario described in the previous section is here reproposed by adding the population of commensal bacteria in the simulations. A comparison between CRISPRcut and CRISPRi technologies, either programmed to target plasmid or chromosome-borne resistances, was thus performed in order to investigate whether the targeting strategy could affect the final result in presence of a third community of microbes and by maintaining

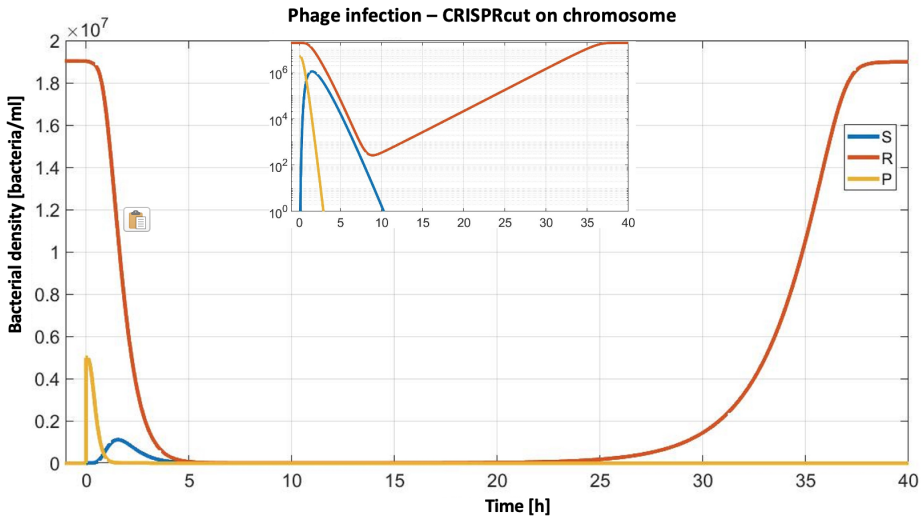

Figure 4.17: **Simulation of a CRISPRcut-based therapy to target chromosome-borne resistances: delivery via phage infection.** Probiotic bacteria engineered with CRISPRcut technology are added to a culture of resistant pathogens growing in a chemostat environment. CRISPRcut circuitry is delivered via phage infection in absence of commensal microbes. In the graph, bacterial density is plotted over time (the inset refers to the same simulation but with semi-logarithmic scale on the y axis). S: susceptible cells; R: resistant pathogens; P: probiotics.

phage infection as the only delivery strategy. In the experimental set-up, bacteria were combined at a pathogens to commensals ratio of 1:4 and the amount of nutrients was increased in order to keep this proportion in a balance until the administration of probiotics. By comparing the results derived from the simulations, the transcriptional inhibition (Figure 4.18) or enzymatic degradation (Figure 4.19) of plasmid-borne target genes do not result in relevant differences despite the presence of commensal bacteria; indeed, upon infection, pathogens rapidly evolve from the resistant to the susceptible state, thus the values of bacterial density at the end of the simulation are not distant from the ones shown in previous section.

Considered scenario	**Resistant Bacteria at 20h**
Phage infection - CRISPRi with commensals	43.5 bacteria/ml
Phage infection - CRISPRcut on plasmid with commensals	23.9 bacteria/ml
Phage infection - CRISPRcut on chromosome with commensals	29.7 bacteria/ml

The results change considerably (compared with the simulations in absence of commensal community) when the target gene is placed on the bacterial chromosome (Figure 4.20); in this case, the final outcome achieved with CRISPRcut technology is comparable with the one observed in the other two scenarios (CRISPRi and CRISPRcut on plasmid). In more detail, as the majority of pathogens die due to the Cas9 cleavage of chromosome-borne resistances, the amount of commensal bacteria can increase by lever-

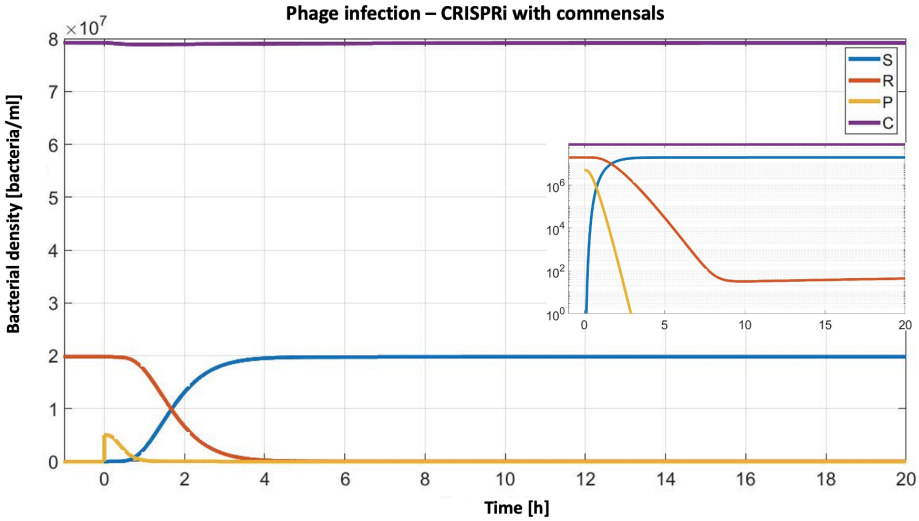

Figure 4.18: **Simulation of a CRISPRi-based therapy to target antibiotic resistances: delivery via phage infection in presence of commensals.** Probiotic bacteria engineered with CRISPRi technology are added to a culture of resistant pathogens growing in a chemostat environment. CRISPRi circuitry is delivered via phage infection in presence of commensal microbes. In the graph, bacterial density is plotted over time (the inset refers to the same simulation but with semi-logarithmic scale on the y axis). S: susceptible cells; R: resistant pathogens; P: probiotics.

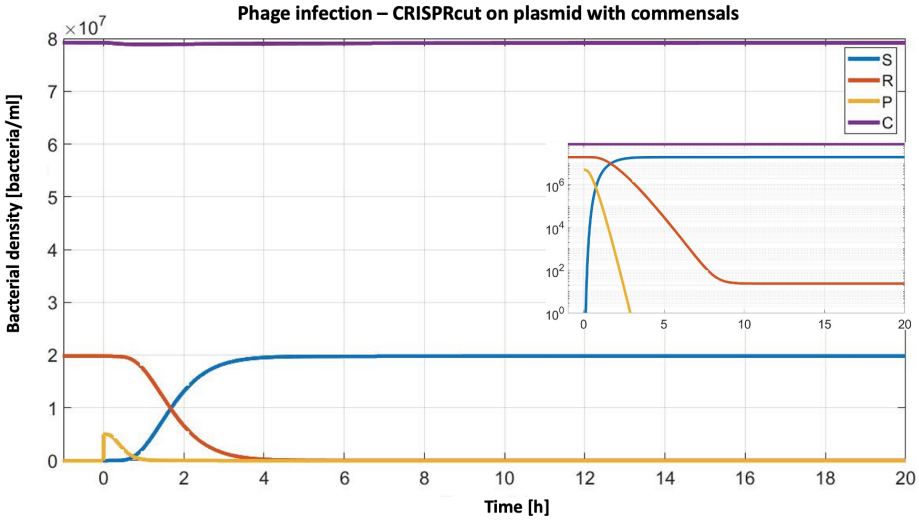

Figure 4.19: **Simulation of a CRISPRcut-based therapy to target plasmid-borne resistances: delivery via phage infection in presence of commensals.** Probiotic bacteria engineered with CRISPRcut technology are added to a culture of resistant pathogens growing in a chemostat environment. CRISPRcut circuitry is delivered via phage infection in presence of commensal microbes. In the graph, bacterial density is plotted over time (the inset refers to the same simulation but with semi-logarithmic scale on y the axis). S: susceptible cells; R: resistant pathogens; P: probiotics.

aging the absence of other microbial community competing for the shared resources. At the beginning of the simulation, thanks to the availability of nutrients, the community of

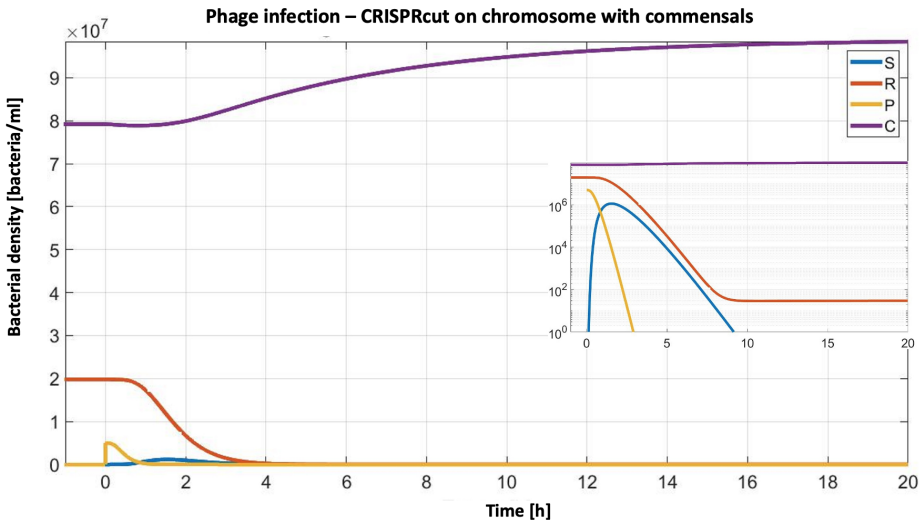

Figure 4.20: **Simulation of a CRISPRcut-based therapy to target chromosome-borne resistances: delivery via phage infection in presence of commensals.** Probiotic bacteria engineered with CRISPRcut technology are added in a culture of resistant pathogens growing in a chemostat environment. CRISPRcut circuitry is delivered via phage infection in presence of commensal microbes. In the graph, bacterial density is plotted over time (the inset refers to the same simulation but with semi-logarithmic scale on the y axis). S: susceptible cells; R: resistant pathogens; P: probiotics.

microbes within the chemostat reaches a bacterial density of 10^8 bacteria/ml: this value included both pathogens ($2 \cdot 10^7$ bacteria/ml) and commensal bacteria ($8 \cdot 10^7$ bacteria/ml). However, when resistant cells die due to chromosome degradation, the initial balance in the microbial community is compromised; taking advantage from this outcome, commensal bacteria can proliferate and consume nutritional resources that are provided with a continuous flux; finally, the chemostat is saturated by the bacterial culture that reaches a density of 10^8 bacteria/ml. In this context, thanks to the presence of commensals that colonize the same habitat, the population of resistant pathogens is eradicated without antibiotic therapy. Indeed, to treat AMR-associated infections, the CRISPR-Cas9 technology has already been proposed as a means to kill resistant bacteria harbouring chromosome-borne resistance genes [49, 50, 51]. Considering the results after 20 hours from the administration of probiotics, still resistant pathogens are present in a small proportion compared to the entire microbial population. Moreover, also in this scenario, the CRISPRi technology does not show relevant advantages: indeed, the evolution of loss of function mutations within the synthetic circuitry can impede the inhibition of resistance genes that are still present and not degraded within the target cell.

CRISPRi technology with two delivery strategies in presence of commensal bacteria

The third comparison proposed in this section aimed at investigating which delivery strategy, between bacterial conjugation and phage infection, could result most effective in the eradication of MDR pathogens. This scenario was investigate by considering CRISPRi technology as the only targeting mechanism and a steady state condition for both commen-

sal and pathogenic bacteria within the chemostat. Considering the results of simulations reported in Figure 4.18 and Figure 4.21, three main differences can be observed:

- the population of probiotics remains until the end of the simulation; indeed, unlike phage infection that occurs upon cell lysis, bacterial conjugation involves a donor cell which delivers the CRISPR circuitry to resistant cells via a cytoplasmic bridge that establishes a cell to cell contact. Moreover, once the first round of conjugation is completed, a time lag of 30 minutes occurs before the beginning of a second conjugative transfer;
- probiotics compete with other members of microbial community for nutritional resources. In case of phage infection, this phenomenon is not observed because probiotics die to release phage particles. This means that the resources in the chemostat are contended by the three different populations of probiotics, pathogens and commensals. As discussed in previous section, pathogens and commensals saturate the chemostat when the bacterial density reaches the value of 10^8 bacteria/ml. However, upon probiotics administration, the culture exceeds the saturation limit; as a consequence, to restore the initial steady state of 10^8 bacteria/ml, the bacterial density of both pathogens and commensals decreases;
- the transition from resistant to susceptible state is slower than in case of phage infection. Indeed, the transmission of the CRISPR circuitry depends on the relative amount of donor and recipient cells. If we consider phage infection as delivery mechanism, donor cells are represented by phage particles: about 100 phages are released by each probiotic, thus the proportion between phages and target cells is 25:1. Although phages can deliver the synthetic circuit only once, their number is large enough to quickly infect all the pathogens within the chemostat. Otherwise, in case of bacterial conjugation, the proportion between donor and recipient cells is 1:4, thus probiotics are outnumbered. It is also worth mentioning that, although CRISPRi circuitry can be delivered several times by probiotics and even by pathogens that have become donor themselves, a time lag of 30 minutes always occurs between two gene transfer events. Considering this aspect, the delivery through bacterial conjugation results slower than the one performed with phage infection.

As shown in the following Table, the number of residual pathogens at the end of the simulation is very similar with both delivery strategies.

Considered scenario	**Resistant Bacteria at 20h**
Phage infection - CRISPRi with commensals	43.5 bacteria/ml
Conjugation - CRISPRi with commensals	41.3 bacteria/ml

However, in case of conjugation, the time required to transfer the genetic circuit is longer than in case of phage infection. This could be a disadvantage as, during this additional time, pathogens or CRISPRi circuitry could evolve mutations that impede an efficient repression of target genes. As a consequence, comparing conjugation and phage infection, a grater number of resistant bacteria is expected in the first case. However, this intuitive outcome is not consistent with the model prediction as, due to the presence of probiotics, the amount of both commensal and pathogenic bacteria decreases, also resulting in a reduction of resistant cells at the end of the simulation.

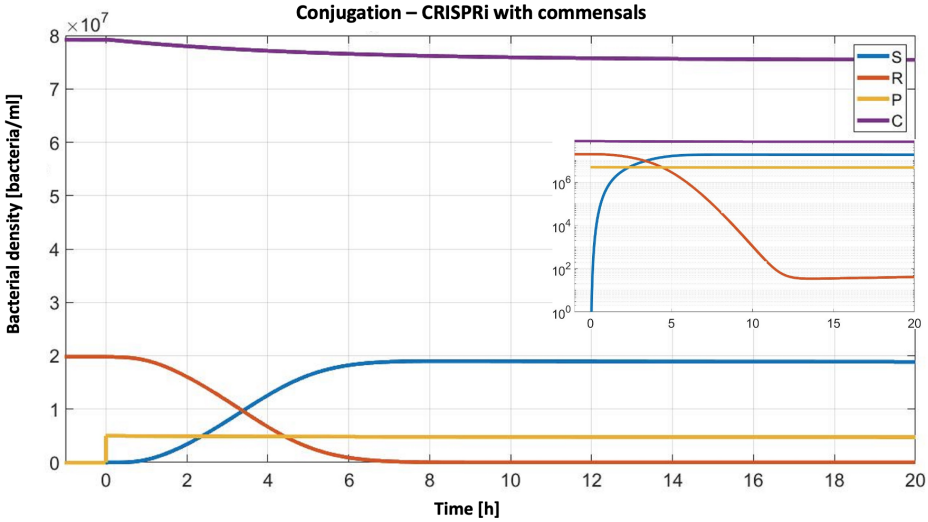

Figure 4.21: **Simulation of a CRISPRi-based therapy to target antibiotic resistances: delivery via conjugation in presence of commensals.** Probiotic bacteria engineered with CRISPRi technology are added to a culture of resistant pathogens growing in a chemostat environment. CRISPRi circuitry is delivered via self-transmissible conjugation in presence of commensal microbes. In the graph, bacterial density is plotted over time (the inset refers to the same simulation but with semi-logarithmic scale on the y axis). S: susceptible cells; R: resistant pathogens; P: probiotics.

CRISPRcut technology with two delivery strategies in presence of commensal bacteria

The fourth scenario proposed in this section aimed at comparing bacterial conjugation and phage infection in a case study in which the CRISPRcut technology is programmed to target chromosome-borne resistance genes, always in presence of commensal bacteria. The simulation of the same case study, discussed as second comparison, revealed that the delivery via phage infection could represent an efficient strategy to treat AMR-associated infections. Indeed, as shown in Figure 4.17, almost the entire population of resistant bacteria is killed due to the Cas9 cleavage of target DNA, while the community of commensals saturates the chemostat by leveraging the absence of other microbes competing for nutritional resources. On the other hand, in case of delivery via bacterial conjugation, the biological process evolves with longer temporal dynamics (Figure 4.22).

Considered scenario	**Resistant Bacteria at 20h**
Phage infection - CRISPRcut on chromosome with commensals	29.7 bacteria/ml
Conjugation - CRISPRcut on chromosome with commensals	2601 bacteria/ml

Indeed, even after 20 hours from the administration of probiotics, the number of resistant pathogens is still decreasing (see the graph in semi-logarithmic scale in Figure 4.22). As a consequence, the bacterial densities computed for both strategies at the end of the simulations are significantly different. The prolonged temporal dynamics observed in

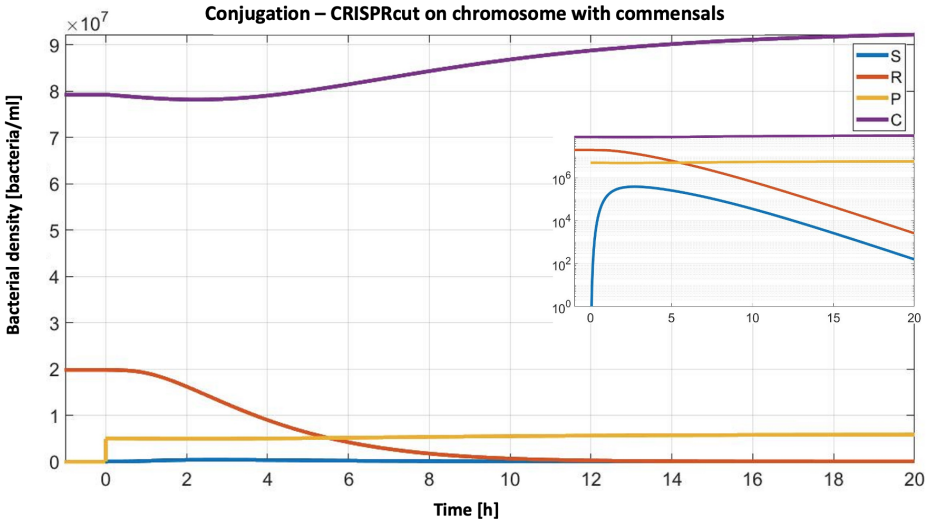

Figure 4.22: **Simulation of a CRISPRcut-based therapy to target chromosome-borne resistances: delivery via conjugation in presence of commensals.** Probiotic bacteria engineered with CRISPRcut technology are added to a culture of resistant pathogens growing in a chemostat environment. CRISPRcut circuitry is delivered via self-transmissible conjugation in presence of commensal microbes. In the graph, bacterial density is plotted over time (the inset refers to the same simulation but with semi-logarithmic scale on the y axis). S: susceptible cells; R: resistant pathogens; P: probiotics.

case of conjugative transfer depends on the ratio between donor and recipient cells; indeed, the strength of conjugation derives from the self-transmissible feature of the conjugative plasmid which, once mobilized in resistant cells, can be delivered to other pathogens within the same community. However, if the transmissible vector encodes a CRISPRcut circuitry programmed to target a chromosomal locus, the Cas9 cleavage of bacterial DNA kills the majority of cells, thus impeding subsequent rounds of conjugation from re-sensitized bacteria. Without the ripple effect induced by the increasing of donor cells, conjugation loses its strength and, due to the prolonged temporal dynamics, even the efficiency of the CRISPR-based treatment is reduced. Overall, from the analysis of this comparison, phage infection results as the best transfer mechanism to quickly deliver CRISPRcut circuitry to the target population, without the need for an antibiotic treatment.

CRISPRi technology with self and non-self transmissible conjugation in presence of commensal bacteria

The last comparison analysed in this study aimed at investigating the role that a conjugation performed by resistant bacteria could have on the final therapeutic outcome. In more detail, considering bacterial conjugation as transfer mechanism and CRISPRi technology as targeting strategy, always in presence of commensals, a new scenario was simulated in order to test whether an amplified transfer of the synthetic circuitry could enhance the efficiency of the CRISPRi-based therapy. With this purpose, the considered case study was analysed under two conditions: in the first one, already described in Figure 4.21, a self-transmissible conjugation is performed by leveraging an autonomous conjugative plasmid which carries the CRISPRi circuitry along with the conjugative machinery;

in the second one, a non-self-transmissible conjugation is performed with a conjugative vector carrying only the CRISPRi circuitry (Figure 4.23). In the latter case, as the conjugative machinery is expressed in *trans* from an helper plasmid or chromosomal DNA within the donor cell, all the recipient bacteria that have received the mobilizable vector cannot become donors themselves due to the lack of transfer and replication functions needed to support a subsequent round of conjugation.

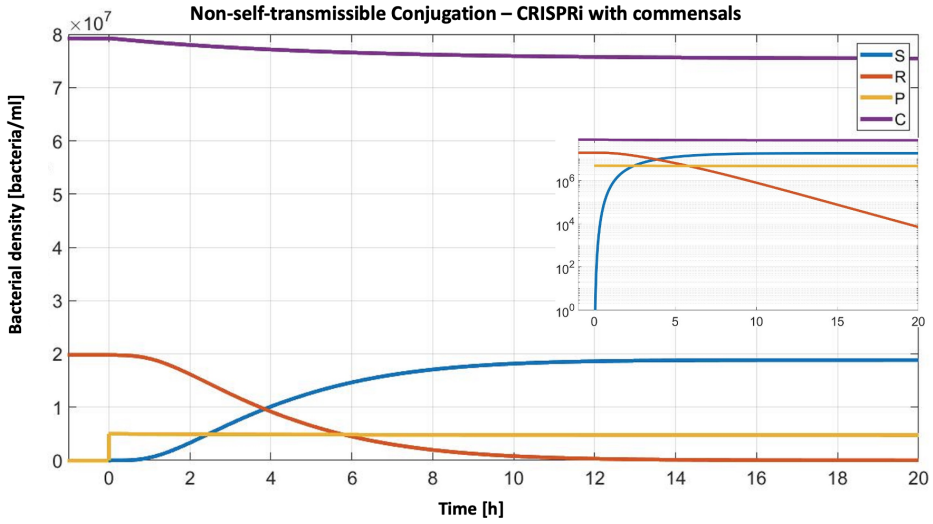

Figure 4.23: **Simulation of a CRISPRi-based therapy to target antibiotic resistances: delivery via non-self transmissible conjugation in presence of commensals.** Probiotic bacteria engineered with CRISPRi technology are added to a culture of resistant pathogens growing in a chemostat environment. CRISPRi circuitry is delivered via non-self-transmissible conjugation in presence of commensal microbes. In the graph, bacterial density is plotted over time (the inset refers to the same simulation but with semi-logarithmic scale on the y axis). S: susceptible cells; R: resistant pathogens; P: probiotics.

Considered scenario	**Resistant Bacteria at 20h**
Self-transmissible conjugation CRISPRi with commensals	41.3 bacteria/ml
Non-Self-transmissible conjugation CRISPRi with commensals	7199 bacteria/ml

The main difference observed between these two conditions is the rate at which the transition from resistant to susceptible state occurs. In the first case, as shown from the graph in semi-logarithmic scale, this transition needs 12 hours to reach the end; otherwise, in the second case, the system requires more than 20 hours to complete its dynamic evolution. As a consequence of a non-self transmissible conjugation, the amount of resistant bacteria at the end of the simulation is greater than the one computed in case of a self-conjugative transfer. This result is in agreement with data reported in the literature: as described in [48], an higher conjugation efficiency can be achieved by leveraging a self-transmissible plasmid (*cis* conjugative set-up) rather than a mobilizable vector (*trans* conjugative set-up).

4.4 Comparison with experimental data

The mathematical model herein presented was employed to simulate a set of experiments with data already published in the literature and also obtained in this thesis work; this approach aimed at investigating the performances of the model by comparing the predictions obtained *in silico* with experimental data derived from *in vitro* and *in vivo* experiments. The first comparison with the literature was carried out by considering the research work conducted by Rodrigues et al. [66]. In this study, a pheromone-responsive plasmid was employed to deliver the CRISPR/Cas9 machinery from an non-pathogenic (donor cell) to an antibiotic resistant (recipient cell) strain of *E. faecalis* via conjugation. From an experimental point of view, the conjugation was performed by combing the mating pair at a 1:9 donor to recipient ratio. As the gene conferring antibiotic resistance in the recipient strain was placed on a plasmid, the Cas9 cleavage of target DNA was expected to restore antibiotic susceptibility without killing the cell. Based on data reported in this study, the conjugative plasmid carrying the CRISPR circuitry was efficiently delivered to resistant recipient cells; indeed, upon antibiotic administration, the target population was reduced by 3- to 6-fold depending on the recipient strain (*E. faecalis* OG1SSp or V583) or the target gene (*tetM*, tetracycline resistance; *ermB*, erythromycin resistance). Starting from the same initial conditions established in [66], the same experimental set-up was simulated with our model. Results revealed that the conjugative plasmid was delivered to the entire bacterial population which, in response to plasmid curing, was reduced by 6-fold. Although this comparison provided an encouraging result, data from *in vitro* experiments showed that the killing efficiency of CRISPR circuitry can be affected by some context-dependent sources such us binding affinity between Cas9:gRNA complex and the respective target sequence (i.e., Cas9 cleavage of target DNA resulted more efficient in case of *ErmB* rather than *TetM* gene) or loss of function mutations that could comprise the role of CRISPR machinery and evolve at rate higher than the one fixed in our model.

A second comparison with the literature was carried out by considering the research work of Hamilton et al. [48], again focused on the eradication of pathogenic bacteria thorough the deployment of CRISPR/Cas9 technology. In this study, a conjugative platform either based on a self or non-self transmissible plasmid was developed to deliver CRISPR machinery from *E. coli* (donor cell) to *S. enterica* (recipient cell). As already mentioned, in a self-transmissible conjugation (*cis* set-up), recipient bacteria become themselves donors able to perform subsequent rounds of conjugation; in case of non-self-transmissible conjugation (*trans* set-up), recipient cells cannot deliver the mobilizable plasmid to other bacteria due to the lack of the conjugative machinery. Experimental data reported in this work showed that a conjugation performed with a self-transmissible plasmid resulted in an exponential increase of the conjugative events, as recipient cells could contribute to disseminate the plasmid once become donors themselves. The simulation of this scenario was already addressed in the last comparison discussed in Section 4.3 (Figure 4.23). Starting from data presented in [48], the same experiment was simulated by modifying the initial conditions. In particular, the number of probiotics was reduced (donor to recipient ratio of 20:1) in order to visualize in a more detail the temporal dynamics followed by the conjugative transfer. Results of model simulations are reported in Figure 4.24 and confirm that a self-transmissible conjugation allows to maximize the amount of transconjugant cells with a dynamic that follows an exponential increase. The research work conducted by Citorik et al. [51] was also considered as last case study. In this work, CRISPR/Cas9 technology was *ad hoc* programmed to target virulence and antibiotic resistance genes either integrated on the chromosome or on plasmids harboured by *E. coli*. The delivery

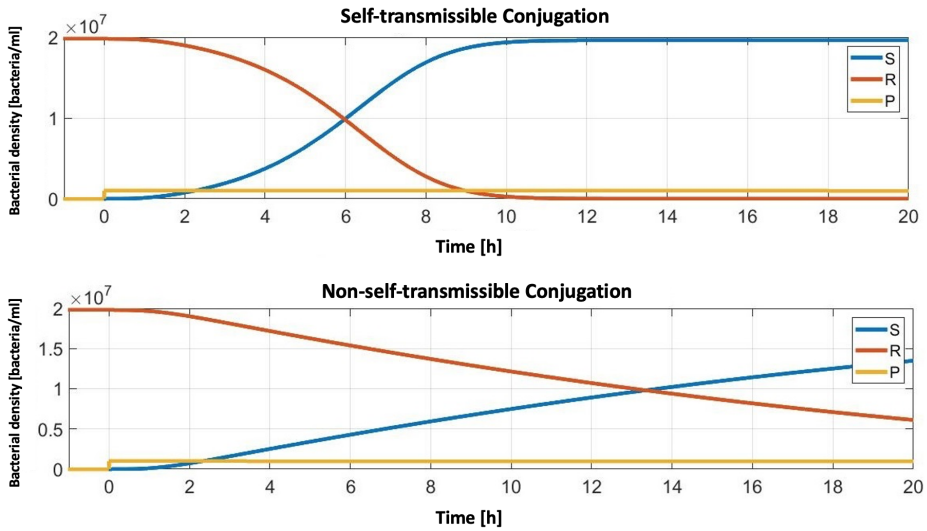

Figure 4.24: **Simulation of a self and non-self transmissible conjugation.** Comparison between two conjugative platforms: in the first one (graph above), a self-conjugation is performed with an autonomous conjugative plasmid that can be mobilized within the microbial community even by recipient cells that have become donors themselves; in the second one (graph below), a non-self-transmissible conjugation is carried out with a conjugative vector that, once acquired by recipient cells, cannot be further mobilized to other bacteria due to the lack of the conjugation machinery. In the graph, bacterial density is plotted over time. S: susceptible cells; R: resistant pathogens; P: probiotics.

of the synthetic circuitry was addressed by employing both phage infection and bacterial conjugation. In case of delivery with phage particles, experimental results were in agreement with model simulations as, with a MOI>10 (ratio of released phages to single recipient cells), the entire bacterial population was infected with CRISPR circuitry. Indeed, if in [51] the experiments were carried out at MOI 20, in our model the same value was fixed at 25. Moreover, in Citorik et al. the Cas9 cleavage of a chromosome-borne resistance resulted in a 5-fold reduction of bacterial density; similarly, in model simulations, the amount of target bacteria decreased by 6-fold due to phage infection. With regard to plasmid-borne resistance, Citorik et al. reported that a 4-fold reduction in the population of re-sensitized bacteria was achieved upon carbenicillin administration. In the same study, bacterial conjugation was also exploited to deliver a CRISPR circuitry programmed to target chromosome-borne resistances. Although target population was significantly reduced due to Cas9 cleavage of the chromosome, a low value of conjugation efficiency was reported as the number of viable recipients was only reduced by 2- to 3-fold compared to controls. In this case, experimental data were not comparable with model simulations or with the results reported in [48] and [66]. Finally, model predictions were compared with the experimental data obtained in this thesis work. As discussed in the previous sections, a non-self transmissible conjugation was here performed to deliver the CRISPRi circuitry to resistant bacteria bearing plasmid-borne resistance genes. The experimental set-up exploited in *in vivo* experiments was simulated by fixing the ratio between donor and recipient cells at 1:1. According to model predictions, almost the entire population of resistant pathogens receive the synthetic circuitry and evolve from resistant to susceptible state at the end of the simulation. This result differs significantly from the experimental data obtained in this thesis, in which the final amount of cells transformed in transconjugants resulted in a value of conjugation efficiency (susceptible cells relative

to total recipients) consistently lower. This outcome can be explained by considering that all the comparisons analysed in this section were carried by simulating an experimental set-up that was slightly different from the one exploited in *in vivo* experiments. Indeed, model simulations were carried out in the chemostat environment, in which the bacterial culture is well stirred in a liquid medium over time; conversely, in this work, the conjugation assay was performed on agar plates, thus preventing a homogeneous distribution of the bacterial culture during the conjugation event. This particular experimental set-up can be characterized by some biological or experimental aspects that could represent the limiting steps of a bacterial conjugation and that must be modelled more accurately in order to obtain more reliable predictions.

4.5 Main considerations on model predictions

The computational biology work herein presented aimed at simulating the effect of a CRISPR-based therapy on the eradication of AMR-associated infections. In particular, to identify *in silico* the best therapeutic strategy to use *in vivo*, a mathematical model was developed and then used to simulate and compare different biological scenarios. In more detail, the model aimed at simulating an experimental set-up where an engineered probiotic bacterium is employed as a delivery vehicle of the CRISPR circuitry to a population of antibiotic-resistant pathogens. This scenario was investigated by comparing two different delivery strategies, bacterial conjugation and phage infection, and DNA targeting mechanisms, CRISPRcut and CRISPRi technologies. First, a detailed revision of the literature was required to identify the most suitable models to describe the biological processes and to retrieve a specific set parameters. Then, each process was modeled with a system of differential equations implemented and solved with the software Matlab. By varying initial conditions, experimental set-up and parameters, different therapeutic solutions were modeled. Depending on the simulated scenario, the system consisted of 30 differential equations in case of targeting with CRISPRi and delivery via phage infection, up to 60 equations in case of targeting with CRISPRcut and delivery via bacterial conjugation. Model simulations revealed that the best therapeutic outcome was achieved by combining CRISPRcut technology and delivery via phage infection. This result was supported by two main observations: the high transfer rate of the synthetic circuit within the population of resistant pathogens and the targeting efficiency of the Cas9:gRNA complex. In more detail, the following considerations can be highlighted:

- starting from the same amount of probiotics at the beginning of the simulation, phage infection showed a temporal dynamics faster than bacterial conjugation; as the number of released phages was sufficient to infect the entire target population in few hours, DNA delivery resulted more efficient than in case of conjugative transfer;
- the Cas9 cleavage of target genes evolves with a dynamic faster than the one of HR-based repair, thus the DSB always resulted in DNA degradation. In case of plasmid-borne resistances, this event restored antibiotic susceptibility without killing the cells; otherwise, in case of chromosome-borne resistances, the DSB rapidly induced bacterial cell death. On the other hand, CRISPRi technology acted by inhibiting the expression of resistance genes without degrading the relative nucleotide sequences; this meant that, along with inactivating mutations within the CRISPRi circuitry, the target sequence could also mutate and provide immunity against antibiotic treatment.

4.5. Main considerations on model predictions

Model performances were also evaluated by comparing the predictions generated *in silico* with experimental data in which CRISPR/Cas9 or CRISPRi/dCas9 technologies, either delivered through phage infection or bacterial conjugation, were employed to target antibiotic resistant bacteria. Although model simulations predicted experimental data with satisfying performances, these comparisons highlighted some limitations. For example, to more accurately describe the biological processes involved in the therapeutic treatment, at least two aspects must be deepened: chemical and physical variables affecting DNA targeting mechanism and the evolution of nucleotide mutations in response of DNA damage. Moreover, a spatial distribution of the microbial communities was not considered in this model, although this aspect can significantly affects a realist prediction of the interactions that could occur among different microbes within the same habitat. In the future, to achieve a more faithful description of the desired scenario, the model can be refined by including some important aspects such as the spatial structure of the microbial population, which affects the efficiency of a genetic transfer, and the inherent stochasticity of living systems, which takes into account the heterogeneity of physiological behaviours shown by single individuals belonging to the same species and the outcome of the comparisons carried out in this work may change in one or more of the described cases. Finally, although the best strategy was identified as CRISPRcut with phage infection, the use of CRISPRcut instead of CRISPRi only leads to a modest improvement in pathogen re-sensitization, while the delivery strategy plays a more relevant role. Nonetheless, the choice of the two strategies should also consider other aspects, like the specificity and the availability of the delivery strategy and the potential mutations in the target DNA, reported to occur using CRISPRcut but not with CRISPRi, as described in this work. A more rational choice of therapeutic strategy will include a trade-off of all these aspect.

Chapter 5

Overall Conclusions

Antibiotic resistance is one of the major global health concern of our time. The ability of microbes to withstand the treatment with an antibiotic to which they were originally sensitive undermines the efficacy of even last resort drugs and threatens a return to a pre-antibiotic era in which human health could be again jeopardized by common infections. This scenario poses the need of huge scientific efforts to develop new therapies able to arrest the spread of MDR pathogens, evade bacterial defence mechanisms and preserve the antimicrobial activity of available drugs. In this work, a novel therapeutic strategy based on CRISPRi technology was proposed to address the threat of antibiotic resistance. In particular, the research work aimed at designing and characterizing a CRISPRi-based platform *ad hoc* programmed to inhibit the expression of antibiotic resistances and suitable for the delivery into resistant cells via bacterial conjugation. First, a synthetic platform carrying the CRISPRi circuitry was developed by including different genetic modules to drive the expression of single sgRNAs, dCas9 protein and *rfp* reporter gene chosen as repressible target. The quantitative characterization of each module revealed that the platform was highly flexible, as it included functional constitutive or inducible modules to finely regulate the expression of its components; moreover, its low impact on metabolic load was proven over traditionally adopted transcriptional regulators; finally, the tunability of the circuitry was demonstrated by leveraging an approach based on modifications of sgRNA sequence, which also allowed to restore the predicted logic function of a non-working synthetic circuit. However, the rational design of sgRNAs with the desired repression efficiency requires a deep characterization as reliable predictions of mismatches identity or site specificity is still a major hurdle to overcome. Despite this aspect, all the aforementioned attractive features made the CRISPRi-based platform a suitable solution to address the purpose of this work. Taking advantage from its high programmable nature, the CRISPRi platform was then repurposed to target antibiotic resistance genes in two case studies: model and clinically relevant resistances. Inhibition of target genes was expected to restore antibiotic susceptibility in resistant *E. coli* strains. By leveraging the pre-characterized gRNA module expressing single sgRNAs, the repression efficiency was investigated by determining the MIC of each target antibiotic in CRISPRi engineered strains upon drug administration in liquid and plate culture assays. A feasibility study was first carried out by redirecting the CRISPRi repressor complex towards *bla* and *tetA*, two example of model ARGs which confer resistance to ampicillin and tetracycline, respectively. Interesting results emerged from this pilot study: although the copy number of plasmid-borne resistance genes affected

the level of repression efficiency, even the expression of a target gene placed on high-copy plasmid was successfully inhibited, thus providing an encouraging result towards the treatment of highly expressed resistances; however, depending on the location of the target site, a reduction in repression strength was observed; moreover, the delay in growth recovery exhibited by CRISPRi-engineered strains upon antibiotic exposure was used to quantify the repression efficiency and also allowed to investigate more accurately the phenomena responsible for the rescue of survivor cells. The scale-up of the synthetic platform was then addressed in order to investigate the multi-targeting capability of CRISPRi system. Two novel genetic architectures, identified as sgRNA Cassettes and CRISPRi Array, were thus implemented with two different gRNAs; both were quantitative characterized in the transcriptional inhibition of the same model ARGs. Results revealed a reduction in repression efficiency due to the competition between gRNAs for the shared pool of dCas9 proteins. To counteract competition, a tuning of dCas9 intracellular level was carried out by replacing its constitutive expression module with an inducible device. Although this strategy allowed to find an optimal dCas9 expression level for target gene repression, the efficiency of single sgRNAs was not reached. An alternative strategy, based on already existing therapies, could be represented by the simultaneous administration of both antibiotics to test whether their combined effect can definitively arrest the growth of resistant cells. The genetic architecture based on CRISPRi Array, preferred to sgRNA cassettes because of its more compact structure, was then reprogrammed with single and double gRNAs to inhibit *NDM-1* and *mcr-1* genes, conferring resistance to meropenem and colistin, two broad-spectrum antibiotics used to treat MDR infections. Even in this case study, promising results were achieved as the susceptibility to both antibiotics was efficiently restored in almost the entire population of resistant cells. Moreover, the inhibition of *NDM-1* gene with a CRISPRi Array encoding for a non-specific gRNA (Array NDM1-mcr1) did not show a substantial reduction in repression efficiency compared to the same Array expressing only the specific gRNA (Array NDM-1). Compared to model ARGs (*bla* gene in HC plasmid), in this case the competition effect was probably mitigated by the lower copy number of the target plasmid (*NDM-1* in MC plasmid). Overall, starting from plate culture assays, the collection of circuits tested showed a repression efficiency ranging from 98% to 99,95% in case of *tetA*, *NDM-1* and *mcr-1* genes. The only exception was represented by *bla* gene: a repression efficiency of 99,58% was achieved only with a single sgRNA cassette targeting the promoter region while, in the remaining cases, the same value ranged from a minimum of 3,3% (CRISPRi Array) to a maximum of 50,6% (single sgRNA Cassette targeting *bla* gene CDS). With particular regard to *bla* gene, these results confirmed the ranking of repression efficiencies related to the different genetic architectures characterized (also demonstrated in liquid culture assays) but they did not represent the maximum level of transcriptional inhibition achievable in CRISPRi engineered strains. Indeed, as exploratory tests, plate culture assays were carried out with a single antibiotic concentration, which can be increased to verify if a MIC value could be established by administering a larger amount of drug. In case of liquid assays, as the control strain (*resistant strain*) always withstood even the highest antibiotic concentration between those tested, the reduction in the MIC value for a target antibiotic was not specifically defined. Only in case of *mcr-1* gene, the colistin MIC was reduced by 2.5 fold in CRISPRi-engineered cells (*silenced strain*) compared to the control strain. These results were comparable with previously published works in which CRISPR/Cas9 technology was exploited to tackle AMR. Indeed, the research works in which CRISPR/Cas9 was reprogrammed to target, and subsequently cleave, plasmid or chromosome-borne resistances reported a value of killing efficiency ranging from 90% to 99% in resistant strains of *S. aureus* [50], *E.coli* [51], *E.*

faecalis [66] and *C. rodentium* [70]; the same result was achieved with CRISPRi technology redirected towards a resistance gene placed on a plasmid [70] while, based on data reported in [74], the IC_{50} value for two resistances expressed from the IntI integron was reduced by 8 to 32 fold in *E.coli*. In this work, we have also investigated the rescue of survivor cells, defined as "escapers", recovered from a background of re-sensitized bacteria upon the exposure to target antibiotic. This phenomenon was analysed with liquid culture assays and sequencing analysis: the former allowed to identify two different bacterial antibiotic responses (resistance and resilience) from the growth profiles of survivor cells; the latter proved that, although loss of function mutations within the CRISPRi circuitry could not be avoided, the nucleotide sequence of target gene was never altered by CRISPRi-mediated repression. This was a relevant result as it proves that the transcriptional inhibition, rather than the Cas9-mediated cleavage of target genes, could provide a silent but also efficient strategy to circumvent the risk of generating new variants of resistance determinants. To our knowledge, this is the first report in which even the nature of CRISPRi escapers was investigated, while the mutations within target gene [46, 48, 70, 71, 72] or CRISPR/Cas9 machinery [48, 50, 51, 68, 68] have already been reported by different research groups. The delivery of CRISPRi circuitry to target bacteria, which is one of the main obstacle to translate this technology in a viable therapeutic, was addressed by developing a *trans*-conjugative platform suited to perform a non-self-transmissible conjugation from donor to resistant recipient bacteria harbouring *bla* or *mcr-1* gene. In both cases, under selection for cells that have received the CRISPRi circuitry, a low value of conjugation efficiency was measured (ranging from $1x10^{-5}$ to $3x10^{-3}$), although the same was consistent with the literature [48]. On the other hand, the CRISPRi-mediated inhibition of target genes in recipient cells resulted in a killing efficiency of 96% and 99,58% in case of *bla* and *mcr-1* gene, respectively. These results demonstrated that the high repression capability of the CRISPRi circuitry is unavoidably limited by the low frequency of the conjugative transfer which, to date, represents the bottle-neck of the entire process. Finally, the therapeutic outcomes derived from a CRISPR-based treatment of AMR infections were investigated by implementing a mathematical model: the latter simulated the delivery (via bacterial conjugation or phage infection) of a CRISPR circuitry (CRISPR/Cas9 or CRISPRi/dCas9) from a probiotic bacterium to a population of resistant cells colonizing an habitat (chemostat) in which the flux of nutrients in input and the removal of waste in output mimics the exchange of organic material observed, for instance, in the human intestine. Model simulations confirmed experimental data as both targeting strategies resulted extremely efficient in the re-sensitisation of antibiotic resistant bacteria. However, due to the fast dynamics of Cas9 cleavage, the number of resistant cells at the end of the simulations was always lower with CRISPR/Cas9 than CRISPRi technology, which preserved target sequence from degradation but not from the risk of evolving mutations impeding the same CRISPRi targeting. Moreover, due to its prolonged temporal dynamics, the genetic transfer via bacterial conjugation resulted less efficient than the one based on phage infection, which allowed a rapid transmission of CRISPR circuitry to the entire target population. However, the described dynamics could be significantly altered by the presence of commensal microbes: indeed, regardless of targeting technology or delivery mechanism, the contribution of commensals in consuming shared nutrients and occupying available space was always necessary to limit the proliferation of resistant bacteria. It is also worth noting that the final outcome is expected to be dependent on the basal mutation rate in target cells, due to its role in the evolution of mutations inactivating CRISPR machinery or modifying the target sequence. With this regard, the role of SOS response in increasing the basal mutation rate upon exogenous DNA uptake or Cas9 cleavage needs to be

investigated in depth. Nevertheless, model predictions must be reviewed by considering the following aspects: first, although their efficacy is known, the use of bacteriophages as therapeutics could be limited by their narrow host range and by the potential evolution of resistance in target bacteria; second, even if CRISPR/Cas9 technology seemed to be the most attractive strategy to eradicate AMR infections, several research works have already shown that the evolution of mutations within resistance genes can rescue the cell from Cas9 cleavage while, as demonstrated in this thesis, the same outcome can be prevented by employing CRISPRi technology. This is an important consequence to highlight as, in case of mutations within CRISPRi machinery, a second administration of engineered probiotics and antibiotics could be still considered to definitively eradicate the infection; the same strategy would be useless if the residual population has evolved mutations in target sequence that provide immunity against CRISPR targeting.

The research work herein presented has provided promising results but has also encouraged the investigation towards the scientific efforts needed to translate the CRISPRi-based platform in a viable therapeutic. The entire genetic platform must be customized in order to address the spectrum of biological conditions associated with an AMR infection. First, a probiotic bacterium that naturally colonizes the treated niche (for instance, a specific district of the human intestine) must be selected and engineered as a vehicle for the *in situ* delivery of the CRISPRi circuitry to the population of resistant pathogens. To this aim, an *E. coli* strain (e.g. *E. coli Nissle* 1917) or a member of the *Lactobacillales* approved for probiotic use could be considered for the clinical context. Second, the overall conjugation frequency must be increased in order to mobilize the synthetic circuit in the largest number of resistant cells. With this purpose, a self-transmissible conjugation could be explored in order to amplify the spread of the CRISPR therapeutic within the target microbial community. Moreover, an effective plasmid delivery only to recipient pathogens requires the identification of the most suitable conjugative vector from a collection of broad and narrow-host range plasmids. Finally, to complete the design of a host-specific platform, even the regulatory parts driving the expression of the CRISPRi circuitry must be customized. Obviously, each inducible device needs to be replaced with a constitutive expression module suited to guaranteeing an effective antimicrobial activity within target recipient pathogens but also no toxicity when expressed in donor cells. Indeed, to date, the characterization of constitutive dCas9 expression modules has been hampered by the toxic effect exhibited above a threshold value in host cells. Two main approaches can be exploited to address the construction of a host-specific antimicrobial: the first is based on the characterization of specific regulatory elements known to be functional in the host organism; the second relies on the identification of the most suitable biological parts by performing iterative cycles with available libraries of transcriptional regulators. This last solution, which requires a significant investment in terms of money and time, can be overcome by the development of new technologies able to support the rational choice of, for example, promoters and RBSs or to provide new regulatory parts with increased portability in different host strains. Clearly, this future plan presupposes the ability to engineer the host strain with the collection of candidate circuits delivered via conjugation. Lastly, the biocontainment of engineered donor cells harbouring the CRISPRi circuitry must be addressed in order to create a genetic platform which is suitable for the designed antimicrobial function but also compliant with the regulatory requirements concerning genetically modified microorganisms (GMMs). The herein presented CRISPRi-based therapy starts with the oral administration of a GM probiotic which can be subsequently released in the environment through fecal waste. In particular, the antibiotic resistance cassette used as selective marker in the plasmide-borne CRISPRi circuitry has the potential to

be acquired by other microorganisms upon probiotic lysis (as extracellular DNA) or via HGT mechanisms. Although the antibiotic therapy used to eradicate the population of re-sensitized pathogens is expected to kill even engineered donor cells, different biocontainment approaches can be harnessed to minimize the environmental escape of the engineered biological system. For example, two of the major chemical biocontainment strategies aim at inhibiting bacterial replication or the horizontal exchange of genetic material. In our case study, the proliferation and subsequent colonization of the treated niche by engineered cells could be hampered by employing an auxotrophic GMM whose growth is dependent on a key metabolite, supplied only in the laboratory experimental set-up [126]; on the other hand, the release of resistant determinants via bacterial conjugation can be controlled by identifying a collection of narrow-host range conjugative plasmids suitable to restrict the spectrum of targeted cells. The aforementioned approaches allow to reduce the escape rate of GMMs but do not completely avoid the release of resistance genes in the natural environment. To address this challenge, the CRISPRi platform can be equipped with an inducible biocontainment module programmed to kill the cell (i.e. toxin-antitoxin systems, inhibition of essential genes expression) or degrade plasmid DNA (plasmid curing) in presence of a localized endogenous signal. The biocontainment system can be implemented with synthetic circuits encoding for transcriptional factors that regulate gene expression or by harnessing the CRISPR/Cas9 technology, which allows sequence-specific degradation of target DNA [127]. Along with the chemical approaches, a physical biocontainment technology has been recently proposed to overcome the basal mutation rate in GMMs, which may deactivate the biocontainment module. An encapsulation system, based on suited polymers like hydrogels, can be leveraged to construct a physical barrier between cells and the natural environment, ensuring the uptake of essential and functional molecules but also the biological containment of the engineered cells [128]. However, this latest strategy may not be suitable for our case study as the hydrogel barrier can prevent cell to cell contact, including bacterial conjugation. Finally, a resolutive way to address the biosafety concerns depends on the possibility to engineer endogenous plasmids in the chassis microorganism and eliminate all the antibiotic resistance cassettes that have been conveniently used in this work during strain characterization.

In conclusion, the research work presented in this thesis aimed at developing a CRISPRi-based platform to treat AMR-associated infections. Two main genetic architectures were characterized and compared in order to measure repression capability and identify the major limitations of the designed platform. Overall, the results obtained suggested that the transcriptional inhibition of target genes can be adopted as an effective silent strategy to tackle AMR, although the low efficiency of bacterial conjugation limits the CRISPRi antimicrobial action. Huge scientific efforts are still needed to optimize the synthetic platform and to translate the same in an effective therapy, but the work herein presented laid the foundations for further investigating the potential of CRISPRi technology in the global fight against antibiotic resistance.

Appendix A

Supplementary Information for Chapter 2 and 3

A.1 Materials and Reagents

In this chapter all the materials and methods used are listed. First, all reagents, growth media and bacterial strains employed are illustrated in Section A.1. Secondly, a description of the molecular biology techniques adopted to obtain the engineered bacterial strains is reported in Section A.2. Finally the genetic architectures herein exploited are described with detailed information about design specifications (Section A.2.3) and the complete lists of basic biological parts, primers and final synthetic circuits obtained are reported in separate tables (Section A.2 and Section A.2.4).

A.1.1 Culture Media and Bacterial Strains

Two major types of culture media were used in this study to support bacterial growth and perform cell culture assays.

- **Luria-Bertani (LB)** is a nutritionally rich medium that was used to propagate recombinat bacterial cultures, prepare glycerol stock and perform liquid or soldid culture assays. The medium is composed of: sodium chloride 10 g/l, tryptone 10 g/l, yeast extract 5g/l. For solid media, 15 g/l of agar was added; antibiotics, listed in the following section, were added as required to prepare selective media.

- **M9** is a minimal growth medium that was used for quantitative fluorescence assays thanks to its low auto-fluorescence. The medium is composed of: M9 salts 11.28 g/L, thiamine hydrochloride 1 mM, MgSO4 2 mM, CaCl2 0.1 mM, casamino acids 2 g/L and glycerol 0.4%. When required, antibiotics were added to prepare selective media.

All the experiments were performed in the bacterium *E. coli* chosen as model organism. The list of strains employed included: TOP10, TOP10 F', DH5α (bearing the plasmids pGDP1_NDM1 or pGDP2_mcr1) and DH10B (bearing the plasmid pTA-Mob).

A.1.2 Antibiotics

In this study, antibiotics were used for two main purposes: to propagate and select recombinant bacteria bearing one or more plasmids encoding the correspondent resistance genes; to perform liquid and solid culture assays aimed at investigate the MIC of engineered strains with CRISPRi circuitry towards a target antibiotic. The list of antibiotic used is reported below.

- **Chloramphenicol (Cm)**: the molecule inhibits bacterial protein synthesis by binding the 50S ribosomal subunit and thus blocking the translational process of mRNAs. Chloramphenicol was used as a marker for the selection of bacteria bearing the low-copy number vector pSB4C5. The antibiotic is conserved at -20°C at a concentration of $34mg/ml$; the working concentration is $12.5\mu g/ml$.
- **Kanamycin (Kan)**: the molecule inhibits bacterial protein synthesis by binding the 30S ribosomal subunit and thus blocking the translational process of mRNAs. Kanamycin was used as a marker for the selection of bacteria bearing the medium-copy number vector pSB3K3 or medium copy plasmids pGDP1-NDM1 and pGDP2-mcr1. This molecule is conserved at -20°C in a concentration of $50mg/ml$; the working concentration is $25\mu g/ml$.
- **Ampicillin (Amp)**: is a β-lactam antibiotic that inhibits bacterial cell-wall synthesis by inactivating transpeptidase enzyme. Ampicillin was used as a marker for the selection of bacteria transformed with the high-copy number vector pSB1A2 and to propagate the *E. coli* strain bearing the pRK2 plasmid (RK2 ATCC #37125). This molecule is conserved at -20°C at a concentration of $100mg/ml$; the working concentration depends on the final application:
  - $100\mu g/ml$ to select bacteria bearing the high-copy vector pSB1A2 and to perform plate culture assays with CRISPRi engineered strains;
  - $50\mu g/ml$ to select bacteria bearing the pRK2 plasmid;
  - a range of concentrations in liquid assays performed to investigate the MIC of CRISPRi engineered strains;
  - 100 and $1000\mu g/ml$ in conjugation assay to evaluate conjugation and killing efficiency.
- **Tetracycline (Tetra)**: the molecule inhibits bacterial protein synthesis by binding the 30S ribosomal subunit and thus blocking the translational process of mRNAs. Tetracycline was used as a marker for the selection of the *E. coli* TOP 10 F' strain naturally bearing the F' plasmid. This molecule is conserved at -20°C at a concentration of $5mg/ml$; the working concentration depends on the final application:
  - $15\mu g/ml$ to select bacteria bearing the F' plasmid and to perform plate culture assays with CRISPRi engineered strains;
  - a range of concentrations in liquid assays performed to investigate the MIC of CRISPRi engineered strains.
- **Gentamicin (Genta)**: the molecule inhibits bacterial protein synthesis by binding the 30S ribosomal subunit and thus blocking the translational process of mRNAs. Gentamicin was used as a marker for the selection of the *E. coli* DH10B strain bearing the plasmid pTA-Mob [88]. This molecule is conserved at -20°C in a concentration of $50mg/ml$; the working concentration is $20\mu g/ml$.

- **Meropenem (Mero)**: the molecule is a ultra-broad spectrum β-lactam antibiotic that inhibits bacterial cell-wall synthesis by covalently bindind specific penicillin-binding proteins (PBP). *NDM1* gene, which confers resistance to this antibiotic, is placed on pGDP1-NDM1 plasmid (Addgene n.#112883). Meropenem powder is diluted in deionyzed water containing $10.4 mg/ml$ of sodium carbonate and conserved at -20°C in a concentration of $50 mg/ml$; the working concentration depends on the final application:
  - $64 \mu g/ml$ in plate culture assays with CRISPRi engineered strains;
  - a range of concentrations in liquid assays performed to investigate the MIC of CRISPRi engineered strains.
- **Colisin (Colis)**: the molecule is a broad spectrum antibiotic that binds the lipid A (a component of LPS) and disrupts the integrity of the outer cell membrane in Gram negative bacteria. *mcr-1* gene, which confers resistance to this antibiotic, is placed on pGDP2-mcr1 plasmid (Addgene n.#118404). Colistin powder is diluted in deionyzed water and the stock conserved 20°C in a concentration of $60 mg/ml$; the working concentration depends on the final application:
  - $1 \mu g/ml$ in plate culture assays with CRISPRi engineered strains and in conjugation assay to evaluate conjugation and killing efficiency;
  - a range of concentrations in liquid assays performed to investigate the MIC of CRISPRi engineered strains.

A.1.3 Inducers

Inducers are small molecules that regulate gene expression by repressing or activating the transcriptional activity of a promoter placed upstream the target gene. In this study, the two inducer molecules HSL and IPTG were used to activate the Lux- and Lac-circuitries, respectively.

- **N-(3-oxohexanoyl)-L-homoserine lactone (HSL)**: it is a small molecule able to freely permeate through bacterial membrane. The binding between HSL molecule and LuxR protein forms an active complex responsible for the activation of the transcriptional activity of P_{Lux} promoter. The HSL molecule was purchased from Sigma Aldrich (K3007), dissolved in deionized water at final concentration of $200 mM$ and conserved at -20°C.
- **Isopropyl β-D-thiogalactopyranoside (IPTG)**: it is a synthetic, structural analogue of allolactose, the molecule that naturally triggers the expression of genes placed in lac operon. Like allolactose, IPTG binds to the lacI protein and releases the tetrameric repressor from the lac operator, thereby allowing the transcription of genes placed under P_{Lac} promoter. Unlike allolactose, IPTG is not metabolized thus providing a constant concentration of the inducer within the cell. IPTG molecule was purchased from Sigma Aldrich (I1284) in a ready to use solution at a concentration of $2 mM$ and conserved at -20°C.

A.2 Cloning

A.2.1 BioBrick™ Standard Assembly

The *E. coli* TOP10 (Invitrogen) strain was used as a host for cloning and *in vivo* propagation of the plasmids. The strain was transformed by heat shock according to manufacturer's instructions and recombinant bacteria were propagated in LB at 37°C, 220 rpm. Glycerol stocks were prepared with 750 μl of saturated culture with proper antibiotics and 250 μl of glycerol 80%, and stored at -80°C. All the plasmids used in this study were assembled through the BioBrick™ Standard Assembly [129] and conventional molecular biology techniques. As a result, standard DNA junctions (TACTAG upstream of coding sequences, TACTAGAG otherwise) are present between assembled parts. The basic or composite parts used for DNA assembly were retrieved from three main sources: existing plasmids avaliable in the MIT Registry of Standard Biological Parts (see Table A.3); customized gene blocks (purchased from Genscript DNA synthesis service); purified strains (RK2 #37125 from the ATCC culture collection). The adopted cloning protocol is described below:

- plasmid DNA was extracted from saturated 5 ml cultures (grown in LB at 37°C, 220rpm) through the NucleoSpin Plasmid kit (Macherey-Nagel), according to manufacturer's protocol;
- purified DNA was digested as appropriate with EcoRI/XbaI/SpeI/PstI enzymes, according to the BioBrick™ Standard Assembly procedure; fragments of interest were extracted from 1% agarose gel by NucleoSpin Extract II Kit (Macherey-Nagel) and PCR cleanup before proceeding with ligation;
- inserts were ligated into vectors with T4 DNA ligase and the reaction was incubated at 16°C overnight.
- a diagnostic restriction digest of each construct was perfomed to identify correctly assembled clones, that were further sequence-verified via the Eurofins Genomics Germany GmbH DNA analysis service (Ebersberg, Germany)

All the restriction enzymes were purchased from Thermo Fisher Scientific, while T4 DNA ligase were purchased from Invitrogen. The described protocol was also performed to ligate customized gene blocks in existing plasmids. To this aim, each gene block was provided with tails of additional nucleotides carrying a properly specified restriction site. The basic parts composing each gene block and the name of the resulting plasmid where the same was cloned are reported in Table A.1. The complete list of constructs obtained in this study is reported in Table A.4.

Table A.1: **Synthetic gene blocks.** The table shows the gene blocks used in this study. The BioBrick^{TM} code of individual parts composing each block is reported along with the name of the resulting plasmid where the same was cloned.

Name	Parts	Recipient plasmid
Array gAmpR_gtetA	XbaI + BBa_J23100 + tracrR + BBa_B1002 + SpeI + BBa_R0011 + repeat + gAmpRpromoter + repeat + gtetA + repeat + BglII + BBa_B1006 + NotI + PstI	Array gAmpRpromoter_gtetA and AE$_{-3A}$dArray gAmpRpromoter_gtetA
Array NDM1	XbaI + BBa_J23100 + tracrR + BBa_B1002 + SpeI + BBa_R0011 + repeat + gNDM1 + repeat + BglII + BBa_B1006 + NotI + PstI	AE$_{-3A}$dArray_NDM1
Array NDM2	BBa_J23100 + tracrR + BBa_B1002 + SpeI + BBa_R0011 + repeat + gNDM2 + repeat + BglII + BBa_B1006 + NotI + PstI	AE$_{-3A}$dArray_NDM2
Array NDM1_NDM2	BBa_J23100 + tracrR + BBa_B1002 + SpeI + BBa_R0011 + repeat + gNDM1 + repeat + gNDM2 + repeat + BglII + BBa_B1006 + NotI + PstI	AE$_{-3A}$dArray_NDM1_NDM2
Array NDM1_mcr1	BBa_J23100 + tracrR + BBa_B1002 + SpeI + BBa_R0011 + repeat + gNDM1 + repeat + gmcr1 + repeat + BglII + BBa_B1006 + NotI + PstI	AE$_{-3A}$dArray_NDM1_mcr1

A.2.2 Mutagenesis

The mutagenesis protocol was performed to modify the sequence of a template plasmid or to amplify a DNA fragment from an existing vector by extending its sequence with selected restriction sites. In particular, mutagenesis with divergent primers was adopted to construct custom sgRNAs and simultaneously delete nucleotides after the transcription start sites of the used promoters, where indicated. The plasmid harbouring the perfectly-matching guide RNA was used as template in the mutagenic PCR. *Reverse* primers annealed the sequence of the promoter placed upstream the guide to be mutagenized. *Forward* primers had two regions: the first carried the sequence of the sgRNA with the desired mutation (deletions or mismatches); the second, annealed the 5' end of

tracrRNA, in order to have always at least 20 perfectly-matching nucleotides at the 3' end of the primer. Mutagenesis with convergent primers was instead performed to amply a DNA fragment from genomic template in order to provide the PCR amplicon with tails of additional nucleotides carrying the XbaI restriction site. The complete list of primers used in this study is reported in Table A.2. The experimental protocol was performed as follows.

- The template DNA was purified through the NucleoSpin Plasmid kit (Macherey-Nagel) in case it was a plasmid from a bacterial culture; otherwise, in case of amplification from genomic template, a bacterial colony was suspended in 100 μl of deionyzed water and 1 μl was used for the PCR protocol. Phusion Hot Start Flex II (ThermoFisher Scientific) was used to perform the PCR reaction according to manufacturer's protocol; in the reaction mix was added the appropriate primer pair, for which annealing temperatures was estimated on the free online tool T_m Calculator (ThermoFisher Scientific) with parameters set to "Phusion or Phire DNA polymerase".
- At the end of PCR reaction, the methylated template DNA was digested at 37°C for 1 h with DpnI (Thermo Scientific), directly added in the reaction mix; the PCR products were run in a 1% agarose gel and then purified with NucleoSpin Extract II Kit (Macherey-Nagel).
- In case of mutagenesis with divergent primers, fifty nanograms of the blunt-ended linear fragments were phosphorylated by polynucleotide kinase (PNK, Thermo Scientific) using the T4 ligase buffer. The reaction was carried out at 37°C for 20 minutes, then 1 μl of ligase was added and incubated for 16 h at 16°C. In case of mutagenesis with convergent primers, the amplicon with XbaI restriction sites at both ends was digested and purified with PCR clean up protocol; the same was further ligated in the recipient vector previously dephosphorylated with Antartic Phosphatase (NEB), according to the manufacturer's protocol.
- Finally, at the end of the ligation reaction, the enzymes were deactivated for 10 min at 75°C, if present PNK and Ligase, or 65°C, if present only ligase. The ligation product was transformed in *E. coli* competent cells and the mutagenized plasmid was screened via restriction enzymes digestion and sequencing.

Table A.2: **Primers used in this study.** For each template reported in the first column, the primer pairs used to obtain the final product are shown; the purpose of each DNA manipulation is outlined, together with the final product obtained.

Template	Primer Pairs	Sequence (5' - 3')	Aim	Product
AEgPtet_PtetRFP	FW_gPtet_DM1	tgtctaactctatcactgatg ttttagagctagaaatagca	Insert gPtet_DM1 and remove three adenide nucleotides located after TSS of P_{Lux}	$AEgPtet_{DM1}$ _PtetRFP
	RV_Plux-3A	attcgactataacaaaccat tttcttgcgtaaacctgtac		
AEgPtet_PtetRFP	FW_gPtet_DM3	tgtcaatcactataactgatg ttttagagctagaaatagca	Insert gPtet_DM3 and remove three adenide nucleotides located after TSS of P_{Lux}	$AEgPtet_{DM3}$ _PtetRFP
	RV_Plux-3A	attcgactataacaaaccat tttcttgcgtaaacctgtac		
AEgPtet_PtetRFP	FW_gPtet_DM4	tgtcaatctctatccctgttg ttttagagctagaaatagca agtt	Insert gPtet_DM4	$AEgPtet_{DM4}$ _PtetRFP
	RV_Plux AAA	tttattcgactataacaaacc attttcttgcgtaaacctg		

Continues on next page...

Table A.2 – *...continued from previous page*

Template	Primer Pairs	Sequence (5' - 3')	Aim	Product
AEgPtet_PtetRFP	FW_gPtet_DM5	tgtcaatctctatcacggacg ttttagagctagaaatagca agtt	Insert gPtet_DM5	AEgPtet$_{DM5}$ _PtetRFP
	RV_Plux AAA	tttattcgactataacaaacc attttcttgcgtaaacctg		
AEgPtet_PtetRFP	FW_gPtet_d5	atctctatcactgatgtttta gagctagaaata	Remove 5 nucleotides from gPtet to obtain gPtet_d5	AEgPtet$_{d5}$ _PtetRFP
	RV_Plux AAA	tttattcgactataacaaacc attttcttgcgtaaacctg		
AEgPtet_PtetRFP	FW_gPtet_d7	ctctatcactgatgttttaga gctagaaatagcaa	Remove 7 nucleotides from gPtet to obtain gPtet_d7	AEgPtet$_{d7}$ _PtetRFP
	RV_Plux AAA	tttattcgactataacaaacc attttcttgcgtaaacctg		
AEgPtet_PtetRFP	FW_gPtet_d10	tatcactgatgttttagagct agaaatagcaagt	Remove 10 nucleotides from gPtet to obtain gPtet_d10	AEgPtet$_{d10}$ _PtetRFP
	RV_Plux AAA	tttattcgactataacaaacc attttcttgcgtaaacctg		
AEgPtet_PtetRFP	FW_gPtet_d15	ctgatgttttagagctagaa atagcaagttaaaa	Remove 15 nucleotides from gPtet to obtain gPtet_d15	AEgPtet$_{d15}$ _PtetRFP
	RV_Plux AAA	tttattcgactataacaaacc attttcttgcgtaaacctg		
AEgPtet_PtetRFP	FW_gPtet_degenerato	tgtcaatctctNtcNcNga tgttttagagctagaaatag	Insert gPtet variants with degenerate nucleotides	AEgPtet$_{(DEG)}$ _PtetRFP
	RV_Plux AAA	tttattcgactataacaaacc attttcttgcgtaaacctg		
gBlock_Plac_gComp	FW_gAmpR_promoter	cagggttattgtctcatgag gttttagagctagaaatagc aagttaaaat	Insert the sgRNA gAmpRpromoter under P_{LlacO1} in LC plasmid	gAmpR_promoter
	RV_Plac	tgtgctcagtatcttgttatc cgctc		
gBlock_Plac_gComp	FW_gAmpR_gene	ttactttcaccagcgtttctg ttttagagctagaaatagca agttaaaat	Insert the sgRNA gAmpRgene under P_{LlacO1} in LC plasmid	gAmpR_gene
	RV_Plac	tgtgctcagtatcttgttatc cgctc		
gBlock_Plac_gComp	FW_tetA	catgataaggccaatcccca gttttagagctagaaatagc aagttaaaat	Insert the sgRNA gtetA under P_{LlacO1} in LC plasmid	gtetA
	RV_Plac	tgtgctcagtatcttgttatc cgctc		
pRK2	FW_14	tcatatctagagacgcccgt gattttgtagc	Amplify oriT sequence by adding XbaI restriction sites at the end of the PCR amplicon	oriT_AE$_{-3A}$d Array NDM1 \NDM2 \NDM1_NDM2 \NDM1_mcr1
	RV_4	tatactctagattgccaaag ggttcgtgtag		
AE$_{-3A}$d Array	C0062_VF	gaatgtttagcgtgggcatg	Sequencing of CRISPRi Array and dCas9 gene from all the circuits holding NDM and mcr spacers	
	FW_dCas9	caatccatcactggtctttat g		
pGDP1_NDM-1	FW_pGDP	cgtatcggtgattcattctgc	Sequencing of NDM-1 target gene	
pGDP2_mcr-1	FW_pGDP	cgtatcggtgattcattctgc	Sequencing of mcr-1 target gene	

A.2.3 sgRNA cassette and CRISPRi Array design

All the sgRNAs used in this study were designed via the Benchling CRISPR tool, setting a guide length of 20 nucleotides, NGG from *S. pyogenes* as PAM sequence, GCA_00005845.2 as reference genome, and using the Optimized Score described in [130]. The sgRNA cassette was based on the design by Jinek et al. [42], and a 20-nt sequence was designed to target the P_{LtetO1}, P_{LlacO1}, P_{bla} promoters as well as the coding sequence of *bla* and *tetA* genes. Along with the customized guide sequence, each sgRNA had a constant region com-

prised the gRNA linker and tracrRNA with its own terminator (BBa_J107201). All the sgRNAs were obtained through the Mutagenesis protocol described in Section A.2.2 and with a specific pair of primers listed in Table A.2. Benchling platform was also adopted for the design of CRISPRi Arrays with single or double spacers targeting P_{bla} promoter or the coding sequence of *tetA*, *NDM1* and *mcr-1* genes. The 30-nt sequence composing each spacer was selected within the CDS of the relative gene and in a locus proximal to the start codon, except in case of gNDM2 (gNDM1 and gNDM2: +13 and + 208 bp of NDM-1 coding sequence, respectively; gmcr: +29 bp of mcr-1 coding sequence). The spacer sequence was the only customized part of the CRISPRi Array as the other components derived from the synthetic architecture characterized in [131]. The Arrays used in this study are all listed in Table A.1 and were implemented in synthetic circuits according to the Cloning protocol described in Section A.2.1. Nucleotide sequences of target genes were retrieved from online databases such us iGEM Parts Registry (*bla* gene within pSB1A2 vector), NCBI (tn10 Transposon encoding *tetA* gene, GenBank: J01830.1) and CARD (for *NDM1* and *mcr-1* genes variants). For the design of gNDM1 and gmcr1, targeting the relative resistance genes, the Clustal Omega tool was used to perform multiple sequence alignment with the all know variants of both genes. oriT sequence was amplified from pRK2 through a mutagenic PCR with convergent primers (see Table A.2), as described in Section A.2.2. The amplicon was cloned upstream the CRISPRi Arrays in low copy vector mobilized by the the conjugative machinery expressed in *trans* by the pTA-Mob helper plasmid [1] [88].

A.2.4 List of constructs

The biological parts used in this study, as well as the final synthetic constructs obtained, are reported in this section and separately listed in two tables.

Table A.3: **BioBrick™ parts and constructs used in this study for circuits assembly.**

Name	BioBrick Code	Description
P_{Lux}	BBa_R0062	LuxR positive-inducible promoter
P_{LtetO1}	BBa_R0040	tetR repressible promoter
P_{LlacO1}	BBa_R0011	IPTG-inducible promoter
P_R	BBa_R0051	Constitutive promoter from λ bacteriophage for LuxR expression
J23100	BBa_J23100	Constitutive promoter placed in the Monitor cassette and upstream tracrRNA in CRISPRi Array
J23101	BBa_J23101	Reference constitutive promoter

Continue on next page...

[1] pTA-Mob plasmid was kindly provided by Prof. Rahmi Lale (Norwegian University of Science and Technology).

Table A.3 – *...continued from previous page*

Name	BioBrick Code	Description
J23116	BBa_J23116	Weak constitutive promoter
J23119	BBa_J23119	Strong constitutive promoter
B0030	BBa_B0030	Strong RBS of LuxR
B0031	BBa_B0031	Weak RBS
B0032	BBa_B0032	Medium-strength RBS
B0034	BBa_B0034	Strong RBS
B0015	BBa_B0015	Double transcriptional terminator
B1006	BBa_B1006	Synthetic transcriptional terminator
B1002	BBa_B1002	Synthetic transcriptional terminator for tracrRNA in CRISPRi Array
LuxR	BBa_C0062	LuxR coding sequence
LacI	BBa_C0012	LacI coding sequence
mRFP1	BBa_E1010	RFP coding sequence
GFPmut3b	BBa_E0040	GFP coding sequence
dCas9	BBa J107200	Coding sequence of Sp. dCas9 from Addgene plasmid #44249 with B0034 RBS and B0015 terminator.
tracr	BBa_J107201	tracr RNA for Sp.dCas9 with tetraloop and trasnscriptional terminator from Addgene plasmid #44251
tracrR	ggaaccattcaaaacagcatagcaagttaaaataaggctagtccgttatcaacttgaaaaagtggcaccgagtcggtgctttttt	tracr RNA inserted in CRISPRi Array and derived by [131]
Repeat	gttttagagctatgctgttttgaatggtcccaaaac	Repeat sequence placed between spacers in CRISPRi Array derived by [131]
J116dCas9	BBa_J107202 + pSB3K3	Constitutive dCas9 cassette in MC plasmid
A37	BBa_J23100 + BBa_B0032 + BBa_E0040 + BBa_B0015 + pSB4C5	GFP-based burden monitor in LC plasmid
AE	A37 + BBa_R0051 + BBa_B0030 + BBa_C0062 + BBa_B1006 + BBa R0062 + pSB4C5	Burden monitor and HSL-inducible module under the control of the wilde-type P_{Lux} promoter in LC plasmid

Continue on next page...

Table A.3 – *...continued from previous page*

Name	BioBrick Code	Description
AE_3Ad	J107216	Burden monitor and HSL-inducible dCas9 under the control of P_{Lux-3A} promoter in LC plasmid

Table A.4: **Synthetic constructs obtained in this study.** The table shows the list of constructs obtained in this study. The BioBrick™ code of individual parts composing each plasmid is reported along with the function designed for the same circuit.

Name	Construct	Purpose
AE_3Ad_J116gPtet	J107217 + pSB4C5	CRISPRi efficiency characterization on P_{LtetO1} promoter with inducible dCas9 and weak constitutive gPtet in LC plasmid
AE_3Ad_J100gPtet	J107218 + pSB4C5	CRISPRi efficiency characterization on P_{LtetO1} promoter with inducible dCas9 and medium-strength constitutive gPtet in LC plasmid
AE_3Ad_J119gPtet	J107219 + pSB4C5	CRISPRi efficiency characterization on P_{LtetO1} promoter with inducible dCas9 and strong constitutive gPtet in LC plasmid
AE_3Ad_J116gPlac	J107220 + pSB4C5	CRISPRi efficiency characterization on P_{LlacO1} promoter with inducible dCas9 and weak constitutive gPlac in LC plasmid
AE_3Ad_J100gPlac	J107221 + pSB4C5	CRISPRi efficiency characterization on P_{LlacO1} promoter with inducible dCas9 and medium-strength constitutive gPlac in LC plasmid
AE_3Ad_J119gPlac	J107222 + pSB4C5	CRISPRi efficiency characterization on P_{LlacO1} promoter with inducible dCas9 and strong constitutive gPlac in LC plasmid
AEgPtet_PtetRFP	J107249 + pSB4C5	CRISPRi efficiency characterization on P_{LtetO1} promoter with constitutive dCas9 in MC and inducible gPtet in LC plasmid

Continues on next page...

Table A.4 – *...continued from previous page*

Name	Construct	Purpose
AEgPtet$_{(n)}$_PtetRFP	J107249 + pSB4C5	CRISPRi efficiency characterization on P_{LtetO1} promoter with constitutive dCas9 in MC and inducible gPtet variants with [n]-nt truncations in LC plasmid
AEgPtet$_{(DM)}$_PtetRFP	J107249 + pSB4C5	CRISPRi efficiency characterization on P_{LtetO1} promoter with constitutive dCas9 in MC and inducible gPtet variants with double mismatches in LC plasmid
AEgPtet$_{(DEG)}$_PtetRFP	J107249 + pSB4C5	CRISPRi efficiency characterization on P_{LtetO1} promoter with constitutive dCas9 in MC and inducible gPtet variants with degenerate nucleotides in LC plasmid
AEgPtet$_{DEG9}$_PtetRFP	J107252 + pSB4C5	CRISPRi efficiency characterization on P_{LtetO1} promoter with constitutive dCas9 in MC and inducible gPtet$_{DEG9}$ with in LC plasmid
AE$_{-3A}$gPtet$_{DEG9}$_PtetRFP	J107254 + pSB4C5	CRISPRi efficiency characterization on P_{LtetO1} promoter with constitutive dCas9 in MC and inducible gPtet$_{DEG9}$ under P_{Lux-3A} promoter in LC plasmid
Final cascade	J107255 + pSB4C5	CRISPRi efficiency characterization for a transcriptional cascade including the inducible gPtet$_{DEG9}$ variant and a lacI-based logic inverter in LC plasmid
gAmpRpromoter	BBa_R0011 + gAmpRpromoter + BBa_J107201 + pSB4C5	Single sgRNA cassette efficiency characterization in the transcriptional inhibition of *bla* gene placed in HC plasmid with constitutive dCas9
gAmpRgene	BBa_R0011 + gAmpRgene + BBa_J107201 + pSB4C5	Single sgRNA cassette efficiency characterization in the transcriptional inhibition of *bla* gene placed in HC plasmid with constitutive dCas9

Continues on next page...

Table A.4 – *...continued from previous page*

Name	Construct	Purpose
gtetA	BBa_R0011 + gtetA + BBa_J107201 + pSB4C5	Single sgRNA cassette efficiency characterization in the transcriptional inhibition of *tetA* gene placed in LC plasmid with constitutive dCas9
gAmpRpromoter_gtetA Cassettes	BBa_R0011 + gAmpRpromoter + BBa_J107201 + BBa_R0011 + gtetA + BBa_J107201 + pSB4C5	Double sgRNA cassettes efficiency characterization in the transcriptional inhibition of *bla* and *tetA* gene placed in HC and LC plasmid with constitutive dCas9
Array gAmpRpromoter _gtetA	BBa_J23100 + tracrR + BBa_B1002 + BBa_R0011 + repeat + gAmpRpromoter + repeat + gtetA + repeat + BBa_B1006 + pSB4C5	CRISPRi Array efficiency characterization in the transcriptional inhibition of *bla* and *tetA* gene placed in HC and LC plasmid with constitutive dCas9
AE_{-3A}d gAmpRpromoter _gtetA Cassettes	J107216 + BBa_R0011 + gAmpRpromoter + BBa_J107201 + BBa_R0011 + gtetA + BBa_J107201 + pSB4C	Double sgRNA cassettes efficiency characterization in the transcriptional inhibition of *bla* and *tetA* gene placed in HC and LC plasmid with inducible dCas9
AE_{-3A}dArray gAmpRpromoter _gtetA	J107216 + BBa_J23100 + tracrR + BBa_B1002 + BBa_R0011 + repeat + gAmpRpromoter + repeat + gtetA + repeat + BBa_B1006 + pSB4C5	CRISPRi Array efficiency characterization in the transcriptional inhibition of *bla* and *tetA* gene placed in HC and LC plasmid with inducible dCas9
AE_{-3A}dArray_NDM1	J107216 + BBa_J23100 + tracrR + BBa_B1002 + BBa_R0011 + repeat + gNDM1 + repeat + BBa_B1006 + pSB4C5	CRISPRi Array efficiency characterization in the transcriptional inhibition of *NDM1* gene placed in MC plasmid with single spacer and inducible dCas9
AE_{-3A}dArray_NDM2	J107216 + BBa_J23100 + tracrR + BBa_B1002 + BBa_R0011 + repeat + gNDM2 + repeat + BBa_B1006 + pSB4C5	CRISPRi Array efficiency characterization in the transcriptional inhibition of *NDM1* gene placed in MC plasmid with single spacer and inducible dCas9
AE_{-3A}dArray NDM1_NDM2	J107216 + BBa_J23100 + tracrR + BBa_B1002 + BBa_R0011 + repeat + gNDM1 + repeat + gNDM2 + repeat + BBa_B1006 + pSB4C5	CRISPRi Array efficiency characterization in the transcriptional inhibition of *NDM1* gene placed in MC plasmid with two spacers and inducible dCas9

Continues on next page...

Table A.4 – *...continued from previous page*

Name	Construct	Purpose
AE_{-3A}dArray NDM1_mcr1	J107216 + BBa_J23100 + tracrR + BBa_B1002 + BBa_R0011 + repeat + gNDM1 + repeat + gmcr1 + repeat + BBa_B1006 + pSB4C5	CRISPRi Array efficiency characterization in the transcriptional inhibition of *NDM1* and *mcr1* gene placed in MC plasmid with single spacer and inducible dCas9
oriT_AE_{-3A}dArray gAmpRpromoter _gtetA	$oriT_{RK2}$ + J107216 + BBa_J23100 + tracrR + BBa_B1002 + BBa_R0011 + repeat + gAmpRpromoter + repeat + gtetA + repeat + BBa_B1006 + pSB4C5	Characterization of CRISPRi conjugative transfer and transcriptional inhibition of *bla* gene placed in HC plasmid with inducible dCas9
oriT_AE_{-3A}dArray NDM1_mcr1	$oriT_{RK2}$ J107216 + BBa_J23100 + tracrR + BBa_B1002 + BBa_R0011 + repeat + gNDM1 + repeat + gmcr1 + repeat + BBa_B1006 + pSB4C5	Characterization of CRISPRi conjugative transfer and transcriptional inhibition of *mcr-1* gene placed in MC plasmid with inducible dCas9

Bibliography

[1] Jocelyne Piret and Guy Boivin. Pandemics throughout history. *Frontiers in microbiology*, 11, 2020.

[2] Centers for Disease Control and Prevention. Control of infectious diseases. *MMWR. Morbidity and mortality weekly report*, 48(29):621–629, 1999.

[3] World Health Organization. Antimicrobial resistance. *https://www.who.int/news-room/fact-sheets/detail/antimicrobial-resistance*.

[4] World Health Organization et al. 2019 antibacterial agents in clinical development: an analysis of the antibacterial clinical development pipeline. Technical report, 2019.

[5] Mulatu Gashaw, Melkamu Berhane, Sisay Bekele, Gebre Kibru, Lule Teshager, Yonas Yilma, Yesuf Ahmed, Netsanet Fentahun, Henok Assefa, Andreas Wieser, et al. Emergence of high drug resistant bacterial isolates from patients with health care associated infections at Jimma university medical center: a cross sectional study. *Antimicrobial Resistance & Infection Control*, 7(1):1–8, 2018.

[6] US Centers for Disease Control and Prevention. Antibiotic resistance threats in the United States. Technical report, Atlanta, GA: US Centers for Disease Control and Prevention, 2019.

[7] World Health Organization et al. Antibacterial agents in preclinical development: an open access database. Technical report, World Health Organization, 2019.

[8] Jim O' Neill. Antimicrobial resistance: Tackling a crisis for the health and wealth of nations. In *The Review on Antimicrobial Resistance Chaired*, pages 1–20. HM Government Wellcome Trust, 2014.

[9] Mohammad Ahmad and Asad U Khan. Global economic impact of antibiotic resistance: a review. *Journal of global antimicrobial resistance*, 19:313–316, 2019.

[10] Rustam I Aminov. The role of antibiotics and antibiotic resistance in nature. *Environmental microbiology*, 11(12):2970–2988, 2009.

[11] Johan Bengtsson-Palme, Erik Kristiansson, and DG Joakim Larsson. Environmental factors influencing the development and spread of antibiotic resistance. *FEMS microbiology reviews*, 42(1):fux053, 2018.

[12] Dan I Andersson and Diarmaid Hughes. Persistence of antibiotic resistance in bacterial populations. *FEMS microbiology reviews*, 35(5):901–911, 2011.

[13] Aimee K Murray, Lihong Zhang, Jason Snape, and William H Gaze. Comparing the selective and co-selective effects of different antimicrobials in bacterial communities. *International journal of antimicrobial agents*, 53(6):767–773, 2019.

[14] Craig Baker-Austin, Meredith S Wright, Ramunas Stepanauskas, and JV McArthur. Co-selection of antibiotic and metal resistance. *Trends in microbiology*, 14(4):176–182, 2006.

[15] Centers for Disease Control and Prevention. How antibiotic resistance happens. *https://www.cdc.gov/drugresistance/about/how-resistance-happens.html*.

[16] Matthew I Hutchings, Andrew W Truman, and Barrie Wilkinson. Antibiotics: past, present and future. *Current opinion in microbiology*, 51:72–80, 2019.

[17] Garima Kapoor, Saurabh Saigal, and Ashok Elongavan. Action and resistance mechanisms of antibiotics: a guide for clinicians. *Journal of anaesthesiology, clinical pharmacology*, 33(3):300, 2017.

[18] Pew Charitable Trusts. A scientific roadmap for antibiotic discovery. *https://www.pewtrusts.org/it/research-and-analysis/reports/2016/05/a-scientific-roadmap-for-antibiotic-discovery*.

[19] Ursula Theuretzbacher and Laura JV Piddock. Non-traditional antibacterial therapeutic options and challenges. *Cell host & microbe*, 26(1):61–72, 2019.

[20] Jordi Vila. Microbiota transplantation and/or CRISPR/Cas in the battle against antimicrobial resistance. *Clinical Microbiology and Infection*, 24(7):684–686, 2018.

[21] Fankang Meng and Tom Ellis. The second decade of synthetic biology: 2010–2020. *Nature Communications*, 11(1):1–4, 2020.

[22] Tim Lewens. From bricolage to BioBricks^{TM}: Synthetic biology and rational design. *Studies in History and Philosophy of Biological and Biomedical Sciences*, 44(4):641–648, 2013.

[23] Anum Azam, Cheng Li, Kevin J Metcalf, and Danielle Tullman-Ercek. Type III secretion as a generalizable strategy for the production of full-length biopolymer-forming proteins. *Biotechnology and bioengineering*, 113(11):2313–2320, 2016.

[24] Lorenzo Pasotti, Davide De Marchi, Michela Casanova, Ilaria Massaiu, Massimo Bellato, Maria Gabriella Cusella De Angelis, Cinzia Calvio, and Paolo Magni. Engineering endogenous fermentative routes in ethanologenic Escherichia coli W for bioethanol production from concentrated whey permeate. *New biotechnology*, 57:55–66, 2020.

[25] Shimyn Slomovic, Keith Pardee, and James J Collins. Synthetic biology devices for in vitro and in vivo diagnostics. *Proceedings of the National Academy of Sciences*, 112(47):14429–14435, 2015.

[26] Xiao Tan, Justin H Letendre, James J Collins, and Wilson W Wong. Synthetic biology in the clinic: engineering vaccines, diagnostics, and therapeutics. *Cell*, 2021.

[27] Andrea C Wong and Maayan Levy. New approaches to microbiome-based therapies. *MSystems, American Society for Microbiology*, 4(3):e00122–19, 2019.

[28] JW van Mierlo. *Tackling antimicrobial resistance: the role of synthetic biology*. PhD thesis, Faculty of Science and Engineering, 2016.

[29] Yong Fan and Oluf Pedersen. Gut microbiota in human metabolic health and disease. *Nature Reviews Microbiology*, 19(1):55–71, 2021.

[30] Giovanni Cammarota, Gianluca Ianiro, Herbert Tilg, Mirjana Rajilić-Stojanović, Patrizia Kump, Reetta Satokari, Harry Sokol, Perttu Arkkila, Cristina Pintus, Ailsa Hart, et al. European consensus conference on faecal microbiota transplantation in clinical practice. *Gut*, 66(4):569–580, 2017.

[31] Josef R Bober, Chase L Beisel, and Nikhil U Nair. Synthetic biology approaches to engineer probiotics and members of the human microbiota for biomedical applications. *Annual review of biomedical engineering*, 20:277–300, 2018.

[32] Juan Borrero, Yuqing Chen, Gary M Dunny, and Yiannis N Kaznessis. Modified lactic acid bacteria detect and inhibit multiresistant enterococci. *ACS synthetic biology*, 4(3):299–306, 2015.

[33] Luciano A Marraffini. CRISPR-Cas immunity in prokaryotes. *Nature*, 526(7571):55–61, 2015.

[34] Jennifer A Doudna and Emmanuelle Charpentier. The new frontier of genome engineering with CRISPR-Cas. *Science*, 346(6213), 2014.

[35] Mario Alberto Garza-Elizondo, DR Rodríguez-Rodríguez, R Ramírez-Solís, MDL Garza-Rodríguez, and HA Barrera-Saldaña. Genome editing: A perspective on the application of CRISPR/Cas9 to study human diseases. *Int. J. Mol. Med*, 43:1559–1574, 2019.

[36] Prarthana Mohanraju, Kira S Makarova, Bernd Zetsche, Feng Zhang, Eugene V Koonin, and John Van der Oost. Diverse evolutionary roots and mechanistic variations of the CRISPR-Cas systems. *Science*, 353(6299), 2016.

[37] Francisco JM Mojica, César Díez-Villaseñor, Jesús García-Martínez, and Cristóbal Almendros. Short motif sequences determine the targets of the prokaryotic CRISPR defence system. *Microbiology*, 155(3):733–740, 2009.

[38] Kira S Makarova, Yuri I Wolf, Jaime Iranzo, Sergey A Shmakov, Omer S Alkhnbashi, Stan JJ Brouns, Emmanuelle Charpentier, David Cheng, Daniel H Haft, Philippe Horvath, et al. Evolutionary classification of CRISPR-Cas systems: a burst of class 2 and derived variants. *Nature Reviews Microbiology*, 18(2):67–83, 2020.

[39] Zeynep Baharoglu, David Bikard, and Didier Mazel. Conjugative DNA transfer induces the bacterial SOS response and promotes antibiotic resistance development through integron activation. *PLoS genetics*, 6(10):e1001165, 2010.

[40] Patrick D Hsu, Eric S Lander, and Feng Zhang. Development and applications of CRISPR-Cas9 for genome engineering. *Cell*, 157(6):1262–1278, 2014.

[41] Cui Zhang, Renfu Quan, and Jinfu Wang. Development and application of CRISPR/Cas9 technologies in genomic editing. *Human molecular genetics*, 27(R2):R79–R88, 2018.

[42] Martin Jinek, Krzysztof Chylinski, Ines Fonfara, Michael Hauer, Jennifer A Doudna, and Emmanuelle Charpentier. A programmable dual-RNA-guided DNA endonuclease in adaptive bacterial immunity. *Science*, 337(6096):816–821, 2012.

[43] Lei S Qi, Matthew H Larson, Luke A Gilbert, Jennifer A Doudna, Jonathan S Weissman, Adam P Arkin, and Wendell A Lim. Repurposing CRISPR as an RNA-guided platform for sequence-specific control of gene expression. *Cell*, 152(5):1173–1183, 2013.

[44] Matthew H Larson, Luke A Gilbert, Xiaowo Wang, Wendell A Lim, Jonathan S Weissman, and Lei S Qi. CRISPR interference (CRISPRi) for sequence-specific control of gene expression. *Nature protocols*, 8(11):2180–2196, 2013.

[45] Mazhar Adli. The crispr tool kit for genome editing and beyond. *Nature communications*, 9(1):1–13, 2018.

[46] Lun Cui and David Bikard. Consequences of Cas9 cleavage in the chromosome of Escherichia coli. *Nucleic acids research*, 44(9):4243–4251, 2016.

[47] Svitlana Malyarchuk, Douglas Wright, Reneau Castore, Emily Klepper, Bernard Weiss, Aidan J Doherty, and Lynn Harrison. Expression of mycobacterium tuberculosis ku and ligase d in escherichia coli results in reca and recb-independent dna end-joining at regions of microhomology. *DNA repair*, 6(10):1413–1424, 2007.

[48] Thomas A Hamilton, Gregory M Pellegrino, Jasmine A Therrien, Dalton T Ham, Peter C Bartlett, Bogumil J Karas, Gregory B Gloor, and David R Edgell. Efficient inter-species conjugative transfer of a CRISPR nuclease for targeted bacterial killing. *Nature communications*, 10(1):1–9, 2019.

[49] Kurt Selle, Joshua R Fletcher, Hannah Tuson, Daniel S Schmitt, Lana McMillan, Gowrinarayani S Vridhambal, Alissa J Rivera, Stephanie A Montgomery, Louis-Charles Fortier, Rodolphe Barrangou, et al. In vivo targeting of Clostridioides difficile using phage-delivered CRISPR-Cas3 antimicrobials. *Mbio*, 11(2):e00019–20, 2020.

[50] David Bikard, Chad W Euler, Wenyan Jiang, Philip M Nussenzweig, Gregory W Goldberg, Xavier Duportet, Vincent A Fischetti, and Luciano A Marraffini. Exploiting crispr-cas nucleases to produce sequence-specific antimicrobials. *Nature biotechnology*, 32(11):1146–1150, 2014.

[51] Robert J Citorik, Mark Mimee, and Timothy K Lu. Sequence-specific antimicrobials using efficiently delivered RNA-guided nucleases. *Nature biotechnology*, 32(11):1141–1145, 2014.

[52] Yoo Kyung Kang, Kyu Kwon, Jea Sung Ryu, Ha Neul Lee, Chankyu Park, and Hyun Jung Chung. Nonviral genome editing based on a polymer-derivatized CRISPR nanocomplex for targeting bacterial pathogens and antibiotic resistance. *Bioconjugate chemistry*, 28(4):957–967, 2017.

[53] Geeta Ram, Hope F Ross, Richard P Novick, Ivelisse Rodriguez-Pagan, and Dunrong Jiang. Conversion of staphylococcal pathogenicity islands to CRISPR-carrying antibacterial agents that cure infections in mice. *Nature biotechnology*, 36(10):971–976, 2018.

[54] Rosalind J Allen and Bartlomiej Waclaw. Bacterial growth: A statistical physicist s guide. *Reports on Progress in Physics*, 82(1):016601, 2018.

[55] Hal L Smith and Paul Waltman. *The theory of the chemostat: dynamics of microbial competition*, volume 13. Cambridge university press, 1995.

[56] Zhenmao Wan, Joseph Varshavsky, Sushma Teegala, Jamille McLawrence, and Noel L Goddard. Measuring the rate of conjugal plasmid transfer in a bacterial population using quantitative pcr. *Biophysical journal*, 101(1):237–244, 2011.

[57] Saptarshi Sinha, Rajdeep K Grewal, and Soumen Roy. Modeling bacteria–phage interactions and its implications for phage therapy. *Advances in applied microbiology*, 103:103–141, 2018.

[58] Iman Farasat and Howard M Salis. A biophysical model of CRISPR/Cas9 activity for rational design of genome editing and gene regulation. *PLoS computational biology*, 12(1):e1004724, 2016.

[59] Dennise Palacios Araya, Kelli L Palmer, and Breck A Duerkop. CRISPR-based antimicrobials to obstruct antibiotic-resistant and pathogenic bacteria. *PLoS Pathogens*, 17(7):e1009672, 2021.

[60] Fen Wan, Mohamed S Draz, Mengjie Gu, Wei Yu, Zhi Ruan, and Qixia Luo. Novel Strategy to Combat Antibiotic Resistance: A Sight into the Combination of CRISPR/Cas9 and Nanoparticles. *Pharmaceutics*, 13(3):352, 2021.

[61] Muhammad Abu Bakr Shabbir, Muhammad Zubair Shabbir, Qin Wu, Sammina Mahmood, Abdul Sajid, Muhammad Kashif Maan, Saeed Ahmed, Umer Naveed, Haihong Hao, and Zonghui Yuan. CRISPR-cas system: biological function in microbes and its use to treat antimicrobial resistant pathogens. *Annals of clinical microbiology and antimicrobials*, 18(1):1–9, 2019.

[62] Rotem Edgar and Udi Qimron. The Escherichia coli CRISPR system protects from λ lysogenization, lysogens, and prophage induction. *Journal of bacteriology*, 192(23):6291–6294, 2010.

[63] Ahmed A Gomaa, Heidi E Klumpe, Michelle L Luo, Kurt Selle, Rodolphe Barrangou, and Chase L Beisel. Programmable removal of bacterial strains by use of genome-targeting CRISPR-Cas systems. *MBio*, 5(1):e00928–13, 2014.

[64] Ido Yosef, Miriam Manor, Ruth Kiro, and Udi Qimron. Temperate and lytic bacteriophages programmed to sensitize and kill antibiotic-resistant bacteria. *Proceedings of the national academy of sciences*, 112(23):7267–7272, 2015.

[65] Elizabeth Pursey, David Sünderhauf, William H Gaze, Edze R Westra, and Stineke van Houte. CRISPR-Cas antimicrobials: Challenges and future prospects. *PLoS pathogens*, 14(6):e1006990, 2018.

[66] Marinelle Rodrigues, Sara W McBride, Karthik Hullahalli, Kelli L Palmer, and Breck A Duerkop. Conjugative delivery of CRISPR-Cas9 for the selective depletion of antibiotic-resistant enterococci. *Antimicrobial agents and chemotherapy*, 63(11):e01454–19, 2019.

[67] Haisi Dong, Hua Xiang, Dan Mu, Dacheng Wang, and Tiedong Wang. Exploiting a conjugative CRISPR/Cas9 system to eliminate plasmid harbouring the mcr-1 gene from Escherichia coli. *International journal of antimicrobial agents*, 53(1):1–8, 2019.

[68] Peng Wan, Shiyun Cui, Zhenbao Ma, Lin Chen, Xiaoshen Li, Ruonan Zhao, Wenguang Xiong, and Zhenling Zeng. Reversal of mcr-1-mediated colistin resistance in escherichia coli by crispr-cas9 system. *Infection and drug resistance*, 13:1171, 2020.

[69] Wenyan Jiang, David Bikard, David Cox, Feng Zhang, and Luciano A Marraffini. RNA-guided editing of bacterial genomes using CRISPR-Cas systems. *Nature biotechnology*, 31(3):233–239, 2013.

[70] Audrey Reuter, Cécile Hilpert, Annick Dedieu-Berne, Sophie Lematre, Erwan Gueguen, Guillaume Launay, Sarah Bigot, and Christian Lesterlin. Targeted-antibacterial-plasmids (TAPs) combining conjugation and CRISPR/Cas systems achieve strain-specific antibacterial activity. *Nucleic acids research*, 49(6):3584–3598, 2021.

[71] Pengxia Wang, Dongmei He, Baiyuan Li, Yunxue Guo, Weiquan Wang, Xiongjian Luo, Xuanyu Zhao, and Xiaoxue Wang. Eliminating mcr-1-harbouring plasmids in clinical isolates using the CRISPR/Cas9 system. *Journal of Antimicrobial Chemotherapy*, 74(9):2559–2565, 2019.

[72] Susan Fischer, Lisa-Katharina Maier, Britta Stoll, Jutta Brendel, Eike Fischer, Friedhelm Pfeiffer, Mike Dyall-Smith, and Anita Marchfelder. An archaeal immune system can detect multiple protospacer adjacent motifs (PAMs) to target invader DNA. *Journal of Biological Chemistry*, 287(40):33351–33363, 2012.

[73] Karissa Wang and Matthew Nicholaou. Suppression of antimicrobial resistance in MRSA using CRISPR-dCas9. *American Society for Clinical Laboratory Science*, 30(4):207–213, 2017.

[74] Qingyang Li, Peng Zhao, Lili Li, Haifeng Zhao, Lei Shi, and Pingfang Tian. Engineering a CRISPR interference system to repress a class 1 integron in Escherichia coli. *Antimicrobial agents and chemotherapy*, 64(3):e01789–19, 2020.

[75] Massimo Bellato, Angelica Frusteri Chiacchiera, Elia Salibi, Michela Casanova, Davide De Marchi, Ignazio Castagliuolo, Maria Gabriella Cusella De Angelis, Lorenzo Pasotti, and Paolo Magni. CRISPR interference modules as low-burden logic inverters in synthetic circuits. *Frontiers in Bioengineering and Biotechnology*, 2022.

[76] J. Christopher Anderson. Anderson promoter collection. *http://parts.igem.org/Promoters/Catalog/Anderson*.

[77] Lorenzo Pasotti, Massimo Bellato, Michela Casanova, Susanna Zucca, Maria Gabriella Cusella De Angelis, and Paolo Magni. Re-using biological devices: a model-aided analysis of interconnected transcriptional cascades designed from the bottom-up. *Journal of biological engineering*, 11(1):1–19, 2017.

[78] Francesca Ceroni, Rhys Algar, Guy-Bart Stan, and Tom Ellis. Quantifying cellular capacity identifies gene expression designs with reduced burden. *Nature methods*, 12(5):415–418, 2015.

[79] Andras Gyorgy, José I Jiménez, John Yazbek, Hsin-Ho Huang, Hattie Chung, Ron Weiss, and Domitilla Del Vecchio. Isocost lines describe the cellular economy of genetic circuits. *Biophysical journal*, 109(3):639–646, 2015.

[80] Massimo Bellato. *Overcoming metabolic burden in synthetic biology: a CRISPR interference approach*. PhD thesis, Faculty Engineering, Department of Industrial and Information Engineering, 2018.

[81] Patrick D Hsu, David A Scott, Joshua A Weinstein, F Ann Ran, Silvana Konermann, Vineeta Agarwala, Yinqing Li, Eli J Fine, Xuebing Wu, Ophir Shalem, et al. DNA targeting specificity of RNA-guided Cas9 nucleases. *Nature biotechnology*, 31(9):827–832, 2013.

[82] John G Doench, Ella Hartenian, Daniel B Graham, Zuzana Tothova, Mudra Hegde, Ian Smith, Meagan Sullender, Benjamin L Ebert, Ramnik J Xavier, and David E Root. Rational design of highly active sgRNAs for CRISPR-Cas9-mediated gene inactivation. *Nature biotechnology*, 32(12):1262–1267, 2014.

[83] Samuel H Sternberg, Sy Redding, Martin Jinek, Eric C Greene, and Jennifer A Doudna. DNA interrogation by the CRISPR RNA-guided endonuclease Cas9. *Nature*, 507(7490):62–67, 2014.

[84] Lun Cui, Antoine Vigouroux, François Rousset, Hugo Varet, Varun Khanna, and David Bikard. A CRISPRi screen in E. coli reveals sequence-specific toxicity of dcas9. *Nature communications*, 9(1):1–10, 2018.

[85] Yili Qian, Hsin-Ho Huang, José I Jiménez, and Domitilla Del Vecchio. Resource competition shapes the response of genetic circuits. *ACS synthetic biology*, 6(7):1263–1272, 2017.

[86] Lorenzo Pasotti, Massimo Bellato, Nicolò Politi, Michela Casanova, Susanna Zucca, Maria Gabriella Cusella De Angelis, and Paolo Magni. A synthetic close-loop controller circuit for the regulation of an extracellular molecule by engineered bacteria. *IEEE transactions on biomedical circuits and systems*, 13(1):248–258, 2018.

[87] Georgina Cox, Arthur Sieron, Andrew M King, Gianfranco De Pascale, Andrew C Pawlowski, Kalinka Koteva, and Gerard D Wright. A common platform for antibiotic dereplication and adjuvant discovery. *Cell chemical biology*, 24(1):98–109, 2017.

[88] Trine Aakvik Strand, Rahmi Lale, Kristin Fløgstad Degnes, Malin Lando, and Svein Valla. A new and improved host-independent plasmid system for rk2-based conjugal transfer. *PLoS One*, 9(3):e90372, 2014.

[89] Caroline A Schneider, Wayne S Rasband, and Kevin W Eliceiri. Nih image to imagej: 25 years of image analysis. *Nature methods*, 9(7):671–675, 2012.

[90] Barrick Lab. General conjugation protocol. *https://barricklab.org/twiki/bin/view/Lab/ProtocolsConjugation*.

[91] B Denise Raynor. Penicillin and ampicillin. *Primary Care Update for OB/GYNS*, 4(4):147–152, 1997.

[92] Ian Chopra and Marilyn Roberts. Tetracycline antibiotics: mode of action, applications, molecular biology, and epidemiology of bacterial resistance. *Microbiology and molecular biology reviews*, 65(2):232–260, 2001.

[93] Hannah R Meredith, Virgile Andreani, Helena R Ma, Allison J Lopatkin, Anna J Lee, Deverick J Anderson, Gregory Batt, and Lingchong You. Applying ecological resistance and resilience to dissect bacterial antibiotic responses. *Science advances*, 4(12):eaau1873, 2018.

[94] June Rothman Scott. Regulation of plasmid replication. *Microbiological reviews*, 48(1):1–23, 1984.

[95] Daniel Schultz, Adam C Palmer, and Roy Kishony. Regulatory dynamics determine cell fate following abrupt antibiotic exposure. *Cell systems*, 5(5):509–517, 2017.

[96] Beatriz Suay-García and María Teresa Pérez-Gracia. Present and future of carbapenem-resistant enterobacteriaceae (cre) infections. *Antibiotics*, 8(3):122, 2019.

[97] Zahra Aghapour, Pourya Gholizadeh, Khudaverdi Ganbarov, Abed Zahedi Bialvaei, Suhad Saad Mahmood, Asghar Tanomand, Mehdi Yousefi, Mohammad Asgharzadeh, Bahman Yousefi, and Hossein Samadi Kafil. Molecular mechanisms related to colistin resistance in enterobacteriaceae. *Infection and drug resistance*, 12:965, 2019.

[98] Wenjing Wu, Yu Feng, Guangmin Tang, Fu Qiao, Alan McNally, and Zhiyong Zong. Ndm metallo-β-lactamases and their bacterial producers in health care settings. *Clinical microbiology reviews*, 32(2):e00115–18, 2019.

[99] The comprehensive antibiotic resistance database (card). *https://card.mcmaster.ca/*.

[100] Brian P Alcock, Amogelang R Raphenya, Tammy TY Lau, Kara K Tsang, Mégane Bouchard, Arman Edalatmand, William Huynh, Anna-Lisa V Nguyen, Annie A Cheng, Sihan Liu, et al. Card 2020: antibiotic resistome surveillance with the comprehensive antibiotic resistance database. *Nucleic acids research*, 48(D1):D517–D525, 2020.

[101] Multiple sequence alignment, clustal omega. *https://www.ebi.ac.uk/Tools/msa/clustalo/*.

[102] Fabian Sievers, Andreas Wilm, David Dineen, Toby J Gibson, Kevin Karplus, Weizhong Li, Rodrigo Lopez, Hamish McWilliam, Michael Remmert, Johannes Söding, et al. Fast, scalable generation of high-quality protein multiple sequence alignments using clustal omega. *Molecular systems biology*, 7(1):539, 2011.

[103] Marco Falcone, Giusy Tiseo, Alberto Antonelli, Cesira Giordano, Vincenzo Di Pilato, Pietro Bertolucci, Eva Maria Parisio, Alessandro Leonildi, Noemi Aiezza, Ilaria Baccani, et al. Clinical features and outcomes of bloodstream infections caused by new delhi metallo-β-lactamase–producing enterobacterales during a regional outbreak. 7(2):ofaa011, 2020.

[104] Thibault Stalder and Eva Top. Plasmid transfer in biofilms: a perspective on limitations and opportunities. *NPJ biofilms and microbiomes*, 2(1):1–5, 2016.

[105] Laurent A Lardon, Brian V Merkey, Sónia Martins, Andreas Dötsch, Cristian Picioreanu, Jan-Ulrich Kreft, and Barth F Smets. idynomics: next-generation individual-based modelling of biofilms. *Environmental microbiology*, 13(9):2416–2434, 2011.

[106] James Dickson Murray. *Mathematical Biology I. An Introduction*. Springer, 2002.

[107] Jacques Monod. The growth of bacterial cultures. *Annual review of microbiology*, 3(1):371–394, 1949.

[108] Athanasios Kakasis and Gerasimia Panitsa. Bacteriophage therapy as an alternative treatment for human infections. a comprehensive review. *International journal of antimicrobial agents*, 53(1):16–21, 2019.

[109] Radojka M Savic, Daniël M Jonker, Thomas Kerbusch, and Mats O Karlsson. Implementation of a transit compartment model for describing drug absorption in pharmacokinetic studies. *Journal of pharmacokinetics and pharmacodynamics*, 34(5):711–726, 2007.

[110] Darja Zgur Bertok and Zdravko Podlesek. The DNA damage inducible SOS response is a key player in generation of bacterial persister cells and population wide tolerance. *Frontiers in Microbiology*, 11:1785, 2020.

[111] Benjamin J Cairns, Andrew R Timms, Vincent AA Jansen, Ian F Connerton, and Robert JH Payne. Quantitative models of in vitro bacteriophage–host dynamics and their application to phage therapy. *PLoS Pathogens*, 5(1):e1000253, 2009.

[112] Richard E Lenski. Dynamics of interactions between bacteria and virulent bacteriophage. *Advances in microbial ecology*, pages 1–44, 1988.

[113] Richard E Lenski and Bruce R Levin. Constraints on the coevolution of bacteria and virulent phage: a model, some experiments, and predictions for natural communities. *The American Naturalist*, 125(4):585–602, 1985.

[114] SJ Schrag and JE Mittler. Host-parasite coexistence: the role of spatial refuges in stabilizing bacteria-phage interactions. *The American Naturalist*, 148(2):348–377, 1996.

[115] Sylvia H Duncan, Petra Louis, John M Thomson, and Harry J Flint. The role of ph in determining the species composition of the human colonic microbiota. *Environmental microbiology*, 11(8):2112–2122, 2009.

[116] Richard R Stein, Vanni Bucci, Nora C Toussaint, Charlie G Buffie, Gunnar Rätsch, Eric G Pamer, Chris Sander, and Joao B Xavier. Ecological modeling from time-series inference: insight into dynamics and stability of intestinal microbiota. *PLoS computational biology*, 9(12):e1003388, 2013.

[117] A Massoudieh, A Mathew, E Lambertini, KE Nelson, and TR Ginn. Horizontal gene transfer on surfaces in natural porous media: conjugation and kinetics. *Vadose Zone Journal*, 6(2):306–315, 2007.

[118] Phillip Nazarian, Frances Tran, and James Q Boedicker. Modeling multispecies gene flow dynamics reveals the unique roles of different horizontal gene transfer mechanisms. *Frontiers in microbiology*, 9:2978, 2018.

[119] Hal L Smith and RT Trevino. Bacteriophage infection dynamics: multiple host binding sites. *Mathematical Modelling of Natural Phenomena*, 4(6):109–134, 2009.

[120] Bruce R Levin, Frank M Stewart, and Lin Chao. Resource-limited growth, competition, and predation: a model and experimental studies with bacteria and bacteriophage. *The American Naturalist*, 111(977):3–24, 1977.

[121] SB Santos, C Carvalho, J Azeredo, and EC Ferreira. Population dynamics of a salmonella lytic phage and its host: Implications of the host bacterial. 2014.

[122] David T Kysela and Paul E Turner. Optimal bacteriophage mutation rates for phage therapy. *Journal of Theoretical Biology*, 249(3):411–421, 2007.

[123] Chaoyong Huang, Tingting Ding, Jingge Wang, Xueqin Wang, Liwei Guo, Jialei Wang, Lin Zhu, Changhao Bi, Xueli Zhang, Xiaoyan Ma, et al. CRISPR-Cas9-assisted native end-joining editing offers a simple strategy for efficient genetic engineering in Escherichia coli. *Applied microbiology and biotechnology*, 103(20):8497–8509, 2019.

[124] Hanna Engelberg-Kulka, Shahar Amitai, Ilana Kolodkin-Gal, and Ronen Hazan. Bacterial programmed cell death and multicellular behavior in bacteria. *PLoS genetics*, 2(10):e135, 2006.

[125] John W Drake. A constant rate of spontaneous mutation in DNA-based microbes. *Proceedings of the National Academy of Sciences*, 88(16):7160–7164, 1991.

[126] Vincent M Isabella, Binh N Ha, Mary Joan Castillo, David J Lubkowicz, Sarah E Rowe, Yves A Millet, Cami L Anderson, Ning Li, Adam B Fisher, Kip A West, et al. Development of a synthetic live bacterial therapeutic for the human metabolic disease phenylketonuria. *Nature biotechnology*, 36(9):857–864, 2018.

[127] Jeong Wook Lee, Clement TY Chan, Shimyn Slomovic, and James J Collins. Next-generation biocontainment systems for engineered organisms. *Nature chemical biology*, 14(6):530–537, 2018.

[128] Tzu-Chieh Tang, Eléonore Tham, Xinyue Liu, Kevin Yehl, Alexis J Rovner, Hyunwoo Yuk, Cesar de la Fuente-Nunez, Farren J Isaacs, Xuanhe Zhao, and Timothy K Lu. Hydrogel-based biocontainment of bacteria for continuous sensing and computation. *Nature Chemical Biology*, 17(6):724–731, 2021.

[129] Thomas Knight. Idempotent vector design for standard assembly of biobricks. 2003.

[130] John G Doench, Nicolo Fusi, Meagan Sullender, Mudra Hegde, Emma W Vaimberg, Katherine F Donovan, Ian Smith, Zuzana Tothova, Craig Wilen, Robert Orchard, et al. Optimized sgRNA design to maximize activity and minimize off-target effects of CRISPR-Cas9. *Nature biotechnology*, 34(2):184–191, 2016.

[131] Carlotta Ronda, Lasse Ebdrup Pedersen, Morten OA Sommer, and Alex Toftgaard Nielsen. CRMAGE: CRISPR optimized mage recombineering. *Scientific reports*, 6(1):1–11, 2016.

List of publications

Published Article

- Massimo Bellato, *Angelica Frusteri Chiacchiera*, Elia Salibi, Michela Casanova, Davide De Marchi, Ignazio Castagliuolo, Maria Gabriella Cusella De Angelis, Paolo Magni, Lorenzo Pasotti. *CRISPR interference modules as low-burden logic inverters in synthetic circuits.* Frontiers in Bioengineering and Biotechnology, 2022.

Contributions to conference proceedings

- Massimo Bellato, Lorenzo Pasotti, Elia Salibi, *Angelica Frusteri Chiacchiera*, Pin-Yi Chen, Yili Qian, Michela Casanova, Maria Gabriella Cusella De Angelis, Domitilla del Vecchio and Paolo Magni. *CRISPRi for rational design of genetic circuits in Synthetic Biology.* Proceeding of the 2018 GNB conference. June 25-27, Milan, Italy.
- *Angelica Frusteri Chiacchiera*, Lorenzo Pasotti, Massimo Bellato, Elia Salibi, Michela Casanova, Davide De Marchi, Maria Gabriella Cusella De Angelis, Paolo Magni. *Approaches to optimize CRISPRi based gene regulation toolkit in E. coli.* Proceeding of the 6th International Synthetic and System Biology Summer School (SSBSS). Pisa, Italy, 2019.